CAR COOLING SYSTEMS AND THEIR PUMPS

FARROKH EIMIEH

Presented for the Degree of Master of Philosophy

1975

UNIVERSITY OF SOUTHAMPTON

DEPARTMENT OF

MECHANICAL ENGINEERING

ABSTRACT

FACULTY OF ENGINEERING & APPLIED SCIENCE

DEPARTMENT OF MECHANICAL ENGINEERING

Master of Philosophy

CAR COOLING SYSTEMS AND THEIR PUMPS

by Farrokh Elmieh

Circulating pumps for automotive coolant systems (cars and trucks) are sold in very large numbers, but in comparison with other rotodynamic pumps the best efficiency points of automotive pumps are distinctly poorer; less than 40% for the designs tested.

The introduction discusses current tendencies in car (liquid) cooling systems and is followed by an historical survey of automotive cooling systems.

Continuing, two main subjects (automotive cooling systems and cavitation) are discussed with particular emphasis on E.G/W mixtures. There is no separate literature review, but the work of others has been brought in throughout the thesis where relevant.

The closed system test rig has been designed to examine commercial pumps. This has provision to run at temperatures up to 130^{o}C and a coolant system pressure up to 1.8 bar (gauge). A 230 litre vessel incorporates a pneumatic pressure controller and thermostated heater. A special housing has been made to simulate installations where a pump discharges directly into the cylinder block.

The last major section of the thesis gives results obtained with the three types of pumps tested, with graphical displays in both dimensional and non-dimensional form. Cavitation in these pumps is discussed with comment on apparent differences between water and ethylene-glycol/water mixture.

Finally, the suggested programme for future work is outlined.

ACKNOWLEDGEMENT

The work presented in this thesis was conducted under the direction of Mr. M.T. Thew, to whom the author is greatly indebted for his guidance and advice throughout the research.

The author acknowledges the help of Mr. M.A. Batey and the mechanical engineering workshop staff and to Mr. J.D. Sewill and the electronic workshop staff for their work and advice on the test facility. Mr. G.N. Spencer assisted with much of the experimental work and performed many of the modifications to the test rig. The help of Mr. Bellamy and the National Motor Museum staff for finding the information for the review is gratefully acknowledged.

Thanks are also due to Mr. R. Herbert for his help on measuring and analysing the vibration of the test rig and to Mrs. Lampard for typing this thesis.

The project was partially financed until May 1973, by the Ford Co. (U.K.). The author is also most grateful that the research was subsequently supported by a grant from The Advanced Studies Committee of the University of Southampton. The personal financial support of a University Research Studentship with a British Council Fees Award is gratefully acknowledged.

Last but not least, grateful thanks are due to my wife for her great patience and encouragement during the hard times which we had.

CONTENTS

LIST OF FIGURES

SUMMARY

Circulating pumps for automotive coolant systems (cars and truck) are sold in very large numbers, but in comparison with other motodynamic pumps the best efficiency points of automotive pumps are distinctly proven; less than 40% for the designs tested.

The introduction discusses current tendencies in car (liquid) cooling systems and is followed by an historical survey of automotive cooling systems.

Continuing, two main subjects (automotive cooling systems and cavitation) are discussed with particular emphasis on E.G/W mixtures. There is no separate literature review, but the work of others has been brought in throughout the thesis where relevant.

The closed system test rig has been designed to examine commercial pumps. This has provision to run at temperatures up to 130°C and a coolant system pressure up to 1.8 bar (gauge). A 230 litre vessel incorporates a pneumatic pressure controller and thermostated heater. A special housing has been made to simulate installations where a pump discharges directly into the cylinder block.

The last major section of the Thesis gives results obtained with the four types of pumps tested, with graphical displays in both dimensional and non-dimensional form. Cavitation in these pumps is discussed with comment on apparent differences between water and ethylene-glycol/water mixture.

Finally, the suggested programme for future work is outlined.

NOTATION

A_r	radiator surface area m^2
A	constant
a	constant
B	thermal cavitation parameter $B = \frac{v_g}{v_f} \times \frac{C_p}{h_{fg}} \times \frac{dT_{sat}}{dT_{pV}}$ Nm^{-2}
B'	constant
B_1	thermal cavitation parameter $B_1 = \frac{B}{\Delta NPSH}$
C	constant
$\overline{C}$	calorific value of petrol J/kg
C_{30}	constant
C_p	specific heat at constant pressure KJ/kg deg K
$\overline{C}_p$	pressure coefficient dimensionless $\overline{C}_p = \frac{p_\infty - \bar{p}}{\frac{1}{2}\rho U_\infty^2}$
D	diameter of impeller m
$\bar{D}$	characteristic body dimension m
E	chemical potential
ΔE_v	decrease in vapour energy $\Delta E_v = g\Delta h_V$ J/kg
Δe_v	internal energy of vaporization J/kg
G	mass flow of air per unit time divided by the cross sectional of flow area (air) kg m^{-2} s^{-1}
G_w	mass flow rate of coolant kg/hr
g	gravity acceleration ms^{-2}
Δh_v	the decrease in vapour pressure due to vaporization expressed in metre of liquid
h_{fm}	enthalpy of liquid mixture kJ/kg
h_{gm}	enthalpy of vapour mixture kJ/kg
h_{fgm}	latent heat of vaporization of the mixture kJ/kg
h_{fgG}	latent heat of vaporization of the glycol kJ/kg
h_{fgW}	latent heat of vaporization of the water kJ/kg
Δh_f	increment of liquid enthalpy kJ/kg
h_{fg}	latent heat of vaporization kJ/kg
h	Planck constant 6.6256×10^{-34} Js
ΔH	activation energy for motion J/kg mole
K_1 & K_2	constant
k	thermal conductivity of saturated liquid J/(m)(sec)(K)

K_r	coefficient depending on core design and viscosity and thermal conductivity of air
L	typical length of the core section (air side) m
M_i	molecular weight of component i kg mole
N	speed of rotation rev/sec
N_A	Avegadro constant 6.02252×10^{23} $mole^{-1}$
n_{sf}	shape number dimensionless $n_{sf} = \frac{\omega \sqrt{Q}}{(Y)^{\frac{3}{4}}}$
NPSE	net positive suction energy Jkg^{-1} NPSE = gNPSH
$NPSE_{GW}$	net positive suction energy of ethylene-glycol/water mixture $NPSE_{GW} = g\ NPSH_{GW}$ J/kg
$NPSE_W$	net positive suction energy of water J/kg
ΔNPSE	NPSE reduction J/kg
δNPSE	additional decreases in NPSE in two component liquid J/kg
NPSH	net positive suction head m
p	local liquid pressure Nm^{-2} $(K_{gm}^{-1}\ s^{-2})$
$\bar{p}$	mean value of the liquid pressure adjacent to a bubble Nm^{-2}
p_A	absolute pressure at a liquid free surface Nm^{-2}
p_C	critical pressure Nm^{-2}
p_i	internal pressure of a bubble Nm^{-2}
p_G	pressure exerted by the non-condensable gases Nm^{-2}
p_L	suction line losses Nm^{-2}
p_p	pressure rise by pump Nm^{-2}
p_S	static suction pressure $(\pm)$ Nm^{-2}
p_{TR}	reduction in the liquid pressure due to turbulence and surface roughness Nm^{-2}
p_V	vapour pressure Nm^{-2}
p_∞	reference pressure Nm^{-2}
$p_{\infty d}$	" " for desinent cavitation Nm^{-2}
$p_{\infty i}$	" " " incipient " Nm^{-2}
Δp_V	reduction in vapour pressure due to local cooling Nm^{-2}
p_{VA}	partial vapour pressure of (A) above a solution Nm^{-2}
p^o_{VA}	the vapour pressure of pure liquid A Nm^{-2}
Q	flow rate $m^3\ s^{-1}$
Q_W	flow rate of water $m^2\ s^{-1}$
Q_{GW}	" " " E.G/W $m^3\ s^{-1}$

P_m	power lost in mechanical friction including the power lost in water pump and oil pump
P_r	Pradntl number $P_r = \frac{C_p \mu}{k}$
q	engine jacket loss J
q_t	total heat dissipated per unit time Js^{-1}
q_g	heat from the gases per unit time Js^{-1}
q_1	heat to the coolant radiator per unit time Js^{-1}
q_2	" " " oil " " " " Js^{-1}
q_3	heat escaping directly from the engine including radiation and heat lost in the exhaust gases per unit time Js^{-1}
Re	Reynolds number $Re = \frac{ND^2}{\nu^2}$
$\bar{R}$	is bubble radius m
R	universal gas constant equals 8.3143 JK^{-1} kg mole
S	suction specific speed $S = \frac{N\sqrt{Q}}{(NPSH)^{\frac{3}{4}}}$
S_{sf}	non dimensional form of suction specific speed $S_{sf} = \frac{\omega\sqrt{Q}}{(NPSE)^{\frac{3}{4}}}$
S_b	surface tension Nm^{-1}
Str	Strouhal number $Str = \frac{t \cdot U_\infty}{X}$
T	absolute temperature deg K
T_{sat}	saturation temperature K
T_o	outlet coolant temperature from the engine
T_i	inlet " " to the cylinder block
T_r	average temperature of the radiator surface equal to the mean water temperature since the tubes are thin and have a high conductivity
T_a	ambient air temperature
t	time s
U	local velocity ms^{-1}
U_∞	reference velocity ms^{-1}
ΔU	internal activation energy J/kg mole
U_1	mean axial inlet velocity ms^{-1}
V_g	volume of vapour produced L^3
V_f	volume of liquid L^3
v_g	specific volume of vapour $m^3\ kg^{-1}$
v_f	specific volume of liquid m^3 kg

v_{fm}	specific volume of fluid mixture m^3kg^{-1}
v_{gm}	specific volume of vapour mixture m^3kg^{-1}
v_{fgm}	difference of specific volume of vapour and liquid in the mixture m^3kg^{-1}
V_i	molar volume of component i m^3/kg mole
W	engine power output kw
$\bar{w}$	fuel consumption kg/kw
ω	speed of rotation rad/sec
ΔX	cavity length m
X_i	mole fraction of component i
x	space coordinate in direction of flux
$\bar{X}_i$	weight fraction of component i
Y	total specific energy J/kg
ΔY	reduction in total specific energy J/kg
$\bar{\alpha}$	dissolved air content
α	thermal diffusivity $\frac{k}{\rho_f C_p}$ m^2/sec
β	Henry's law constant
σ	cavitation number $\sigma = \frac{p_\infty - p_V}{\frac{1}{2}\rho U_\infty^2}$
σ_d	desinent cavitation number $\sigma_d = \frac{p_{\infty d} - p_V}{\frac{1}{2}\rho U_\infty^2}$
σ_i	incipient cavitation number $\sigma_i = \frac{p_{\infty i} - p_V}{\frac{1}{2}\rho U_\infty^2}$
σ_{th}	thoma cavitation number $\sigma_{th} = \frac{NPSE}{Y}$
ρ	density kg/m^3
η	efficiency of pump
μ	absolute viscosity $NS\,m^{-2}$
ν	kinematic viscosity m^2s^{-1}
Φ	flow coefficient dimensionless $\Phi = \frac{Q}{ND^3}$
ψ	head coefficient " $\psi = \frac{Y}{N^2D^2}$
λ_p	power coefficient " $\lambda_p = \frac{\text{power}}{\rho N^3 D^5}$
J_i	flux of component i m/sec
D_{12}	diffusion coefficient m^2/sec
D_T	thermal diffusion constant dimensionless

J_{TDi}	flux due to thermal diffusion of component i	m/sec
E.G/W	ethylene glycol water mixture	

OBJECTIVES

There are two main objectives for this experiment, to examine automotive pump performance and to further basic cavitation studies. During the experiment the two aspects of the work were often merged together.

Pump Performance

Pump performance tests include measuring the performance of a variety of pump design fitted to engines, over a range of water-glycol concentrations with and without cavitation. Differences arising due to mass production tolerances in components are to be examined.

By using these results in non-dimensional correlations, we hope to redesign pumps and housing to seek improved head/flow and cavitation performance, with due regard to cost, reliability, durability and size. (Co-operation with engine manufacturers is essential).

During experiments pump seal performance is to be checked for weak points and improve design.

Cavitation Studies

By measuring pump performance under cavitation conditions with a range of water glycol concentrations, the standard predictive correlations will be checked.

Using water glycol mixture as a circulant we are going to attempt to derive correlations applicable to two-component liquids and compare the cavitation damage from two-component mixtures with established data for standard liquids.

These are ultimate objectives even though personal problems cut short the programme.

CHAPTER I

INTRODUCTION

In terms of size, the circulating pump for automotive liquid coolant systems is amongst the smaller sizes of pump marketed. Because of the high volume of sales at $> 10^6$ p.a. in the U.K. alone (though diminution in demand might be anticipated in the near future) the cumulative value is very large.

The need for a performance and cavitation investigation in automotive water pumps is accentuated by the worldwide tendency to buy and use a one engine package and the use of air conditioning systems. It follows that cooling systems must cope with a very wide variety of environmental conditions. Because of the variety of climates and height above sea level, sealed cooling systems are accepted and used by many automotive manufacturers. Water glycol mixture is used as a coolant in most pressurized systems which are fitted with an expansion and header tank. This type of system has some advantages, such as, higher NPSE at pump inlet, smaller radiator[15] (because of the larger temperature difference between coolant and air compared with older cooling systems), reduction of boiling effect after stopping, reduced sensitivity to fall of boiling point with altitude; hence minimizing coolant loss, and also giving a lower freezing point.

It might also be noted that combustion characteristics have to be carefully controlled and coolant temperature control can help to secure improved emission. By using water/glycol mixtures as a coolant in a pressurized system, it is more difficult to find out the cavitation behaviour of the automotive water pump; because of two-component liquid effects, flowrate prediction is difficult.

Lack of space around the engine because of car styling and the cost of production, causes automotive circulating pumps to be made without a volute in a large number of cars, with discharge straight into the cylinder block. Thus there is a highly irregular cavity to receive flow from the impeller.

Truck engines require larger fans and radiators, and because of higher power, need a bigger circulating pump than passenger cars. So the cooling system and automotive circulating pump is more important in trucks than in cars, especially as system specifications are higher. Diesel engines are often selected for motor trucks because of higher efficiency especially at part-load. In this case vibration becomes very important in the cavitation at cylinder liners and the pump blades as vibration accelerates the cavitation damage. It is suggested that by increasing the pressure in cooling systems, the amplitude of vibration reduces considerably.[26] The recommended pressure value varies for different vehicles, such as, for cars 1.9 - 2.04 bar abs., light trucks 1.49 - 2.04 bar abs., medium trucks 1.49 - 1.9 bar abs. and heavy trucks 1.28 - 1.63 bar abs.[15]

CHAPTER II

HISTORICAL INTRODUCTION TO COOLING SYSTEMS

2.1 Introduction

Earlier water cooling systems consisted of a 10 gallon drum (45 litres), mounted above the engine, which supplied water to the jacket around the engine by means of a centrifugal friction driven on a semi rotary type of pump. Since there was no radiator, the evaporation of water did not take very long and it was usually necessary to renew the water supply every thirty miles.(1)

The early motorists had to have a good knowledge of every pump and horse trough and pond within one hundred miles of their home.

The first cars with radiators did not have any fans for forced circulation of air through the radiators thus continuous hill-climbing, with the engine running at its greatest speed, sometimes resulted in over-heating, even though the water circulation may have been satisfactory. This was even more likely to heppen if the radiation was not subjected to a through current of air.

There was a great tendency for pioneers to use air cooled engine. Cooling by means of direct heat dissipation from the cylinder barrel and head to the surrounding air was employed in small engines (Franklin) and in almost all motor cycles. Natural flow air-cooling was very difficult to regulate and as the size of cylinder increased, the difficulties became very serious, because the heat generated increases with the volume of cylinder, whilst the dissipation is proportional to the area of radiating surface. Air cooled engines had the reputation of being noisier than the water cooled ones. Very few instances of fan-cooled (forced circulation direct air cooling) engines were on the market between 1910 - 1920. The Kruff flat four was a successful example.(2)

2.2 Different varieties of early cooling system

Some of the earlier cars employed a combination of water cooling for the combustion head and valve passages and seatings, and air or oil cooling for the cylinder barrel.

There were two principal methods of cooling systems with water in the early twentieth century, these were

1 - the natural convection, or thermo syphon system

2 - forced circulation

The principle of natural circulation depends upon the convection circulation. In the case of automobile engine, the hottest part is the space around the cylinder head, and the hot water rises from this part to the top of the radiator, thence down the numerous passages in the radiator and along to the lowest part of the water jacket, Fig. (1).

In order to ensure a constant, as against a more or less intermittent flow of the cooling water throughout the circulation system, many makers used some sort of a pump driven either by friction from the periphery of the fly wheel, or by means of some positive system of chain or gear drive, Fig. (2).

The average volume of water per KW power output for engines with natural convection circulation was slightly more than that for others[5] Fig. (3). The amount of water required to cool an average car was about 1 gallon per 10 b.h.p. for engines with pumps and 1¼ gallon per 10 b.h.p. for engines with thermosyphon cooling systems. Thermo syphon cooling systems were very popular especially on family cars even after the 2nd World War. The advantages of the thermo syphon system were its simplicity; it had no glands, no moving parts and never required adjustment. An important advantage of thermo syphon system was that if the car stood for some length of time in cold weather, the possibility of the water jacket bursting due to the water freezing was very remote. As the temperature of the water fell, a certain amount of circulation was set up because of convection which could not be obtained if a pump was fitted.

The respective percentage of cars fitted with thermo syphon cooling systems at the Olympia Motor Show were 8% in 1905, 11% in 1906[3]. The percentage of cars with thermo syphon cooling system increased to 31% in 1918[4].

The disadvantages of thermo syphon cooling system were:

1 - Circulation was not satisfactory unless the water pipes were of ample diameter, the jacket comparatively unrestricted, and the cylinders must be fitted low enough in relation to the bottom of radiator (a styling problem), but it is doubtful whether this was necessary, as the bottom of the cylinder block could not be very warm.

2 - It is essential always to maintain the water level at such a height that the outlet from the cylinders to the radiator is always submerged. This was a big problem in warm weather and tropical countries, due to evaporation of water in the cooling system.

The main disadvantage of forced circulation cooling systems was leakage which was caused by failure of the pump's seal. Also in forced circulation systems, the use of dirty water caused serious problems especially when eccentric positive throw pumps or gear pumps were employed. Motorists were advised to use rain water for the coolant by many manufacturers, especially for those who lived in the countryside.[13] There were advertisements stating that only a pint of water for every 300 to 500 miles was required depending on the nature of roads encountered[13], or a pint of water every day!![12]

2.3 Early Automotive Water Pumps

There were three types of pumps which were in common use in early cars.

1 - eccentric positive throw pump (vane pump)

2 - gear wheel pump.

3 - centrifugal pump.

The eccentric positive throw pumps are perhaps the oldest type of rotary pump used on motor cars, Fig. (4). This type of pump usually had a strainer to prevent the dirt going in to the pump[6]. The strainer had to be cleaned occasionally. This type of pump had a tendency to wear the pump case, since the blades had to be close fit in the case to prevent significant leakage. Fig. (5 & 6), show a modification of Fig. (4), which was liable to wear[3].

Fig. (7) shows a gear pump which was in common use in early 1900. This type of pump was liable to wear from dirt in the water more than

other types of pump. Some used double helical gear wheels for pumping, Fig. (8).

Fig. (9) shows a centrifugal pump which was used on early cars. Centrifugal pumps were very popular because there is only one moving part, and the impeller need not be water tight. The main advantage of centrifugal pumps over gear pumps and eccentric positive throw pumps was that if any small object, such as a stick or pebbel should get into the circulating system, no serious harm would result, whereas with the other types of pumps, damage was almost certain to ensue. Another advantage is that, there is a free passage for the water when the pump is not operating, thus in event of a breakdown of the driving mechanism of the pump, the possibility of a (reduced) natural thermosyphon circulation remains.

The circulating pump was driven in different ways. The older way of driving the pump was to have a small friction wheel running against the flywheel of the engine. This was rather complicated, as a spring was required for keeping the friction wheel in position, and either the pump had to be mounted so that it could move slightly to accommodate this, or the shaft had to have a flexible joint in it. The advantage of this method was that the pump speed could exceed that of the engine, which allowed use of a smaller pump. This method was not very successful as failure of the bearings was more likely at higher speed. Gear driven or direct drive were other options for car manufacturers. Table I shows the respective percentage of various cooling systems which were exhibited at the Olympia Motor Show and Stanley Show Agricultural Hall in London in 1905 and 1906.

Table I Respective Percentage of Various Cooling Systems in Cars in 1905 and 1906.

YEAR	Thermo syphon	Gear pump Gear driven	Centrifugal Gear driven	Centrifugal Friction driven	RADIATOR	
					Gilled	Honeycomb
1905	8%	33%	43%	16%	41%	59%
1906	11%	27%	61%	1%	37%	63%

One of the famous companies which changed its pump from gear pump to centrifugal type in 1906 was Rolls Royce.

In early pumps both the spindle and the bearings in which it ran, were made from brass, which occasionally caused great wear. The problem was lack of lubrication caused by leakage of grease out of pump bearings. At the time, the brass spindle and white metal bearings (80% Zn, 16% tin and 4% Cu) were the most usual materials. There was usually a stuffing-box to prevent leakage where the spindle passed out of the pump casing as in Fig. (10). Sometimes the spindle had a very long bearing, and grease was used to keep it water tight, but wear of the bearings led to leakage. Another plan was to drive the pump by a spring, Fig. (11) fitting into a notch at the end of the spindle, and pressing against a collar with enough force to keep it tight.

In July 1911 Albion patented a cooling system with pump impellor inside the cylinder block[5]. This system saved considerable piping and connection problems, Fig. (12). This system is in common use nowadays.

2.4 Thermostat

The use of cars in countries with a great variation of temperature, increased the tendency to use a thermostatically controlled cooling system. This was achieved by using a valve which is put into operation automatically (Bellows thermostat in Cadillac in 1918), Fig. 14, hand operated (in Daimler) Fig. (13) or by radiators fitted with shutters so that either the whole or a part of the cooling surface can be blanketed from action at the will of the driver (Rolls Royce, Sunbeam and Hudson).

2.5 Radiator

In the early types of motor cars, pipes curled in front of the engine contained the circulating cooling water to radiate the heat from the cylinders of the engine. These were simply pipes with fins of iron or zinc brazed to them so as to give them the additional surface needed to cool the engine efficiently. The German Daimler Company was responsible for producing the honeycomb type radiator[8] which is the principal fashion for present day motor vehicles. Table 1 shows the tendency of using honeycomb radiator in 1905 and 1906.

2.6 Antifreeze

The use of antifreeze was suggested by some specialists in early 1900[6]. The most common antifreeze was 30% glycerine. It was soon realized that glycerine affected the rubber hose of the piping system adversely[9]. Other types of antifreeze on the market were, wood alcohol (Methanol), Glycerine, alcohol and calcium chloride. A combination solution of alcohol and glycerine in water was most satisfactory but expensive[4]. In cars using the alcohol and water mixture as antifreeze the alcohol tended to evaporate preferentially, so it was necessary to refill the tank with alcohol. Drivers had to be very careful that the percentage of alcohol did not exceed 50% as this increased the fire risk. Calcium chloride or any alkaline solution was corrosive to metal parts. The pH value of ($CaCl_2$) could be increased by neutralizing the solution by means of ammonia and sodium carbonate.

2.7 Pressurized Cooling System

The existing systems of water cooling before the 2nd World War were recognized as inefficient and they were the subject of a great deal of experiment in Europe and America. Pressurized cooling systems using a high boiling point coolant were suggested before the 2nd World War[10]. The 1939-1945 war initiated a demand for vehicles for the Allied Armies in Africa and Asia, so pressurized cooling system were almost in common use after the 2nd World War. A pressurized cooling system is similar to the atmospheric pressure ones, except that, instead of its having a radiatior overflow pipe to the air, a safety valve is fitted to the top of radiator and the overflow pipe is attached to the safety valve outlet. A vacuum valve is also provided Fig. (15). Pressurized cooling systems were not very successful at the beginning because of the failure or hysteresis of the blow-off valve and increased probability of a vapour lock due to increased temperature[11]. Ethylene glycol was used as a coolant in aero engines between the two wars, after it had been suggested as a coolant for engines in the late 1930's[10]. Ethylene glycol water mixture was not in common use as a year round coolant until sealed cooling systems were employed.

Table II shows the specification of cooling systems of some popular cars from 1910.

Table II. Improvement of Cooling System of Some Automotive Engines.

Model of Car	Cooling system	Thermostat	Shutter on front of radiator	Production year	Remark
Ford Model 'T'	Ts. F.	No	No	1909-1928	
Austin	Ts.	No	No	1910	
Austin	Pu.	No	No	1914-1915	
Austin 20	Pu. F.	No	No	1921-1932	
Austin 7	Ts.	No	No	1923	
Cadillac	Pu. F.(1)	Bellows	No	1923-1924	Two pumps
Cadillac	Pu. F.(2)	No	au	1924-1939	
Austin 7	Ts. F.	No	No	1924-1938	
Rolls Royce Phantom	Pu. F.	No	ha	1925-1928	
Ford 14 & 24 HP.	Ts.Pu.F.(4)	No	No	1928-1934	
Rolls Royce (Phantom)	Pu. F.	No	au	1929-1939	
Austin 20	Pu. F.	Yes (3)	No	1932-1936	
Austin 10-4	Ts. F.	No	No	1932-1934	
Ford Model (Y)	Ts. F.	No	No	1933-1946	
Austin 10-4	Ts. F.	Yes (3)	No	1934-1936	
Ford Delux 4 cylinder	Ts. F.	No	No	1935-1937	
Austin 10-4	Ts. F.	Bellows	No	1936-1947	
Austin Big 7	Ts. F.	No	No	1937-1938	
Austin 20	Pu. F.	Bellows	No	1937	
Ford Prefect	Ts. F.(5)	No	No	1939-1957	
Austin 8	Ts. F.	No	No	1939-1952	
Ford Anglia	Ts.F.(6)	No	No	1945-1950	
" "	Ts.Pu.F.	No	No	1951-1956	
Ford Popular	Ts.F.	No	No	1953-1960	
Ford Prefect	Ts.Pu.F.P.	Bellows	No	1957-1960	Pressurized at 4 PSI
Ford Anglia	Ts.Pu.F.P.	"	No	1957-1963	Pressurized at 7 PSI
" "	Ts.Pu.F.P.	Wax	No	1963 →	"

Abbreviation

Ts. Thermosyphon system

Pu. pump circulating

Ts, Pu. Thermosyphon and an impeller assisted circulation

F. fan

P. pressurized system

au automatic

ha hand operated

Notes

(1) They used a condenser, in order to prevent the loss of the cooling water by evaporation. The operation of the condenser required an air tight seal at the radiator filler cup. This model was produced for only 2 years.

(2) Water pump installed with spring loaded packing, Fig. (11)

(3) The Smith R.R. thermostat with on-off knob.

(4) Centrifugal pump was installed at the front of the cylinder head, before water inlet to the radiator.

(5) Pump could be installed with it, as a supplementary, after 1954.

(6) In early Anglia model, pump could be fitted if heater was installed.

CHAPTER III

AUTOMOTIVE COOLING SYSTEMS

3.1 Different Varieties of Cooling Systems

Fig. 1 shows the basic design of automotive liquid cooled systems. In this system the fan moves ambient air over the engine and through the radiator. Most of the heat which has crossed from the cylinder into the surrounding metal, is eventually removed by a stream of cooling air which is passing through the radiator. Some is transferred to the coolant or oil which is cooled directly by the cooling air which has passed through the radiator.

The are two principal types of cooling systems for motor vehicles operating on the land. These two systems are direct and indirect air cooling. The amount of heat carried off by the cooling air depends upon the following items in air cooled engines:

1 - surface of the fins around cylinder

2 - the velocity of cooling air

3 - the temperature of the cooling air, cylinder and fins

Air cooled engines in the past have been noted for their higher oil consumption[32] due to some of the lubricating oil being burnt in the combustion chamber where temperature at the cylinder walls is high. This system is still undoubtedly noisier in action. The additional noise of air-cooled engine, apart from the valves and silencer, may be due to the fact that there is no outer jacket and water content to damp down the noise as with the water cooled types, so that the surface vibrations are of large amplitude, and the emitted sounds therefore greater. The fins are also less stiff than the outside of a water coolant cylinder jacket which cause more vibration.

There is dimension low in amount of heat produced by fuel and heat carried off by cylinder, i.e. more space will be needed for big cylinder for spacing the fins around engine. Because of higher thermal conductivity of water, the larger heat fluxes are collected in liquid

cooling system. For most average truck applications, liquid cooled engines are desired because the liquid gives more efficient heat transfer and more nearly uniform metal temperature.

In the case of water-cooled engines, it is necessary to dissipate the heat conducted through the cylinder walls by circulating the water past the cylinder walls and circulating the water through a cooling device, known as the radiator, There are three principal methods of circulating in present use

1 - natural convection, or thermo-syphon, Fig. (1)

2 - impeller-thermo-syphon, Fig. (12)

3 - Full pump circulation (Fig. 2)

There is also steam cooling which can reduce the weight of cooling system considerably.

In order to reduce the weight of cooling liquid carried and also that of the radiator, other liquids with higher boiling points such as ylene-glycol water mixture must be used. The boiling point can be increased by pressurization. Nowadays there are two common cooling systems

1 - pressurized cooling system

2 - sealed cooling system

In the pressurized system of cooling, which is widely used in American car engines and on most British ones, the cooling system radiator filler cap is fitted with two valves, namely a vacuum valve and a pressure valve as shown in Fig. (15).

Recently, sealed cooling systems have been introduced in engines; in principle, this is again a normal pressurised system fitted with an expansion and header tank. When the liquid coolant is heated its volume increases and this amount of volume goes to the closed header tank mounted at a well cooled point. When the engine cools, the volume of coolant decreases again and the radiator automatically refills from the header tanks.

Fig. (16) shows a sealed cooling system, so that the pressure through the system can be maintained at a constant level above atmospheric pressure.

Most of the new cars have a thermostat which controls the coolant temperature. It is obvious that at a definite mean temperature for the cooling water the engine works at its best efficiency. When an engine is started in the cold condition, it frequently takes an appreciable times before it attains its correct working temperature, as all of the water in the system has to be heated up. Thermostat can control the temperature of the jacket cooling water of engines. This is usually effected by cutting out the radiator when the engine is cold and by varying an opening in the outlet water pipe to the radiator according to the temperature of the engines. Typical values are 88 deg. C control temperature for a 118 deg. C. boiling point in a car engine of a commercial vehicle. There are two types of thermostat in common use: Bellows type, Fig. (14), and wax pellet element thermostat, Fig. (17). Some cars use a shutter control thermostat which controls the amount of air coming through radiators. The disadvantage of this system is the higher resistance between the body and air in cold weather.

3.2 The Circulating Pump in Relation to Cooling System Demand

The coolant pump circulates the coolant through the cooling system; coolant is pumped from the radiator into the cylinder block, past the cylinder head and back to the radiator. Pumps are often installed to discharge directly into the cylinder block when they have only a rudimentary volute or none at all. Because of economy and car design requirements the car manufacturers want to use a smaller radiator. The best way to get substantial gains in heat rejection per volume of radiator core is to increase the mean temperature difference between the coolant and cooling air. This can be done by raising the boiling point of the coolant, using increased pressure and/or a liquid with higher boiling point, such as, ethylene-glycol/water mixture. The performance is improved by about 14% when increasing the inlet coolant temperature by going from 1 to 1.5 bar radiator top tank operating pressure and 26% at 2 bar pressure.(33)

Heat rejection is increased at higher speeds and on gradients. Moore[14] found, when road speed increased from 50 km/hr to 128 km/hr the average metal temperature of an aluminium engine increased by about 20°C and 25°C in cast-iron engine. At constant speed but on a 1:10 positive gradient, the average metal temperature increased by about 20°C. He also showed that at higher speeds a substantially increased flowrate through the automotive circulating pump was required. When the car speed changes from 50 km/hr to 128 km/hr at ambient temperature (between 18 and 38°C ambient temperature), it is noticed that the flowrate doubled.[19]

The automotive water pump has certain different characteristics as compared with other centrifugal pumps. Ideally the head/flow curve should be rather flat to avoid excessive pressure on the block and hoses when the thermostat is shut, yet give an adequate flowrate when it opens. The head/speed curve should also be rather flat to avoid excessive pressures when the engine speed is high and still give an adequate flow when moving slowly in traffic.

When the vehicle is climbing a steep hill, the road speed is reduced, in this case the quantity of heat conveyed from the engine to the radiator is more than that carried away by the air, so the temperature of the cooling liquid rises to boiling point. There is also gear change problem with highly rated engines i.e. between two gears with slow engine speed the temperature of cylinder is high but there is not enough flow circulating around the cylinder (water pump is linearly dependent on the speed of engine). There is a space limit for installing cooling equipment on account of styling, such as - radiator, circulating pump, fan, pipes and housing which connect the radiator to the circulating pump, and cylinder block to the radiator in modern passenger cars. Circulating pumps may then be positioned to suit space criteria with a belt driven or may be mechanically coupled to the engines. The ratio of the pump to the crackshaft speed is generally around (1 - 1.5)[15], so that the flow rate of coolant is related to the engine speed rather than coolant temperature, i.e. heat release rate. An electrical driven pump is feasible but does not appear economically viable, though electrically driven fans are in use in some passenger cars. Typical flowrates for modern vehicles without auxilaries such as

air conditioning, are 2.7 lit/min KW[15] and 1.5 - 2 litre/min. KW for naturally aspirated diesel engines.[16]

3.3 Coolant Liquids and Inhibitors

Over the years many coolants have been tried in automotive engines, but water has been used in automotive engines since the beginning of the industry.

Water has the best combination of availability, high specific heat, low viscosity, non toxic and low price required for a car engine coolant. But water has some disadvantages which are shown below:

1) the water freezing point is higher than the lowest ambient temperature in some locations

2) it is corrosive to all metals used for components in car cooling systems (like cast iron, aluminium, brass, etc.)

3) water expands upon freezing

4) rather low boiling point.

Many liquids have been added to water to reduce its freezing point; these liquids include sugar, glycerine, methanol, ethanol, isopropanol, ethylene glycol (ethanedial), calcium chloride, magnesium chloride.[17]

Of all additives used to decrease the water freezing point, only two of them are in common use today, methanol and ethylene glycol. Ethylene glycol is increasing in use and methanol is decreasing, because methanol has a boiling point of 65°C which is below the desired minimum engine coolant operating temperature of 82°C, but it produces the bigger freezing point depression compared with other liquids.

Water as used in car cooling systems is natural water and it is likely to contain calcium, magnesium and sodium as cations: chloride, sulphate and bicarbonate as anions, with lower concentrations of nitrate, phosphate and silica, some of them make the water more corrosive, so corrosion inhibitors must be added to water. In emergency cases where hard water is used as a coolant it can reduce the heat transfer between

the cylinder and coolant considerably by forming a layer between the cylinder and coolant. This sort of water was often used in Army vehicles

Physical properties of ethylene-glycol $(CH_2OH)_2$ have been published [18] (see Appendix VI) and they show that glycol begins decomposing even below its boiling point.[19] The mechanism of thermal decomposition of glycol is oxidation; this produces various acids, the main one being formic acid. Thermal decomposition is catalysed by the presence of acids and possibly copper ions in the solution.[20]

The amount of ethylene-glycol vapour in voids in the ethylene-glycol/water liquid mixture is very low compared with water vapour. For example, the mole fraction of glycol in the vapour from 50% by weight ethylene-glycol/water mixture is about 0.2%[21] (1.2% by weight) at saturation point. The vapour fraction of ethylene-glycol does not change much with pressure when the glycol concentration is less than 60% by weight at least for pressures higher than 0.6 bar absolute at saturation. However, it reduces to between 0.2 to 0.3% by weight when the pressure in the system is reduced to 0.3 bar absolute in the mixture.[21]

Because of the corrosiveness of water and the decomposition of ethylene-glycol, it is customary to add corrosion inhibitors to the ethylene-glycol/water mixture. For these reasons commercially available brands of ethylene-glycol (antifreeze) generally contain corrosion inhibitors which are basically standardized.[22] Corrosion in car cooling systems is a complex action and formulating corrosion inhibitors and antifreeze compound is difficult work. These inhibitors must be sufficient for a wide range of temperatures from ambient to boiling point of the coolant under pressure and must operate for a considerable time. The inhibitors must also cope with combustion gases which acidify the coolant, and as far as possible they must reduce the corrosion rate in all materials found in engines. Also they have to effectively prevent acid build-up due to thermal decomposition, and the formation of copper ions in the mixture which catalyse the thermal decomposition.[23] When choosing a proper inhibitor, the heat transfer between a metal surface and a coolant must be mentioned. The deposition of corrosion products

and scale in the cylinder head can seriously affect heat trasnfer processes which may cause the metal to crack.[23] Recently there was an attempt to use soluble oil as an inhibitor (railways and military vehicles) which gave good results in many cases,[24,25] except in one case where damage was mentioned in hose connection and seals.[26]

Figs. (18,19,20) show the effect of antifreeze with different type of inhibitors on different types of materials. It is easy to see that the inhibited coolant (B) is more adequate than coolant 'A' for service under high temperature. Coolant (C) could be said to be equivalent to coolant (B) at high temperature, except for higher solder corrosivity.[27]

3.4 Choice of Coolant Temperature and Pressure Level.

Experience has shown that the hotter engines can work with fewer problems [redacted]. In warm engines the thermal efficiency is higher and also because of that the petrol consumption is reduced and the power output is greater than cold engines. For normal running, the temperature of coolant at the top of radiator should lie between 75°C and 85°C. This allows a sufficient margin for temperature increase when climbing long hills on lower gears.

By considering that engine horse power has been increased in recent years because of high speed requirement, also in some cases air conditioning has been used, both effects produce a bigger heat loss. So a bigger radiator must be designed for them. The best way to get substantial gains in heat rejection per volume of radiator core is to increase the mean temperature difference between the coolant and cooling air. This can be done by increasing the boiling point of the coolant by increasing the pressure level of a cooling system or by using a liquid with higher boiling point. Some manufacturers use ethylene glycol water mixture as a whole year coolant in a sealed pressurized cooling system.

A low coolant temperature increases temperature stresses in the cylinder block and increases the size of radiator because of low temperature difference between coolant and air compared with high coolant temperature.

Pressure level at the top tank is usually between 0.28 - 0.48 bar (4 - 7 PSI), although on some American cars it is as high as 1.03 bar (15 PSI). Pressurized cooling system affords a good protection when running at high altitude and tropical conditions; also for long hard driving periods.

3.5 Flow Rate in Coolant System

A considerable proportion of the heat of combustion of the fuel is lost so far as useful work on power is concerned, and only relatively small proportion is available for useful power purposes. Exhaust gases carry most of the heat which is produced by combustion of the fuel. Next in importance are the losses of heat to the combustion chamber, cylinder walls and piston. Friction losses radiation and the heating of the lubricating oil are minor losses in engine. Fig. (21) shows the percentage of total heat which is carried off by exhaust gas, useful power, coolant and friction losses[28]. It can be seen that for passenger cars with compression ratio of 10, 23% of heat must be carried off by cooling system. This percentage increases as compression ratio reduces.

We can write that the heat dissipated by an engine is equal[29] to:

$$q_t = q_g + \frac{P_m}{J} = q_1 + q_2 + q_3 \qquad 3\text{-}1$$

where q_t = total heat dissipated per unit time
q_g = heat from the gases
P_m = power lost in mechanical friction including the power lost in water pump and oil pump
q_1 = heat to the coolant radiator
q_2 = heat to the oil radiators (if any)
q_3 = heat escaping directly from the engine including radiation and heat lost in the exhaust gases

In general most small gasoline engines have no oil radiator so the heat to the oil radiator is zero and the oil is cooled partly by the jacket water and partly by direct loss from the engine, thus the amounts of q_1 and q_3 are increased.

The internal combustion engine of a modern day automobile has a max. thermal efficiency of about 30%[30]. Thus about 60% of the heat of combustion of the fuel must be dissipated either by the exhaust gases or through the cooling system. The cooling system of a modern engine is expected to dissipate more than half of the waste heat of the engine cycle, or to put it another way the cooling system must dissipate approximately 20-40 percent of the energy in the fuel supplied to an engine, dependent on the comparative ratio of the engine. So we can approximately write

$$q_t = k_1 \bar{w} W \bar{c}$$

where $\bar{w}$ = fuel consumption kg/kw, W is engine power output kw

$\bar{c}$ = calorific value of petrol Joules/kg

k_1 and k_2 are dimensionless and roughly constants

$$q_1 = k_2 q_t = k \bar{w} W \bar{c} \quad \text{where } k = k_1 k_2 \qquad 3.2$$

$$q_1 = G_w \, Cp(T_o - T_i) \qquad 3.3$$

where G_w = mass flow rate of coolant kg/hr

Cp = specific heat at constant pressure Joules/kg^{o}C

T_o = outlet coolant temperature from the engine

T_i = inlet coolant temperature to the cylinder block

From equation (No. 3-1 and 3-2) (above) we can find the flow rate of coolant system for a known engine, since k is found experimentally to be 0.3 - 0.4.

3.6 Radiator

At the radiator, heat is transferred via a two stage process, first from the coolant to the radiator metal and then from the metal to the ambient air.

Tubes and tank which contact the coolant are usually made of brass. The secondary surface, fins or spacers are generally made of thin copper strips. Tube thickness varies from 0.114 mm to 3.05 mm and fins are made of 0.076 - 0.127 mm[31], the smaller thickness is predominant because

of cost, greater thicknesses are used where strength requirement demands it (commercial vehicles).

Heat flow from the radiator to the air is equal[29]

$$q = A_r K_r G_a^n L^{n-1} (T_r - T_a) \qquad 3\text{-}4$$

where q = engine jacket loss

A_r = radiator surface area

G = mass flow of air per unit time divided by the cross sectional of flow area (air)

L = typical length of the core section (airside)

T_r = average temperature of the radiator surface, equal to the mean water temperature, since the tubes are thin and have a high conductivity

T_a = Ambient air temperature

K_r = coefficient depending on core design and viscosity and thermal conductivity of air

To obtain the dimensions of K_r we write:

$$K_r = \frac{q}{A_r G_a^n L^{n-1} (T_r - T_a)} \qquad 3\text{-}5$$

when we put the dimensions of physical quantities of each symbol in the equation No. 3-2 we have

$$D_{K_r} = \frac{HT^{-1}}{L^2 (\frac{M}{L^2 T})^n \times L^{n-1} \theta} = \frac{HT^{-1} T^n}{M^n L^{1-n} \theta}$$

$$D_{K_r} = \frac{H L^{-1} T^{-1} \theta^{-1}}{M^n L^{-n} T^{-n}} =$$

the dimension of thermal conductivity is

$D_K = HL^{-1}T^{-1}\theta^{-1}$ and the dimension of viscosity is

$D_\mu = ML^{-1}T^{-1}$.. So the dimension of K_r is equal to

$$D_{K_r} = \frac{k}{\mu^n} \qquad 3\text{-}6$$

Radiators are formed by an assembly of sheets or tubes, called a core, which contains many similar passages for air flow, the walls of which also form the passages to carry the coolant.

Selection of an approximate core design fixes the value of K_r, L and n; since n for radiators usually lies between 0.7 and 0.8, increasing the value T_r will reduce $A_r G^n$, this is the reason that pressurized radiator or high-boiling-point liquids are used when it is important to decrease the radiator capacity.

Core heat transfer being directly proportional to the temperature difference between coolant and air, a pressurized system permits the use of less core, for example, a core might require 2.1 mm pitch (12 fins per inch) with an atmospheric pressure but might only need 2.82 mm pitch (9 fins per inch) with a 0.28 bar (4 PSIG) pressure cap value.

CHAPTER IV

CAVITATION.

4.1 Cavitation Inception

Cavitation is the result of a reduction of the local pressure in a disturbed or flowing liquid to a level at, or near to, its vapour pressure. If the liquid contains much dissolved gas, then as the pressure is reduced the gas comes out of solution and forms cavities in which the pressure will be greater than the vapour pressure of the liquid. Even if there are no visible gas bubbles, the presence of submicroscopic gas bubbles may provide nuclei which cause cavitation at pressures above the vapour pressure. Tiny bubbles filled with gas or vapour appear and grow rapidly. Then as they move along the liquid to a point where the local pressure is high enough - or, in a stationary liquid, when the pressure intensity is raised - the bubbles collapse, the entire cycle taking perhaps within a few milliseconds or less. Bubbles may follow each other so rapidly that they appear to the eye to form a single continuous cavity.

If no nuclei are present, the liquid may actually stand negative pressures or tensions without undergoing cavitation. Theories have been produced to show that liquid should be able to withstand tensions equivalent to thousands of bars. For example, estimation shows that water will withstand a tension ranging from 300 to 10,000 bars[34]. Practically, with extremely careful filtration of the liquid and with pre-pressurisation of several hundred bars, it has ruptured at tensions of 300 bars. According to Plesset[35] water without nuclei theoretically will withstand tensions of about 15,000 bars.

Physically, cavitation gives rise to a number of other phenomena. During the final collapse phase, it has been found that a very weak emission of light may come from the bubble. The cause of this sonoluminescence is not known, but one idea is that the flash is due to the recombination of free ions produced by thermal or mechanical dissociation of molecules on the bubble surface. The flash may last for a period between one twentieth and one thousandth of a second[36]. In 1960

Jarman[34] and co-worker put forward strong evidence to indicate that sonoluminescence is due to the incandescence of the gas in the bubble resulting from the high pressures and temperatures during collapse. The intensity of the light is dependent on the gas present; there will be no light if there is no gas in the bubble.

When the cavities collapse, high pressures and temperatures are generally thought to occur; surrounding fluid temperature as high as 10,000°K have been suggested while Wheeler[38] has concluded from his experiments that temperature rises to 500 to 800°C can occur in the material at the centre of an implosion. As ultra high speed cine films have shown the collapse is completed in a period of milli or even micro seconds. Harrison[39] showed that the resulting shock waves radiated through the liquid adjacent to the bubble may have a pressure difference as high as 4,000 bars.

The exact events in the inception and development of cavitation depend on the condition of the liquid, including the presence of solid particles or of gas bubbles, and on the pressure field in the zone of cavitation. The pressure field is largely dependent on the geometry of the solid boundary, but the nature of solid boundaries may be important in itself.

4.2 Significant Dimensionless Groups

Cavitation flows are commonly described by the cavitation number σ:

$$\sigma = \frac{p_\infty - p_V}{\frac{1}{2}\rho U_\infty^2} \qquad 4\text{-}1$$

The limit of cavitation for a particular boundary geometry has been determined experimentally by holding the velocity constant, establishing cavitation and then increasing the pressure until the cavitation disappears at the desinence pressure, $p_{\infty d}$. This state is referred to as desinent cavitation. Thus the desinent cavitation number, σ_d is defined as

$$\sigma_d = \frac{p_{\infty d} - p_V}{\frac{1}{2}\rho U_\infty^2} \qquad 4\text{-}2$$

For incipient cavitation there will correspond a particular value of p called the "inception pressure" $p_{\infty i}$. Thus the incipient cavitation number, σ_i, is defined as

$$\sigma_i = \frac{p_{\infty i} - p_V}{\frac{1}{2}\rho U_\infty^2} \qquad 4\text{-}3$$

Incipient cavitation and desinent cavitation are only identical when $p_{\infty i} = p_{\infty d}$. The cavitation is more developed as $p_{\infty i}$ drops below $p_{\infty d}$. The difference between $p_{\infty d}$ and $p_{\infty i}$ is often called "cavitation hysteresis". In terms of the cavitation number, incipient and desinent cavitation are related by the expression

$$\sigma_d \geq \sigma_i$$

Thus, for a given flow condition, σ_d appears to be the upper limit for σ_i. Furthermore, incipient cavitation is random in nature whereas desinent cavitation is repeatable.

Let us consider a body which is operating in the state of desinent cavitation. We assume that this state may be characterised by a single bubble which is in a stationary position and thus we are ignoring all dynamic effects due to translation of bubble.

At equilibrium the pressure on the bubble must be balanced. Thus[40]

$$p_i = p + \frac{2S_b}{\bar{R}} \qquad 4\text{-}4$$

where $\bar{R}$ is bubble radius
S_b is the surface tension
p is the local liquid pressure
p_i is the internal pressure of the bubble

The internal pressure can also be written in the form:

$$p_i = p_V - \Delta p_V + p_G \qquad 4\text{-}5$$

where p_V is the vapour pressure at the bulk temperature of the fluid
Δp_V is the reduction in vapour pressure due to local cooling

due to the temperature drop of the liquid resulting from the vaporization.

p_G is the pressure exerted by the non-condensable gases.

The liquid pressure can also be written in the form:

$$p = \bar{p} - p_{TR} \qquad 4\text{-}6$$

where $\bar{p}$ is the mean value of the liquid pressure adjacent to the bubble

p_{TR} is the reduction in the liquid pressure due to turbulence and surface roughness.

Substituting equations (4-6) and (4-5) into (4-4) we have

$$- p_V = - \bar{p} + p_G + p_{TR} - \frac{2S_b}{R} - \Delta p_V \qquad 4\text{-}7$$

If we put equation (4-7) in equation (4-2) we can write

$$\sigma_d = \bar{C}_p + \frac{p_G}{\frac{1}{2}\rho U_\infty^2} + \frac{p_{TR}}{\frac{1}{2}\rho U_\infty^2} - \frac{2S_b/\bar{R}}{\frac{1}{2}\rho U_\infty^2} - \frac{\Delta p_V}{\frac{1}{2}\rho U_\infty^2} \qquad 4\text{-}8$$

where $\bar{C}_p$, a pressure coefficient at the location of the characteristic bubble, is defined as

$$\bar{C}_p = \frac{p_\infty - \bar{p}}{\frac{1}{2}\rho U_\infty^2} \qquad 4\text{-}9$$

Equations like (4-8) have been derived by several authors[41,42,43,44]. It is seen that high gas contents, turbulence and surface roughness tend to increase σ_d whereas surface tension and heat transfer have the opposite effect.

The pressure coefficient ($\bar{C}_p$) is a function of Reynolds Number and may increase or decrease depending on boundary-flow conditions. For immersed bodies, $\bar{C}_p$ is known to become nearly constant at sufficiently high Reynolds Number[42]. At high Reynolds number the effect of turbulence and surface roughness ($\frac{p_{TR}}{\frac{1}{2}\rho U_\infty^2}$) is becoming negligible.

The cavitation parameter, σ, is a very useful measure for many different aspects of the cavitation phenomenon. For example, in centrifugal pumps, the normal location at which cavitation first appears when the machine is operated under unfavourable conditions is along the inlet edges of the impeller vanes and on the adjacent shrouds. However, it is rather difficult to determine the local pressures and velocities at these points, so that it is much easier to calculate the cavitation parameter for, say, the flow at the inlet flange to the pump. The value of σ at which cavitation inception occurs somewhere in the pump is designated as σ_i.

Another useful cavitation parameter is σ_{th} which is now commonly known as the Thoma sigma. It is a very useful parameter in turbo-machinery equipment. For general use with pumps or turbines σ_{th} is equal to

$$\sigma_{th} = \frac{NPSE}{Y} \qquad 4\text{-}10$$

where NPSE is net positive suction energy and

Y is the total specific energy equal to $\frac{p_P}{\rho}$ where

p_P is the total pressure rise by pump.

It is possible to write for net positive suction energy

$$NPSE = \frac{1}{\rho}\left(\pm p_S - p_L + p_A - p_V\right) \qquad 4\text{-}11$$

where p_S = static suction (+) or lift (-)

p_L = suction line losses (friction, entrance and fitting)

p_A = absolute pressure at the liquid free surface

p_V = vapour pressure of liquid at pumping temperature

Another useful parameter is suction specific speed

$$S = \frac{N\sqrt{Q}}{(NPSH)^{\frac{3}{4}}} \qquad 4\text{-}12$$

where N is rotation per sec.

This has different values according to the units. It is preferable

therefore to use the non dimensional form of suction specific speed

$$S_{sf} = \frac{\omega \sqrt{Q}}{(NPSE)^{\frac{3}{4}}} \qquad 4\text{-}13$$

where ω is rad/sec and Q is m^3/sec and NPSE is in J/Kg.

This parameter is widely used for pumping machinery. It should be noted that σ_{th} and S_{sf} vary in the opposite direction as the severity of the cavitation condition changes; that is, as the tendency to cavitate increases, σ_{th} decreases, but S_{sf} increases. One can find the relation between S_{sf}, σ_{th} and n_{sf} where n_{sf} is shape number

$$n_{sf} = \frac{\omega \sqrt{Q}}{(Y)^{\frac{3}{4}}} \qquad 4\text{-}14$$

The following interrelation between S_{sf}, n_{sf}, σ_{th} is obtained from Equations (4-10), (4-13) and (4-14).

$$\frac{n_{sf}}{S_{sf}} = (\sigma_{th})^{\frac{3}{4}}$$

$$\left(\frac{n_{sf}}{S_{sf}}\right)^{4/3} = \sigma_{th} \qquad 4\text{-}15$$

The cavitation characteristic is often presented as in Fig. (22) for a constant speed and flow (possibly at the best efficiency point), specific energy or head or efficiency is plotted against NPSE(NPSH) or σ_{th}. The figure shows the typical wide difference in NPSE between inception and performance breakdown. It can be seen that the inception of cavitation does not necessarily cause a reduction in pump head or efficiency, since a rise in head prior to the final breakdown has frequently been observed. This slight rise in head is usually explained by a reduction in the skin friction following the formation of a thin layer of vapour at the surface of the impeller vanes. This explanation is in agreement with the fact that the rise in performance is most frequently observed under conditions tending towards instabilities, such as the stalling of propeller vanes or airfoils. Under such conditions, a reduction in the skin friction obviously would have the most

pronounced influence since such instabilities are controlled by the skin friction[45]. The increased head during the early stages of cavitation development is similar to the increased lift found for the sharp edged, thin profiles of Numachi[46,47], which he tested singly and in decelerating cascades. It has been suggested that if impeller vanes had had a shape equivalent to that of Numachi's NAS.10168 profile, the increase in head might have been even greater[46].

As opposed to running with cavitation just above the 'breakdown' point, a much larger and more expensive pump is necessary to satisfy the condition of no cavitation, and for this reason it is rarely done in commercial practice. However, the disadvantage of running with cavitation is the risk of erosion damage .

4.3 Air Content Effect

In order to clearly bring out the problem for consideration it is necessary to distinguish between two broad categories of cavitation. Vaporous cavitation is the sudden expansion and the collapse of a vapour bubble due to vaporization of the liquid at the bubble wall whereas gaseous cavitation is the relatively slow expansion of a gas bubble due to diffusion. When a desinent cavitation test was carried out, it was found that as the vaporous cavitation disappeared, a few isolated bubbles persisted to much higher pressures[43]. It was hypothesized that these stationary 'spots of cavitation' were in fact gaseous cavitation. With this as the predominant phenomenon, Equation (4-8) reduces to[43]

$$\sigma_d = \bar{C}_p + \frac{p_G}{\frac{1}{2}\rho U_\infty^2} \qquad 4\text{-}16$$

From Equation (4-16) one can find the difference between the desinent cavitation number (for the gaseous cavitation) and that for the vaporous cavitation is directly proportional to the p_G and inversely proportional to the square of velocity. If the bubble becomes saturated with air,

$$p_G = \bar{\alpha}\beta \qquad 4\text{-}17$$

where $\bar{\alpha}$ is the dissolved air content and β is the Henry's Law constant[41].

Therefore the difference between σ_d for gaseous and vaporous cavitation is directly proportional to the dissolved air content.

Equation (4-16) shows that cavitation number is dependent on air content. Figure (23) shows the effect of air content on cavitation number at inception point, before breakdown and at breakdown[48].

4.4 Thermodynamic Effects

The cavitation characteristics of most centrifugal pumps operating on cold water are either known from actual tests or can be established fairly closely from the available information on similar pumps. The NPSE of pumps handling liquid other than cold water are usually estimated (often with a considerable discrepancy) by considering the performance of the same pump on a water test. It has been found experimentally that for liquids other than water, NPSE can be reduced below or increased above their values for cold water, when the density of the liquid is more than that of cold water, e.g. glycol, glycerine, etc. Stepanoff[49] presented experimental results on a pump handling water up to 150°C and demonstrated that less NPSE was required at the higher temperature. Figure (24) shows that the cavitation performance of pumps in water at high temperature is better than cold water. Stepanoff also proposed that thermodynamic effects limit the flashing of water into steam caused by a given pressure drop below the initial vapour pressure. The limitation, arising from heat transfer constraints in the vicinity of the bubble, he called 'dynamic depression' and he suggested that the volume of the vapour thus formed decreases as the temperature increases. The thermal cavitation parameter, B, which is presented by Stepanoff and Stahl[50] for inception point can be expressed as:

$$B = \frac{V_g}{V_f} \qquad 4\text{-}18$$

where V_g is volume of vapour per unit mass of mixture if the pressure and temperature are given time to reach equilibrium and V_f is volume of the liquid at the same condition. Approximately one can roughly write

$$B = \frac{v_g \Delta h_f}{v_f h_{fg}} \qquad 4\text{-}19$$

where v_g is the specific volume of the vapour
v_f is the specific volume of the liquid
h_{fg} is latent heat of vaporization J/Kg
Δh_f is an increment of liquid enthalpy corresponding to the energy reduction ΔNPSE (J/Kg) below the saturation conditions

Since equilibrium conditions are not realised during liquid passage through the low pressure zones, the ratio $\frac{V_g}{V_f} = B$ does not represent the vapour/liquid ratio by volume for the whole flow and B is used merely as an index of the 'tendency' of the liquid to boil or its 'readiness' to flash into vapour. Thus it is indicative of the 'rate of vaporization' of the liquid under cavitation conditions producing the measurable effect of $\frac{\Delta Y}{Y}$.

By simple algebraic manipulation and the Clausius-Clapeyron Equation (4-19) is transformed to:

$$B = \frac{\Delta NPSE}{h_{fg}^2} \times C_p T \left[\frac{v_g}{v_f}\right]^2 \qquad 4\text{-}20$$

where C_p is specific heat of liquid Joules/Kg deg K
T is temperature of liquid ^{o}Kelvin

or

$$B_1 = \frac{g B}{\Delta NPSE} = \frac{B}{\Delta NPSH} = \frac{C_p T}{h_{fg}^2} \left[\frac{v_g}{v_f}\right]^2 \qquad 4\text{-}21$$

For liquid other than cold water we can write

$$(NPSE)_{liquid} = (NPSE)_{water} \pm |\Delta NPSE| \qquad 4\text{-}22$$

Equation (4-22) with minus sign is presented elsewhere[49,50,51,52] the present author added the plus sign for liquids in which the density and viscosity are greater than water. One can write

$$(\sigma_{th})_{liquid} = (\sigma_{th})_{water} \pm \left| \frac{\Delta NPSE}{Y} \right| \qquad 4\text{-}23$$

The determination of ΔNPSE is important for knowing the cavitation behaviour for liquids other than water.

Spraker[51] suggested that depression in net positive suction energy is a function of inverse of thermal cavitation parameter.

$$\frac{\Delta NPSE}{g} = f\left(\frac{1}{B}\right) \qquad 4\text{-}24$$

where the cold water cavitation characteristics are used as a reference.

Ward and Sutton[52] suggested that in absence of information one can approximately use

$$\frac{V_g}{V_f} = 0.244 \qquad \text{(SI unit)} \qquad 4\text{-}25$$

Equations 4-25 and 4-21 can give us an approximate indication of the reduction in NPSE below that of cold water.

Dimensional analysis was applied for finding a relation between fluid properties and cooling effect[44] due to vaporization. He found that

$$\frac{\Delta p_v}{\rho_L U_\infty^2} = Re^{0.55} \times P_r^{-1.03} \left(\frac{h_{fg}}{T.C_p}\right)^{3.3} Str^{-4.8} \qquad 4\text{-}26$$

where $Re = \dfrac{U_\infty \rho \Delta X}{\mu}$ Reynolds number

$P_r = \dfrac{C_p \mu}{k}$ Prandtl number

$Str = \dfrac{t.U_\infty}{\Delta X}$ Strouhal number

t time

ΔX cavity length

Equation 4-26 tends to underestimate the cooling effect compared

with the experimental data. Spraker[51] showed that Stepanoff's factor (B) can be applied to a first degree of approximation and Furness[44] showed that the use of B overestimated thermodynamic effects. Chivers[53] solution based on Lord Rayleigh's bubble growth theory shows quite remarkable agreement with the experimental data obtained from his own pump, operating in water at different temperatures. His solution is not applicable to different fluids but only the same fluid at different temperature [54].

The cavity pressure depression which is caused by the decrease of vapour pressure in the cavitating region due to evaporation of the liquid layer adjacent to the bubble, was calculated by Ruggeri and Moore.[55,56,57,58] Their calculation based on theoretical and experimental consideration. The assumptions which were involved were

1 - Steady flow

2 - negligible net work and heat transfer during the vaporization (flashing) process.

3 - negligible surface tension

4 - negligible body forces

5 - no liquid tension

6 - fluid in thermodynamically stable equilibrium throughout the process

A good agreement was obtained in comparison between experimental and predicted results. The cavity pressure depression which was calculated by Ruggeri equal to

$$\Delta E_v = g\Delta h_v = \left(\frac{\rho_g}{\rho_f}\right)^2 \left(\frac{h_{gf}}{C_p T}\right)^2 \left(\frac{V_g}{V_f}\right) \qquad 4\text{-}27$$

where Δh_v decrease in vapour pressure due to vaporization, metre of liquid

$\Delta E_v = g\Delta h_v$ decrease in vapour energy J/kg

ρ_g saturated vapour density kg/m^3

ρ_f " liquid " kg/m^3

C_p specific heat of liquid J/(kg)(K)

Vapour liquid volume ratio $\frac{V_g}{V_f}$ is not possible to measure directly and thus the value of this ratio can be used only in a relative sense. Their calculation shows that in a venturi[58].

$$\left(\frac{V_g}{V_f}\right)_{Pred} = \left(\frac{V_g}{V_f}\right)_{Ref} \left(\frac{\alpha_{ref}}{\alpha}\right)\left(\frac{U_1}{U_{1_{ref}}}\right)^{0.8} \left(\frac{\bar{D}}{D_{ref}}\right)^{0.2} \frac{\left(\frac{\Delta x}{D}\right)^{0.3}}{\left(\frac{\Delta x}{D}\right)_{ref}} \qquad 4\text{-}28$$

$$\frac{(NPSE)_{ref} + (\Delta E_v)_{ref}}{(NPSE)_{Pred} + (\Delta E_v)_{Pred}} = \left(\frac{U_{1_{ref}}}{U_1}\right)^2 \qquad 4\text{-}29$$

where α is thermal diffusivity $\alpha = \frac{k}{C_p \rho_f}$ m^2/sec

k " " conductivity of saturated liquid J/(m)(sec) (K)

U_1 mean axial inlet velocity m/sec

$\bar{D}$ characteristic body dimension m

Δx length of cavitated region m

With flow similarity, the fluid velocity at the pump inlet is proportional to pump rotational speed. Also for a pump working at a constant flow coefficient and a constant value of ψ/ψ_{NC}, Δx of equation (4-28) was considered constant for various liquids, liquid temperature, and pump rotative speeds. Thus one can write

$$\frac{(NPSE)_{ref} + (\Delta E_v)_{ref}}{(NPSE)_{Pred} + (\Delta E_v)_{Pred}} = \left(\frac{N_{ref}}{N}\right)^2 \qquad 4\text{-}30$$

$$\left(\frac{V_g}{V_f}\right)_{Pred} = \left(\frac{V_g}{V_f}\right)_{ref} \left(\frac{\alpha_{ref}}{\alpha}\right)\left(\frac{N}{N_{ref}}\right)^{0.8} \qquad 4\text{-}31$$

For an estimation of ΔE_v $(g\Delta h_v)$, there is a need to have two sets of experimental data at the same ψ/ψ_{NC} and constant Φ (flow coefficient). Tests need not be for the same liquid or the same rotative speeds, but they have to be for pumps with similar geometry. Good examples were presented in Ref. (58). Their calculation was applicable only when there is no permanent gas present.

Experiments with mercury showed that for all gas contents, the cavitation number reaches a maximum for an intermediate temperature and then decreases substantially[59]. This effect is most pronounced for the lower gas content.

4.5 Cavitation Behaviour of Mixtures with Particular Emphasis on E.G/W Mixture

For a mixture of two or more liquids, Stepanoff[60] suggested that one can assume that each component contributes a fraction of its individual NPSE equal to its weight fraction in the mixture. Spraker[51] found that hydrocarbon mixtures have an additional decrement in NPSE over that for pure fluids having the same thermal cavitation parameter (B), and this additional decrement is temperature dependent. Therefore Spraker hypothesized that

$$\Delta NPSE_{mix} = \Delta NPSE_{pure} + \delta NPSE \qquad 4\text{-}32$$

$$\delta NPSE = f(T) \qquad 4\text{-}33$$

The relations found by Spraker between δNPSE and temperature should be applicable to petroleum-based hydrocarbon mixtures over the temperature range tested. Other types of mixtures such as water/glycol might be expected to exhibit a similar relationship, but not necessarily identical. Ethylene-glycol itself has a better cavitation behaviour than water[61], and its incipient cavitation number at constant temperature and velocity is lower, i.e. it is less likely to cavitate[61]. This is maybe because of the higher viscosity of ethylene-glycol $(CH_2OH)_2$ which generates a lower bubble collapse speed than water near the solid surface. Plesset[62] shows that as one goes from pure water to pure glycerol $(C_3H_5(OH)_3)$ through mixtures in various proportions there is a minimum damage rate at about 25% water and 75% glycerol. The damage rate in pure glycerol reaches only about 50% of the rate observed in pure water. At temperatures lower than 80°C glycol has a better cavitation behaviour than water, but when the temperature rises, water has a better behaviour,[63] and in 20% water-glycol mixture: weight loss of specimens is more like water than the proportional weight fraction of the mixture. The same weight loss at the same temperature of the specimen in water and 20% water glycol mixture can be

foreseen and accounted for as there is almost no glycol vapour present in the vapour present in the vapour mixture.

The calculated value based on equation 4-27 for cavity pressure depression for 54/46% of E.G/W shows that Δh_v values at 102°C are about half of those of water, Fig. (25) which shows that the cooling effect in E.G/W is not as important as for water. Fig. (26) shows the variation of thermal cavitation parameter B as a function of temperature (calculated from empirical equations) for water, ethylene-glycol and 54/46 E.G/W and also methanol. It shows that thermal cavitation parameter of the E.G/W mixtures is more like that of water.

The cooling effect becomes complex when one uses a mixture of fluids. The cooling effect can be explained by considering that as a cavity grows, the latent heat of vaporization must be supplied by the liquid adjacent to the cavity boundary which means temperatures near the bubble are less than in the bulk of the fluid. This local temperature drop may be related to the local pressure drop by assuming the change to be slow enough to apply the equilibrium equation of state. The temperature difference adjacent to the bubble surface causes a thermal gradient in the liquid between the surface of the bubble and fluid far from the bubble.

Thermal diffusion effects are treated quantitatively for gases by the kinetic theory and only qualitatively for liquids by the cage model. The cage model considers that each molecule in the liquid is retained temporarily in an equilibrium position by the potential field of the surrounding molecules.[64] Now, because of random motion of liquid molecules,[65] this lets us assume an average kinetic energy for each molecule. (There are molecules with much greater and smaller kinetic energy in the liquid). Therefore the heavier molecules have higher momentum.

The thermal gradient causes an imbalance in the system, i.e. a migration of some molecules from the higher temperature region to the lower temperature region tending to restore the equilibrium. The heavier and larger molecules, because of their higher momentum, are

able to force their way to the cold region and concentrate in that region, i.e. near the expanding bubble surface.

It is possible to calculate the migration of molecules when there is a thermal gradient in the system for the E.G/W mixture. The flux J_1 of component 1 (the component of lower molecular weight in a binary solution) can be expressed in terms of the thermal diffusion constant[64]

$$\vec{J}_1 = - D_{12} \left[\overrightarrow{\text{grad}}\ X_1 - D_T X_1 X_2 \frac{1}{T} \overrightarrow{\text{grad}}\ T \right] \qquad 4\text{-}34$$

where D_T thermal diffusion constant
J_1 flux of component 1 m/sec
D_{12} diffusion coefficient
X_i mole fraction of component i
T absolute temperature (mean)

If x is space coordinate in direction of flux

$$J_1 = - D_{12} \left[\frac{dX_1}{dx} - D_T X_1 X_2 \frac{1}{T} \frac{dT}{dx} \right] \qquad 4\text{-}35$$

So one can write the flux due to thermal diffusion is equal to

$$J_{TD_1} = D_T X_1 X_2 D_{12} \times \frac{1}{T} \frac{dT}{dx} \qquad 4\text{-}36$$

The value for the thermal diffusion constant can be calculated at the steady state[67] when $\vec{J}_1 = 0$

$$\frac{1}{X_1 X_2} \frac{dX_1}{dx} = D_T \frac{1}{T} \times \frac{dT}{dx} \qquad 4\text{-}37$$

By considering the net heat transport at steady state, it is possible to calculate the thermal diffusion constant[66]

$$D_T = \frac{M_2 V_1 + M_1 V_2}{2RT(M_1 X_1 + M_2 X_2)} \left[\frac{\Delta U_2}{V_2} - \frac{\Delta U_1}{V_1} \right] \qquad 4\text{-}38$$

where V_i molar volume of component i m^3/kg mole
R universal gas constant 8.3143 J K^{-1} K $mole^{-1}$
ΔU internal activation energy J/kg mole
M_i molecular weight of component i kg mole

The internal activation energy is equal to

$$\Delta U = \Delta H - p\Delta V \qquad 4\text{-}39$$

where ΔH is activation energy for motion J/kg mole

p is pressure Nm^{-2}

By using the Eyring theory[66] of the variation of viscosity with temperature, the internal activation energy is given by

$$\Delta U = R \left\{ \left[\frac{\partial Ln(\mu V)}{\partial(\frac{1}{T})} \right]_p - pT \left[\frac{\partial Ln(\mu V)}{\partial p} \right]_T \right\} \qquad 4\text{-}40$$

where μ is absolute viscosity kg m/s^{-1}

μ can be found from an empirical equation

$$\mu = A\, e^{C/T}$$

In Eyring equation A and C are functions of the molar volume and internal energy of vaporization[68]

$$\mu = \frac{hNA}{V}\, e^{\Delta e_v / 2.45RT} \qquad 4\text{-}41$$

$$\Delta e_v = h_{fg} - p\Delta V$$

By assuming that the vapour behaves as an ideal gas (when vapour is steam and superheated throughout the process, the approximation is very close to actual behaviour)[93]

$$\Delta e_v = h_{fg} - RT \qquad 4\text{-}42$$

where h_{fg} is the molar heat of vaporization of the liquid.

Δe_v is the internal energy of vaporization J/kg.

h is planck constant 6.6256×10^{-34} J s

NA is Avogadro constant 6.02252×10^{23} $mole^{-1}$

$$\frac{\partial\, \mathrm{Ln}(\mu V)}{\partial \frac{1}{T}} = \frac{\Delta e_v}{2.45R} + \frac{1}{2.45RT} \frac{\partial \Delta e_v}{\partial \frac{1}{T}}$$

$$\frac{\partial\, \Delta e_v}{\partial T} = \frac{\partial h_{fg}}{\partial T} - R$$

$$\frac{\partial\, \Delta e_v}{\partial \frac{1}{T}} = -T^2 \frac{\partial h_{fg}}{\partial T} + RT^2$$

$$\left[\frac{\partial \mathrm{Ln}(\mu V)}{\partial \frac{1}{T}}\right]_p = \left\{\frac{\Delta e_v}{2.45R} + \frac{T}{2.45R}\left[R - \frac{\partial h_{fg}}{\partial T}\right]\right\}_p \qquad 4\text{-}43$$

$$\left[\frac{\partial \mathrm{Ln}(\mu V)}{\partial p}\right]_T = \left[\frac{1}{\mu}\frac{\partial \mu}{\partial p} + \frac{1}{V}\frac{\partial V}{\partial p}\right]_T \qquad 4\text{-}44$$

Using equations 4-43 and 4-44 in 4-40 we have

$$\Delta U = R\left\{\left[\frac{\Delta e_v}{2.45R} + \frac{T}{2.45R}\left(R - \frac{\partial h_{fg}}{\partial T}\right)\right]_p - pT\left[\frac{1}{\mu}\frac{\partial \mu}{\partial p} + \frac{1}{V}\frac{\partial V}{\partial p}\right]_T\right\} \qquad 4\text{-}45$$

At atmospheric pressure the value $p\Delta V$ is negligible but in our case when the pressure at collapse is very high (582000 Atm max. pressure at collapse time was mentioned[46]).

The only part which is difficult to find in equation 4-45 is the variation of viscosity with pressure which is unknown for E.G. By neglecting the $\frac{\partial \mu}{\partial p}$ part in equation 4-45, thermal diffusivity of the ethylene glycol-water mixture near the collapsing bubble was calculated, it shows a negative value for the thermal diffusion constant (-5.2232). This shows that water is concentrating in the ~~warm~~ COLD region. This can be explained by considering that the thermal diffusion is dependent on $(\frac{\Delta U}{V})$, i.e. molecules with high molecular weight and low model volume can press their way to cold region.

Differential migration of molecules due to thermal gradient might be very important at cavitation behaviour of pumping mixed petroleum products.

4.6 Cavitation Erosion

Erosion due to cavitation is a major problem. The capacity of materials to resist cavitation erosion is frequently termed their 'cavitation stability'. The cavitation stability of materials varies within wide limits depending on their physical properties and condition, also upon the hydrodynamic conditions in the flow and the properties of the liquid. Four different possible kinds of attack were delineated elsewhere[46]

1) A mechanical attack characterized by high intensity, relatively infrequent blows due to impingement of either shock waves propagated in the liquid and/or liquid microjets.

2) A chemical attack which is accelerated by both high pressures and high temperatures and often by the presence of free oxygen and water vapour.

3) The development of electrical potentials which may accelerate chemical attack.

4) A slight possibility of a thermal attack, with some evidence of temperatures sufficiently high to cause microscopic melting.

The collapse of a bubble causes the pressure and the temperature of the vapour inside the bubble to be greatly increased.[70] It is not possible to find one single explanation to cover all causes of cavitation damage.

The repetitive nature of bubble collapse probably means that fatigue phenomena are often relevant to cavitation attack.

The most widely used method of determining the cavitation stability of material is by means of a magnetostrictive vibrator. The development of this apparatus for the production of intensive local

cavitation erosion gives us a great deal of information from the viewpoint of materials' resistance to cavitation damage. A series of investigations have been made in recent years of the cavitation stability of materials by using magnetostrictive vibrators at N.E.L.[71,72,73,74] and elsewhere[75]. Figure (27) shows the rate of erosion for different materials versus testing time; one can see most material when subjected to cavitation attack exhibits an initial incubation period during which no erosion occurs. This figure shows three different parts which are described below:

1) Incubation period during which no cavitation occurs (dashed line).

2) A fairly stable state (steady erosion).

3) The rate of erosion falls again when surface becomes very pitted.

4) Steady period.

Matsumura et al.[76] found that the rate time curves of brass, stainless steel, tool steel and mild steel have two peaks in contrast to those of aluminium, cast iron and iron, which have a single peak, and they also found the first peak appears in the rate time curve as temperature rises from 90 to 200°C.

Cavitation-erosion damage increases with temperature up to a maximum at about 50°C after which it decreases owing to the rapidly increasing vapour pressure[78], when the test pressure is atmospheric pressure. The erosion rate also increases with the square of the pressures over a range from 0.35 Bar to 3.0 Bar (5.0 to 43.5 P.S.I.). Figure 28 shows data on the effect of pressure on erosion rate[72] obtained by Hobbs and Laird using a magnetostrictive transducer for these tests. It seems this result is important in automotive coolant system pumps when a pressurization system is used and also where vibration induced cavitation is suggested in the cylinder cooling jacket[79]. But cavitation erosion damage observed in cooling systems is a result of chemical and mechanical effects working together[77], whereas vibrators are normally used to produce pure cavitation. It is therefore difficult to discuss the full implications of Hobbs' experiment in relation to automotive cooling systems. He showed that hardness and tensile strength are the main properties governing erosion

behaviour[73]. Results of laboratory tests indicate that the highest cavitation stability is exhibited by aluminium bronze and stainless steels[73,74].

For economic reasons, the most widely used materials for the construction of large hydraulic machinery are cast iron, cast bronze, or thick steel plate. All these materials exhibit rather poor cavitation stability. Because of this, in the manufacture of components for hydraulic machinery and also when repairing damaged parts, resistive coverings such as stainless steel or aluminium bronze are often employed.

In recent years, the possibility has been investigated of protecting metallic components of hydraulic machines with material such as rubber or plastic (the erosion resistance of nylon and high impact polythene is similar to that of stainless steel). The main difficulty lies in ensuring a sufficiently good bond between the protective material and the surface of the component.

4.7 Cavitation in Centrifugal Pumps

The occurrence of cavitation is a consequence of the reduction in the absolute pressure of a liquid to some critical value; it may be caused by general pressure drop in the system, or it may bear a localized character.

If we know the cause of such a reduction in pressure, we can predict the incidence of cavitation in one or other parts of a centrifugal pump.

The causes of general reduction in pressure in the system may be as follows:

1) Reduction of atmospheric pressure through increase in the altitude of the installation.

2) Reduction of the absolute pressure in the system because of the particular operating conditions of the pump.

3) Increase in the suction lift above the recommended value.

Local reduction in pressure may occur because of one of the following reasons:

1) Additional pressure losses in the suction line or in the pump impeller.

2) Increase in the liquid velocity through increase in pump speed.

3) Deflection of the flow streams from their normal trajectory, which may occur at a bend or through flow round some protruding body.

4) As a result of breakaway or constriction of the flow.

Low absolute pressure and thus cavitation may also take place through unstable operating conditions in the pump such as hydraulic shock in the system when starting or stopping the pump.

Cavitation damage to pump components frequently occurs where there are sudden changes in flow direction or sharp changes in the cross section of channels, e.g. pump C. It occurs only in smooth flow in those cases where the entry pressure is less than the specified minimum allowable value. Cavitation can occur because of vibration in certain parts of the pump in contact with water.

Cavitation in centrifugal pumps may lead to damage to certain parts of the impeller, suction or discharge components, to a reduction in head, to diminished output and efficiency and to an increase in noise level and vibration of the pump. It should be emphasized that noise and the vibration which goes with it occur in any pump under operating conditions which depart appreciably from the condition of maximum efficiency because of non-conformity of the angle of attack at entry to the impeller. Conversely, the operating characteristics of a pump may fall off severely and there may even be a certain amount of damage due to cavitation without any noticeable increase in noise and vibration. In other words, although noise and vibration are causes of cavitation, they do not yet permit the degree of its development to be determined with any degree of accuracy. In this respect the performance loss of pumps under cavitating conditions differs with the type of pump and with the type of installation.

Figure (29) shows typical cavitation characteristics for a centrifugal pump. This shows clearly how the head and pump discharge rate changes with variation in pressure in the suction line, that is, before entry to the impeller[80]. Figure (22) shows constant capacity cavitation test results obtained with a propeller pump. It can be seen a certain increase in head and efficiency of the pump just before commencement of cavitation[45]. This can be explained in that before cavitation commences, the liquid breaks away from the walls of the channels in the impeller and the frictional resistance decreases with a corresponding increase in head and pump efficiency.

The results of many tests on pumps have been correlated by the Hydraulic Institute in the U.S.A.[81] They plotted a graph relating σ_{th} to shape number for critical and other conditions. Figure (30).

4.8 Cavitation in Automotive Water Pump

The material of automotive water pumps is often aluminium or cast iron. Aluminium is attractive material because of its light weight, favourable nature for production techniques and better cavitation pitting resistance than cast iron[70]. But aluminium has a poorer resistance to corrosion when antifreeze (water glycol mixture) is used as the coolant in cooling systems[27]. In addition to mechanical effects of cavitation on the pump, pump damage seems also to be due to chemical effects[79].

Many types of experiments have been used in studying the pump cavitation problem, such as engine dynamometer, tests in a laboratory, sonic vibrator rig, Venturi rig, and car field tests. Car manufacturers independently developed laboratory pump tests to find a representative flow rate and for selection of factory fill coolants. These tests were aimed to produce relative data on materials and antifreeze under accidental cavitation/corrosion conditions, and also to try and design a circulating pump with flat head/flow characteristics, a high flow rate but avoiding excessive pressures at high speed.

The A.S.T.M. tried to standardize a laboratory pump test for cavitation erosion/corrosion and this seems on the way to being accepted by

most interested groups[82,83]. A laboratory pump test according to an A.S.T.M. standard was developed for rating the compatibility of aluminium pumps with various coolants. Pumps were rated for damage visually after 50 hours using a scale from 1 to 10, 1 being perforation and 10 being no damage[82]. Table III gives some typical results of the laboratory pump tests which were done by the G.M. Corporation[77].

Table III Laboratory Pump Test Results - 50 hours.

Type of coolant	Type of inhibitors*	% water	T temperature	Pump damage scale (after a 50 hour run)
Water	-	100%	115°C	8
10% glycol	A	90%	115	1
10% "	A	90%	85	4
25% "	A	75%	115	2
50% "	A	50%	120	2
50% "	B	50%	120	7
50% "	C	50%	120	8

* see reference 22.

Test conditions are very important to this test, which is illustrated in the data of Table III, by the 2nd and 3rd results, where temperature was varied. The fact that different antifreeze corrosion inhibitors have widely varying results when tested similarly, was interpreted as proof that chemical effects were occurring in addition to the mechanical effects of cavitation.

Ethylene glycol has a slight deleterious effect upon most metal and rubber; it attacks lead-tin solders so that it is necessary to use a special cadmium-zinc solder[84].

Cavitation erosion/corrosion or pitting of the water side of water cooled engine can be reduced by such means as:

1. Adding corrosion inhibitor to the water.
2. Reducing the vibratory stresses in the affected area, e.g. by increasing cylinder liner wall thickness and reducing piston clearance. Vibratory stresses are very important in diesel engines.[85]

3a. Making components liable to damage, such as impeller and housing, of a more erosion resistant material.

3b. Coating the liner and impeller surface with a more erosion resistant material.

Many authors have presented data to show that the pressurisation of coolant systems can reduce the cavitation erosion rate in cylinder blocks[36,84,85,15]. It is important to mention that cavitation erosion in automotive water pumps is a combination of cavitation corrosion and erosion. It follows that the trend shown on Figure (28) where Hobbs showed that in vibratory cavitation the erosion rate increased with square of pressure[72], is not necessarily applicable to automotive water pumps[77]. Other ways of reducing pump cavitation damage have been investigated[77]. Small changes in design can often be helpful, as for example where a small change in the housing of the Ford Kent pump was claimed to give a 20% increase in flow rate without cavitation.

Some automotive pumps currently in use resemble open impeller centrifugal pumps which are being successfully employed in the field of chemical and the process industries. The use of a single stage pump impeller running at speeds from 2900 to 25,000 rev/min makes possible a large performance envelope[86], with a flat head/flow characteristic [86,87] which is important in automotive water pumps. But the shape number tends to be lower for process pumps and their tangential conical diffuser may not be convenient for integral installations in the cylinder block. Also, the process pumps showed an output pressure which is very nearly related to $(\text{speed})^2$ and this is rather steep for automotive use.

CHAPTER V

BACKGROUND ON NON CAVITATING PERFORMANCE.

Non dimensional coefficients were used to plot the results

$$\Phi = \frac{Q}{ND^3} \qquad 5\text{-}1$$

$$\psi = \frac{Y}{N^2D^2} \qquad 5\text{-}2$$

$$\lambda_p = \frac{\text{Power}}{\rho N^3 D^5} \qquad 5\text{-}3$$

$$n_{sf} = \frac{N\sqrt{Q}}{(Y)^{\frac{3}{4}}} \qquad 5\text{-}4$$

where Φ is discharge coefficient
ψ is head "
λ_p is power "
n_{sf} is shape number
D is impeller diameter
Q is flow rate m^3/s
Y is specific energy J/kg

But it must be mentioned that when the non dimensional variables vary at cavitating conditions, a single parameter relationship $\psi = f(\Phi)$ is not applicable and other parameters such as scale effect, Reynolds number, thermodynamic effect, surface roughness and turbulence effect are important at cavitating condition. So that these parameters can be added to the one parameter law, we must write

$$\psi = f(Q, Re, \ldots) \qquad 5\text{-}5$$

Experience in the U.S.A. has shown that car engines usually have resistance equivalent to that through a 1.9 - 2.5 cm diameter orifice, while the resistance for a large engine is usually equivalent to that through a 2.8 - 2.9 cm diameter orifice[15]. So that the flow rate/ head loss characteristics of the coolant flow passages obeys the square law.

CHAPTER VI

THE TEST RIG

6.1 Planned Experimental Programme and Test Rig Design

There were two aims in the designing the test rig:

1. To measure the external characteristics of automotive water pumps at various speeds (1500 - 6500 rpm), temperatures (15 - 130°C), top tank pressures and at various concentrations of antifreeze.

2. Look at the cavitation characteristics of automotive water pumps and study the flow distribution in the pump's housing.

To fulfil these two aims a closed test rig was designed to cope with our requirements. The pump circulates coolant through a closed piping loop which includes a pressurized vessel, thermostated heater and a cooling coil.

Experimental studies were performed using a closed circuit as shown in Fig. (31). The test pumps (three types from a U.K. manufacturer) are installed horizontally, Fig. (32), and were mounted on a specially designed square housing which is similar to the cylinder block end Fig. (33), except pump 'C' which has a volute. A special machined face plate was designed for mounting this pump on the bracket Fig. (32a). These pumps can reasonably represent the available circulating pumps which are in common use in ordinary cars when one considers that most water circulating pumps are now installed directly into the cylinder block. Later it had been hoped to test some of the truck water circulating pumps, since these are not only larger but nearer in geometry to conventional pumps.

The square housing has four 25 mm holes Fig. (34), which are connected to a plenum chamber Figs. (35,36). Four 12.5 mm diameter bolts held the housing against the moveable vertical machined face of the bracket which had been designed by Saunders[89]. A 5.6 kw electric motor, coupled to an electro-magnetic induction coupling provides a variable speed drive between 0 and 2400 rpm. A plain spurs gear and

pinion of mild steel step-up the speed after the coupling and provide a maximum speed of 6800 rpm in the secondary shaft. This shaft drives the pumps through a toothed belt with 1 to 1 ratio pulleys. The pump speed was measured by a magnetic pick-up from a 60-tooth wheel with read-out on a digital counter. The shaft torque was measured by using strain gauge type torque meter which is connected to a galvanometer via slip rings.

Fluid is supplied to the test pump through a long suction pipe with strainer, valves and one glass section which is installed upstream of the pump inlet Fig. (31). This pipe is set in a 230 litre capacity (Fig. 38) pressurized tank. The flowrate was measured by a 25 mm stainless steel turbine type flow meter (in the delivery line) a design relatively insensitive to change in viscosity.

Pressures were measured at various points by using a six-way valve and a precision Bourdon pressure gauge. Pressure in the system was controlled by using compressed air which is passed through a filter and precision regulator into a stainless steel bellows (23 cm. dia.) Fig. (37). An expansion tank was designed to collect the liquid expansion; a 1½" relief valve prevents the system pressure rising more than 2.16 bar, gauge (30 psig). A pressurized system was used because it provides high boiling points and is in common use in car cooling systems. Pressurized systems for car cooling were selected by manufacturers because of their ability to work in various environments without having the problem of boiling.

Temperature was controlled by using one 3 kw immersed heater which is controlled by two thermostats and one small shell and tube heat exchanger. Temperatures were measured at suction, discharge, and at the main tank using thermistor probes. For more detailed information see Appendix I.

6.2 Test Rig Development

Galvanized water pipe with screwed joints was used for piping because of its low cost and its good resistance to corrosion. In the majority of joints 'Stag' was used as a sealing compound. Tri-sodium

phosphate was used as an inhibitor at the beginning of the experiment, it was found that Stag was soluble in tri-sodium phosphate solution, and there was noticeable leakage at the joints. Initially, there was no strainer in the system, but because of the seizure of the turbine flow meter which was caused by some materials such as Stag, chalk and pieces of rust (which left the pressure cylinder body as a result of expansion and contraction at various temperatures and the cleaning effect of tri-sodium phosphate), it was decided to put in a 50 mm (2") standard cast iron strainer with stainless steel mesh. The corrosion inhibitor in the water was changed to 'Bryto Fluid' No.5. It was chosen because it is a powerful corrosion inhibitor, although it is only recommended for grinding machine use.

A diaphragm valve was used at the discharge line to control the flowrate. At the beginning of the experiments a 25 mm (1") Warren Morrison diaphragm valve with Butyl rubber diaphragm had been used but this showed leakage at 90°C with ethylene-glycol/water mixture (allowable max. temp. was 120°C for EG/W according to the manufacturers catalogue). It was decided to change the 25 mm diaphragm valve to a 32 mm ($1\frac{1}{4}$") Saunders diaphragm valve with Viton material. This attempt was successful and it produced a lower resistance in the discharge line which is desirable. By using the $1\frac{1}{4}$" Saunders valve, it was realized that to have a good control on the flowrate was impossible especially at low flowrate. So it was decided to put two diaphragm valves in parallel. $1\frac{1}{2}$" and 1" Warren Morrison diaphragm valves with PTFE diaphragms have been used which show no problems so far.

The suction line design has been changed because the previous design Fig. (31) shows the uncontrolled flow pattern (swirling flow) entering the inlet of the pumps. For having a better flow pattern, fluid was supplied through a suction box (this will allow us to use Hewlett Packard quartz thermometer for accurate temperature measurement), a straightener and a glass section which is held by two PTFE bellows, Fig. (42).

0-100 PSIa absolute Statham pressure transducer was purchased to use with Scannivalve[92]. This will allow a future researcher to measure pressure very accurately and to study pressure variation in the pump housing.

The torque meter in shaft drive arrangement had been used for about 9 years before these experiments were started. It soon began to give erratic readings and the repairing of the torque meter took a considerable amount of time. See Appendix II for detailed work which was carried out.

Bearings in the drive shaft arrangement were redesigned because of high torque absorption of the old bearings. The old pre-packed grease bearings were replaced by new oil cooled bearings and the paired thrust bearings at the end of the drive shaft were changed with one journal bearing. The new arrangement reduced torque absorption in the bearings by more than 50%; see Appendix III.

6.3 Test Procedure

At the beginning of the experiment, the galvanometer and other electronic equipment in the test rig were switched on, and oil level in the bearings was checked. Torque meter's calibration curve was occasionally checked statically by dead weight tester (each fortnight). Before any tests, the test rig must be run for about $\frac{1}{2}$ an hour for warming-up at 4000 rpm. (This time had been $1\frac{1}{2}$ hours before repairing the torque meter). The flowrate, pressure at discharge and suction, torque absorption and temperature were measured at constant speed while the top tank pressure was adjusted. This is a normal test procedure for plotting the head/flow curve at constant speed. Time for warming-up at a higher speed than the test speed is about one to two minutes, but when speed is reduced the time required for cooling the bearings and reaching a stable torque reading is about 5 minutes for a 500 rpm. reduction in speed. For testing the pump at cavitating condition, the inlet pressure was changed by adjusting two gate valves and a needle valve on the suction line, Fig. (31), then the results were processed by using a short computer programme which is displayed in Appendix V.

CHAPTER VII

RESULTS AND DISCUSSIONS. NON CAVITATING FLOW

7.1 Introduction

Tests were carried out with four pump types (A, A_1, B and C), using water and 54% by weight of ethylene glycol water mixture, at various temperatures and pressures. Table IV shows the performance of the four pumps at their best efficiency points when E.G/W mixture was used as a fluid in the system.

Table IV. Specification of Pumps Tested.

PUMP	Speed R.P.M	Q Lit/min	Y J/kg	η_{max}	Dia. of Impeller	Shape No.*	Liquid	Tamp °C	Pressure Rise Bar
O.H.C A	5500	118.4	136.4	39.3%	0.071 m	102	54% of EG/W	25.5	1.364
KENT B	5500	102.3	55	24%	0.057 m	188	54% of EG/W	25	0.55
O.H.C A_1	5500	158.4	111.6	23%	0.0715 m	137	54% of EG/W	28	1.116
ESSEX C	6000	13.18	113.3	26%	0.06 m	135	54% of EG/W	23.5	1.133

* Based on experimental results

Pump A is cast iron and B has a cast iron impeller with a cast aluminium housing which may increase the damage due to electrochemical effects. Pump C has a cast iron impeller with a cast aluminium volute. Recently the impeller of pump (A) has been changed to a new type of impeller manufactured from steel sheet S.A.E. 1008 14 gauge (1.897 mm) and the new arrangement termed type A_1. This sheet metal impeller has sharp edges at the inlet and outlet which has a greater change of flow separation at the edges.

7.2 Non-Cavitating Results on Pump B.

Tests were carried out up to 6500 rpm, but a slight efficiency drop was measured at speeds above 5500 rpm. The efficiency value for this pump is doubtful because it was measured before final modifications were made to the torque meter (see Appendix II).

Pressure variation between a flowrate of 10 litre/min (corresponding to a closed thermostat in a car) and 120 litre/minute (high flowrate, when thermostat is open) is about 0.3 bar at high speed (6500 rpm), which meets the objective for the automotive water pump from point of flat head/flow characteristic. This pressure range becomes smaller when the speed is reduced, Figs. (58,59). The head coefficients for the same discharge coefficient were greater at higher speeds, which shows the effect of Reynolds number due to velocity change, Fig. (60). Fig. (61) shows the effect of temperatures on non-dimensional head flow characteristic in pump B when the fluids were 54/46% by weight of EG/W. There is no sign of cavitation in both fluids until 103°C with water and ethylene-glycol/water mixture, during the experiments with pump 'B). It is important to mention at lower temperature the head/flow characteristic is unusual, as it is the same for water and ethylene-glycol/water mixture,(88,97) in spite of the higher viscosity of 54/46% by weight of EG/W which is about four times that of water at room temperature. The difference between the curves rises as the temperature in the system increases. It shows that in pump (B) temperature change reduces the friction losses due to surface roughness in the pump.

7.3 Non-Cavitating Results on Pump A

6500 rpm was the maximum speed at which tests were carried out with pump A. The efficiency drop was observed at speeds more than 5500 rpm.

Fig. (62) shows the head flow curve for pump (A) in non-dimensional form at various speed and constant temperature (about 92°C), when the fluids were water and 54/46% by weight EG/W. One can find a median curve for lower flowrate to a first degree of approximation, but the similarity law is not applicable at higher flowrates in cavitating conditions. When increasing the speed at breakdown point Fig. (63), flow-

rate does not change, i.e. NPSE, but it is influenced by increased temperature. It shows that at the low inlet head in the circulating pump of the car or at high altitude, there is a limit for flowrate which is controlled only by coolant temperature and altitude with the same geometry of the pump. This can be explained by considering the cavitating flow in the impeller eye at the low inlet head when there is low resistance in the discharge line. This effect is more pronounced when theylene-glycol/water mixture is used as a fluid in the system. The ψ/φ curve moved towards the ψ axis at high speed at cavitating condition, Fig. (62), and it must be mentioned that the cavitation numbers for 5% head drop are the same in the case of water at 6500 rpm and 6000 rpm. Cavitation number for 5% head drop varies with speed in ethylene-glycol/water mixture, but in general has a much higher value than for water. Fig. (64) illustrates there are wide differences in ψ/φ curves at cavitating conditions at the same speed but varying temperatures. It is difficult to find any explanation for this range. The probable blockage in the impeller eye which was mentioned before occurred at a lower flowrate after increasing the temperature to 107°C. The bottom end of this curve is doubtful because of the low NPSE at high temperature. There are three possible explanations for this effect:

1 - Two-phase flow in the flow meter because of the presence of vapour bubbles in the mixture when it passes through the flow meter. The possibility of the presence of vapour bubbles after discharge is a likely reason for this occurrence as the pressure in the middle of the square housing is below atmospheric pressure at this temperatures, (boiling point of 54% of ethylene-glycol/water mixture at 1 bar absolute is about 110°C). This is more likely, as the flow meter measures the volumetric flow and the concentration of vapour bubbles dependent on the time (tests were started at point (A)).

2 - Cavitation in flow meter. This might occur when the flow is accelerated as it passes through the flow meter.

3 - There is a slight possibility that the ethylene-glycol/water mixture decomposes at high temperature which means a change in the concentration of the mixture in the cavitation region, i.e. the vapour pressure of the mixture increases. There are three important factors for the decomposition of ethylene-glycol/water mixture.(98)

a - The oxygen content of the coolant.

b - The temperature of the coolant and the temperature of the walls between which the coolant flows.

c - The presence of copper in the system.

Fig. (65) shows a power/flow curve in non-dimensional form. The effect of Reynolds number becomes important at low speed especially at low flowrate. Nominal rating of torque meter is 0 - 15 lb ft., (galvanometer has three scales 0 - 1.5, 0 - 5, 0 - 15 lb ft). The manufacturer claimed that the torque readings were within $\pm$ 1% of the true torque over the major part of each scale. The torque readings show that at high speed (more than 3000 rpm), when the Reynolds numbers are large, the similarity law is applicable. By assuming a mean power coefficient curve in Fig. (65) at high speeds, it was found that the torque readings were within $^{+}$ 2% of the mean torque over the major part of 0 - 1.5 lb ft scale at low speed (1500 rpm). But the torque reading at 1500 rpm shows about 40% error on torque readings compared with the mean curve on Fig. (65) when there is no flowrate. This error decreases to 25% at higher flowrate. There are ~~two~~ three reasons which could be put forward to explain these errors.

1 - The rating of the torque meter is 0 - 15 lb ft and at low speed (1500 rpm) the maximum torque reading was 0.2 lb ft which shows that the torque meter was working at a relatively very low strain. This could explain the error in torque reading. This error has been reduced by using a pair of final drive pulleys with a (2:1) higher speed ratio for driving the pump.

2 - Reynolds number effect should also be considered at low speed (1500 rpm) and low flowrate when the Reynolds number is small. It is about four times smaller than at 6000 rpm ($R = \frac{ND^2}{\nu}$ and $R = \frac{Q}{D}$). Because of the effect of Reynolds number it is almost unacceptable to use the derived mean power coefficient curve for low speeds.

3 - Power absorbed in the pump's seal at low speed might be quite large compared with the power absorbed by pumping the coolant plus power absorbed in seal (see section 7.5).

Fig. (66) shows the effect of external pressure in increasing the flowrate, when the pump is initially working under cavitating conditions. By changing the inlet condition, which means raising the pressure inside the tank by forcing the air pressure into the bellows or by reducing the NPSE by closing the inlet valves, flowrate is increased or reduced as shown in Fig. (66). It shows that pressurization can suppress the presence of cavity bubbles, i.e. give more flowrate in the system, but it does not mean less cavitation damage. By considering two fluids (water and 54% by weight of ethylene-glycol in water) at the same temperature and in cavitating condition (point 0 on the graph Fig. 66), we can approximately say

$$Q_W = 154 \text{ lit/min} \qquad NPSE_W = 74 \text{ J/kg}$$

$$Q_{GW} = 159.1 \text{ lit/min} \qquad NPSE_{GW} = 60 \text{ J/kg}$$

By assuming that we need 170 lit/min of fluid, the required NPSE is equal to

$$NPSE_W = 89.5 \text{ J/kg}$$

$$NPSE_{GW} = 69 \text{ J/kg}$$

The NPSE figures show that in order to reach the proper flowrate by increasing the NPSE, the system must be pressurized by 15.5 J/kg (1.58 m head) in water and 9 J/kg (0.92 m head) in the 54/46 EG/W. In a pressurized system less NPSE was necessary for the EG/W than water, i.e. less top tank pressure. There is a sealing problem at high top radiator tank pressure at high temperature in car. Figure (67) shows the effect of NPSE change at complete breakdown. It demonstrates that for the pump to be working under non-cavitating conditions at 101°C, the top tank pressure must be raised to increase the NPSE by about 100 J/kg (about 9.8 m head). The more or less horizontal line in Fig. (67) when NPSE reduces by closing the valve in suction line, can be explained, by considering that, the pressure drop in the system is changed by closing the suction valve. But, by increasing the top tank pressure at breakdown energy lost in the system is dependent on the flow rate only, i.e. breakdown point moves on the energy lost/flowrate curve in the system towards the head/flow curve of the pump at non cavitating condition.

7.4 Non-Cavitating Results on Pump A_1

As one can see from the Table IV (p.51) the efficiency dropped considerably after changing the impeller, but the flowrate at best efficiency point was increased. This is because the flow passage is much bigger than for the previous impeller. Fig. (68-69) show the dimensional and non-dimensional characteristics of pump A_1. Pump was tested at about 25°C when the top tank pressure was opened to atmosphere, the starting of cavitation was observed at 6500 rpm. By comparing the head flow characteristics of the two pumps at room temperature, the steeper head/flow curve for pump A_1 was observed which is not desirable (Fig. 80-A).

For more investigation on pump A_1 the pressures in the middle of the discharge housing for various flowrates and speeds were measured Fig. (41). The results were plotted in Fig. (70) which shows a maximum at an intermediate flowrate. The pressure falls considerably on either side of the maximum when the top tank pressure is constant. It is very difficult to predict any explanation for this without having the pressure readings in other points of the housing, and was not possible to measure them during the test. At constant pump inlet pressure the maximum in the intermediate flowrate still exists, but the fall in the high flowrate is much less than when there were constant top tank pressures (Fig. (70). It is hoped to study the pressure and velocity distribution of the housing by employing a Scanivalve and absolute pressure transducer in the future. At this stage the following explanation may be advanced.

The housing and the back plate of impeller could be considered as a rotating disk in a large clearance housing. Now considering the three cases of low, medium and high throughflow in the system.

1 - No throughflow at shut-off valve

By employing the Navier-Stokes equation for turbulent flow near the rotating disk with a constant angular velocity (ω) in an open tank, and a surface which flow rotates at a large distance from the surface with the same angular constant velocity (ω).[99] At the neighbourhood of a disk a layer of fluid is carried by the disk because of viscous

forces and the centrifugal forces in the thin layer give rise to secondary flow which is directed radially outward. The outward flow is compensated by particles which flow in an axial direction towards the disk centre. At the neighbourhood of plate, in which the fluid rotates over the wall, there is a similar effect but its sign is reversed, Fig. (71a). At no throughflow the velocity in the housing increases and there is high axial velocity near the middle of the housing which reduces the pressure at that point. Because of this circulation the temperature rise in the square housing was observed, see Fig. (96), on paint spot tests.

2 - Medium throughflow at the discharge.

By opening the discharge valve the fluid in the housings flows from the housing and so it reduces the velocity and temperature rise in the secondary flow between the housing and the rotating disk and the fluid which is carried out by the disk is compensated by fresh fluid in the housing, Fig. (71b).

3 - High throughflow.

When the discharge valve is completely open all the flowrate which pumped by impeller escapes from four passages in the housing. There might be two points for the reduction in pressure at the middle of housing. Firstly because the pressure at the discharge falls at high flowrate (Fig. 68), secondly, the author thinks that there might be a sort of closed secondary flow between the housing and the disk which may create a vapour cavity between the disk and plate, Figs (71c and 97).

It is hoped that a protruding cylindrical surface will be installed in the housing, Fig. (72), which can reduce the distance between the impeller and housing. (This brings the square housing design, the protuberance simulates the side of the front cylinder). By using the new design and measuring the velocity distribution in the housing and the effect of this change on the performance might lead to a better velocity distribution in the cylinder block and better performance of the pump itself.

7.5 Non-Cavitating Results on Pump C

Fig. (73) shows the head/flow characteristics at non-cavitating conditions. The head flow curve is quite steep compared with other pumps. Fig. (80-A). It has to be mentioned that the pressure rise in pump C for same flowrate and speed when water circulates in the system is less than for 54/46% E.G/W, Fig. (74). This is rather interesting as for high viscosity, the head should be higher than that for low viscosity liquid[101]. This might be because of increase of viscosity suppresses the relative circulation within the impeller channel, i.e. more head generation at pump outlet (density of E.G/W is 7% higher than that for water at 20°C). Falling pressure head at high flowrate is because of losses in inlet head.

Fig. (75) shows the non-dimensional head flow characteristic at various speeds. The difference between ψ/φ curves for various speeds shows the Reynolds number effect. Fig. (76) illustrates the dimensionless head flow curve at various temperatures at 6500 rpm.

Fig. (77) shows the non-dimensional power/flow characteristics at various speeds for pump (C). The difference between curves is more pronounced than pump A. This figure indicated that something was probably going wrong in the system. On removal of the pump, it was realized that impeller was touching the case in some parts, Fig. (78). The size of groove in the case was about 80 micron deep. It was decided to machine the back surface of the pump about 80 microns. The results showed improvements (see Fig. 77) but there are differences on the λ_p/φ curves. The torque reductions at various flow rates for the same speed are almost the same, Table V.

Table V. Torque absorption before modification (b.m) and after modification (a.m).

SPEED	φ	Torque absorption lb.ft.		$M_b - M_a$
		b.m	a.m	
6500	0.0	1.90	0.96	0.29000
6500	0.04	1.41	1.19	0.22
1500	0.0	0.25	0.14	0.11
1500	0.04	0.27	0.16	0.11

The new modification does not change the head/flow curves Fig. (79), but it increased the efficiency (see Table (VI).

Table VI. Efficiency Increase After Modification at the Best Efficiency Point.

SPEED	Flow rate Q lit/min		Specific Energy Y J/kg		η_{max}		Temp	
	b.m.	a.m.	b.m.	a.m.	b.m.	a.m.	b.m.	a.m.
7000	149.6	145.1	161.5	161.7	17.0	18.7	25	25
5000	96.1	113	89.5	77	24.2	27.2	23	27.5
1500	34.1	33.2	5.0	7.0	5	12.4	22.5	27.5

The non dimensional power/flow curves are rather flat, by comparing them with λ_p/φ curves for pump A, Fig. (77). This might be because of high mechanical torque absorption in the pump's sealing. In that case the ~~former~~ Torque absorption in the pump is more dependent on the losses in the seal than in handling fluid itself (this is very important at low speed). Torque absorption in the bearing was measured by running the impeller in the air. Table VII shows the amount of torque absorption in the pump seal (considering 96% efficiency for tooth belt).

Table VII Torque Absorption in the Pump's Seal

SPEED	Torque absorption in pump when φ = 0 lb-ft	Torque absorption in the pump's seal when pump running at air lb-ft	λ_p When pump running at air
1500	0.17	0.085	1.3481
3000	0.28	0.104	0.4195
4000	0.53	0.098	0.2196

The tests were performed very quickly and give just a rough idea about why the similarity law is not applicable at low speeds in small pumps. It was impossible to do tests at high speeds as there is problem of failure of pump bearings and seal due to lack of cooling when running in the air.

For more investigation the static pressure at different points of volute of pump C were measured. The effect of cavitation on the

the pressure at the beginning of volute is more pronounced than the pressure at the discharge passage. The static pressure at the beginning of volute is about 33% of that at non cavitating condition. Pressure distributions in the middle of volute casing are almost parallel at different flow rates, Fig. (80).

7.6 Comparing the Non Cavitating Results of Different Tested Pumps

By comparing pumps A, A_1, B and C, it is obvious that pump C has the steepest head/flow characteristic and pump B has the flattest one between the tested pumps, Fig. (80-B).

There are three important factors which can change the shape of head/flow characteristic[101].

1 - Width of the impeller.
2 - impeller vane angle.
3 - number of impeller vanes.

Higher width of the impeller causes a flatter head/flow characteristic. Also radial or spokelike vane can produce a flat ψ/φ characteristic. Reducing the number of the impeller vanes gives the steeper head/flow characteristic[101]. Unfortunately it was not possible to compare four tested pumps with each other because of different diameter of impellers. But in the case of pumps A and A_1, pump A has a wider impeller than pump A_1.

Also it is important to mention that for the same flow coefficient at the same speed flow rates are different in the tested pumps, i.e. pressure drop from reservoir to the impeller eyes is different. Table VIII shows the pressure drop at the impeller eye in respect to pump B (it has the flattest ψ/φ curves).

Table VIII Pressure Drop at the Impeller Eye in Relation to Pump B for φ constant.

Pump	Dia. of impeller	Dia. of impeller eye	Q flow rate	$\Delta h \approx k \frac{V^2}{2}$
A	71 mm	40 mm	$1.93\ Q_B$	$4.20\ \Delta h_B$
A_1	71.5 mm	55 mm	$1.97\ Q_B$	$1.80\ \Delta h_B$
B	57 mm	41.2 mm	Q_B	Δh_B
C	60 mm	36.5 mm	$1.79 Q_B$	$1.9\ \Delta h_B$

This shows that at the same flow coefficient pressure drop at the impeller eye is higher for pumps A, A_1 and C than pump B. As flow coefficient increases this inlet line pressure drop increases, i.e. less head produced at the discharge for pump A, A_1 and C in respect to the normal head rise (steepening the head/flow curve as compared with testing at a constant pump inlet pressure).

Low efficiencies in four tested pumps more or less are due to poor inlet conditions to the pumps. In the case of pump A, A_1 and B fluid enters the pump from one side of the pumps perpendicular to the shafts. This arrangement causes a high preswirling. In pump C, there is a sharp bend which produces a poor distribution,also there is a hole (3.2 mm dia.) between suction line and high pressure region (it is used for air bleeding of the pump). This pressure difference causes an unequal pressure distribution in the suction line, this might produce cavitation in the ~~discharge~~ suction line because of high pressure at suction line.

Fig. (94) shows the efficiency of different tested pumps at 6500 rpm. A maximum efficiency of 37.5% was recorded for pump A. With pump A_1 the efficiency dropped considerably, this might be because of the vanes of the impeller which have sharp edges. After a modification to pump A, the efficiency improved by about 2%. The low efficiency figure in pump C is due to the bad entry condition and the internal circulation of the fluid in the system. See section 7.7 on paint spot tests.

7.7 Paint Spot Tests

To investigate further the flow distribution within the housing of pump C, it was decided to do some tests by using the paint spot technique, although concluding anything from these tests is far from indicating the complete flow distribution because it just gives the flow distribution near the wall. Tests showed that in pump C, there is flow from the high pressure region to the low pressure region between the impeller face and the inlet casing, Fig. (95). This inward flow near the wall of the casing and impeller is increased at the cavitating condition, Fig. (95), and when pump is running at low speeds, Fig. (95), there is also inward flow near the discharge in the volute. The author

thinks that by controlling the axial clearance between the impeller and the inlet casing, designing the air bleeding hole to reduce the disturbance in the suction line to a minimum and removing the sharp bend in the suction entry near the impeller eye can improve the efficiency of pump C without altering the geometry of the impeller itself.

A paint spot test on the housing of pump A_1 shows that near the walls of the housing there is a high radial inward flow, both with no throughflow and also high throughflow, Figs. (96-97). This evidence cannot be used directly to find the flow distribution in the housing away from the wall, but the author thinks that the flow distribution in the housing is probably more like Fig. (71). It is also interesting to mention that the ratio of $\frac{\text{tangential velocity}}{\text{radial velocity}}$ when there is no throughflow is higher than that at high throughflow. This does not mean that the radial velocity is lower than that in high throughflow since the tangential velocity may be higher as the stream lines only show the ratio of the two velocities.

CHAPTER VIII

RESULTS AND DISCUSSION. CAVITATING CONDITION

8.1 Cavitating Results on Pump A

Figs. (81 & 82) show the cavitating characteristics of pump (A) at various temperatures in dimensional and non-dimensional forms. Temperature effect is not very important in cavitation behaviour of pump A as far as tests were carried out with EG/W and assuming that total errors in NPSE are $\pm$4J/kg, (see Appendix IV). Because of the lack of information on the physical property of the ethylene-glycol, the cooling effect due to vaporization of ethylene-glycol at a cavity boundary, cannot be calculated, so that the correction factor which was presented by Furness[44] was not applied to find a cavity pressure. By comparing other results (when the fluids were water) from Stepanoff's[88] and Chivers[102] results Figs. (24,83) with the results of the ethylene-glycol/water mixture, the following points were observed.

1 - NPSE variation as a result of temperature change in the ethylene-glycol/water mixture, is less than the NPSE change in water. The reason for this is higher density and viscosity and less vapour pressure; as a result the cooling effect is not as great as for water. As shown in 4.5, thermal diffusion could not play a strong rule in the case of E.G/W mixture, but it might be important for pumping petroleum products.

2 - Other authors[88-102] show that in water as the temperature increases, NPSE reduces, but in E.G/W by increasing the temperature there was an NPSE increase upto a temperature of 93°C but with a further temperature rise NPSE reduced again. This cannot be explained now as accurate tests will be necessary which were not possible with the test rig when the tests were carried out.

3 - The fall in vapour pressure due to vaporization for 54/46% E.G/W mixture was calculated by using equation 4.27. The calculated values show that cooling effect in 54/46% E.G/W mixture is about half the value of that for water at the same temperature.

An attempt was made to calculate the cavitation performance for E.G/W at 93°C and 102°C by using two sets of (F.E.) available data at 22°C and 92°C for E.G/W but this was unsuccessful as NPSE/temp. curve is not similar to classical theory as used in Ref. 58 where NPSE falls by temperature increase. This might be because of presence of dissolved gases in the system as one can see in Equation 4-8. The same sort of increment was observed by Hammit in mercury.(59)

Values of ΔNPSE as a function of the thermal cavitation parameter are plotted in Fig. (84), which also shows the average curve for the pure fluid from Ref. (51). The data for E.G/W do not agree with the pure fluid data. This is rather interesting when one considers that published data for the cavitation behaviour of fluids with higher density than water is rare except some work(59) which has been done on mercury. The modulus of ΔNPSE was used in Fig. (84) because with the E.G/W, there were NPSE increases due to rise in temperature. At the same temperature the cavitation number is higher for 54/46 E.G/W than water, based on a 5% head drop at the same speed, Fig. (85). The cavitation in 54/46 E.G/W takes place at higher NPSE and lower flowrate than water in automotive cooling pumps at same coolant temperature. The increase in cavitation nunber as a result of temperature rise in water for the tests on pump A is not the same as other published data(88-102). NPSE for 5% head drop when the fluid was water at 6000 rpm shows that there is slight decrease in NPSE when the temperature rises from about 25°C up to 93°C. It shows that there might be speed effects on cavitation number, which at high speed increase the NPSE at high temperature. It is hoped that more tests will be carried out by others in the future on the cavitation characteristics of water and various concentrations of the E.G/W at various temperatures and speeds in order to obtain a clear picture.

8.2 Cavitating Results on Pump B.

After 60 hours running at cavitating and non-cavitating condition with water and 54/46% by weight of E.G/W in pump B, we observed a layer of spongy material deposited on the surface of aluminium housing. The deposit which was analysed by micro probe analyser showed that the more than 50% deposit is copper, and the other major materials were Si, Fe, Al, Ca with almost equal concentrations. Also there were small amounts of

zinc and copper. It can be said that copper deposit comes from a brass pipe in the suction line just upstream of pump inlet (due to de-zincification); that is, the brass is carried away in the solution. Collins[98] observed that some copper was deposited on any exposed aluminium and ferrous metals in the vicinity of brass. In our experiment copper was deposited in the aluminium housing near the brass tube in the pump. Cavitation pittings were found in the housing near the suction line, Fig. (86). Collins[98] also mentioned that copper deposited on the aluminium surface may stimulate the cavitation pitting which was observed in our experiments. It can be said that other deposits such as Si, Zn, Fe, Al, Ca, Cl deposited on the surface of aluminium housings due to electro-chemical effect.

8.3 Cavitating Results on Pump C

Figs. (87 and 88) illustrated the cavitation characteristic of pump C at various temperatures in dimensional and non-dimensional forms when fluid was water. By considering the error in measuring NPSE the NPSE increases due to temperature increases are within the error's limit ($\pm$ 4 J/kg see Appendix V). Figs. (89-90) show the cavitation characteristic with 54/46% E.G/W at various temperatures at 6500 rpm in dimensional and dimensionless form.

The cavity pressure depression for 9% energy loss by using Equations (4-27, 4-30 and 4-31) for water and 54/46% E.G/W mixture in pump C were calculated, with the results at 28°C and 86°C used as reference data. The results were plotted in Fig. (91). The calculated values for the cavity pressure depression are not in agreement with experimental data by assuming Furness[44] hypothesis (one $\psi/(NPSE)_K$ curve at different temperature. For cavitation characteristic of pump $(NPSE)_K = (p - p_v - p_g + \Delta p_v)\frac{1}{\rho}$ for water and 54/46% E.G/W mixture. There is a maximum for the experimental value for cavity pressure depression in 54/46% E.G/W mixture and a minimum in the case of water.

Maximum NPSE at 70°C in water might be because of the presence of differing amount of air in the system, Fig. (92). NPSE vs. temperature is almost straight line in case of E.G/W at 5% head drop. Fig. (92) shows that 54/46% E.G/W has a better cavitation characteristic at cold

condition but at high temperature water has a better cavitation behaviour. This is because at cold condition higher viscosity of E.G/W causes more resistance which can suppress the cavitation appearance but at high temperature vapour pressure is important part at cavitating condition.

By comparing the two pumps A and C it is possible to see that at the same flow rate (not at the same φ) and same speed, NPSE was higher at 5%, head drop for pump (C) than for pump (A), but at breakdown the NPSE was higher in pump A than pump C. Better cavitation breakdown at 5% head drop in pump A is due to bigger diameter of impeller eye, i.e. less pressure drop at the same flow rate. Less NPSE at breakdown for pump C means that pump C is capable to work at cavitating condition better than pump A. The author thinks this is because of the connection hole between discharge and suction (high pressure and low pressure region) which can increase the pressure at the impeller eye when the pressure in the suction line is quite low. Also pre swirling in pump A is higher than pump C because of different inlet geometry of two pumps. In case of water the pump breakdown did not happen at all. Cavitation damage was observed in the tongue of aluminium volute casing.

The value of $|\Delta NPSE|$ as a function of thermal cavitation parameter ($B = \frac{v_g}{v_f} \times \frac{C_p}{h_{fg}} \times \frac{\delta T_{sat}}{\delta p_v}$) are plotted in Fig. (93). The data for 54/46% E.G/W mixture and water do not agree with the pure fluid data from ref. (51). The author thinks the different geometry of tested pumps with pumps tested by others is the main reason of the disagreement between F.E. results and results published at Ref. (51).

CHAPTER IX

CONCLUSIONS

1 - From the pumps tested, pump B showed itself to have a flatter head flow characteristic than the other pumps.

2 - Similarity law is not applicable to the pump types tested at low speed for λ_p/φ as the power absorption in the bearings and seal is quite high.

3 - Corrosion damage due to electro-chemical effect becomes important in a pump made of differing types of material.

4 - The pressurization of the closed system can increase the flow rate in automotive cooling system especially at high temperature, but at some value of external pressure (which is dependent on the temperature and geometry of cooling system) the flow rate and head rise reaches to a plateau.

5 - The low efficiencies in the pumps tested, show that an improvement in efficiency is very important, since for example, there is about 1.5 kw (2 HP) power absorption in the pump C at high speed and high throughflow (about 5% in 75 kw engine). Tests show that by improvement in bearing design, it is possible to increase efficiency considerably (see table VII)

6 - Local cooling effect due to vaporization is less important in E.G/W than water. This can be accounted for as a result of higher viscosity of E.G/W which could suppress the growth of bubble, and lower thermal conductivity of 54/46% E.G/W at high temperature. (The variation of thermal diffusion $\frac{K}{C_p \rho_f}$ is negligible at different temperature).

7 - The calculation of thermal cavitation parameter (B) shows that the B parameter for E.G/W is greater than water at the same temperature, but the thermal cavitation parameter's value for 54/46% by weight of E.G/W is more like water than glycol.

8 - The thermal cavitation parameter as derived by Spraker[51] to hydrocarbon mixtures with density lower than water. It seems more tests will be necessary with polar fluids with a higher density than

water for further conclusions about its more general applicability.

9 - More results will be necessary to predict fully the ethylene-glycol/water mixture's cavitation behaviour as a coolant in automotive cooling systems. (The results have shown that the possibility of cavitation by using ethylene glycol/water mixture is higher than pure water in pump A, but in pump C E.G/W mixture showed a better behaviour than water at low temperature).

10 - 54/46% E.G/W mixture produces higher specific energy at the same flow rate. (This might be because of higher viscosity of E.G/W suppressing the internal circulation within the region between two blades.)

CHAPTER X

FUTURE WORK

Because of high production of the automotive car pumps (10^6 + in U.K. only) the total amount of money involved in production is high (the average purchase price of a pump for an ordinary passenger car is about £5). The rather low performance shows that a slight increase in efficiency can save appreciable power absorption (about 2 kw at high flow rate) in the cooling system. The reduction in cost of manufacturing by making the pump simpler could save a large amount of money without further lowering the performance of the pump. The efficiency of the automotive water pumps tested is low when comparing with other centrifugal pumps. As a result of the author's programme, further work must be carried out on the following topics.

1 - More types of automotive pumps currently in use must be tested in various concentrations of E.G/W and water. During the experiments, temperature and speed must be varied in a controlled manner.

2 - One must change the impeller discharge cavity geometry and find the best type of impeller for the housing by considering the capital cost and durability as well as efficiency.

3 - Examine the plastic type of impeller of the automotive water pump and investigate the cavitation pitting of plastic.

4 - To find out the velocity profile in the discharge cavity (which simulates the cylinder block) by using a pitot-cylinder or laser beam. This velocity profile is going to help to see if there is any possibility to have better distribution of fluid in the cylinder block entry.

5 - To investigate the cavitation behaviour of the automotive water pump in various conditions. Accurate measurement of NPSE, temperature, flowrate and density will be necessary to predict the cavitation behaviour of E.G/W. This might help to find any possible predictive

relationship for cavitation behaviour of E.G/W. Density measurement will be necessary, as it shows the possible change of concentration of E.G/W due to decomposition.

6 - It will be necessary to test similar pumps in order to assess changes in behaviour produced by geometric variation in mass produced items.

7 - Test some pump designs from truck engines, since these are not only larger, but nearer in geometry to conventional pumps.

8 - The amount of soluble gas in the system must be controlled and measured after each test.

9 - Compare the laboratory test results with actual engine.

APPENDIX I

INSTRUMENTATION AND TEST RIG DETAILS

A-1-1 Drive Shaft Arrangement

A 5.6 kw electric motor, coupled to an electro induction coupling provides a variable speed. A plain step-up spur gear, the wheel made from "Tufnol" and the pinion of mild steel connect it to the torque meter drive shaft. This shaft drives the pump through a pair of (3.581" dia.) $\frac{3}{8}$" stock pulleys and toothed belt; this avoids any problems of belt slip. For high speed (10.000 rpm) it is possible to change the pulleys and install a new pair of pulleys (with speed ratio of 2:1) and mounting the bigger pulley on the drive shaft, and by installing the smaller pulley on the pump shaft, it is possible to increase the torque indicating value which is useful when the torque value is very small. This low torque causes error in the reading specially at low speed. Because of safety reasons a sheet metal housing has been installed around the pulleys. Also a wooden box was designed to reduce the level of sound from the spur gears. This was completely successful and at all speeds the noise near the gears (working place) reduced considerably.

The speed in the secondary shaft is measured by means of $\frac{3}{8}$" wide wheel on the shaft which has 60 teeth machined on its periphery. A magnetic impulse pick-up is mounted near this, and connected to a digital counter (Racal SA. 535) set to read cycles per second, thus directly indicating revolutions per minutes. (Now, A.M.F. digital counter Model 7734).

This mild steel shaft and wheel are supported by two oil cooled journal bearsing with a shielf on one side (Appendix III). The final drive shaft is stainless steel and mounted on two journal bearings. Torque transducer is axially mounted between the two shafts with two flexible couplings. Flexible couplings protect the torque meter from any bending load caused by vibration and misalignment.

A-1-2 Pressure and Expansion Tank

A 46 cm. diameter piece of an old $\frac{1}{2}$" plate duct was used for making a 230 litre capacity pressurized vessel. It was impossible to use a standard flange for this cylinder, because it is not a complete circle. So two 25 mm thick mild steel plates were designed for the bottom and top end of the cylinder. Three holes were drilled at the bottom end: one of them is $2\frac{1}{4}$" BSP for heater installation. There are two holes on the top end, see Fig. (38,48). $1\frac{1}{2}$" BSP tapping was used for installing the relief valve.

Two mild steel half rings Fig. (36) (43.5 cm. outside diam. 25.4 cm. inside dia. and 25 mm. thickness) which are overlap jointed, were designed to bolt to the top end with 16 bolts ($\frac{3}{4}$" dia.). Neoprene rubber (34.1 cm. dia.) was used for sealing the bottom of the half rings to the end plate. Stainless steel bellows (23.5 cm. dia.) with two 12.5 mm mild steel end flanges suspended with 8 bolts ($\frac{3}{8}$" dia.) to the half rings, which sealed the bottom of the top bellows' flange recess by a neoprene rubber O-ring (26 cm. dia.) Fig. (37). Two half rings were sealed by two pieces of brown paper gasket and Stag sealant, in overlap jointing position.

Two tee bars were welded inside the tank to prevent over-deflection of the bellows, when the pressure inside the tank is reduced for any reason. The tank was installed on 3 legs (3" dia. pipe and 30 cm. length), three mild steel plates were welded to the 3" pipes for distributing the weight of the tank. The pressure tank was tested successfully at 4 bar gauge (60 psig) with cold water.

A 19 litre expansion tank was designed for collecting the liquid expansion at high temperature, which is shown in Fig. (39) and Fig. (48). It has a sight glass which shows the level of the liquid on the expansion tank. There is $1\frac{1}{2}$" pipe inside the expansion tank which is connected to the relief valve. It prevents any water or steam flush at high temperature through the vent pipe. The expansion tank was installed at the top of the vessel and it can be used as an expansion and make-up tank for experiments.

The rig pressure is controlled pneumatically by using compressed air fed in at the top end of the bellows, giving an operating pressure range of an approximately 1 to 3 bar absolute (15 to 45 psia). Compressed air flows through a filter and a micro air regulator. Relief valve at the top of the pressure tank is set at 3 bar absolute.

A-1-3 Valves and Piping

Galvanized pipe with screwed joints were used for piping. Diaphragm valves were used at the pump outlet and where the pressure is above atmospheric, see Fig. (31). Gate valves and needle valves were chosen for suction line, because at low pressure, the diaphragm of the valve fluttered. Fluid flows in the suction line through a 2" cast iron strainer with stainless steel mesh. There is a glass section at the suction line near the pump's inlet to allow observation for gas bubbles. Because of difference in expansion between glass and galvanized piping and to provide an easy way of changing the pump from housing, steam hose connections were used. Now the steam hoses are changed with 2 PTFE bellows.

Because of lack of money, sundry types of insulation were used to reduce the heat release from the system.

A-1-4 Flow Measurement

A 25 mm. dia. stainless steel commercial turbine type flow meter situated in the pump outlet line measures the flowrate, this meter has been chosen because of its low sensitivity to large changes in viscosity between hot water and cold EG/W. A magnetic pick-up is used for sensing the speed of rotation. Calibration test with digital counter showed $\pm$ 1% was sufficient between flowrate of 25 litres per minute and 300 litres per minute without any error on the reading of the digital counter. So it is necessary to correct the flowrate for lower flowrate than 25 lit/min. The flow meter was installed vertically. A special reducer cone was designed to reduce the diameter of the main piping line from 32 mm to 25 mm dia. at a reduction angle of 15^{o}. This cone, straightener and a 45 cm. long 25 mm stainless steel straight pipe were installed upstream of the flow meter in the vertical line in that order Fig. (31). The signal from the pick-up is fed to the digital counter with $\pm$ 0.1%

accuracy. An adjustable time base may be varied from 1 to 10 seconds in stages of milliseconds, and this provides readings in any desired units. In our case it is set to read litres per minute directly.

Fig. (40) shows calibration curve for 25 mm flow meter. Flowrate less than 25 lit/min was calculated from an empirical equation which was developed by Tan[90,91]. Calibration tests were carried out with a test rig in the University which $\pm$ 0.1% accuracy is claimed.[91] The flow meter was installed in the calibration rig in a vertical position with the cone, straightener and straight pipe.

A-1-5 Pressure Measurement

Pressure measurement was carried out via one six-way valve to a precision (absolute pressure) Bourdon tube gauge (range 9 - 6.9 bar absolute or 0.100 psia). Static pressure was measured at various points such as inlet and outlet of the pump and at the housing. Normally whatever test is in progress, it is necessary to measure several pressures, such as pressure at inlet, outlet, and some pressure reading from the housing. Actually, there are 19 pressure tap holes in the housing for studying pressure distribution inside. Six of them are at the corner of four flow passages and others are located in cross line as shown in Fig. (41). These pressure holes were connected by $\frac{1}{4}$" copper tubes which were brazed to the housing and are connected to the six-way valve by plastic tube. When unused they are blanked off.

Pressure in the reservoir and bellows are measured by two 10 cm. dia. commercial class pressure gauges (range 0 - 4 bar). They were calibrated by the dead-weight gauge tester. The precision Bourdon tube gauge (made by Wallace & Tiernan) appeared to be as accurate as the dead-weight tests.

A-1-6 Temperature Measurement

A multi-way indicator with thermistor temperature probes made by Zeal Ltd. was used to measure temperature (range 10 to 150°C) which Howard[32] used previously. Temperature was measured at four points, inlet and outlet of the pump, main reservoir and ambient temperature.

There is an accuracy of $\pm$ 0.25°C at the reading device. The combination of temperature and pressure measurement at pump inlet enables one to find the net positive suction energy(NPSE).

Experiments showed that there is a temperature rise between suction and discharge, this difference increases when the resistance in the system increases (low efficiency).

A-1-7 Heating, Cooling, Thermostat

A three kw domestic heater was installed at the bottom of the tank, there were two thermostats which control temperature from 25°C to 170°C. An ordinary domestic thermostat which is sufficient to control the temperature range from 25°C to 93°C was installed at the centre of the heater. Another one was installed at 25 cm. from the bottom of the tank. It controls temperatures from 70°C to 170°C. This thermostat has a stainless steel protector sleeve which avoids corrosion problems.

A control panel was designed to control the heater with these thermostats. There is a switch for selecting the appropriate thermostat. The accuracy of thermostats is about $\pm$ 3°C.

There is a small shell and tube heat exchanger which is cooled by City water. This (borrowed) heat exchanger was chosen because, by using it, it was easier to select a constant temperature. Heat transfer in the heat exchanger was controlled by using two hand operated valves Fig. (31). There is some difficulty in maintaining constant temperature because everything is hand operated, but during a long experiment (about 3 hours) it was possible to have a constant temperature within $\pm$ 2°C at the suction line.

APPENDIX II

TORQUE METER PROBLEMS

A Westland Aircraft (now British Hovercraft Corp.) strain gauge torque transducer has been used for ten years to measure the torque in the rotating shaft. A portable galvanometer indicator (which is also ten years old) is employed for indicating the mean torque applied to the torque transducer.

At the first stage of the experiment, an irregular fluctuation was registered on the indicator. The indicator showed that the torque readings were not repeatable as the torque readings were time and temperature dependent.

Several attempts have been made to diminish the torque fluctuations which are shown in Fig. (43). The maintenance of the torque meter and redesigning and replacing of the grease lubricated bearings and wick-fed thrust bearing on the line shaft were carried out together. Bearing re-design is described in Appendix III.

At the last attempt the changing resistance of the old resistors and transducer-mounted potentiometer in the bridge network with the temperature of the torque transducer was investigated. We observed high temperatures ($40^{\circ}C$ after 1 hour running at 4000 rpm) and noticed vibrations on the torque transducer's case (when the speed rises more than 5000 rpm). By replacing the old resistors (22 kΩ $\pm$ 2%) and potentiometer (10 kΩ) and installing the new ones in the indicator, a quite stable reading of torque has been achieved. (Two 24 kΩ $\pm$ 1% resistors and 22 kΩ potentiometers were supplied by British Hovercraft Corporation). The torque meter is calibrated statically and Fig. (44) shows the calibration curve for the torque meter readings. Calibration curve has been checked every other week.

APPENDIX III

REDESIGNING THE BEARINGS

The bearings were redesigned because of torque fluctuation and high parasitic torque absorption in the oil cooled thrust bearings and grease cooled journal bearings of the drive shaft. The disadvantages with the old bearings in the secondary shaft were:

1 - Torque absorption in the preloaded back-to-back pair of ball thrust bearings which were oil lubricated and cooled, were dependent on temperature. At high temperatures because of different expansion rates between the stainless steel shaft and bearings, torque absorption increased with temperature. In our case there was almost no axial load, so, it was decided to remove and change the thrust bearings to a single deep-groove ball journal (oil cooled) bearing. This journal bearing was installed in the position of one of the thrust bearings, then the outer case and inner case of one of the old thrust bearings were used to prevent the axial movement of the journal bearing. The drive shaft, previous thrust bearings and grease lubricated journal bearings are described elsewhere.(89)

2 - Three grease lubricated bearings which were previously used in the drive shaft installation were shown to be inconsistent in their torque absorption when one considered the difference in viscosity due to temperature change. This torque absorption was also too high to be acceptable. As a result of temperature change in the shaft it was not possible to read a single torque absorption reading for one speed without $1\frac{1}{2}$ hours running to reach a constant temperature in the drive shaft arrangement. So it was decided to change the three grease bearings to three oil cooled journal bearings with a shield on one side. The outer race in the other side is held securely in place by a specially designed external sealed mounting. Figs. (45-46) show the external mountings for the two size of bearings which were used. There were two 4 B.A. tap holes and one of them has a feeder on the top end with brazed copper tube on it. The other one is used to stabilize the level of the oil in the housing and to prevent excess lubrication which causes heating of the bearings and accelerates the deterioration of the lubricant.

3 - After installing the new bearings excessive vibration was observed in the system. By checking the installation, it was realized that: there was misalignment due to the bending of the drive shaft during the removing of thrust and pre-packed grease lubricated bearings. Also the flexible couplings mounting the torque meter were not machined properly and they were off centre. The outer case of the coupling was machined and new bushes were put in the coupling which reduced vibration considerably. There is still some vibration in the test rig at speeds greater than 5000 rpm. These vibrations were transferred to the main building structure. In order to avoid this it was necessary to change the present isolator to a better type of isolation or decrease the misalignment in the shaft (the main frequency produced at worse condition is frequency of shaft rotation, see Fig. (47). Fig. (43) shows the progress chart of investigations and maintenance which were carried out. By changing the isolation the vibrations which were transferred to the building were reduced considerably.

By changing the bearings, parasitic torque absorption was reduced considerably more than 50%, see Table IV. Torque absorption in the bearings shows hysteresis with speed on Fig. (49). Higher torque absorption when the speed is reduced can be explained by considering that at high speed the temperature in the bearings is higher than at low speed.

Table IV. Torque Absorption in the Bearings

Speed Rev/min	New Design lb ft.	Old Design lb ft.	% reduction
2000	0.113	0.19	40
3000	0.13	0.22	41
4000	0.143	0.26	45
5000	0.152	0.325	53
6000	0.144	0.384	62
6500	0.129	0.39	67

APPENDIX IV

ERRORS

A-4-1 Shaft Speed Variation

Maximum error by assuming that counter is correct $\pm$ 1 count, is $\pm$ 3 rev/min at low speed (less than 3000 rpm) and $\pm$ 5 rpm at high speed. This error increases after new 2:1 step up pulleys.

A-4-2 Torque Meter

The static calibration shows that the accuracy claimed by the manufacturer was correct (less than 1% over the major part 0 - 15 lb ft). The estimated read-out error was about 0.005 lb ft (0.0068 Nm) for 0 -1.5 lb ft range and 0.0125 lb ft (0 - 0.017 Nm) for 0 - 5 lb ft range. Errors due to torque readings at low speed was doubtful because there is possibility of large error at the lower range of the torque rating. Dynamic calibration will be necessary to find out the actual error variation in the whole range of the torque meter.

A-4-3 Pressure Gauge

There were errors on pressure readings which can be classified as follows:

i - Error due to actual readings (ambiguity in reading the dial and pressure fluctuation) is about 1000 Nm^{-2} or 0.01 bar at low pressure (0.15% of full scale reading (6.9 bar)).

ii - Error due to temperature effect (the pressure gauge was calibrated at 20°C) is about 0.1% of full scale reading (6.9 bar) per 10°C change in ambient from 20°C. Maximum room temperature was about 28°C during the experiment.

iii - Error due to hysteresis (when the pressure falls) is about 0.1% of full scale reading (6.9 bar).

The pressure readings in most conditions (at low pressure) indicated that the total error due to all contributions is equal to

0.35% of full scale or about 0.025 bar, which is equivalent to $\pm$ 2.5 J/kg error. There was also an inaccuracy in vapour pressure which was calculated from empirical equation (A-6-13). By assuming that there is no decomposition in ethylene glycol it can be said that the maximum total error is not more than $\pm$ 4 J/kg at the range of our experiment (allowing 2% error due to empirical relation for vapour pressure).

A-4-4 Temperature Measurements

Errors on temperature readings can be classified in two categories.

i - Error due to actual reading is about $\pm$ 0.5°C.

ii - Error due to changing of temperature which is caused by hysteresis effect of thermostat is about $\pm$ 4°C. This error varies with duration time of experiment, but for an experiment with constant speed the temperature variation is max. $\pm$ 2°C.

APPENDIX V

COMPUTER PROGRAMME

The results were processed by using a short computer programme to calculate the dimensional and non-dimensional coefficients and plot the head/flow curves at various speeds, by reading the flow rate, inlet pressure, discharge pressure and torque.

```
0001                  LIST(LP)
0002                  LIBRARY(ED,SUBGROUPSRGP)
0003                  LIBRARY(SUBGROUPS-RS)
0004                  PROGRAM(F1716)
0005                  INPUT 1=CRD
0006                  OUTPUT 2=LPD
0007                  COMPACT DATA
0008                  COMPRESS INTEGER AND LOGICAL
0009                  TRACE
0010                  END



0011                  MASTER PUMP CHARACTERISTIC
0012                  DIMENSION B(20),D(20),E(20),EE(20),P(20),R(20),S(20),TE(20),U(20),
0013                 1V(20),W(20),Z(20)
0014                  REAL M,NPSE
0015                3 FORMAT(1H1,42X,'DIMENSIONAL KENT , PUMP CHARACTERISTIC',/)
0016                4 FORMAT(32X,'SPEED=',F10.5,5X,'TEMP=',F10.5,5X,'RHO=',F10.5/)
0017                5 FORMAT(11X,'CAPACITY',7X,'SPECIFIC ENERGY',9X,'NPSE',14X,'POWER',8
0018                 1X,'WATER POWER',7X,'EFFICIENCY',/)
0019                6 FORMAT(9X,6(F12.6,6X)/)
0020                7 FORMAT(120(1H-))
0021                8 FORMAT(5X,'CAPACITY',12X,'PI',14X,'PSI',13X,'PLANDA',11X,'ZIGMA',8
0022                 1X,'SHAPE NUMBER',5X,'CAVITATION NO',/)
0023                9 FORMAT(3X,7(F12.6,5X)/)
0024               10 FORMAT(1H1,40X,'NON DIMENSIONAL KENT  PUMP CHARACTERISTIC',/)
0025               11 FORMAT(1H0,38X,'ETHYLENE GLYCOL / WATER MIXTURE 50%OF EACH',/)
0026                  DIMENSION TN(2),XT1(2),YT1(3),XT2(4),YT2(4)
0027                  DATA TN(1)/12HPUMPCHARTAPE/
0028                  CALL LGPCONT (TN,1,0)
0029                  DO 1000 JH=1,2
0030                  DATA XT1(1)/16HCAPACITY LIT/MIN/,YT1(1)/24HSPECIFIC ENERGY  J/KG
0031                 1 /
0032                  DATA XT2(1)/32HFLOW  COEFFICIENT   Q/SPEED**3*D/,
0033                 1YT2(1)/32HHEAD COEFFICIENT Y/SPEED**2*D**2/
0034                  IF(JH,EQ,1) GO TO 16
0035                  IF(JH,EQ,2) GO TO 13
0036               C  **** DRAW AXIS
0037               16 CALL LGP5A(0.,250.,0.,240.,25.,24.,XT1,2,YT1,3,0)
0038                  GO TO 112
0039               13 CALL LGP5A(0.,0.05,0.,0.96,25.,24.,XT2,4,YT2,4,0)
0040               12 FORMAT(I10)
0041               112 READ(1,12)K
0042                  DO 100 IZ=1,K
0043               101 FORMAT(I10,4F0.0)
0044                  READ(1,101)N,SPEED,T,RHO,PV
0045                  IF(JH,EQ,2) GO TO 14
0046                  WRITE(2,5)
0047                  WRITE(2,11)
0048                  WRITE(2,7)
0049                  WRITE(2,4)SPEED,T,RHO
0050                  WRITE(2,5)
0051                  WRITE(2,7)
0052               14 READ(1,201)(B(J),D(J),E(J),EE(J),J=1,16)
0053                  DO200 IT=1,N
0054                  Q=B(IT)
0055                  PS=D(IT)
0056                  PD=E(IT)
0057                  N=EE(IT)
```

```
0058          201  FORMAT(64F0.0)
0059          C    ***** CALCULATE DIMENSIONAL & NONDIMENSIONAL VARIABLES
0060          C    **** DIA OF IMPELLER =0.057 METER
0061               M=M*0.974206
0062               Y=(PD-PS)*10.**5/RHO-0.0001404*Q**2
0063               POWER=0.14190916*M*SPEED
0064               PW=RHO*Q*Y/60000.
0065               EFF=PW/POWER*100.
0066               FI=0.4056597*Q/(0.57**3*SPEED)
0067               PSI=750.2527484*Y/(0.057**2*SPEED**2)
0068               PLANDA=POWER/(0.057**5*SPEED**3)*216000./RHO
0069               NPSE=10.**5*(PS-PV)/RHO+2.*Q**2/(3.14**2*3.01625**4*9.)
0070               ZIGMA=NPSE/Y
0071               IF(Q.EQ.0.0) GO TO 111
0072               CAV=NPSE/(2.*Q**2/(3.14**2*3.01625**4*9.))
0073          111  IF(Q.EQ.0.0) CAV=1000.
0074               SHAPE=SPEED/60.*SQRT(Q/60000.)/(Y**(3./4.))*1000.
0075               IF(JH.EQ.2) GO TO 15
0076               WRITE(2,6)Q,Y,NPSE,POWER,PW,EFF
0077           15  R(IT)=FI
0078               S(IT)=PSI
0079               P(IT)=Q
0080               Z(IT)=Y
0081               TE(IT)=PLANDA
0082               U(IT)=ZIGMA
0083               V(IT)=SHAPE
0084               W(IT)=CAV
0085          200  CONTINUE
0086          C    ****   PLOT GRAPHS OF;
0087          C                              HEAD VS FLOW DIMENSIONAL FORM
0088          C                              PSI VS FI NON DIMENSIONAL FORM
0089               CALL FARPLOT(P,Z,R,S,SPEED,N,JH,K,T)
0090               IF(JH.EQ.2) GO TO 100
0091               WRITE(2,10)
0092               WRITE(2,11)
0093               WRITE(2,7)
0094               WRITE(2,4)SPEED,T,RHO
0095               WRITE(2,8)
0096               WRITE(2,7)
0097               WRITE(2,9)(P(IT),R(IT),S(IT),TE(IT),U(IT),V(IT),W(IT),IT=1,N)
0098          100  CONTINUE
0099          1000 CONTINUE
0100               CALL LGP2
0101               STOP
0102               END
```

```
0103                SUBROUTINE FARPLOT(P,Z,R,S,SPEED,N,JH,X,T)
0104                DIMENSION T(2),P(N),Z(N),XT1(2),YT1(3)
0105                DIMENSION R(N),S(N),XT2(4),YT2(4)
0106                DATA CHAR1/1H*/,CHAR2/1HX/,CHAR3/1H@/,CHAR4/1H#/,CHAR5/1H+/,
0107               1CHAR6/1H£/,CHAR7/1H0/,CHAR8/1H&/,CHAR9/1HQ/,CHAR10/1HD/,CHAR11/1HG
0108               2/
0109                IF(JH.EQ.2) GO TO 1500
0110                IF(SPEED.LT.1501.) GO TO 1001
0111                IF(SPEED.LT.2001.) GO TO 1002
0112                IF(SPEED.LT.2501.) GO TO 1003
0113                IF(SPEED.LT.3001.) GO TO 1004
0114                IF(SPEED.LT.3501.) GO TO 1005
0115                IF(SPEED.LT.4001.) GO TO 1006
0116                IF(SPEED.LT.4501.) GO TO 1007
0117                IF(SPEED.LT.5001.) GO TO 1008
0118                IF(SPEED.LT.5501.) GO TO 1009
0119                IF(SPEED.LT.6001.) GO TO 1010
0120                IF(SPEED.LT.6501.) GO TO 1011
0121           1001 CALL LGP6B(P,Z,N,CHAR1)
0122                GO TO 3000
0123           1002 CALL LGP6B(P,Z,N,CHAR2)
0124                GO TO 3000
0125           1003 CALL LGP6B(P,Z,N,CHAR3)
0126                GO TO 3000
0127           1004 CALL LGP6B(P,Z,N,CHAR4)
0128                GO TO 3000
0129           1005 CALL LGP6B(P,Z,N,CHAR5)
0130                GO TO 3000
0131           1006 CALL LGP6B(P,Z,N,CHAR6)
0132                GO TO 3000
0133           1007 CALL LGP6B(P,Z,N,CHAR7)
0134                GO TO 3000
0135           1008 CALL LGP6B(P,Z,N,CHAR8)
0136                GO TO 3000
0137           1009 CALL LGP6B(P,Z,N,CHAR9)
0138                GO TO 3000
0139           1010 CALL LGP6B(P,Z,N,CHAR10)
0140                GO TO 3000
0141           1011 CALL LGP6B(P,Z,N,CHAR11)
0142                IF(JH.EQ.1) GO TO 3000
0143           1500 IF(SPEED.LT.1501.) GO TO 2001
0144                IF(SPEED.LT.2001.) GO TO 2002
0145                IF(SPEED.LT.2501.) GO TO 2003
0146                IF(SPEED.LT.3001.) GO TO 2004
0147                IF(SPEED.LT.3501.) GO TO 2005
0148                IF(SPEED.LT.4001.) GO TO 2006
0149                IF(SPEED.LT.4501.) GO TO 2007

0150                IF(SPEED.LT.5001.) GO TO 2008
0151                IF(SPEED.LT.5501.) GO TO 2009
0152                IF(SPEED.LT.6001.) GO TO 2010
0153                IF(SPEED.LT.6501.) GO TO 2011
0154           2001 CALL LGP6B(R,S,N,CHAR1)
0155                GO TO 3000
0156           2002 CALL LGP6B(R,S,N,CHAR2)
0157                GO TO 3000
0158           2003 CALL LGP6B(R,S,N,CHAR3)
0159                GO TO 3000
0160           2004 CALL LGP6B(R,S,N,CHAR4)
0161                GO TO 3000
0162           2005 CALL LGP6B(R,S,N,CHAR5)
0163                GO TO 3000
0164           2006 CALL LGP6B(R,S,N,CHAR6)
0165                GO TO 3000
0166           2007 CALL LGP6B(R,S,N,CHAR7)
0167                GO TO 3000
0168           2008 CALL LGP6B(R,S,N,CHAR8)
0169                GO TO 3000
0170           2009 CALL LGP6B(R,S,N,CHAR9)
0171                GO TO 3000
0172           2010 CALL LGP6B(R,S,N,CHAR10)
0173                GO TO 3000
0174           2011 CALL LGP6B(R,S,N,CHAR11)
0175           3000 RETURN
0176                END

END OF SEGMENT, LENGTH   540, NAME  FARPLOT
```

APPENDIX VI

PHYSICAL PROPERTIES OF E.G/W.

Variation of density and vapour pressure versus temperature in various concentrations of ethylene-glycol/water mixture is shown in Figs. (50-51). Fig. (52) illustrates the ethylene glycol's latent heat of vaporization versus temperature.

There is little information available about vapour phase data. It is possible to find out the latent heat of vaporization of ethylene-glycol/water mixture, by assuming that the mixture is homogeneous. By using the Clapeyron equation[93] one can calculate the specific volume of vapour of the ethylene-glycol/water mixture.

$$C_p = \left[C_{30} + a\,(T - 30) \right] 4.1868 \qquad 30 < T < 130$$

A6-1

where C_p is specific heat of the ethylene-glycol/water mixture kJ/kg deg K

T is temperature in ^{o}C

C_{30} and a are constants, Fig. (53) shows the specific heat value of the mixture versus temperature[94].

Denoting h_{fm} as the enthalpy of the fluid mixture, the additional enthalpy introduced by the liquid-vapour phase change is:

$$h_{fgm} = X\,h_{fgG} + (1-X)\,h_{fgW} \qquad \text{A6-2}$$

where X is mole fraction of glycol in the mixture

h_{fgm} is latent heat of vaporization of mixture kJ/kg

h_{fgG} is latent heat of vaporization of glycol kJ/kg

h_{fgW} is latent heat of vaporization of water kJ/kg

Now enthalpy of vapour is equal to

$$h_{gm} = h_{fgm} + h_{fm} \qquad \text{A6-3}$$

where h_{gm} is enthalpy of vapour mixture.

By using the Clapeyron equation:

$$v_{fgm} = v_{gm} - v_{fm} \qquad \text{A6-4}$$

$$v_{fgm} = \frac{h_{fgm}}{T_{sat} \times \frac{dp_v}{dT_{sat}}} \qquad \text{A6-5}$$

where v_{fm} is specific volume of fluid mixture
v_{gm} is specific volume of vapour mixture
v_{fgm} is difference of specific volume of vapour and liquid in the mixture
p_v is vapour pressure N/m^2
T_{sat} is absolute saturation temperature ^oK

Above assumption is applicable only for homogeneous and ideal solution. An ideal solution is defined by complete uniformity of cohesive forces. The partial vapour pressure of a component (A) in a solution is related to the chemical potential E_A. Consider a solution in equilibrium with its vapour. At equilibrium we have

$$E_A^{soln} = E_A^{vapour}$$

$$E_B^{soln} = E_B^{vapour}$$

A solution is said to be ideal if the escaping tendency of each component is proportional to the mole fraction of that component in a solution[95]. The definition of ideality implies that a molecule of A in the solution will have the same tendency to escape into the vapour whether it is surrounded entirely by other A molecules, entirely by B molecules, or partly by A and partly by B molecules. The escaping tendency of component A from such an ideal solution, as measured by its partial vapour pressure, is accordingly the same as that from pure liquid A, except that it is proportionately reduced on account of the

lowered fraction of A molecules in the solution (Raoult Law).

$$p_{vA} = X_A \, p^o_{vA} \qquad \text{A6-6}$$

where p_{vA} is the partial vapour pressure of A above a solution

X_A is the mole fraction of A in the solution

p^o_{vA} is the vapour pressure of pure liquid A

So we can write

$$p_{vm} = X'_A \, p^o_{vA} + (1 - X'_A) p^o_{vB} \qquad \text{A6-7}$$

where p_{vm} is total vapour pressure of mixture

p^o_{vB} is the vapour pressure of pure fluid B

It is possible to use Clapeyron's equation to find the vapour pressure for a pure fluid or an ideal solution. For a pure fluid we have

$$\frac{dp_v}{dT_{sat}} = \frac{h_{fg}}{T_{sat} \times v_{fg}} \qquad \text{A6-8}$$

By assuming that vapour specific volume is much bigger than fluid specific volume ($v_g >> v_f$) we can write

$$v_{gf} \simeq v_g \qquad \text{A6-9}$$

By assuming that vapour is an ideal gas we can transform the equation A6-8 (when vapour is steam and superheated throughout the process, the approximation is very close to actual behaviour)[93] to

$$\frac{d \ln p_v}{d T_{sat}} = \frac{h_{fg}}{R T^2_{sat}} \qquad \text{A6-10}$$

or Eq. A6-10 may be written as

$$d\text{Ln}p_v = -\frac{h_{fg}}{R} d\left(\frac{1}{T_{sat}}\right) \qquad \text{A6-11}$$

By assuming that h_{fg} is constant we can write:

(see Fig. 52 for variation of h_{fg} in water and glycol)

$$\text{Ln}p_v = -\frac{h_{fg}}{R} \times \frac{1}{T_{sat}} + C \qquad \text{A6-12}$$

where C is an integration constant.

By using the equation A6-12 for pure fluid, it is possible to find an equation for the mixture with above properties. So by considering that EG/W obeys Raoult's law fairly closely,[21] we can write for EG/W

$$\text{Log}_{10} p_{vm} = A - \frac{C}{T_{sat}} \qquad \text{A6-13}$$

where A and C are constant. A and C were found by Trimble[21] et al and they deduced a set of equations for various concentrations. In their equations the magnitude of p_{vm} was calculated in mm of Hg. From Equation A6-13 by differentiating with respect to T_{sat} one obtains

$$\frac{dp_v}{dT_{sat}} = p_v \times \frac{C}{T_{sat}^2} \times \text{Log}_e 10 \qquad \text{A6-14}$$

Fig. (54) shows the variation of A and C.

By using Equations A6-(4,5,13,14) it is possible to calculate the value of a specific volume of vapour mixture.

Viscosity of ethylene glycol water mixture can be calculated[68]

$$\eta = A\, e^{B'/T} \qquad \text{A6-15}$$

Where A and B are constant, value of A and B can be calculated by knowing two values of viscosity at different temperatures. Fig. (55) shows the viscosity variation of E.G/W mixture at various concentrations.

Thermal conductivity of pure ethylene glycol can be estimated from equation[18].

$$k_G = 0.30354 - 7.53624 \times 10^{-5} \times t \qquad \text{A6-16}$$

where t is temperature in ^{o}C

k_G is thermal conductivity of glycol $Wm^{-1}\ {}^{o}K^{-1}$

For a mixture of E.G and water one can use the following equations[96].

$$k_{mix} = k_w \bar{X}_w + k_G \bar{X}_G - (k_G - k_w)(1 - \bar{X}_G)\ \bar{X}_G \qquad \text{A6-17}$$

where $\bar{X}_i$ is weight fraction.

Fig. (56) shows the variation of thermal conductivity for various concentrations of E.G/W mixtures at different temperatures. Thermal conductivity of E.G decreases with the temperature as water's increases with temperature. So that in car cooling system the maximum concentration of E.G/W mixture is desirable to be less than 50%. (In this percentage thermal conductivity is almost constant). More than 50% of E.G in water reduces the thermal conductivity, i.e. heat transmission capacity of coolant at high temperature.

Fig. (57) shows the diffusion coefficient of E.G. in water at various temperatures, by using the Othmer and Thakar's nomograph.[68]

APPENDIX VII

REFERENCES

1. LORD MONTAGU "A History of Ten Years of Automobilism" The car illustrated Ltd. London 1906.

2. K. NEWTON, W. STEEDS "The motor vehicles' Iliffe & Sons Ltd.

3. F. STRICKLAND, "A Manual of petrol motors and motor cars". Charles Griffin & Co. Ltd. 1907.

4. "DYKEIS AUTOMOBILE AND GASOLINE ENGINE Encyclopedia" A.L. Dykeis & Pub. 1918.

5. "Some points relating to water cooling" The Automobile Engineer, 1910-1911, p.343-345.

6. WOLSELY INSTRUCTION MANUAL 1902.

7. R. KENNEDI "The Book of Motor Cars" Vol. II Caxton Publishing Co. Ltd. 1922.

8. Motor News, January 1903. Vol. IV. No. I.

9. Cyclopedia of Automobile Engineering Chicago, American Technical Society 1913.

10. C.S. STEADMAN "Automobile Cooling and its Associated Problems" The Proc. of Inst. of Automobile Engineers 1938-1939.

11. C.J.D. CARRUTHERS "Motor Vehicles in Hot Countries" Proc. of Inst. Mech. Eng. Automobile Div. 1951-1952.

12. "The Wolsely Car and Its Mechanism" The Motor News, Nov. 1901, Vol. II No.13.

13. A. FORR "The Darracq and its Management" Liverpool, The School of Motoring, 1905.

14. C.N. MOORE, H.L. HOHENSTEIN & E. GEHRES. "Heat transfer and Engine Cooling Aluminium vs. Cast Iron" S.A.E. Paper No. 494A March 1962.

15. S.R.G. TAYLOR "Cooling system" Automobile Engineer, April, May, June, 1970.

16. B.W. MILLINGTON & H.W. BARNESS-MOSS "Diesel Enginess for Commercial Vehicles" Commercial vehicles engineering and operation conference, Inst. of Mech. Eng. London 1967.

17. C.D. DURKIN & G.G. LEVY "Engine Coolants Corrosion and Cooling System Design" S.A.E. Paper 660B.

18. G.O. CURME, F. JOHNSTON "Glycols" Reinhold Pub. Corporation, A.C.S monograph series 1953.

19. A.F. GALLAUGHER, H. HIBBERT "Studies on reactions relating to carbohydrates and polysaccharides - vapour pressures of the polyethylene glycols and their derivatives". J. Am. Chem. Society 59, 2514 (1937).

20. H.H. COLLINS, & R.I. HIGGINS "The Corrosion of road vehicles engines by anti-freeze solution - 2" Corrosion Rev. and Control 1960 Vol.7 (3) Page 41-48.

21. H.M. TRIMBLE & W. POTTS "Glycol water mixtures, vapour pressure - boiling point. Composition relations" Ind. Eng. Chem., Vol.27 No. 1 Jan 1935, 66-68.

22. B.S. 3150-2 "Corrosion - Inhibited Ethanediol Antifreeze for water-cooled Engines".

23. A.D. MERCER "Corrosion Inhibition" Corrosion & Protection at the NPL, N.P.L. Pub.

24. L.C. ROWE "An evaluation of Inhibitors for Corrosion Prevention in an engine cooling system" Corrosion Vol.13, 1957, p.750t-756t.

25. H. BAUR "Prevention of Cavitation Corrosion on the German Federal Railway" Symp. on Cavitation Corrosion and its prevention in Diesel Engines" 10th Nov. 1956, organized Brit. Rail. Chem. Res. Div.

26. J.A. JOYNER "Reduction of Cavitation Pitting of diesel engine cylinder liner" Trans. S.A.E., Vol.65, p.337-348.

27. H.J. HANNIGAN "Coolant Performance at Higher Temperatures" S.A.E. 680497.

28. D.F. CARIS & E.E. NELSON "Where does all power go" Symposium of Papers, S.A.E. Meeting. Atlantic City, June 1956, S.A.E. Fourn. 65 (1957).

29. C.F. TAYLOR "The internal combustion engine in theory and practise" Pub. M.I.T. Press 2nd edition 1966.

30. W.E. DRINKARD AND M.L. CARPENTIER "Development Highlights and Unique Features of Chrysler V-8 Engine" Presented at S.A.E. Meeting, March 1951.

31. J.D. MORSE "Engine Cooling Radiator" S.A.E. paper 670525.

32. A.W. JUDGE "Automobile Engines" Motor manual 8th ed. Chapman & Hall 1972.

33. F. LUSTMERCK, R. BATSON "New light-weight design copper and brass radiator performance compared with production radiators" S.A.E. paper No. 720012 1972.

34. E.N. HARVEY, W.D. MCELORY & A.H. WHITELEY "On cavity formation in water" J. Appl. Phys. 18, 162-172, 1947.

35. M.S. PLESSET "The tensile strength of liquids" Cavitation state of knowledge ASME 1969.

36. I.S. PEARSALL & E.A. SPENCER "Cavitation" Science Journal May 1966.

37. P. JARMAN "Measurement of sonoluminescence from pure liquids and some aqueous solutions" Proc. Phys. Soc. 73, 628, 1959.

38. W.H. WHEELER "Indentation of metal by cavitation" ASME. Trans. Series D, 82, 184-194, 1960.

39. M. HARRISON "Experimental study of single bubble cavitation noise" J. Acoust. Soc. Amer. 24, p.776. 1952.

40. M.S. PLESSET "Bubble Dynamics" Dept. of the Navy Report No.85-23 Pasadena, C.I.T. Feb. 1967.

41. J.W. HOLL "Limited Cavitation" Cavitation state of knowledge, ASME, 1969.

42. J.W. DAILY & V.E. JOHNSON JR. "Turbulence and Boundary-layer Effects on Cavitation Inception from Gas Nuclei" Trans. ASME Vol.78 1956.

43. J.W. HOLL "An effect of Air Content on the occurrence of Cavitation" Journal of Basic Engineering Trans. ASME Series D, Vol.82 941-946 1960.

44. R.W. FURNESS "Basic Cavitation Studies in a Converging-Diverging Nozzle" Ph.D. Thesis, University of Southampton, Dept. of Mech. Engineering, March 1973.

45. G.F. WISLICENUS "Fluid Mechanics of Turbomachinery" Vol.I, Dover Pub. 1965.

46. R.T. KNAPP, J.W. DAILY & F.G. HAMMIT "Cavitation" McGraw-Hill Pub. Monographs Eng. Soc. 1970.

47. NUMACHI, F. "Cavitation Tests on Hydrofoils in Cascade" Trans. ASME, 75, pp.1257-1269, 1953.

48. I.S. PEARSALL "Cavitation" M & B Monographs, Mechanical Engineering 1972.

49. A.J. STEPANOFF "Pumps & Blowers" John Wiley & Sons Pub. 1965.

50. H.A. STHAL & A.J. STEPANOFF "Thermodynamic Aspects of Cavitation in Centrifugal pumps" Trans. ASME Volume 78, 1961.

51. W.A. SPRAKER "The Effects of fluid properties on cavitation in centrifugal pumps" ASME Paper No. 64-WA/FE-19.

52. T. WARD & M. SUTTON "A Review of the Literature on Cavitation in Centrifugal Pumps with Various Liquids" TN.892 B.H.R.A. Cranfield, April 1967.

53. T.C. CHIVERS "Temperature effects on cavitation in a centrifugal pump theory and experiment" Proc. Instn. Mech. Engrs. 1969-1970 Vol.184 Pt.1 No.1 .37-47.

54. T.C. CHIVERS "The Correlation of Cavitation in a Centrifugal Pump Theory and Experiment" Proc. Instn. Mech. Engrs. 1969-1970 Vol.184, Pt.1, No.2 p.48-68 1969-1970.

55. F.T. GELDER, R.S. RUGGERI, AND R.D. MOORE "Cavitation similarity considerations based on measured pressure and temperature depressions in cavitated regions of Freon-114." NASA TND-3309 1966.

56. R.D. MOORE & R.S. RUGGERI "Venturi scaling studies on thermodynamic effect of Developed Cavitation of Freon 114" NASA TNL-4387 1968.

57. R.D. MOORE & R.S. RUGGERI "Prediction of Thermodynamic Effects of Developed Cavitation based on Liquid Hydrogen and Freon 114 Data in scaled Venturi" NASA TND 4899 1968.

58. R.S. RUGGERI & R.D. MOORE "Method for prediction of pump cavitation performance for various liquids, liquid temperature, and rotative speeds" NASA TND-5292 1969.

59. F.G. HAMMITT, D.M. ERICSON, J.F. LAFFERTY & M.J. ROBINSON "Gas Content, Size, Temperature Effects on Cavitation Inception in a Venturi" ASME Paper 67-WA/FE-22, 1968.

60. A.J. STEPANOFF "Cavitation properties of liquids" Journal of Engineering for power ASME Paper No.64-WA/FE-14.

61. R.S. RUGGERI & R.D. MOORE "Incipient cavitation of ethyleneglycol in a tunnel venturi" NASA TND2722 March 1965.

62. M.S. PLESSET "Cavitation and cavitation damage" Report AD-760 719 Prepared for Office of Naval Research Calif. Inst. of Tech., March 1973.

63. R.W. WILSON "The Control of cavitation damage in diesel engines" Symp. on Cavitation, Corrosion and its prevention in diesel engines No. 10, 1965, organized by Brit. Rail. Chem. Res. Div.

64. J.H. PERRY "Chemical Engineer's Handbook" 4th ed. McGraw Hill Chemical Engineering Series - 1963.

65. BOROWITZ & BEISER "Essentials of Physics" Addison Wesley Publishing Company, 1967.

66. E.L. DOUGHERTY, JR. & H.G. DRICKAMER "Thermal diffusion and molecular motion in liquids" Journal of Phys. Chem. May 1955 Vol.59 p.443-449.

67. E.L. DOUGHERTY, J.R. & H.G. DRICKAMER "A Theory of thermal diffusion in liquids" The Journal of Chemical Physics, Vol.23, No.2 Feb. 1955, 295-309.

68. S. BRETSZNAJDER "Prediction of transport and other physical properties of fluids" Pergamon Press, 1971.

69. S.R. DE GROOT "Thermodynamics of Irreversible Processes" North-Holland Pub. Co. 4th ed. 1961.

70. KARLEIN, V. YA "Cavitation Phenomena in Centrifugal and Axial Flow Pumps" Translated by R.J. Dobble from the Russian edited by N.E.L., Pub. by N.E.L. 1965.

71. J.M. HOBBS, MISS A. LAIRD, BRUNTON, W.C. "Laboratory Evaluation of the Vibrating Cavitation Erosion Test" N.E.L. Report No.271, Jan. 1967.

72. J.M. HOBBS, Miss A. LAIRD. "Pressure, Temperature and Gas Content Effects in the Vibratory Cavitation Test" N.E.L. Report No.438, Oct. 1969.

73. J.M. HOBBS, MISS A.LAIRD, "Comparative Erosion Tests on Ferrous Materials. Part I: Vibratory Cavitation Tests". N.E.L. Report No. 495, Dec. 1971.

74. J.M. HOBBS, MISS A. LAIRD "Comparative Erosion Tests on Non-Ferrous Materials. Part II: Vibratory Cavitation Tests" N.E.L. Report No.496, Dec. 1971.

75. M.S. PLESSET "Pulsing Technique for Studying Cavitation Erosion of Metals". Corrosion, Vol.18, No.5, 181t-188t, May 1962.

76. M. MATSUMURA, Y. SUEZAWA, K. TSUDA "On the Time Dependence of the Rate of Erosion" Polyphase Flow Forum, ASME Publication, 1972.

77. J.B. CLARK "Cavitation-Erosion Damage Control in Aluminium Water Pumps for Cars" S.A.E. Paper No. 680498.

78. M.S. PLESSET "Temperature Effects in Cavitation Damage" ASME Paper No. 71-WA/FE.30.

79. W.C. LEITH & W.S. MCILQUHAM "Accelerated Cavitation Erosion and Sand Erosion" Symp. on Erosion and Cavitation pub. by ASTM No. 307, June 1961.

80. I.S. PEARSELL "Pump Test Circuits" Course Papers, Pump Testing Birniehill Institute, N.E.L. Paper No. 7, 2612 7th Oct. 1971.

81. Standards of the Hydraulic Institute, Hydraulic Institute, New York, 11th ed, 1965.

82. A.S.T.M. Standard Method of Tests for Cavitation Corrosion Characteristics of Aluminium Automotive Water Pumps with Coolants. Test Designation D2809-72, ASTM Part 22-1972.

83. A.S.T.M. Standard Method for Simulated Service Corrosion Testing of Engine Antifreezes. Test Designation D2570-70, ASTM Part 22-1972.

84. A.W. JUDGE "Modern Petrol Engines". Chapman & Hall Ltd., 1965.

85. "Cavitation Erosion in Diesels can be Reduced". S.A.E. Journal, 1957.

86. G. SCOBIE "Advances in Pumping Engineering" Unit Operational Review - Pumps. The Chemical Engineer, September 1972.

87. "Sundyne High Speed Centrifugal Pumps" Bulletin 133, Feb. 1967, Industrial Products Group, Sundstrand Corporation, Denver.

88. A.J. STEPANOFF "Centrifugal and Axial Flow Pumps" John Wiley & Sons, 2nd Ed. 1957.

89. M.G. SAUNDERS "An Investigation on the Hydrodynamic Disc Seals" M.Phil. Thesis, Dept. of Mech. Eng. Southampton Univ. 1968.

90. P.A.K. TAN & S.P. HUTTON "Experimental, analytical and tip clearance loss studies in turbine-type flow meter" Modern Developments in flow measurement, Proc. of the International Conf. held at Harwell, 21st-23rd Sept. 1971, pub. Peter Peregrinus Ltd.London 1972.

91. P.A.K. TAN "Theoretical and experimental studies of turbine flow meter" Ph.D. Tehsis, Dept. of Mech. Eng. Southampton Univ. Dec. 1973.

92. F.B. HOWARD "Aspects of the hydrodynamic disc seal development and performance" Ph.D. Thesis, Dept. of Mech. Eng., Southampton Univ. 1972.

93. ROGERS & MAYHEW "Engineering Thermodynamics Work and Heat Transfer" Longmans Pub. 2nd ed., 1967.

94. J.B. IRVING "Thermodynamic properties of ethylene-glycol" N.E.L. Private communication, July 1973.

95. W.J. MOORE "Physical Chemistry" Longmans Pub. 4th ed., 1966.

96. D.T. JAMIESON, J.B. IRVING "Thermal Conductivity of Binary Liquid Mixtures" N.E.L. Report No.567 Dept. of Industry July 1974.

97. S. LAZARKIEWICZ & A.T. TROKOLANSKI "Impeller Pump" Pergamon Press, Oxford 1965.

98. H.H. COLLINS & R.I. HIGGINS "The Corrosion of Road Vehicles Engines by Anti-freeze Solution". BCIRA Journal of Res. & Development, Vol.7, June 1959, No.12 p.667-691,

99. H. SCHLICHTING "Boundary-Layer Theory" 6th ed. McGraw Hill Book Company, 1968.

100. J.S. ANAND "The Effect of Aqueous Media Drag Reducers on the Performance of the Hydrodynamic Disc Seal" Ph.D. Thesis, Dept. of Mech. Eng., Southampton University, 1974.

101. T.G. HICKS & T.W. EDWARDS "Pump Application Engineering" 1971. McGraw Hill.

102. T.C. CHIVERS "The effect of fluid properties on cavitation in a centrifugal pump" Ph.D. Thesis, Mech. Eng. Dept. University College, Cardiff, 1967.

103. H.T. RUTTER "Modern motors, their construction, management and control" Vol.II 1926.

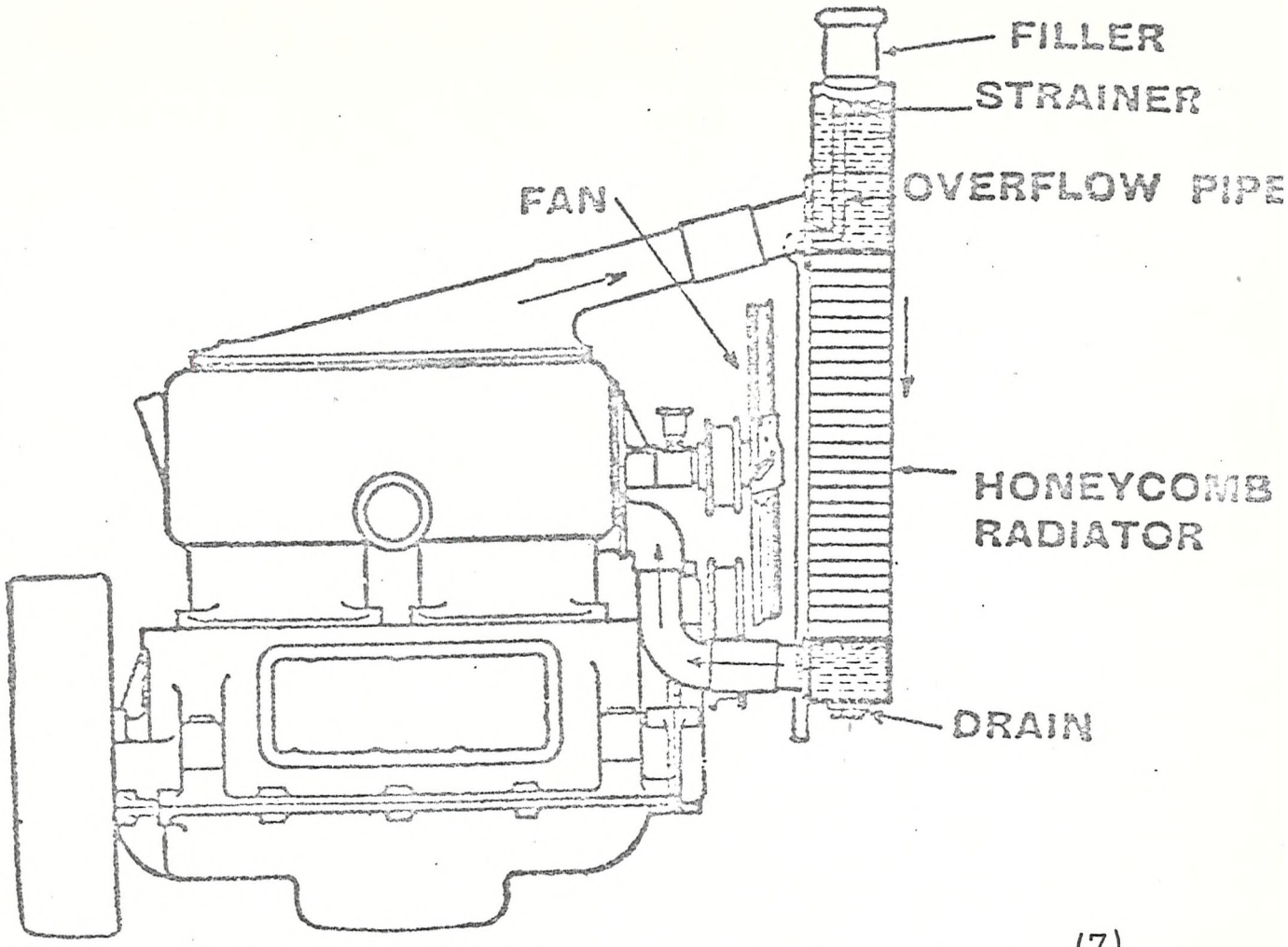

Fig.(1) —Thermo-syphon Cooling with Fan (7)

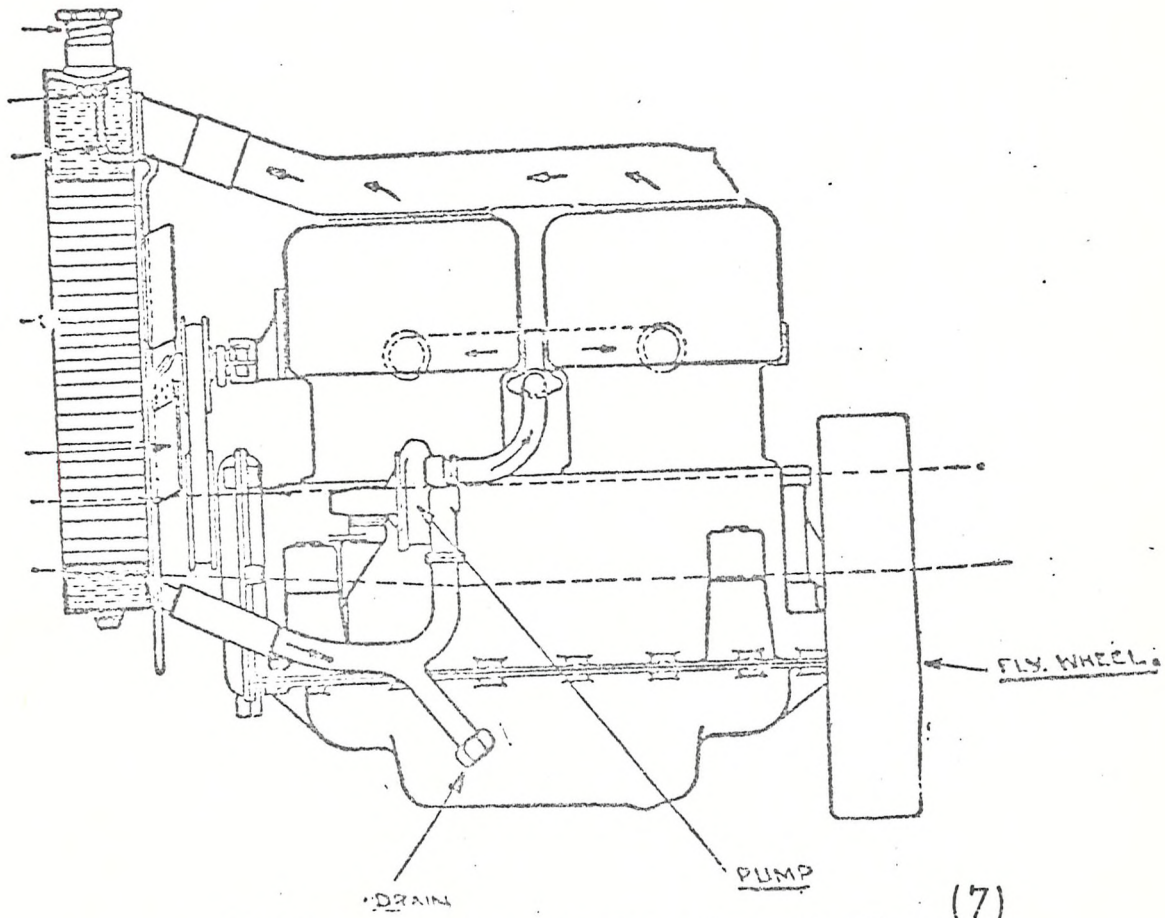

Fig. 2 —Cooling System in Connection with a Pump. (7)

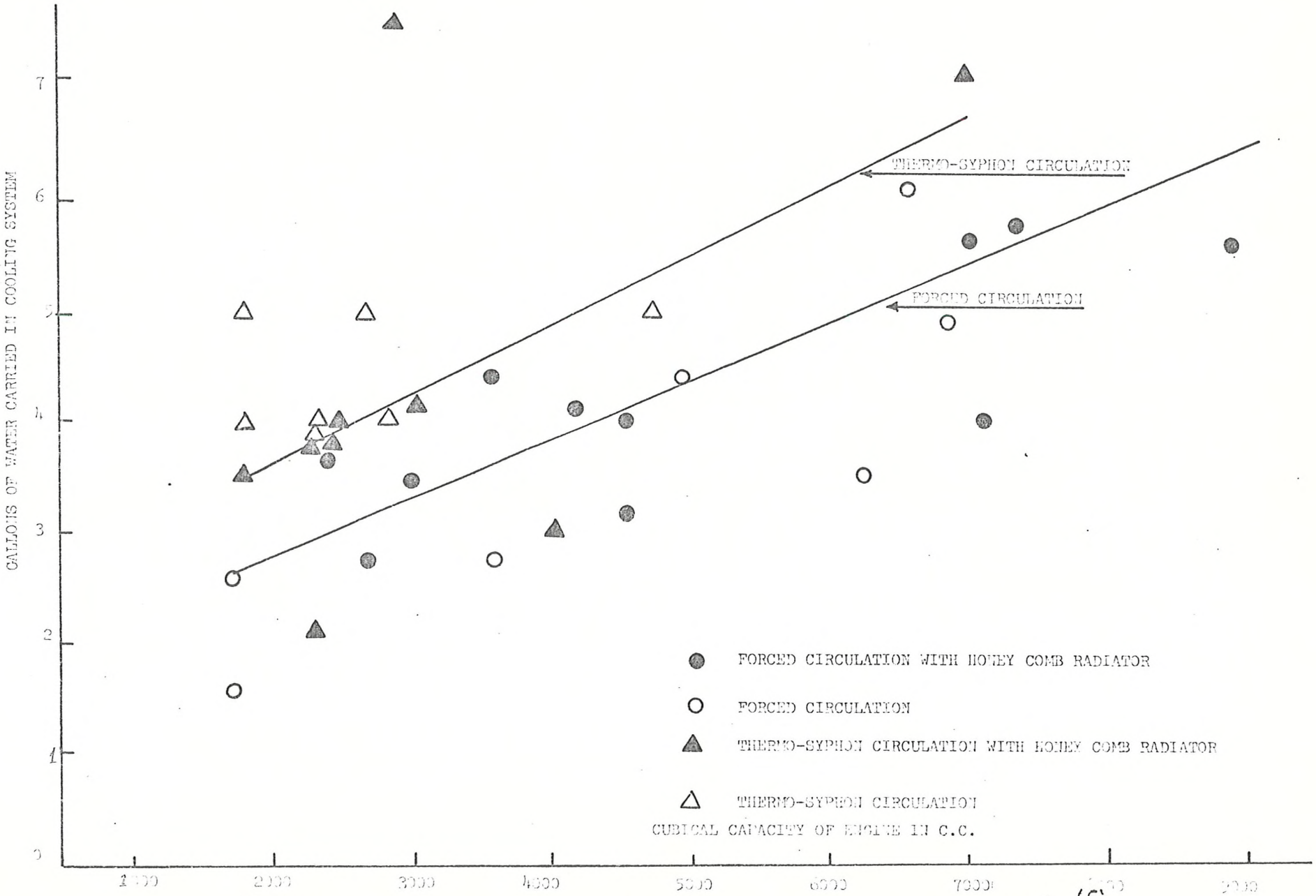

FIG.(3). SUGGESTED CURVES OF COOLING-WATER VOLUME FOR ENGINES OF VARYING CAPACITY (1911) 5:

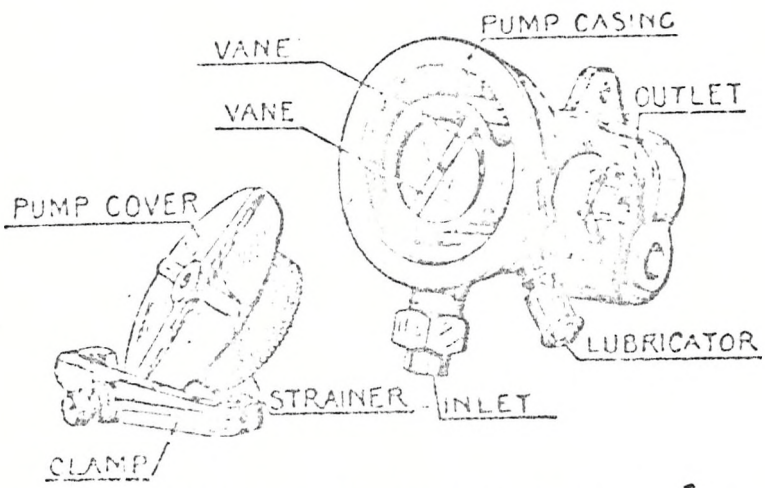

FIG.(4). ECCENTRIC POSITIVE THROW PUMP WITH STRAINER 6

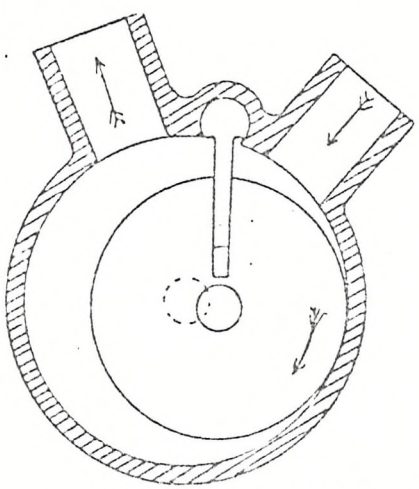

FIG.(5). ECCENTRIC POSITIVE THROW PUMP 3

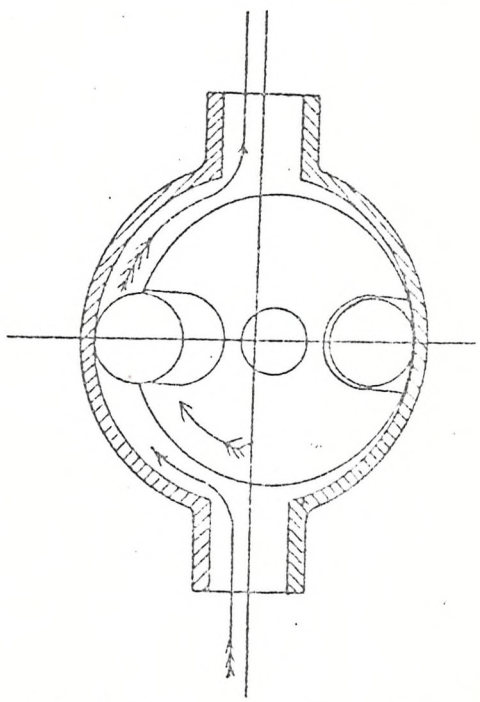

FIG.(6). ECCENTRIC POSITIVE THROW PUMP 3

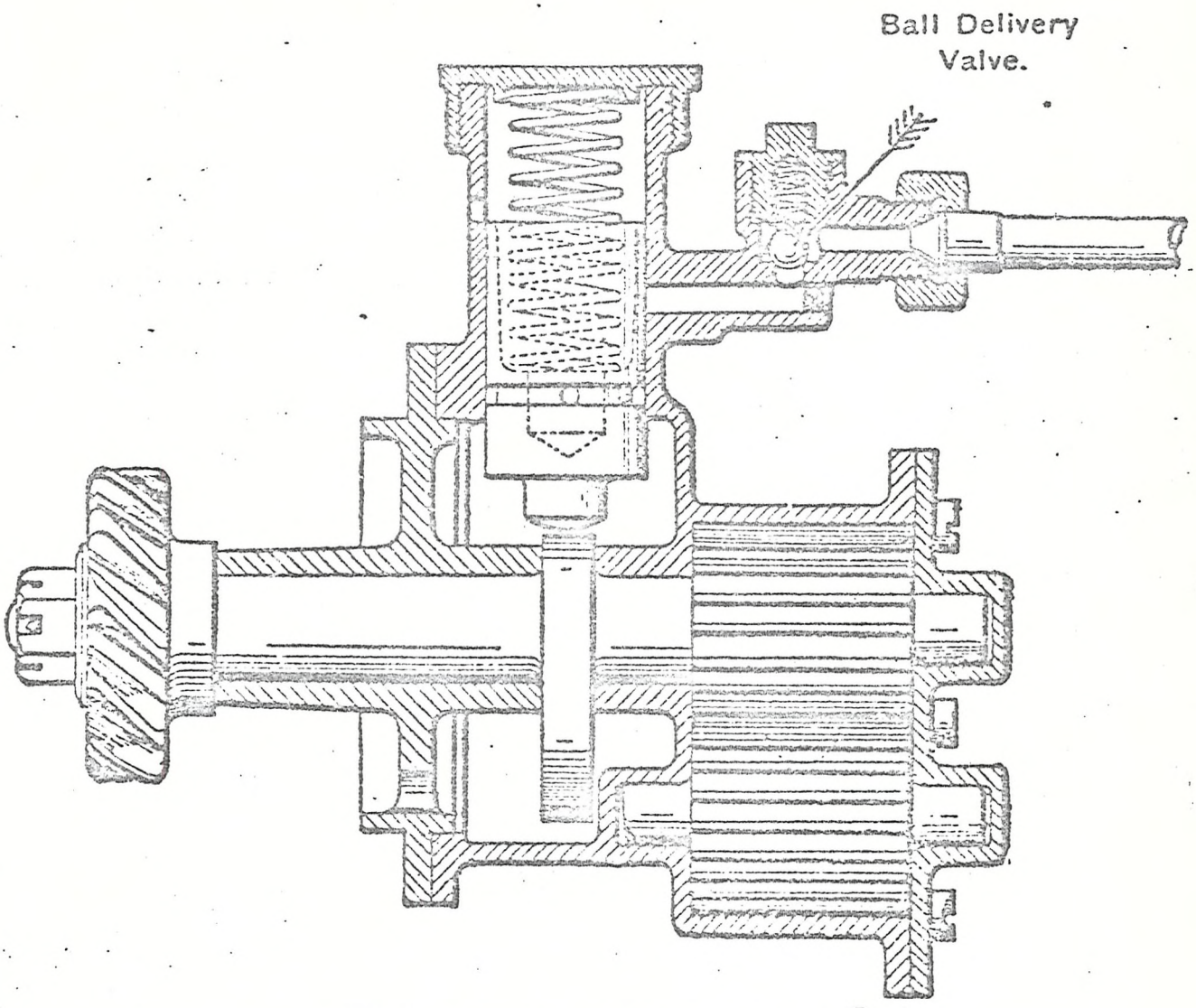

Fig. 7 —Gear Wheel Pump.

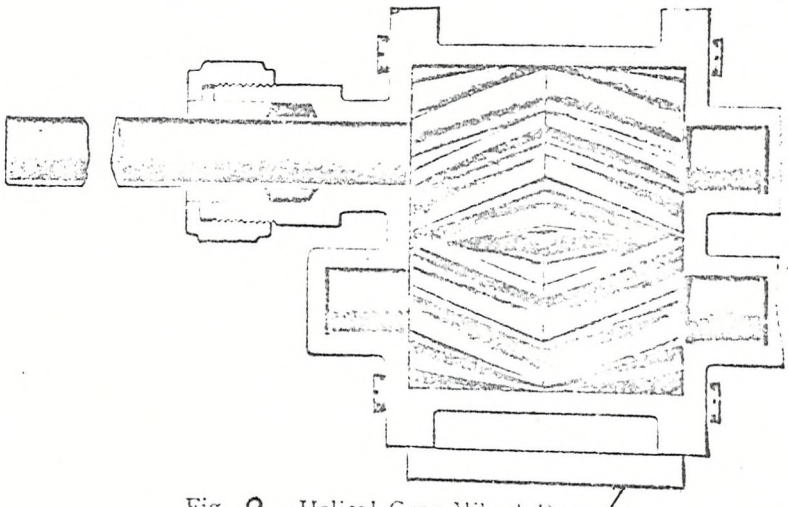

Fig. 8 —Helical Gear Wheel Pump.

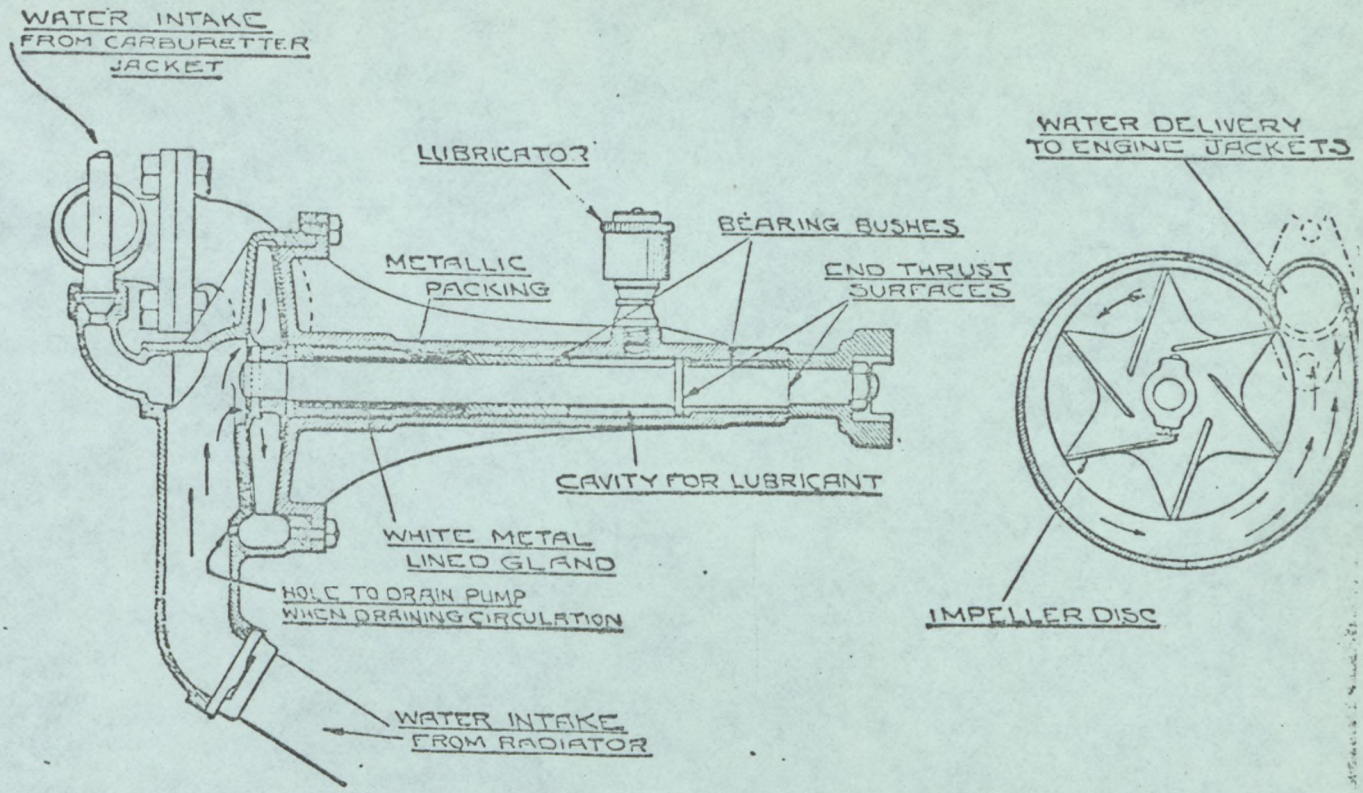

Fig. 9a.—Longitudinal Section of Pump.[7]

Fig. 9b—Section through Pump Impeller.[7]

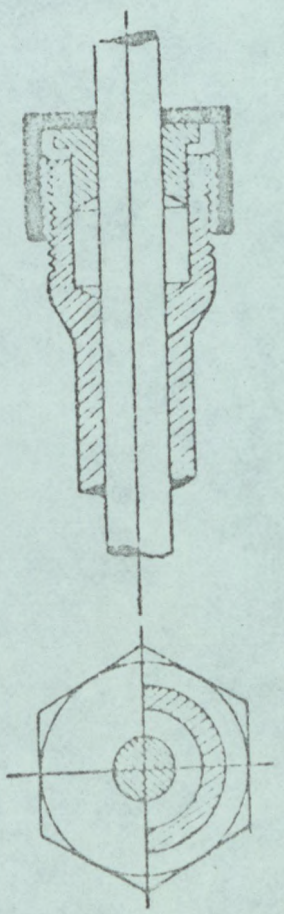

FIG(IO). STUFFING BOX [3]

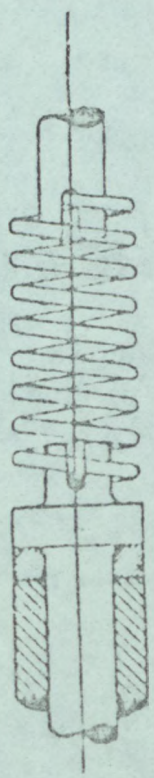

FIG(II). SPRING CONNECTION BETWEEN PUMP & DRIVE SHAFT [3]

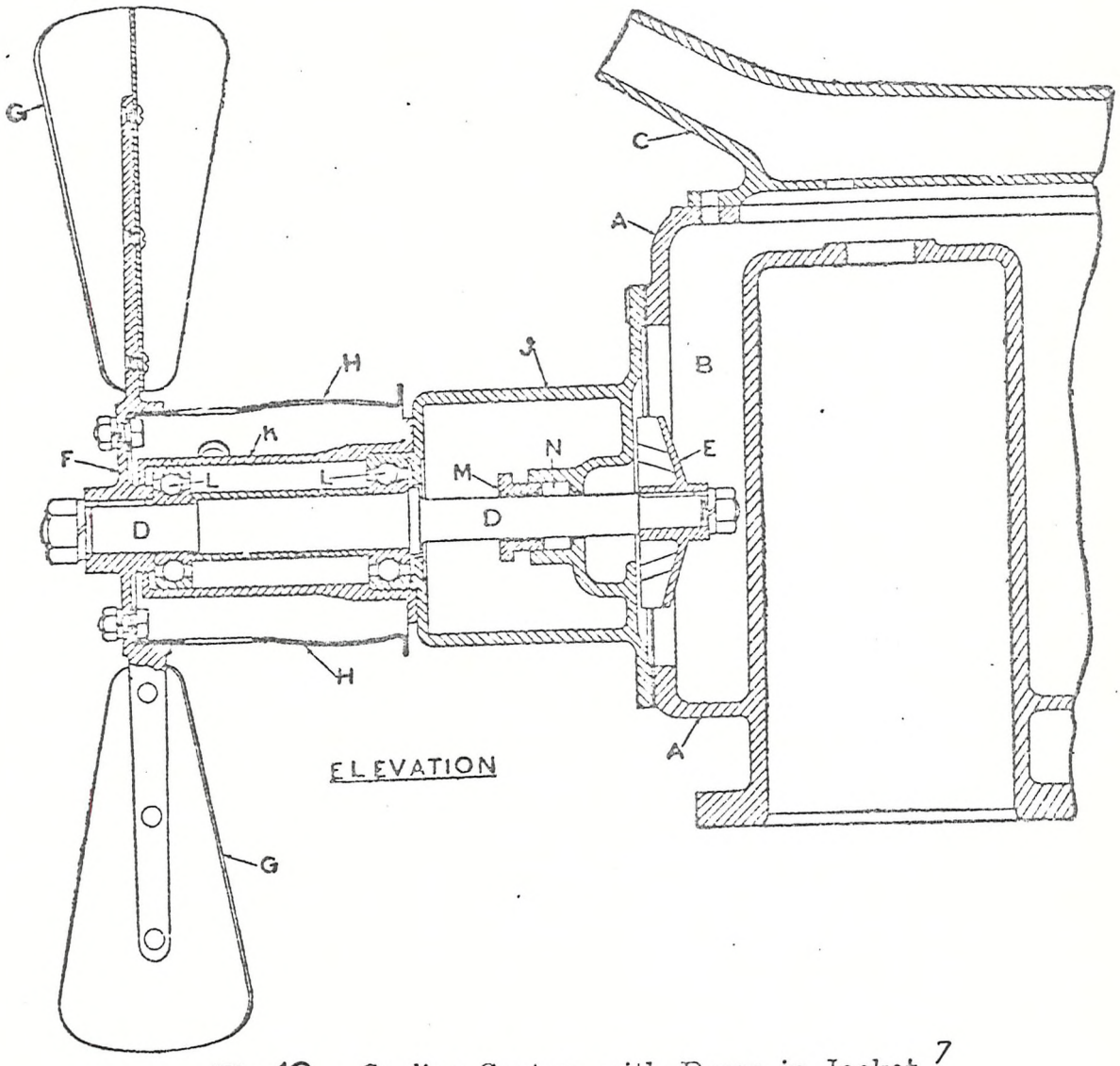

Fig. 12.—Cooling System with Pump in Jacket.[7]

A, CYLENDER WATER JACKET B,WATER SPACE C,WATER JACKET COVER D, PUMP&FAN SPINDLE E,PUMP WHEEL F,FAN SPIDER WITH ARMS G,FAN BLADES H,SMALL FAN PULLEY J,BRACKET ATTACHED TO WATER JACKET K,BRACKET FOR BALL BEARINGS L,OUTER & INNER BALL BEARINGS M, PACKING GLAND N, SPACE FOR PACKING.

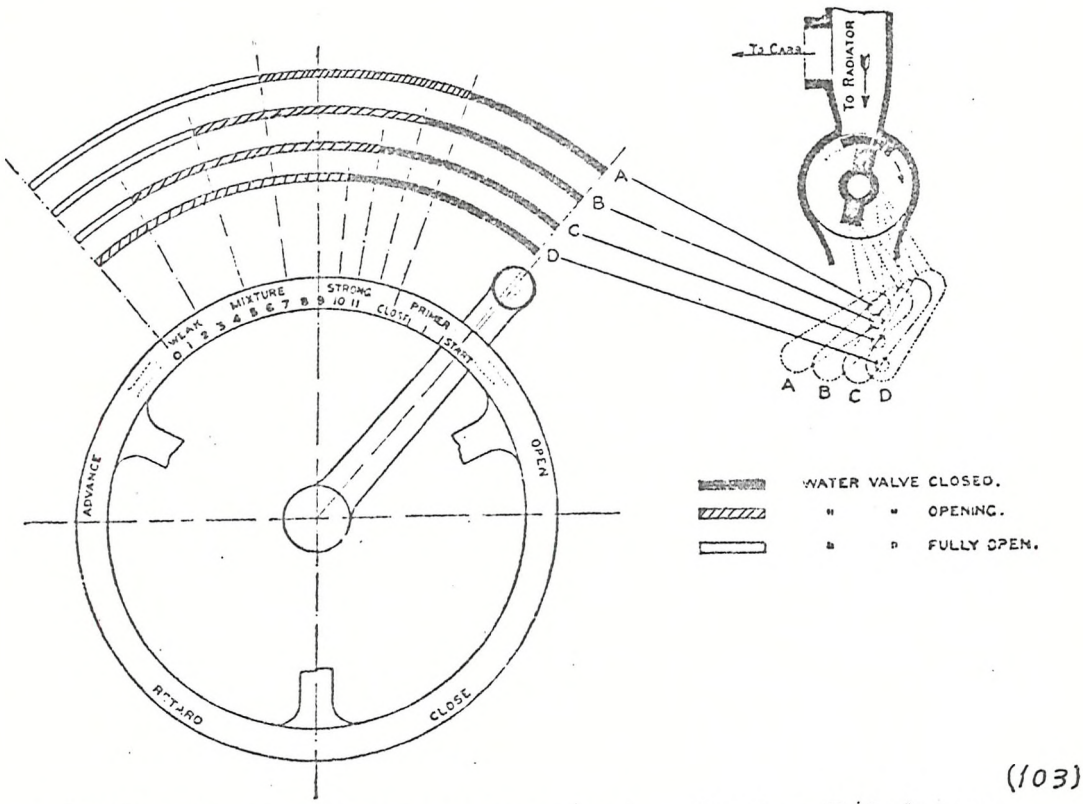

(103)

Fig. 13. — Diagram of water valve control, as fitted on Daimler cars.

his is coupled to the centre or mixture lever of the control on top of the steering wheel, the connections being so arranged that the water valve cuts out the radiator when the hand lever is set at the prima or starting position. Thus in this position the water circulation is confined to the circulating pump, engine, and carburettor only, and therefore very rapid warming of the carburettor jacket ensues, and so the fuel volatilises quicker. Movement of the mixture lever to the left first puts the prima of the carburettor out of action and thereafter gradually opens the water valve, thus allowing normal circulation of the water to take place by degrees, after its previous restriction. The black lines on A, B, C, and D show the position when the water valve is closed, the grey lines when the water valve is open, and the white space when the water valve is fully open.

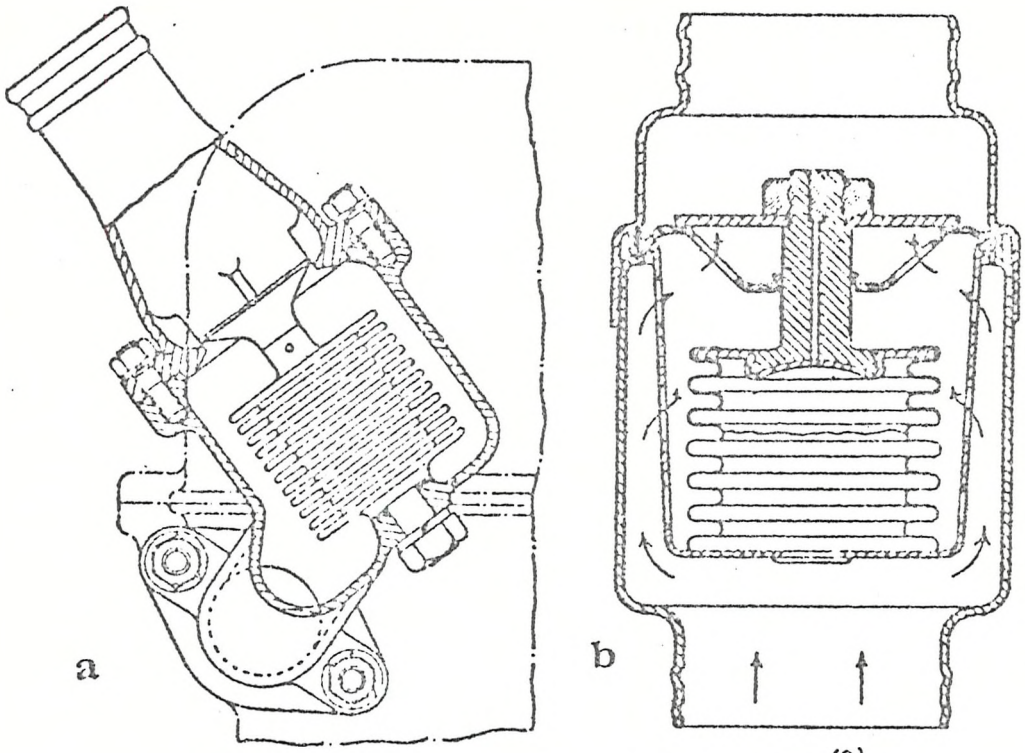

Fig. 14 —Bellows Type Thermostat[2].

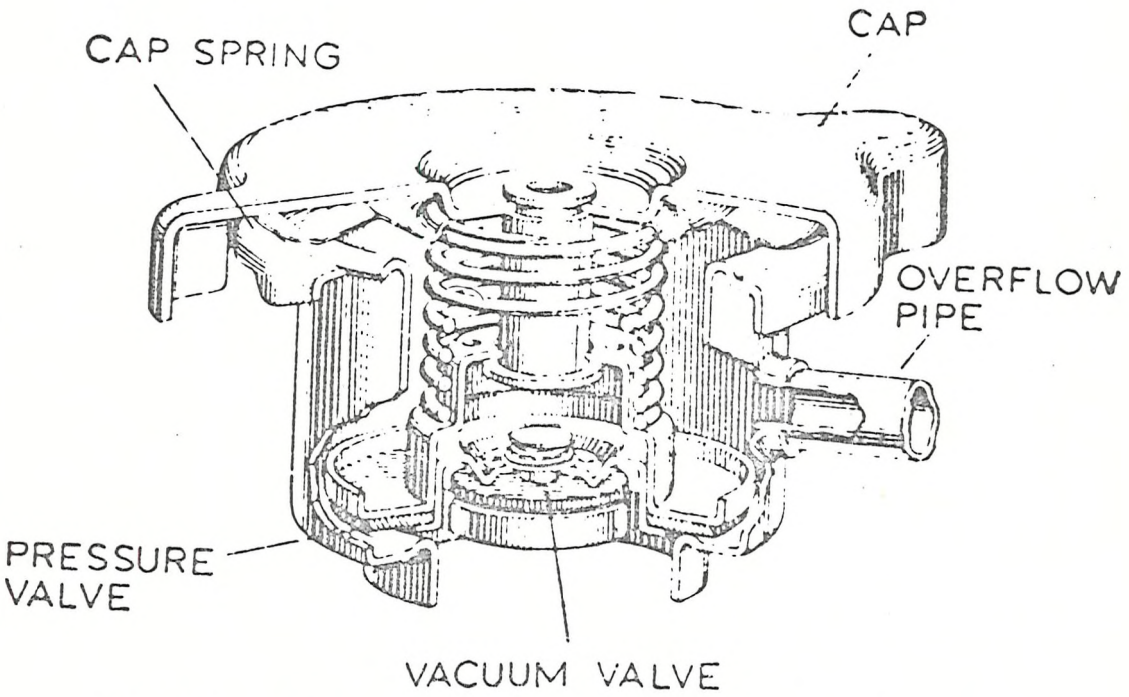

Fig. 15 —The A.C. Delco Radiator Filler Cap, for Pressurized Cooling Systems.[32]

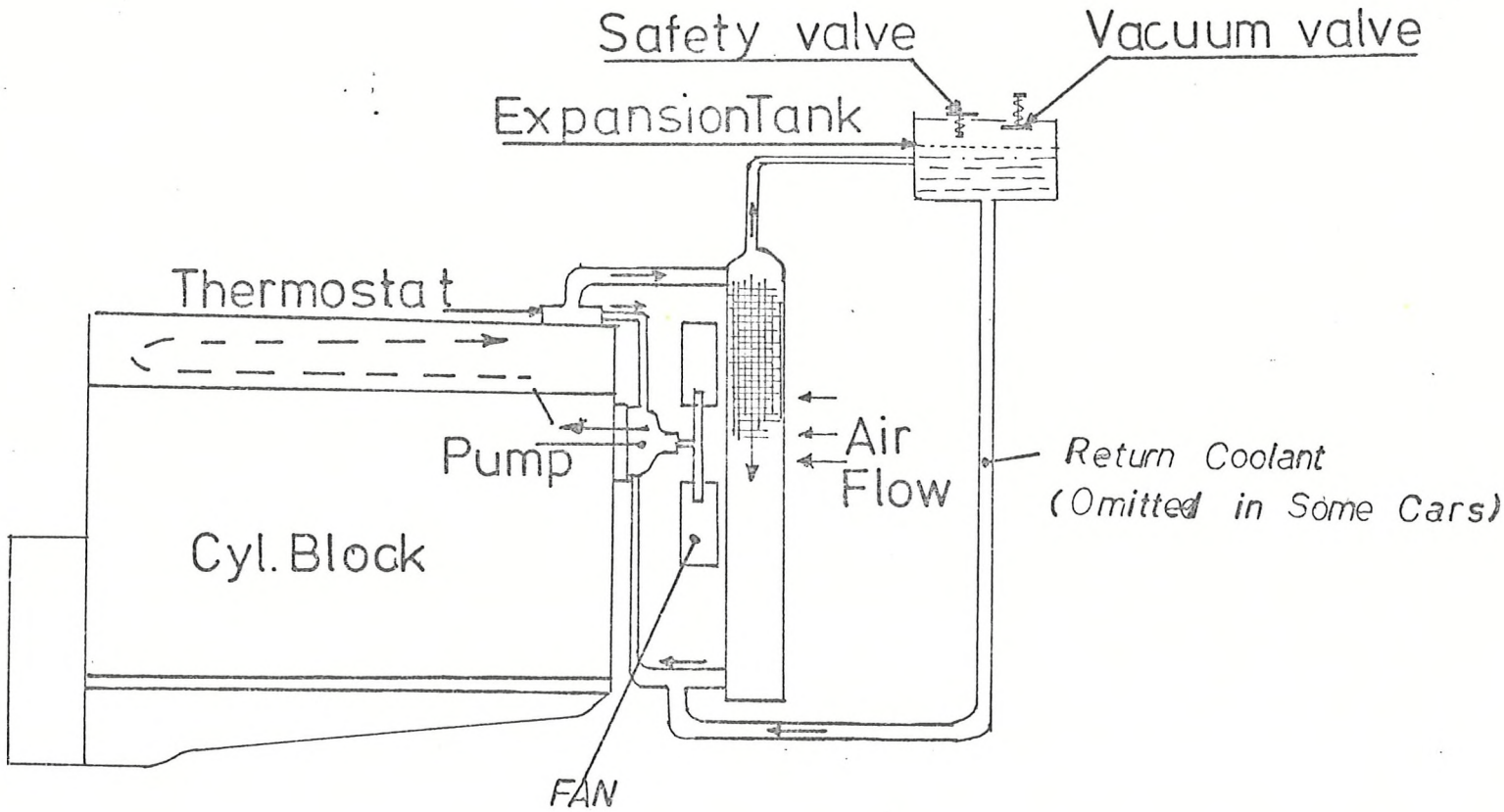

Fig (16) : Sealed cooling system

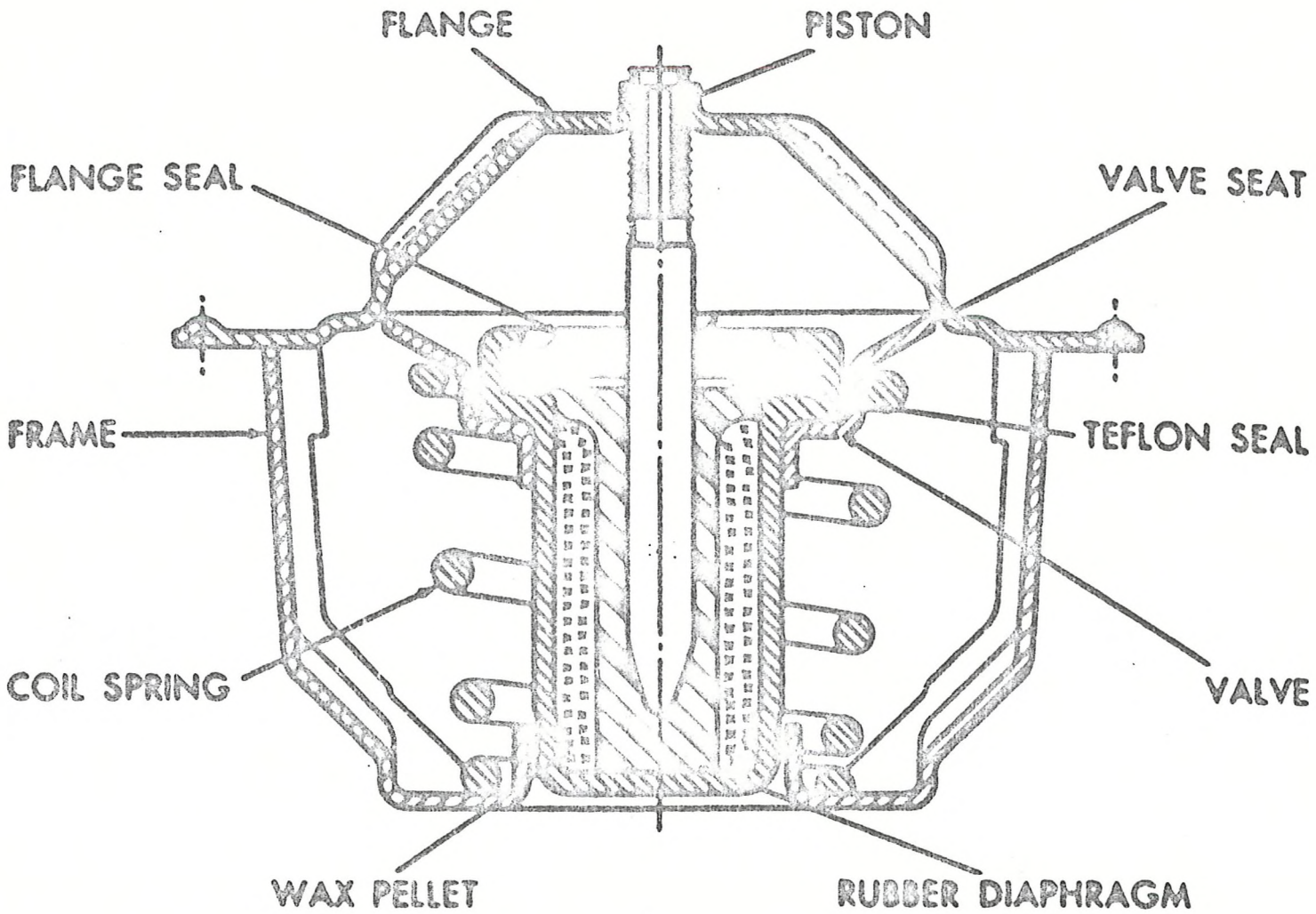

Fig. 17 .—The Wax Pellet Element-type Thermostat.

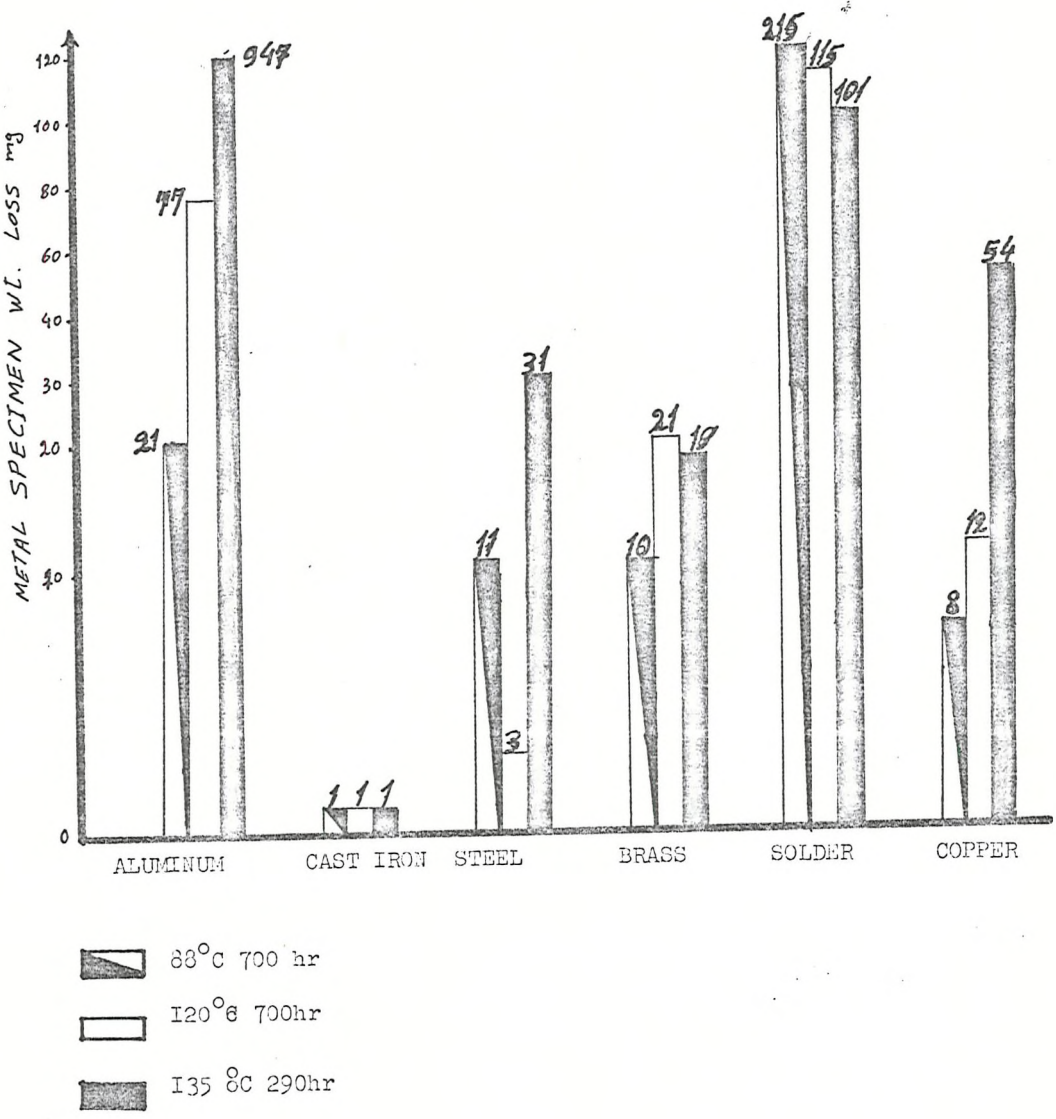

FIG.I8. CORROSION WEIGHT LOSS, COOLANT TEMPERATURE, ENGINE DYNAMOMETER TESTS COOLANT: ANTIFREEZE(A) (40% GLYCOL in 100ppm $\underline{cl}$, $\underline{so}_4$, $\underline{HCO}_3$ &WATER) (27)

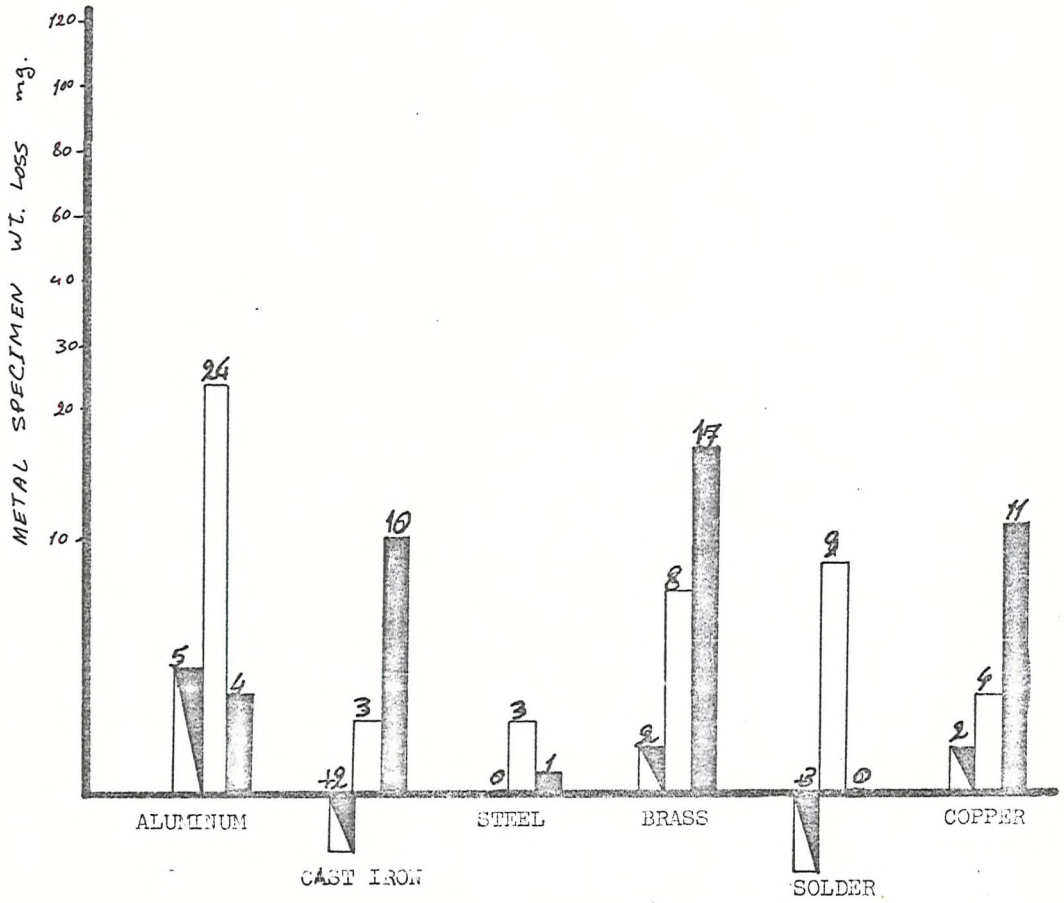

FIG.19 , CORROSION WEIGHT LOSS, COOLANT TEMPERATURE, ENGINE DYNAMOMETER TESTS
COOLANT: ANTIFREEZE (B) (40% GLYCOL in 100ppm $\underline{Cl}$, $\underline{SO_4}$, $\underline{HCO_3}$ & water). Ref(27)

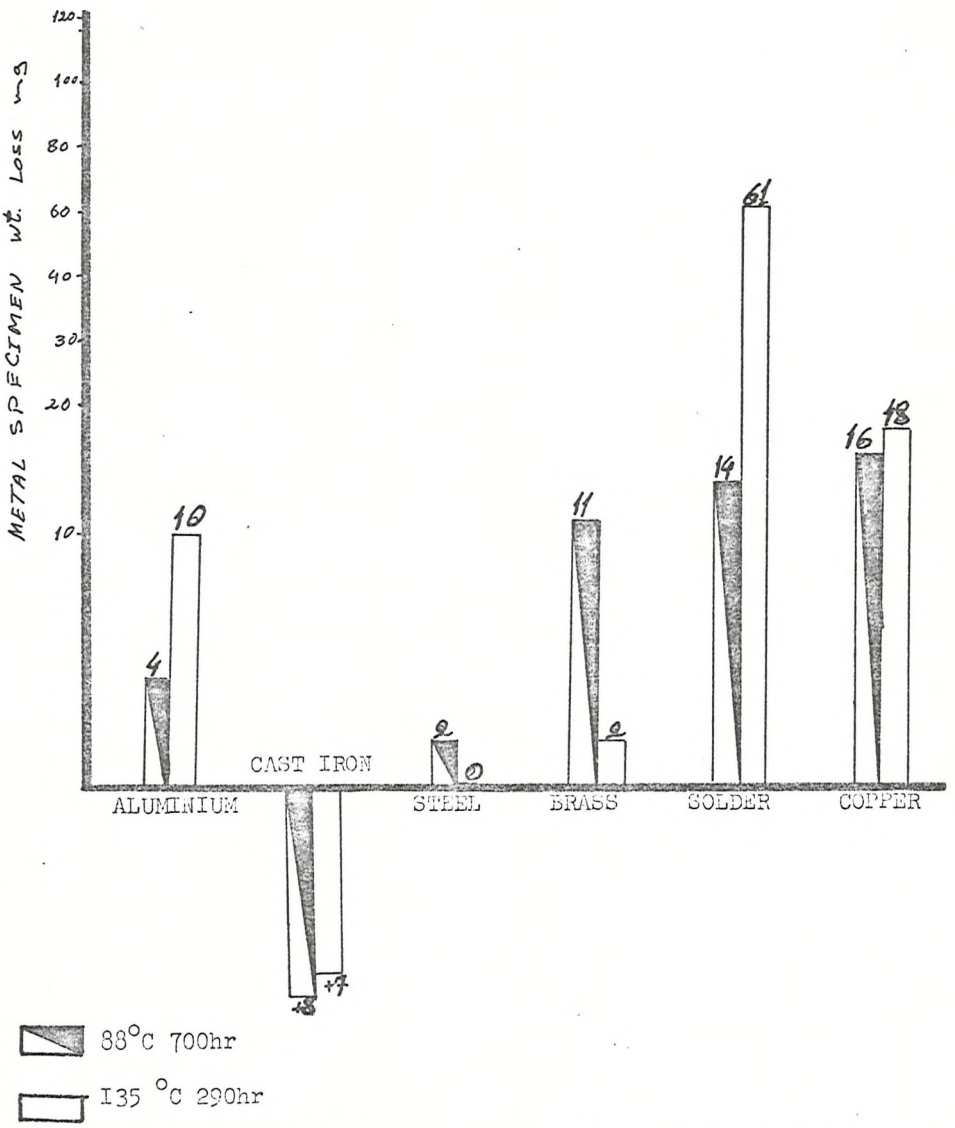

FIG.20. CORROSION WEIGHT LOSS, COOLANT TEMPERATURE, ENGINE DYNAMOMETER TESTS
COOLANT: ANTIFREEZE (C) (40%GLYCOL in 100ppm Cl, SO_4,HCO_3 & WATER). Ref.(27)

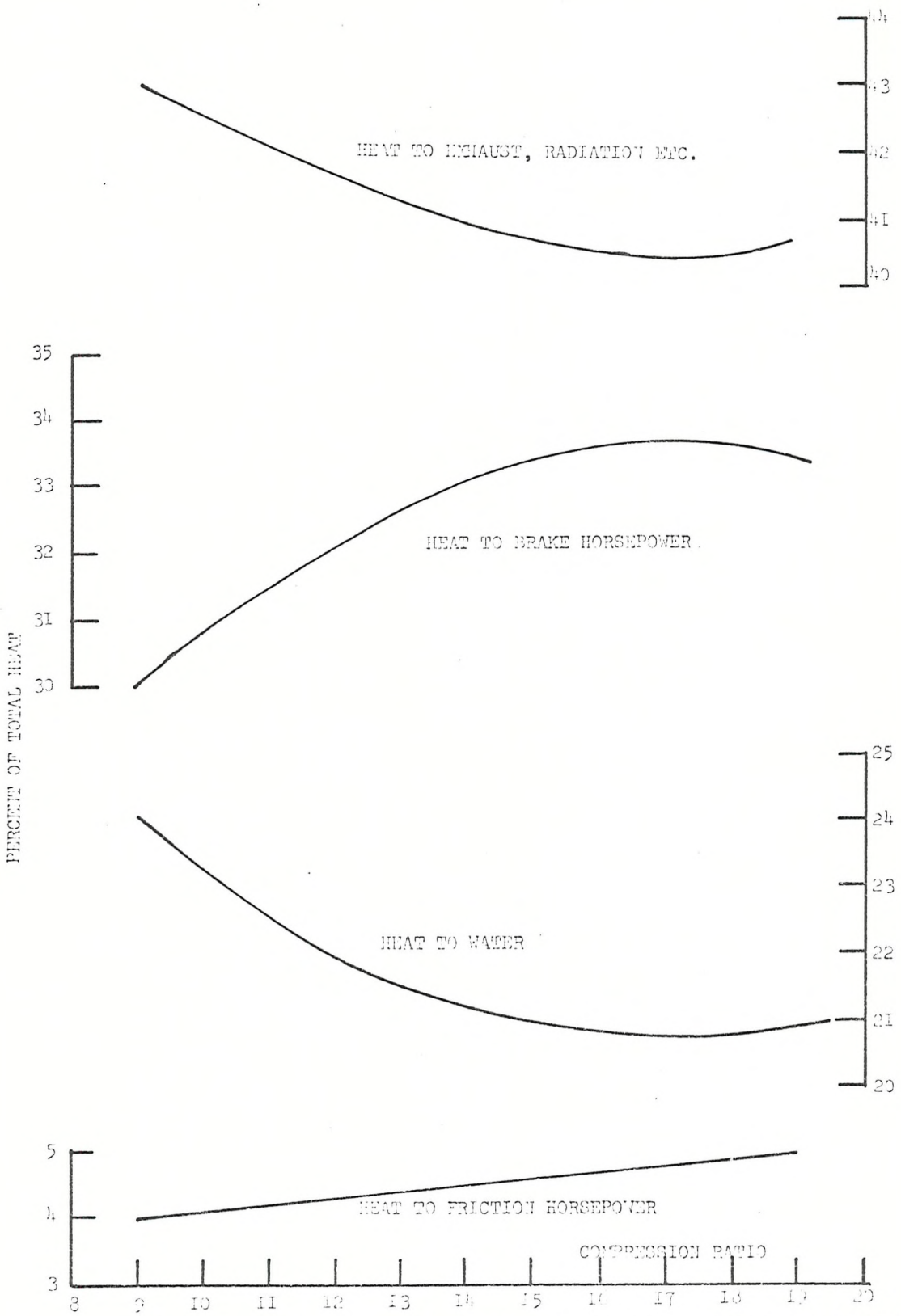

FIG.21. ANALYSIS OF HEAT LOSSES IN VARIABLE COMPRESSION ENGINE FOR A COMPRESSION RATIO RANGE OF 8:1 TO 20:1 Ref.(28)

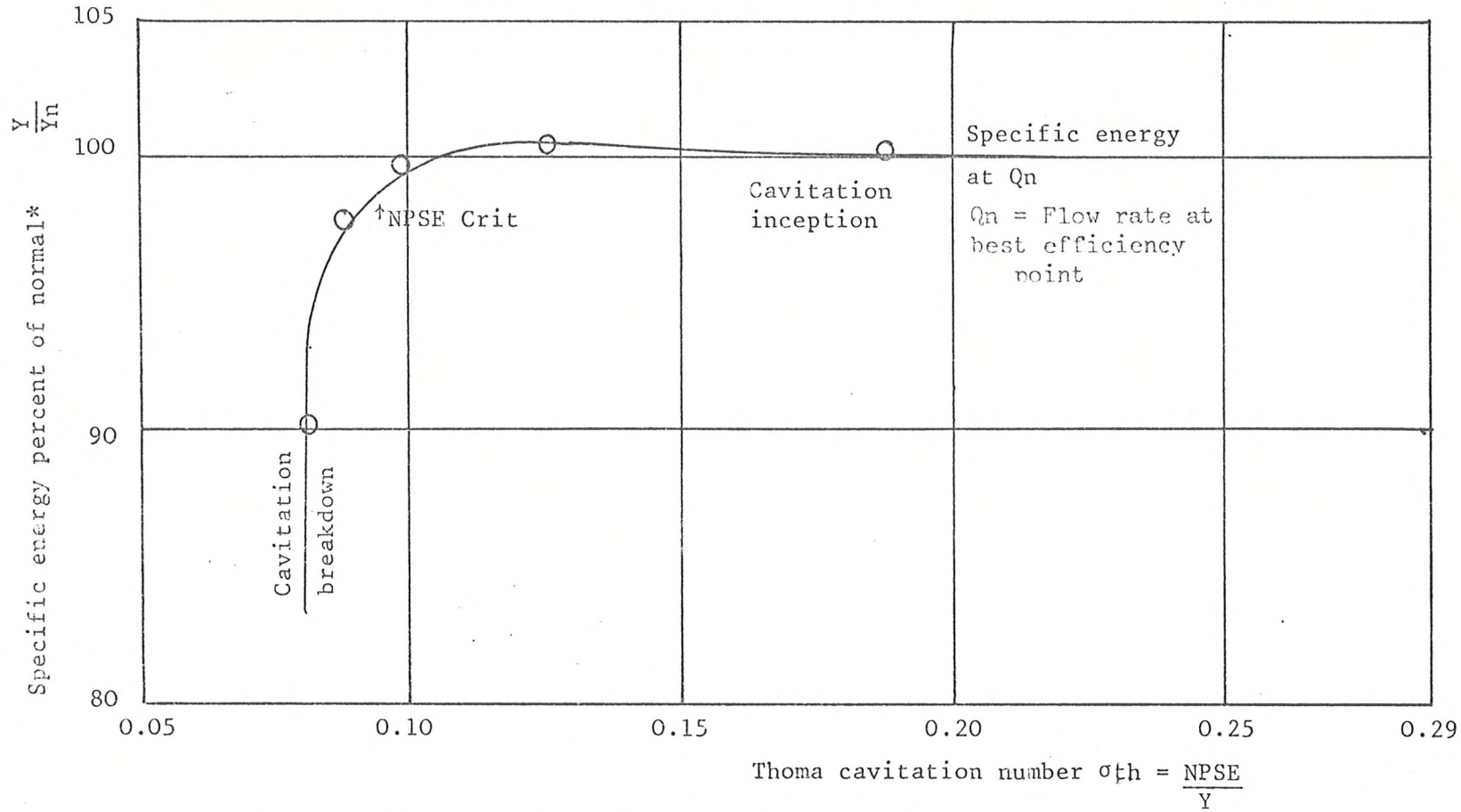

Fig.22 σ_{th} curve for a centrifugal pump at constant speed and discharge. Ref. (46)

* Normal specific energy is the value at the best efficiency point and high σ_{th}

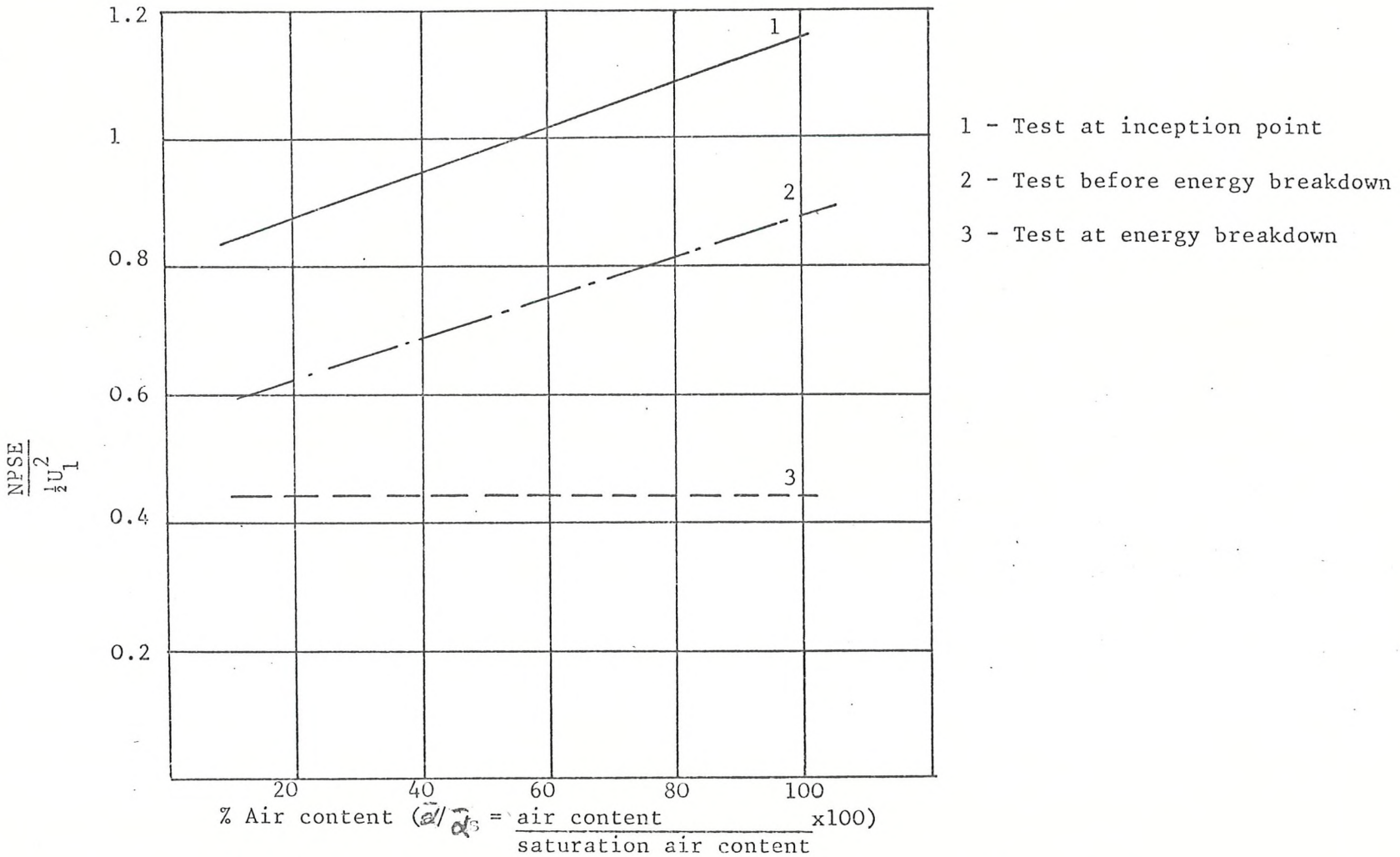

Fig. 23 Effect of air content on cavitation in centrifugal pump Ref. (13)

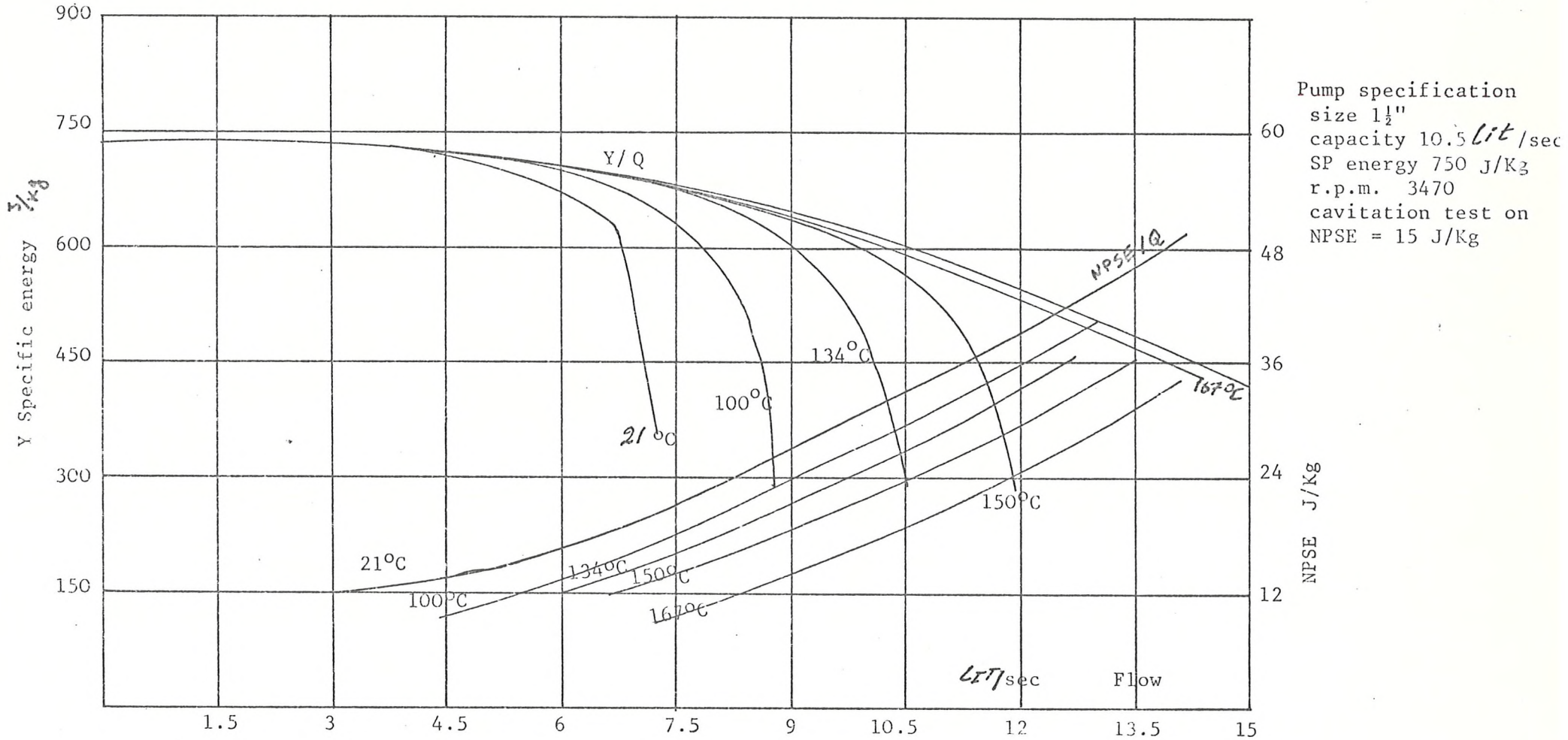

Pump specification
size $1\frac{1}{2}$"
capacity 10.5 lit/sec
SP energy 750 J/Kg
r.p.m. 3470
cavitation test on
NPSE = 15 J/Kg

Fig. 24 Effect of temperature on cavitation in a pump Ref. 49)

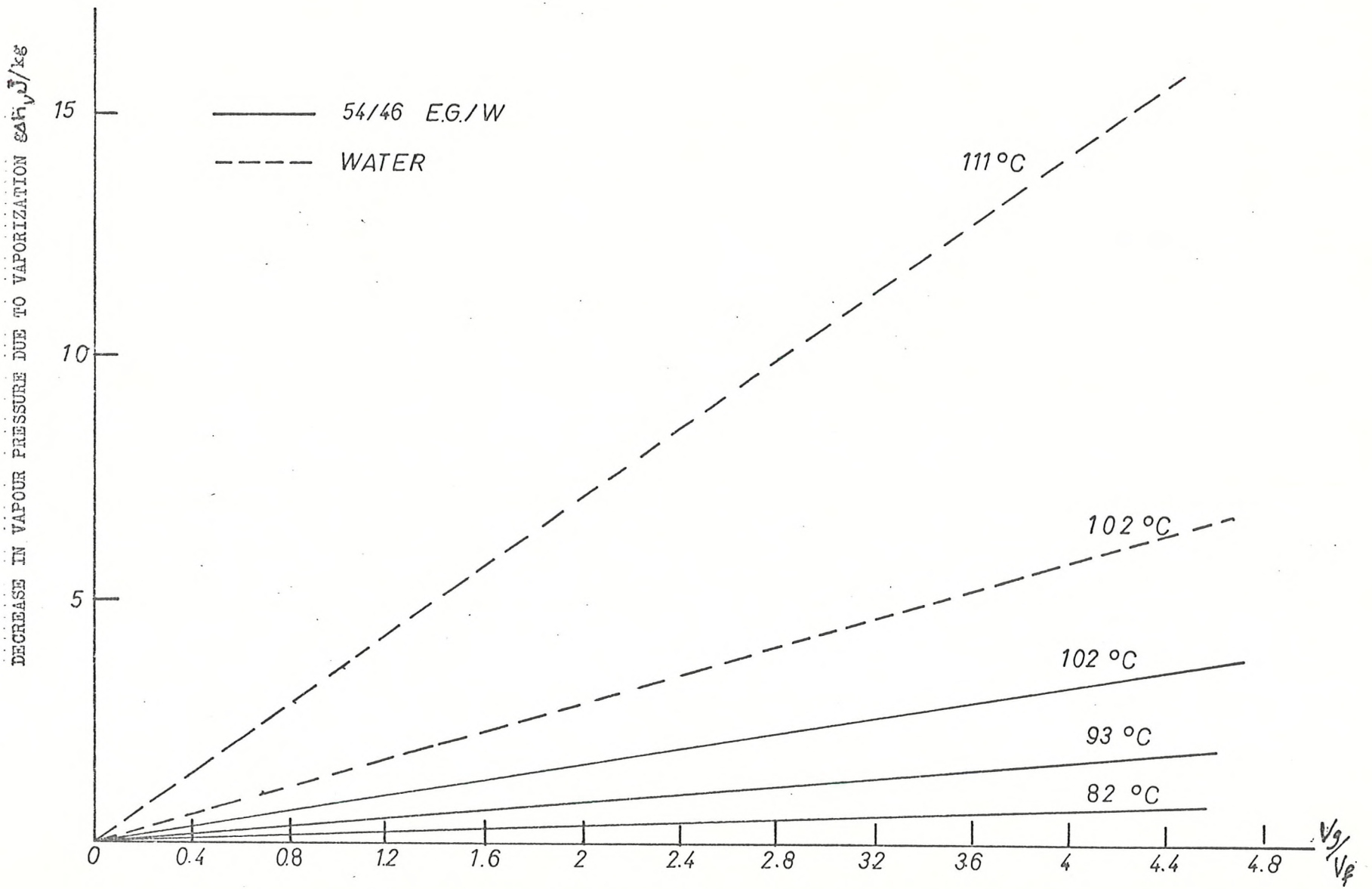

FIG 25: VAPOUR PRESSURE DEPRESSION AS FUNCTION OF VAPOUR-TO LIQUID-VOLUME RATIO FOR E.G./W AND WATER AT VARIOUS TEMPERATURES

FIG 26: THERMAL CAVITATION PARAMETER AS A FUNCTION OF TEMPERATURE FOR WATER; 100% ETHYLENE GLYCOL , 54/46 E.G./W AND METHANOL

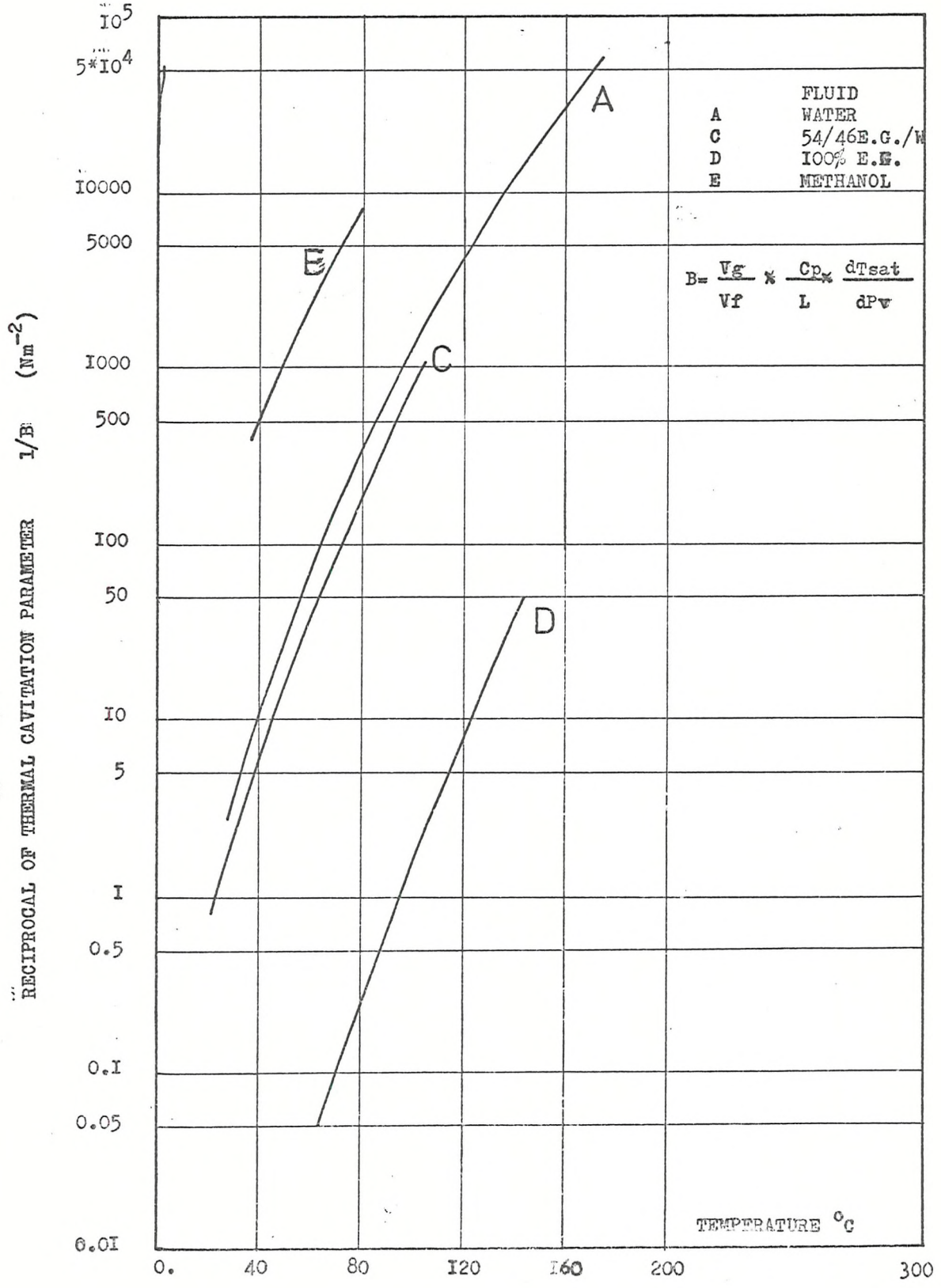

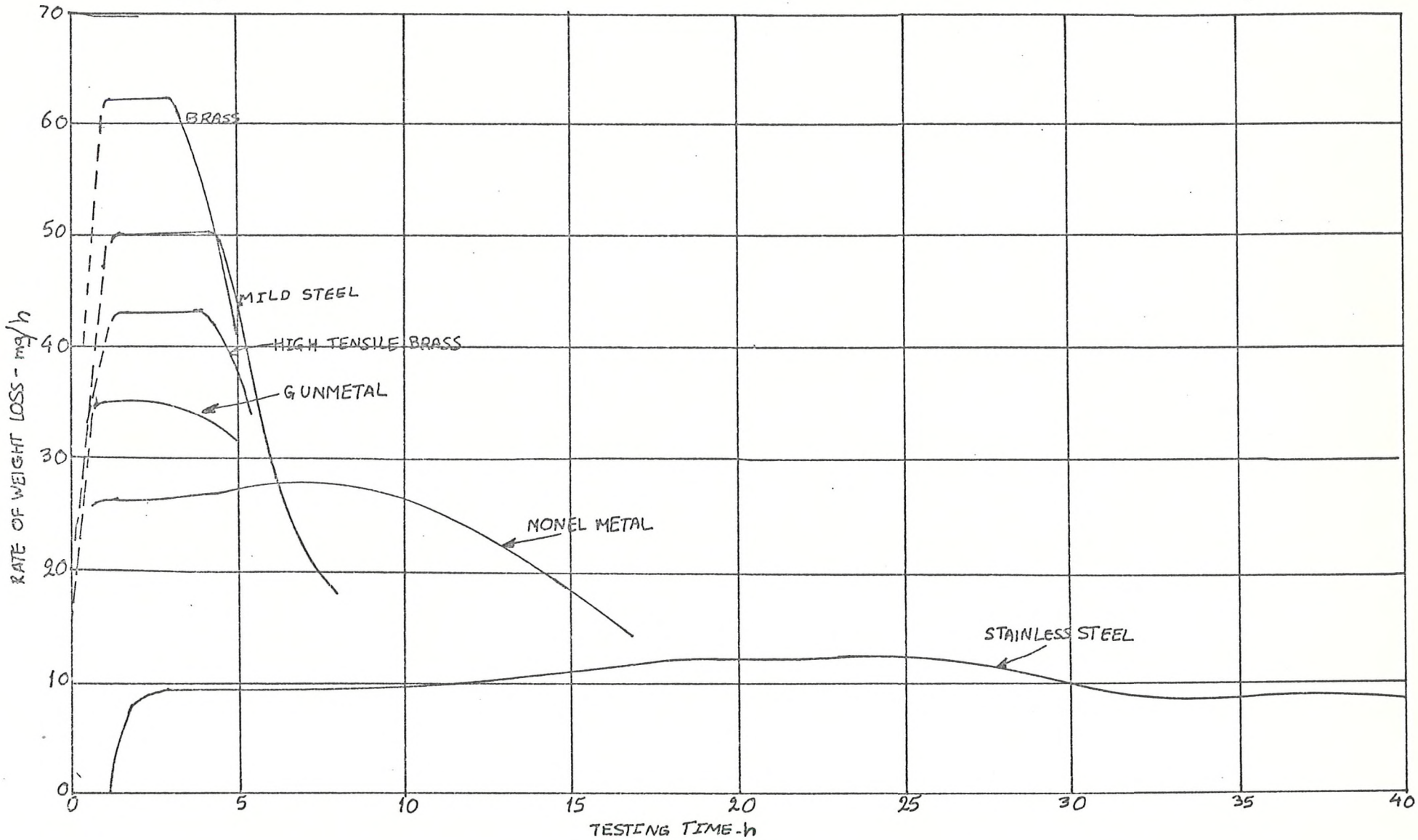

FIG[27] RATE OF EROSION/ TIME CURVES FOR DIFFERENT MATERIALS Ref (74)

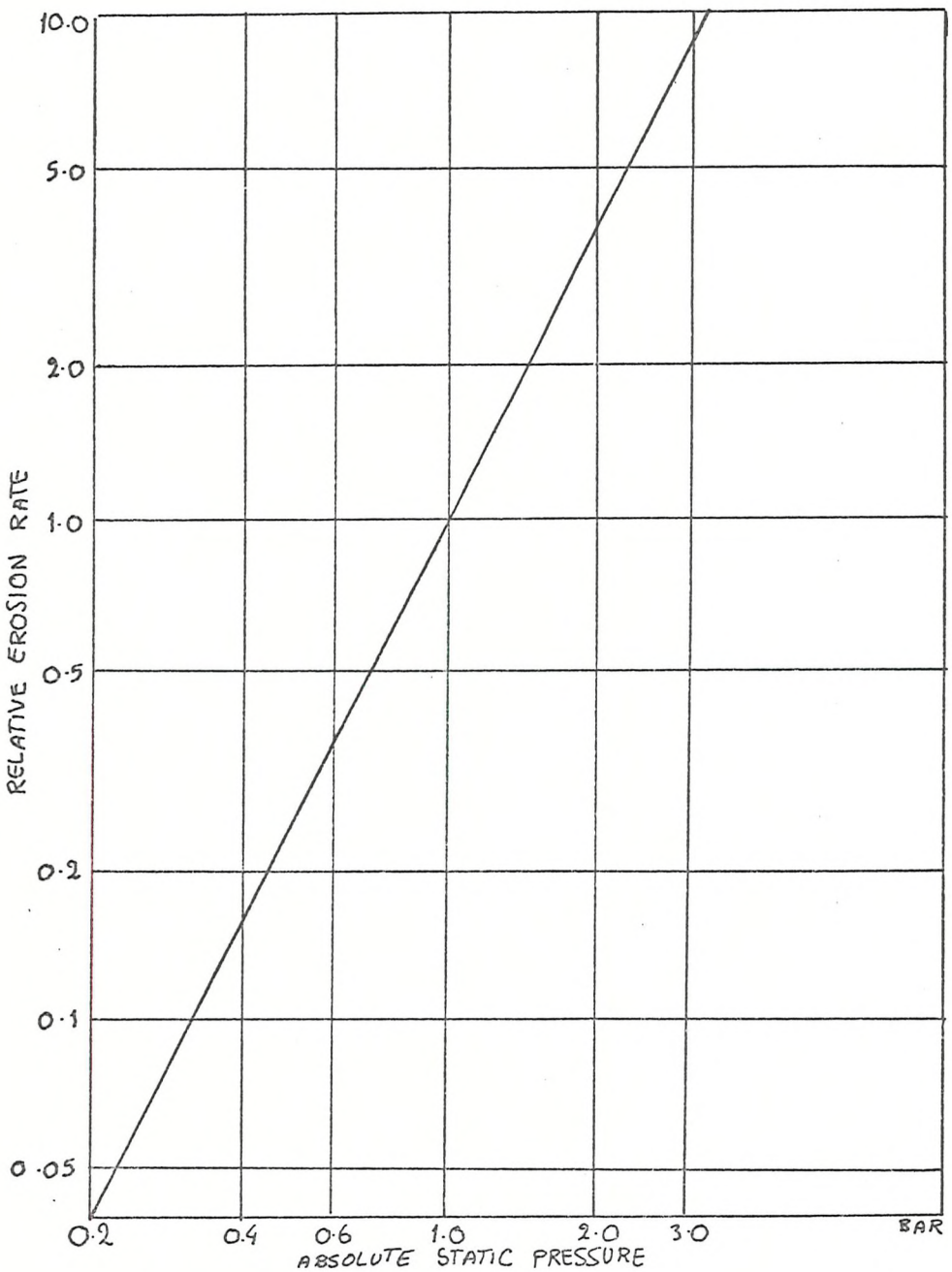

FIG [28] EFFECT OF PRESSURE ON EROSION RATE

(FREQ: 20 KHz Amf.: 50 μm) Ref (72)

$$\text{RELATIVE EROSION RATE} = \frac{\text{EROSION RATE AT VARIOUS PRESSURE}}{\text{EROSION RATE AT ONE BAR}}$$

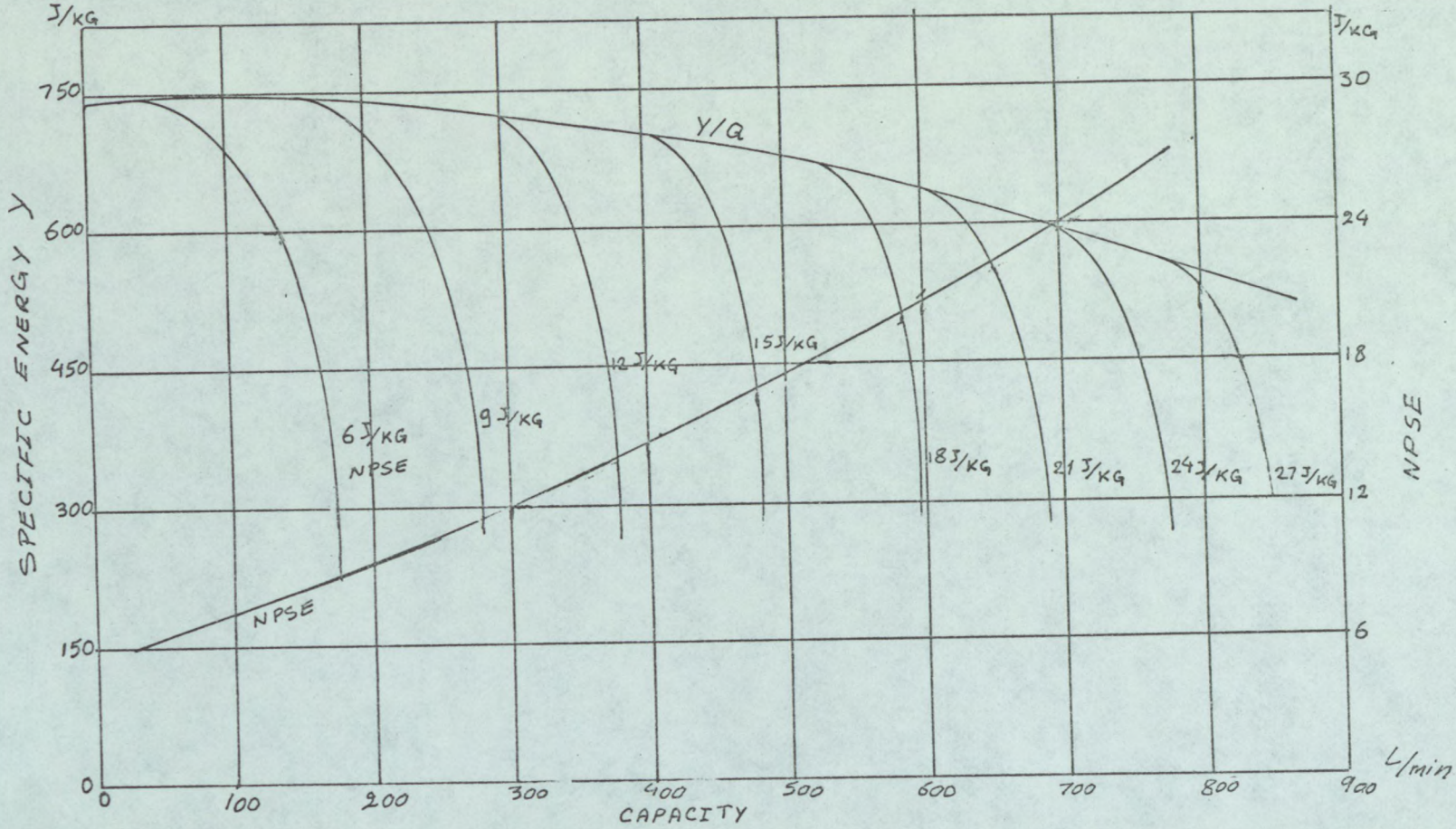

FLUID was water

FIG [29] EFFECT OF CAVITATION ON CENTRIFUGAL PUMP CHARACTERISTIC.

Ref (28)

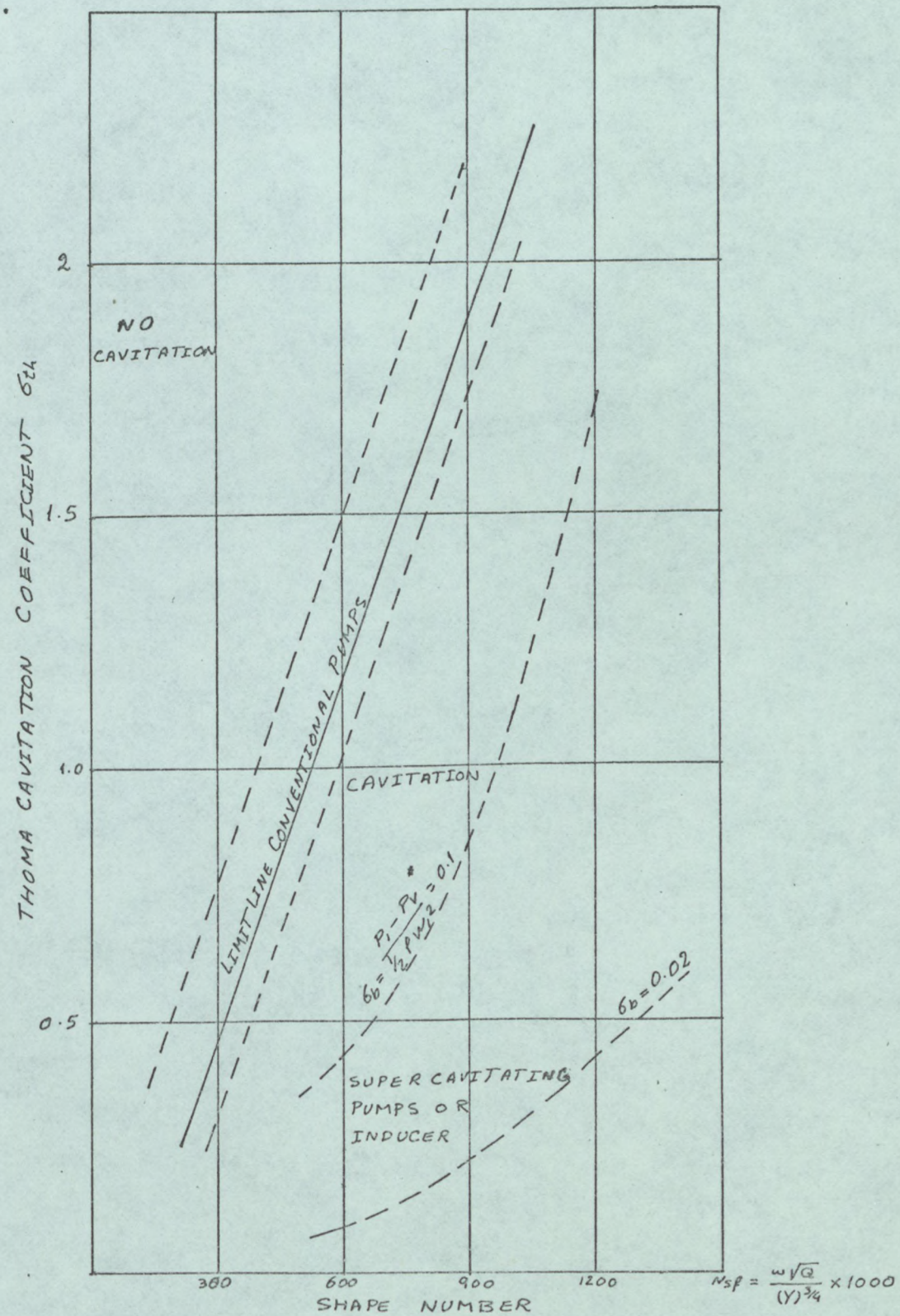

FIGURE [38] CAVITATION LIMIT FOR PUMPS Ref (84)

* σ_b is blade coefficient W_1 relative velocity before blades

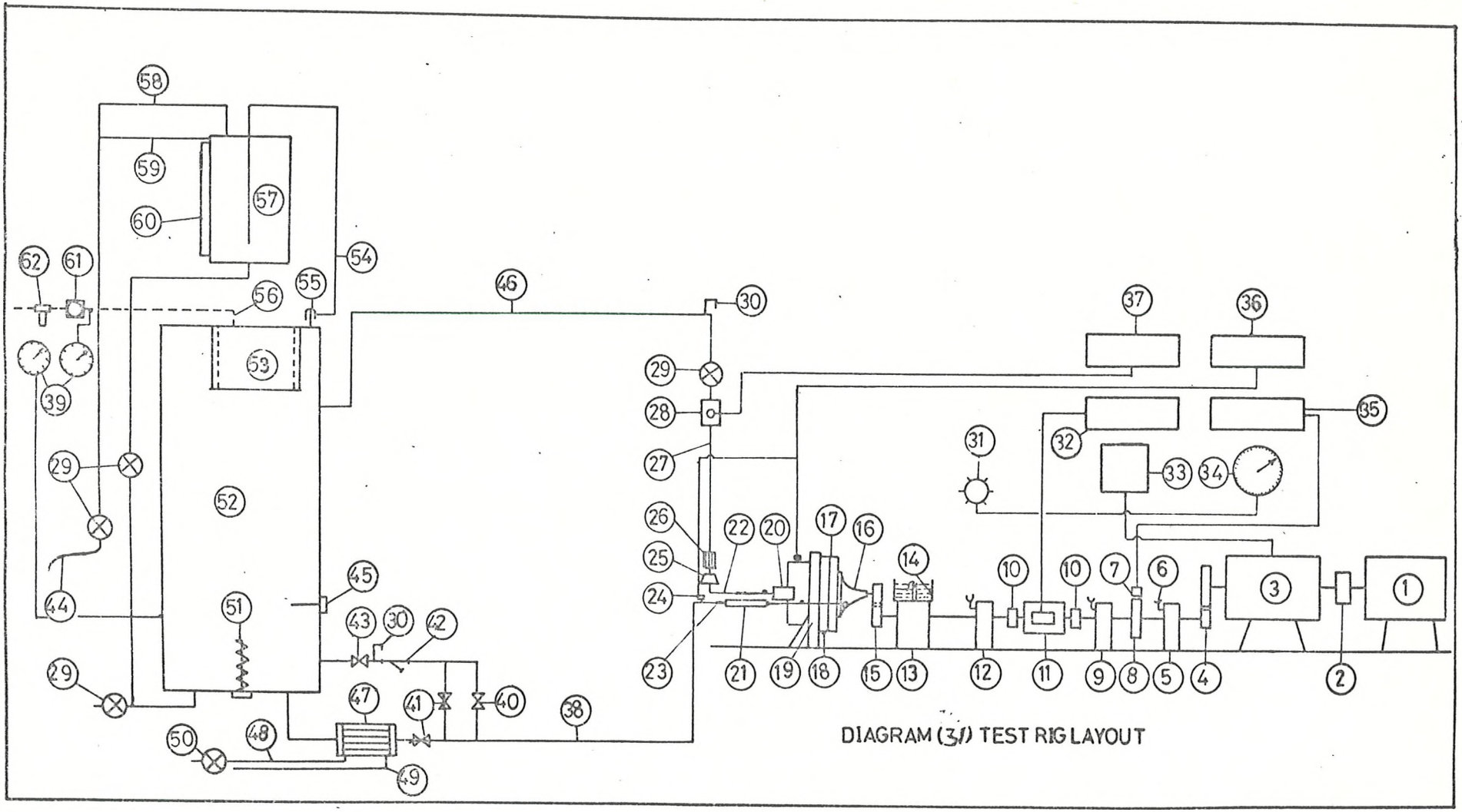

DIAGRAM (31) TEST RIG LAYOUT

RIG DESCRIPTION - Refer to Diagram 31

1. 5.25 Kw (7.5HP) 2700 R.P.M. Electric Motor
2. Disc-type flexible coupling
3. 'PYE TASC' Unit magnetic coupling
4. 2½:1 gearing
5. 30mm dia. journal bearings housing
6. Oil drip funnel
7. Electro-magnetic impulse sensor
8. 60 toothed wheel
9. Housing for 30mm dia. journal bearing
10. Flexible coupling
11. Torquemeter strain gauge type
12. Housing for 25mm dia. journal bearing
13. Oil cooled journal bearing
14. Oil drip feed
15. 1:1 pulleys and 1" toothed belt
16. Test pump
17. Square-type pump housing
18. Pressure tapping
19. Bracket
20. Plenum chamber
21. Glass section 42mm dia. 20cm length
22. 1½" galvanized pipe
23. Steam house 1½"
24. Temperature probe
25. 1½" to 25mm special cone reduction angle 15°
26. 25mm straightener
27. 25mm stainless steel pipe
28. 25mm stainless steel turbine-type flowmeter
29. 1" diaphragm valve
30. ¼" dia. air bleed valve
31. Six-way valve
32. Galvanometer (it is set to read lb.ft directly)
33. Speed remote controller
34. Precision Bourdon gauge 0-6.9bar (abs)
35. Digital counter (R.P.M.)
36. Temperature indicator 10-150°C
37. Digital counter (litre/min)

RIG DESCRIPTION - Refer to Diagram 31 (continued)

38. 1½" galvanized pipe (suction line)
39. Pressure gauges
40. 1½" gate valve (screw-type)
41. 1¼" needle valve (screw-type)
42. 2" cast iron Y-type strainer (screw-type)
43. 2" gate valve (screw-type)
44. 1" flexible pipe
45. Thermostat range 70-150°C
46. 1½" galvanized pipe (discharge line)
47. Shell and tube heat exchanger
48. ½" copper tube from main water supply
49. ½" " " to waste water disposal
50. ½" diaphragm valve
51. 3KW immersion heater with thermostat
52. 230 litre pressure tank
53. 9¼" stainless steel bellows
54. 1½" galvanized pipe
55. 1½" relief valve
56. ¼" copper tube (compressed air line)
57. Expansion tank 19 litre capacity
58. 1" vent pipe (galvanized)
59. 1" overflow pipe (galvanized)
60. 12mm dia. sight glass
61. Air pressure regulator
62. Air filter

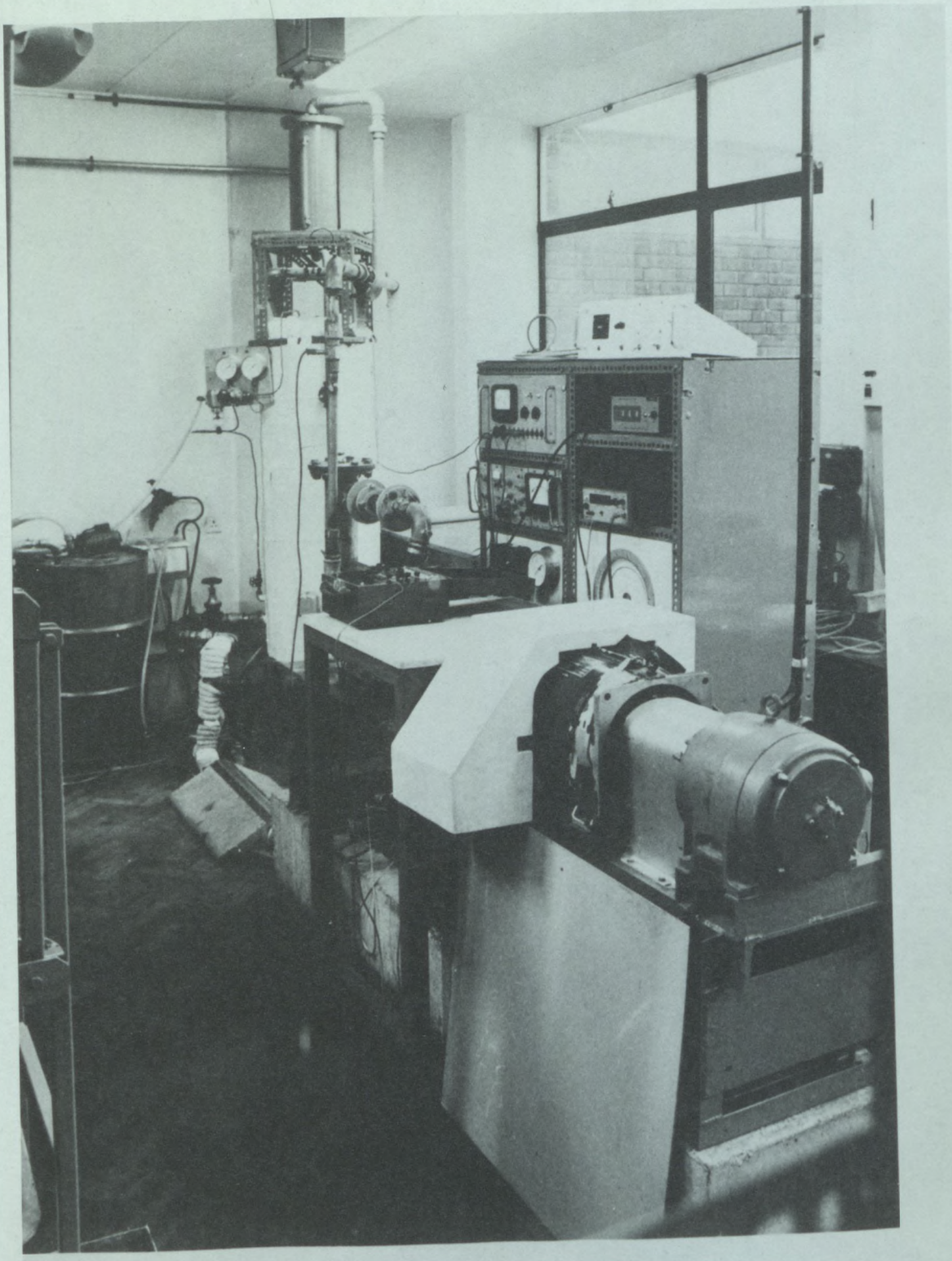

Fig(31_A): TEST RIG AFTER MODIFICATION

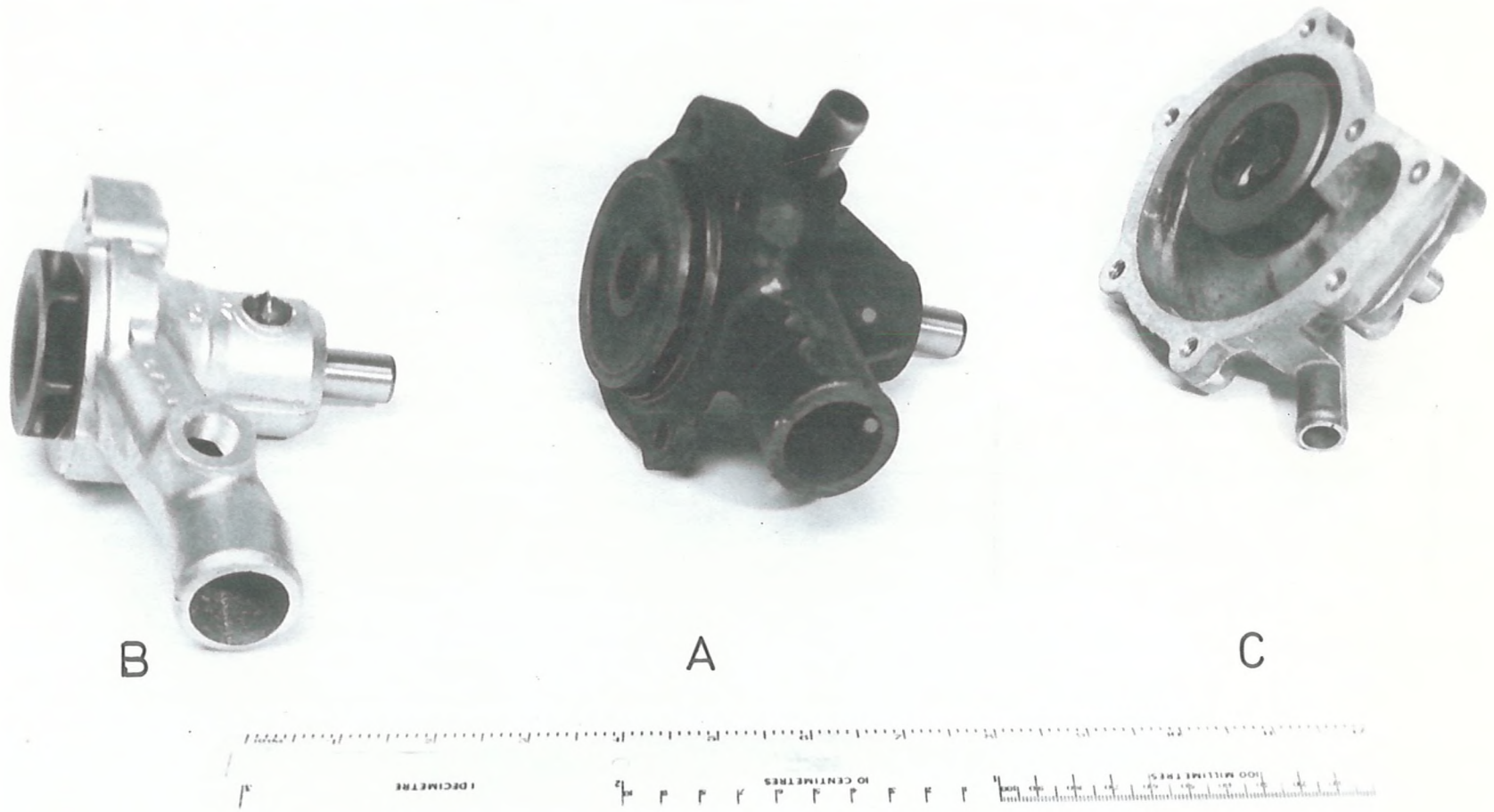

FIG:32 : Pumps Tested

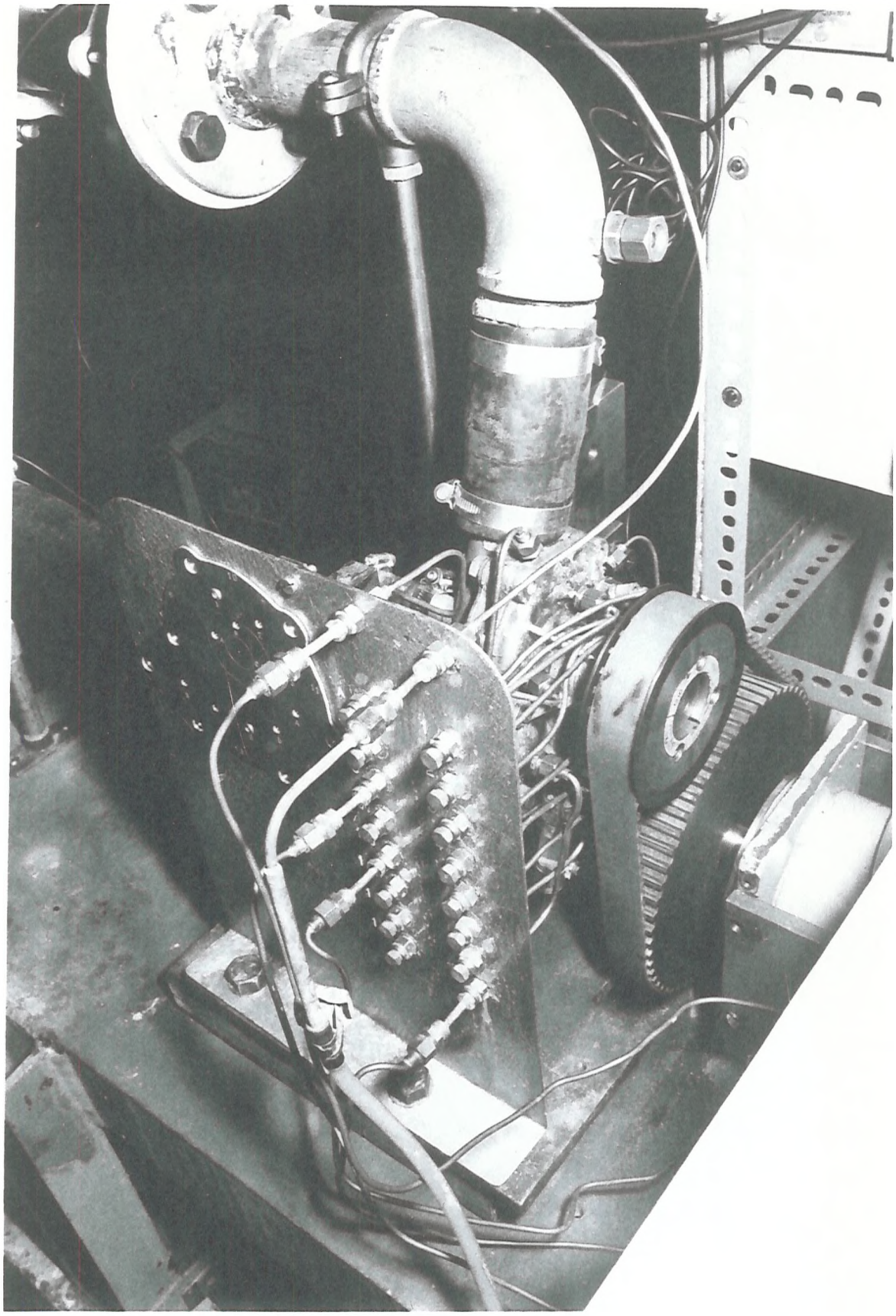

FIG (32-A): Pump "C" Mounted on the Bracket

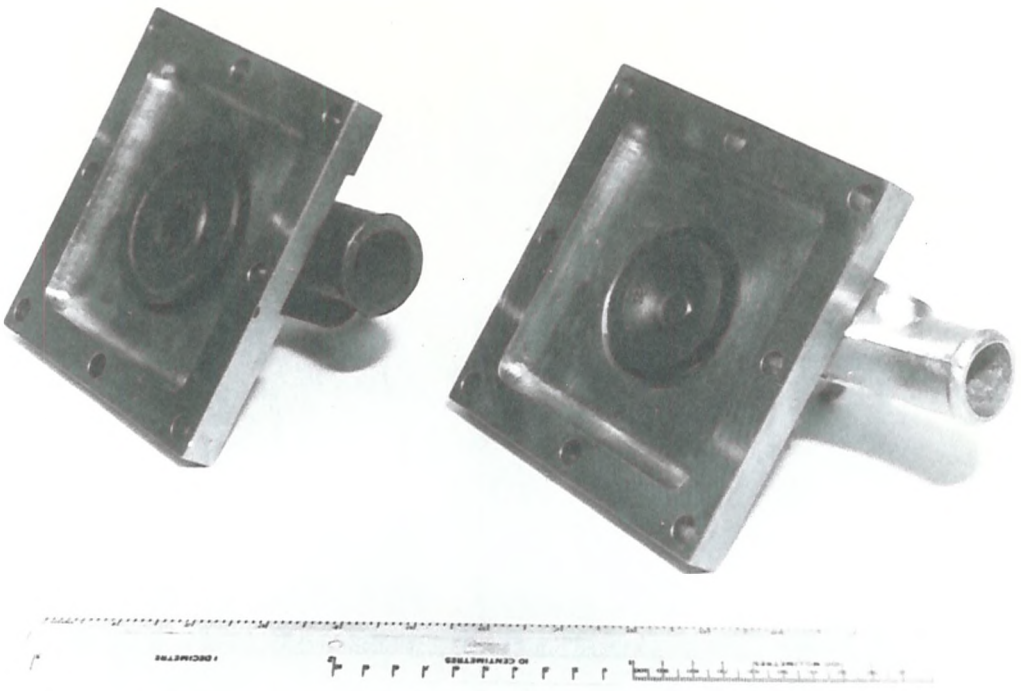

Fig33 Test Rig Housing For Pumps

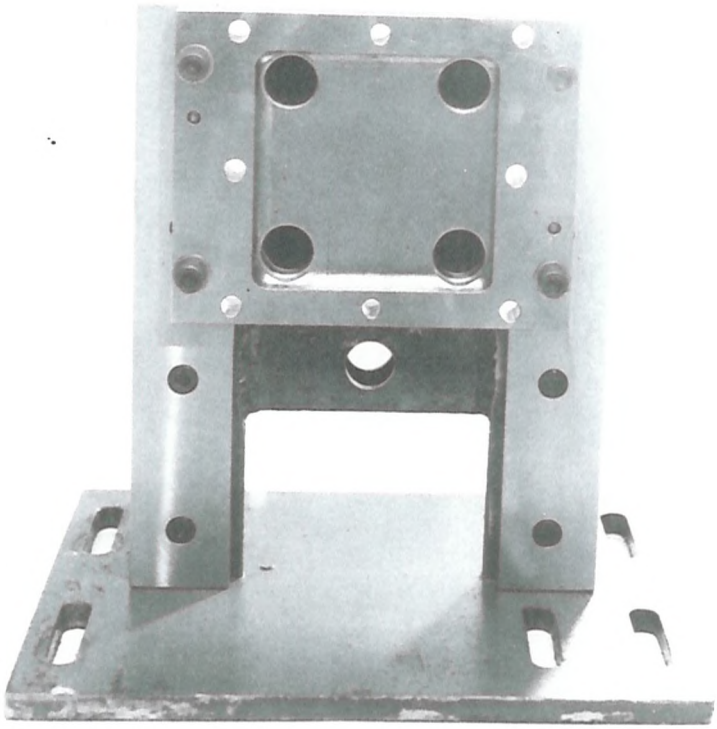

Fig 34 Housing Mounted On The Bracket

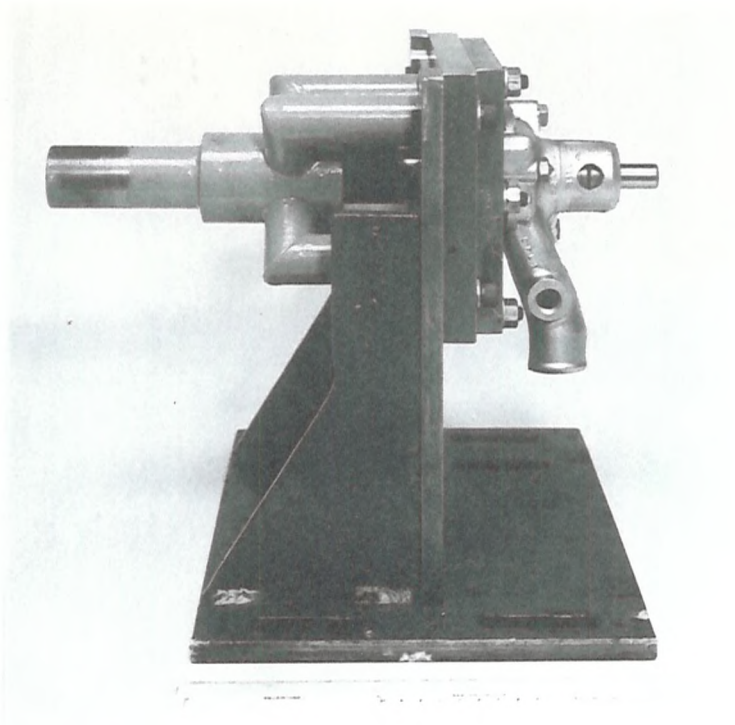

Fig35 Pump B Mounted & Plenum Chamber

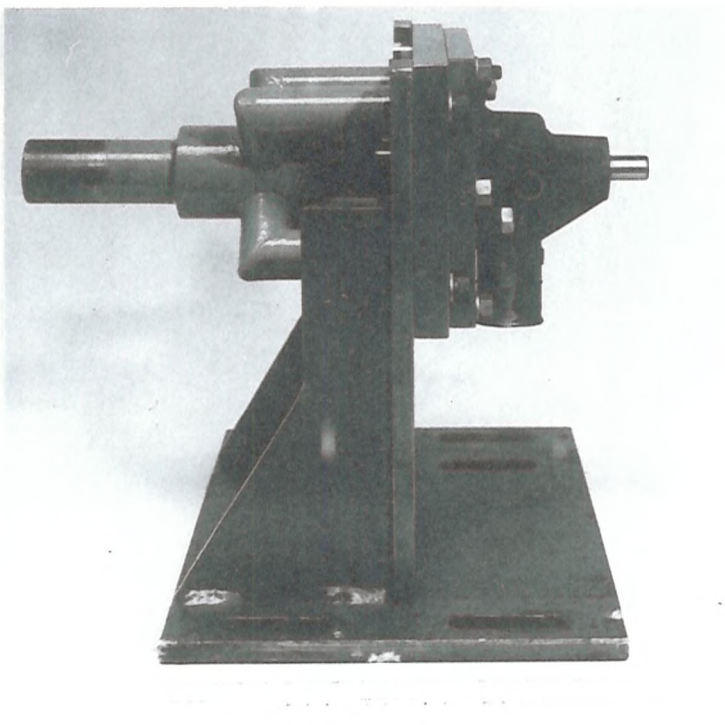

Fig36 Pump A Mounted & Plenum Chamber

Fig 35[A] Bellows (23.5 Cm Dia)

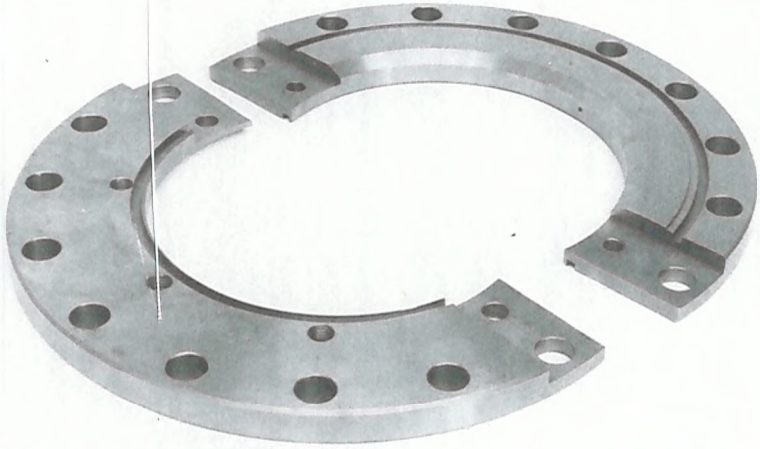

Fig36[A] Split Ring for Bellows Mounting

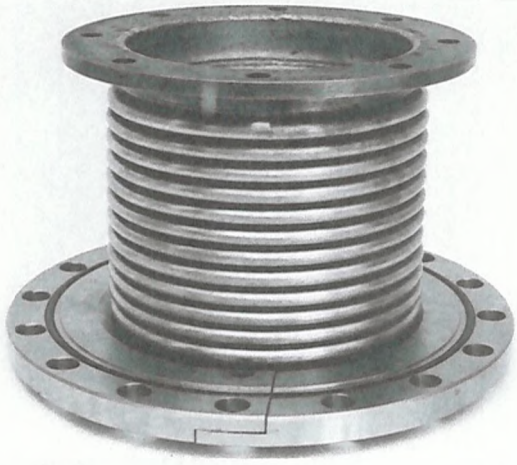

Fig37 Combination of Split Ring & Bellows

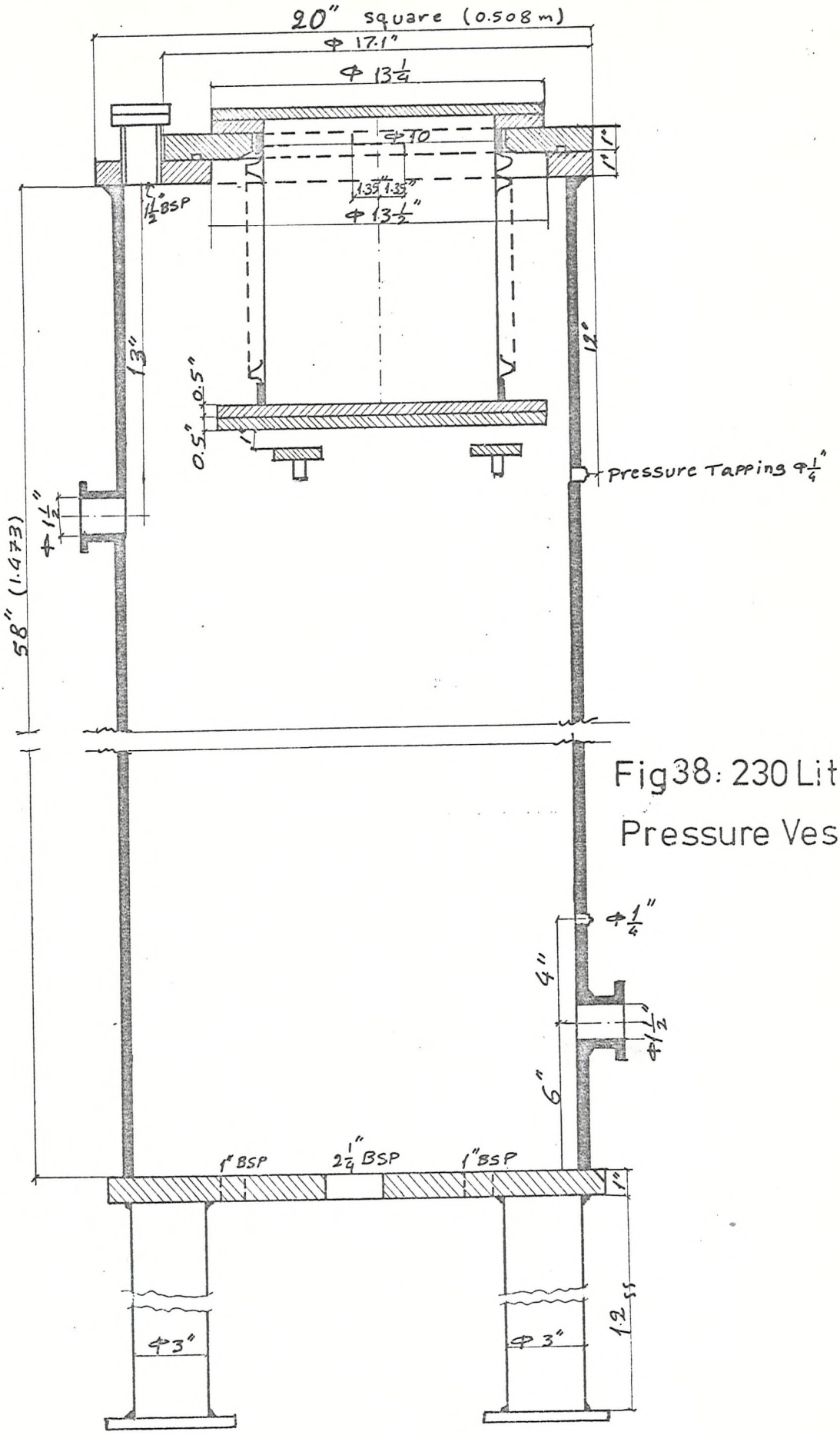

Fig 38: 230 Litre Pressure Vessel

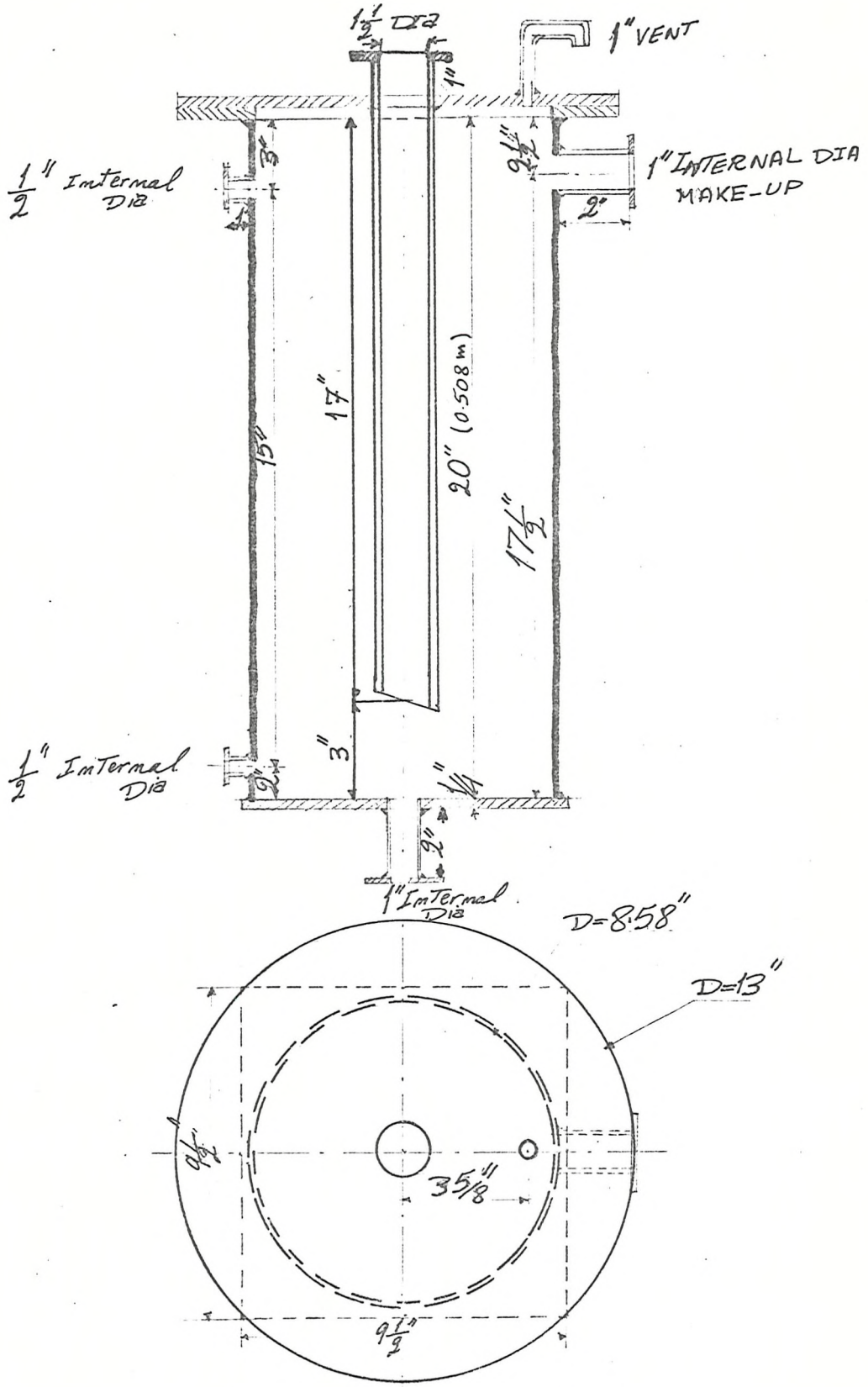

Fig 39 Expansion Tank

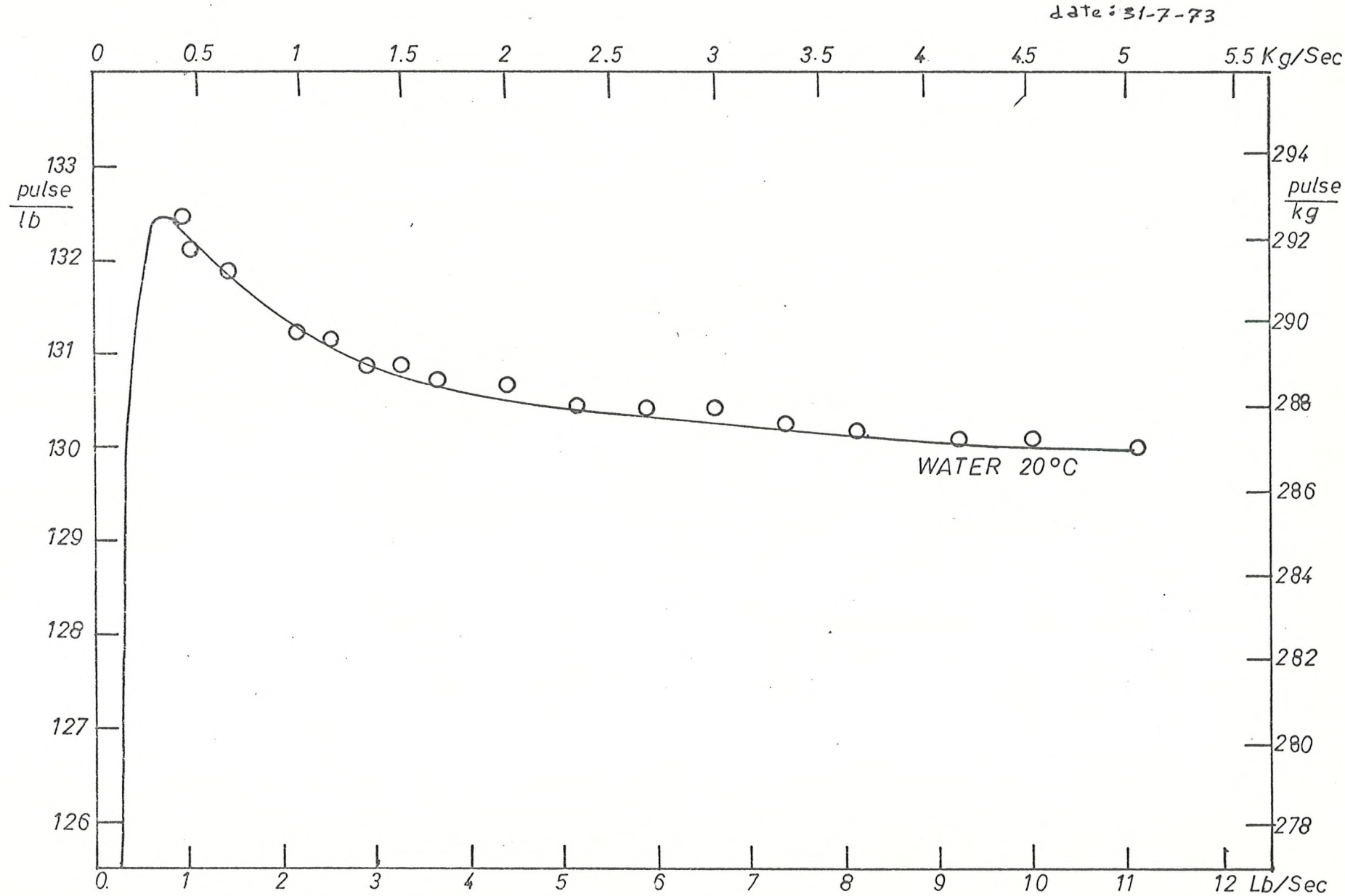

Fig 40 Calibration Curve of the Turbine type Flow Meter

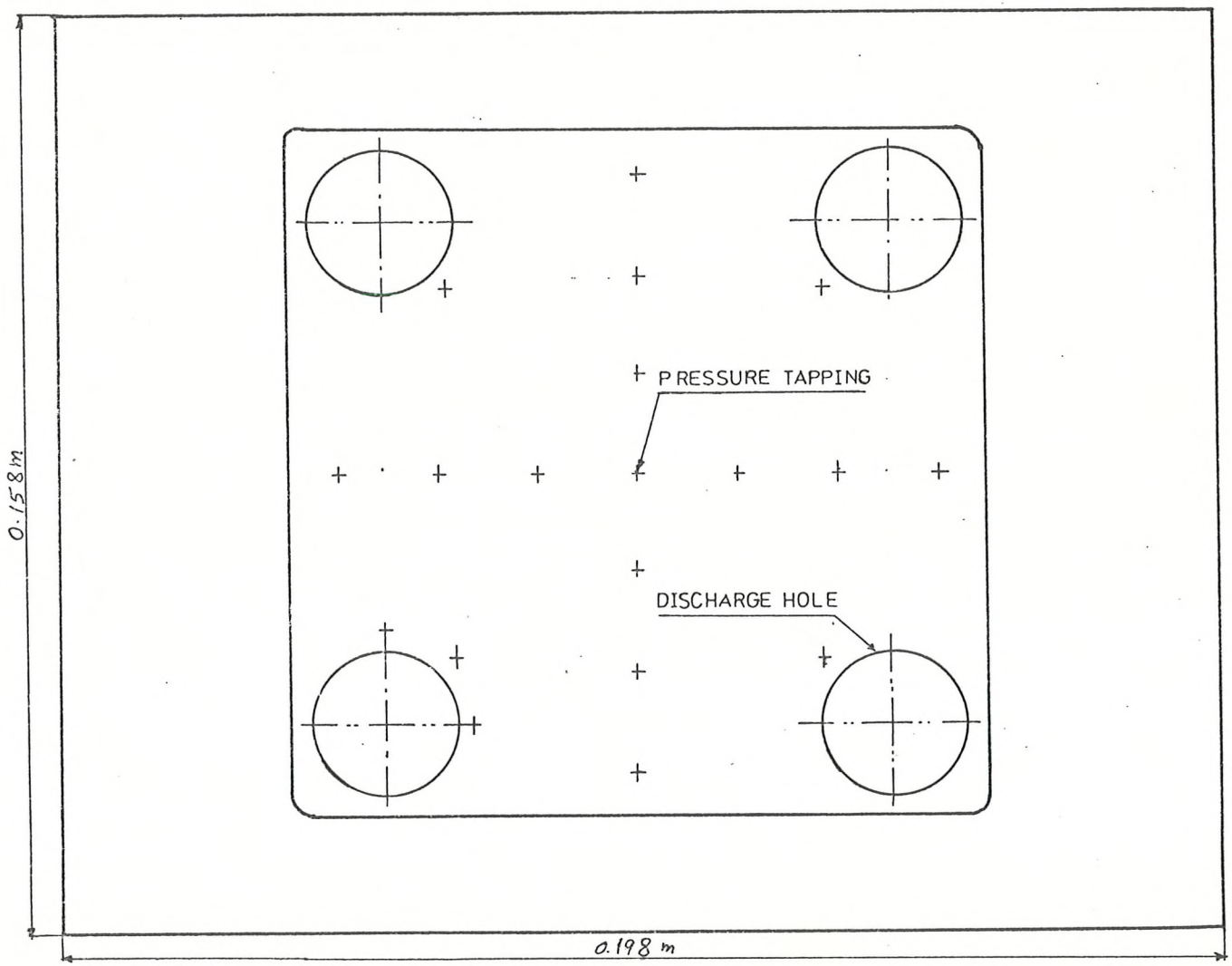

Fig 41: Pressure Tappings in the Square Housing

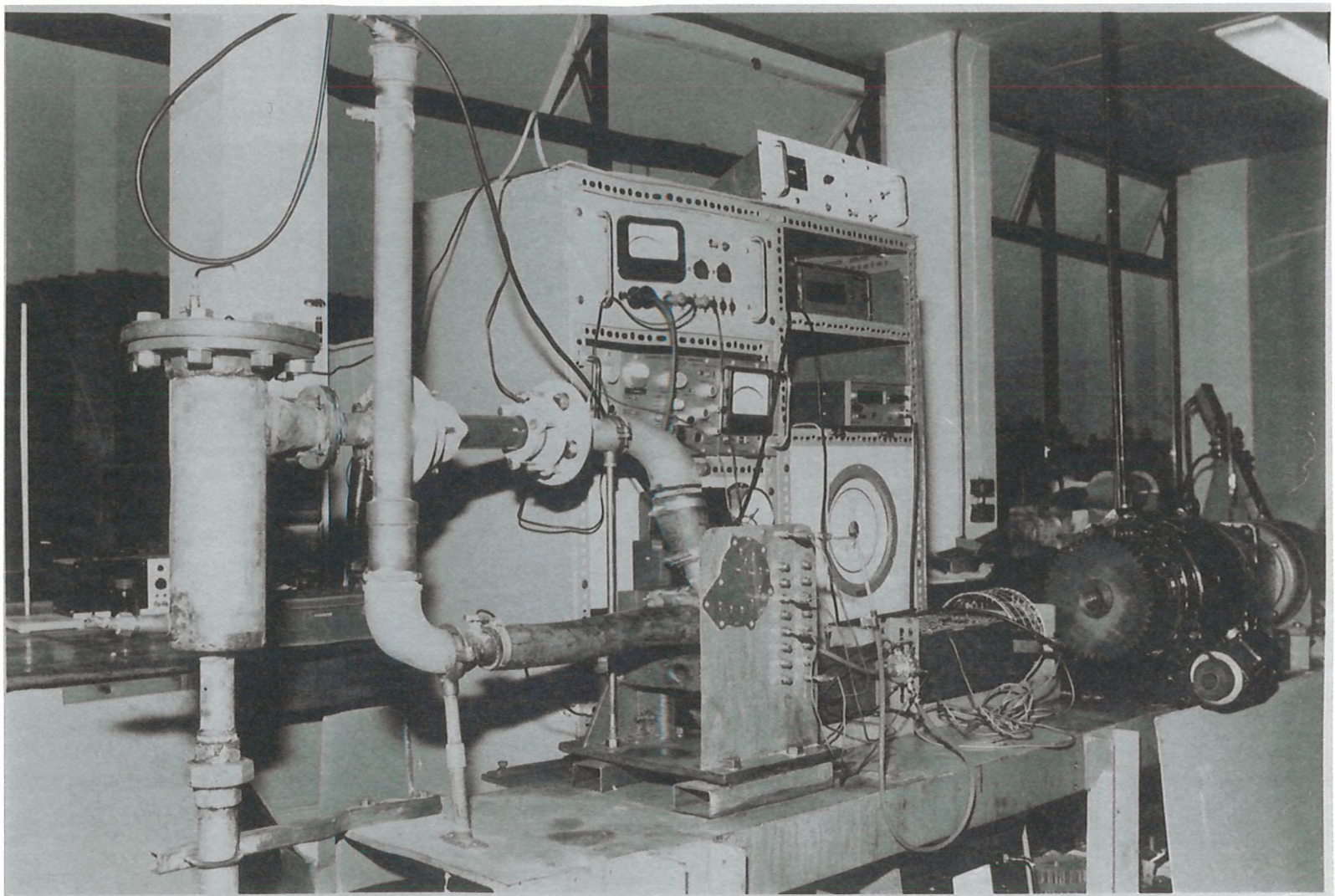

Fig(42) Suction Line Arrangement

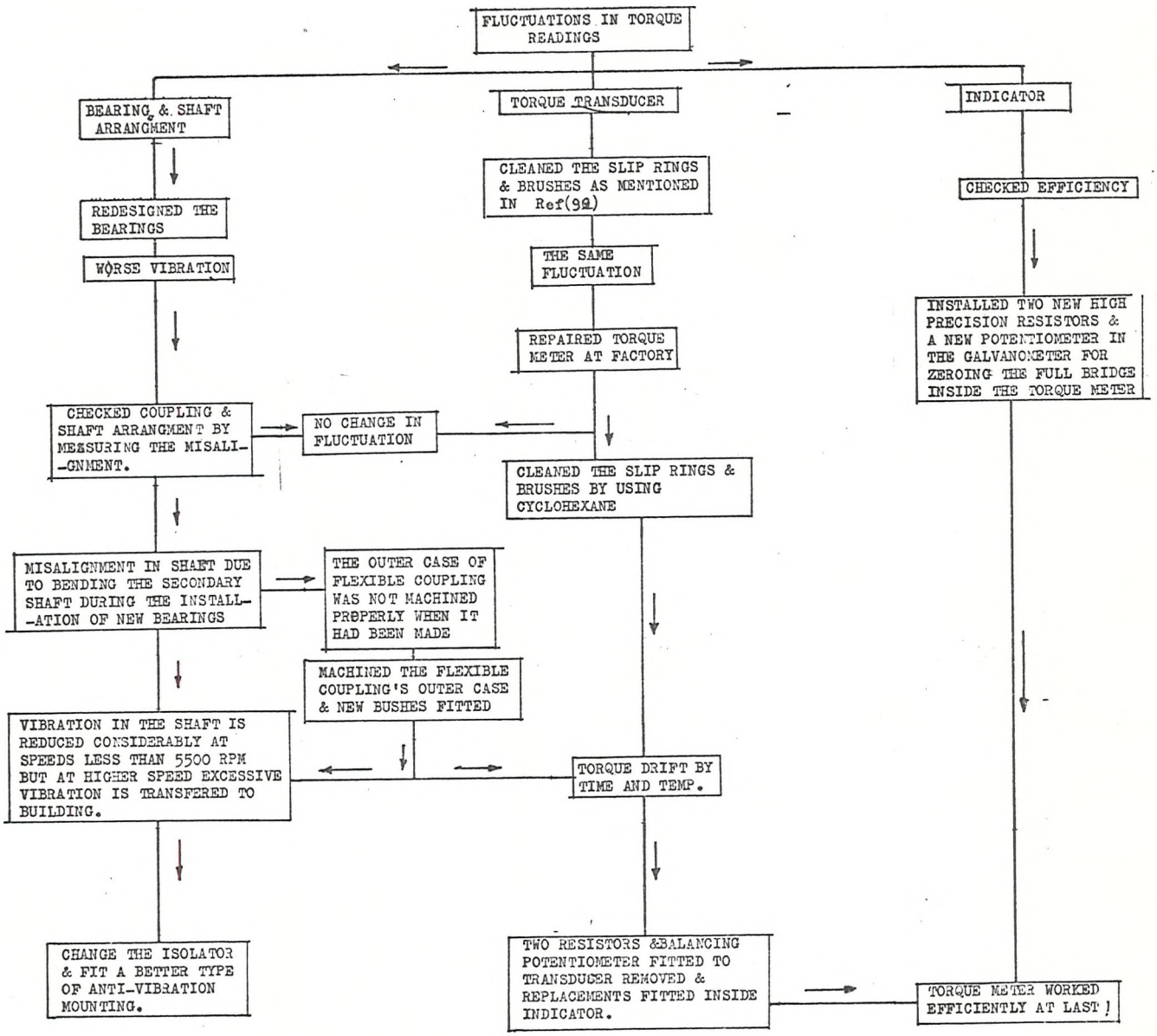

FIG 33: THE PROGRESS CHART OF INVESTIGATION & MAINTENANCE OF TORQUE TRANSDUCER & BEARINGS

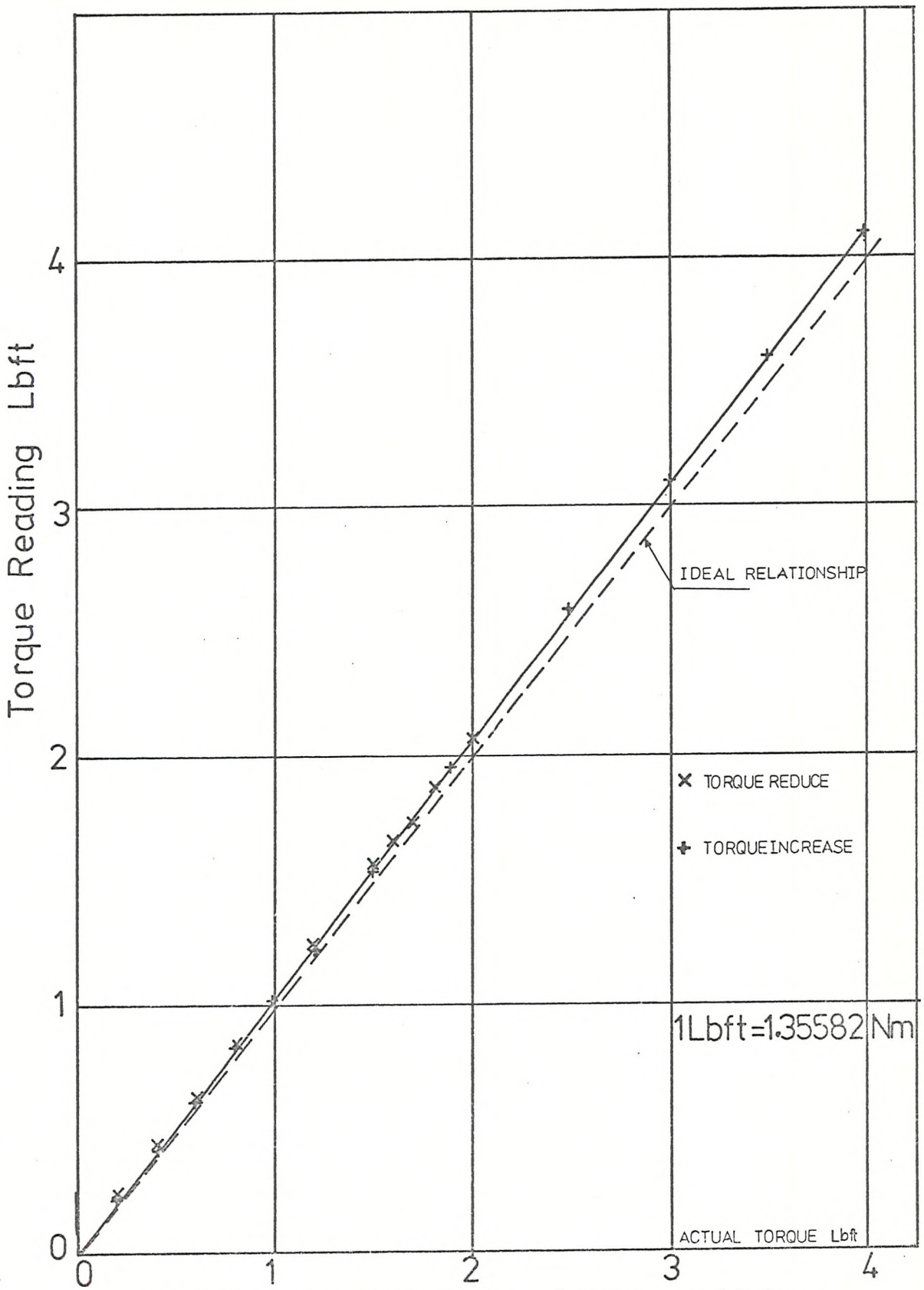

Fig44:Static Calibration Of Torque Meter

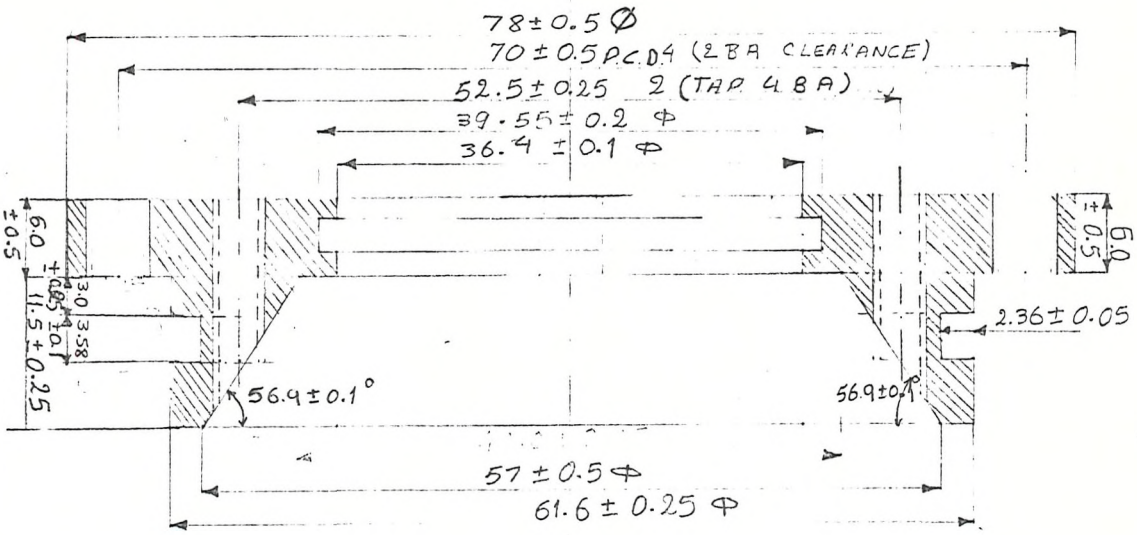

Fig45 : External Mounting of 35mm Oil Cooled Bearings

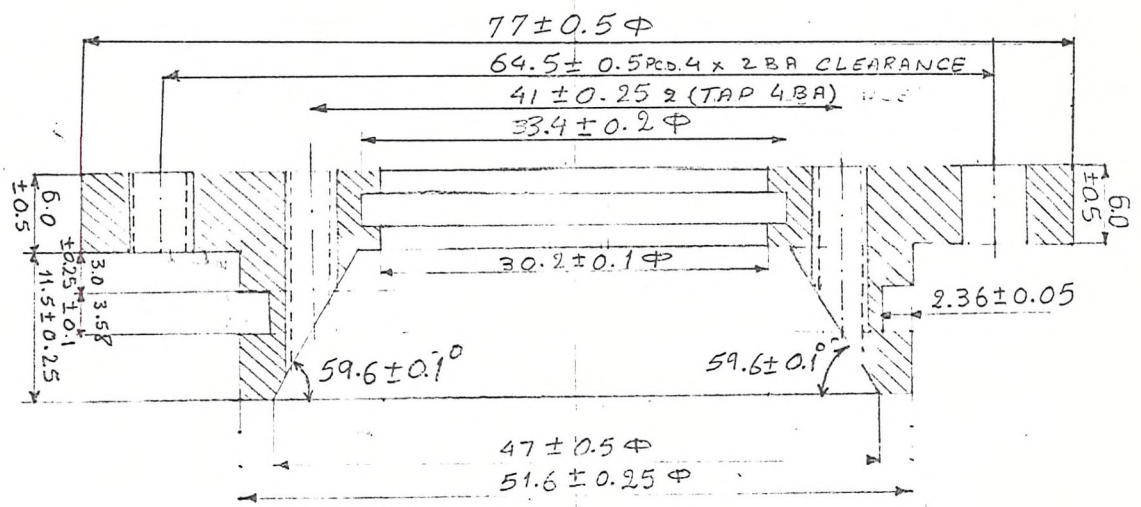

Fig46 : External Mounting of 25mm Oil Cooled Bearing

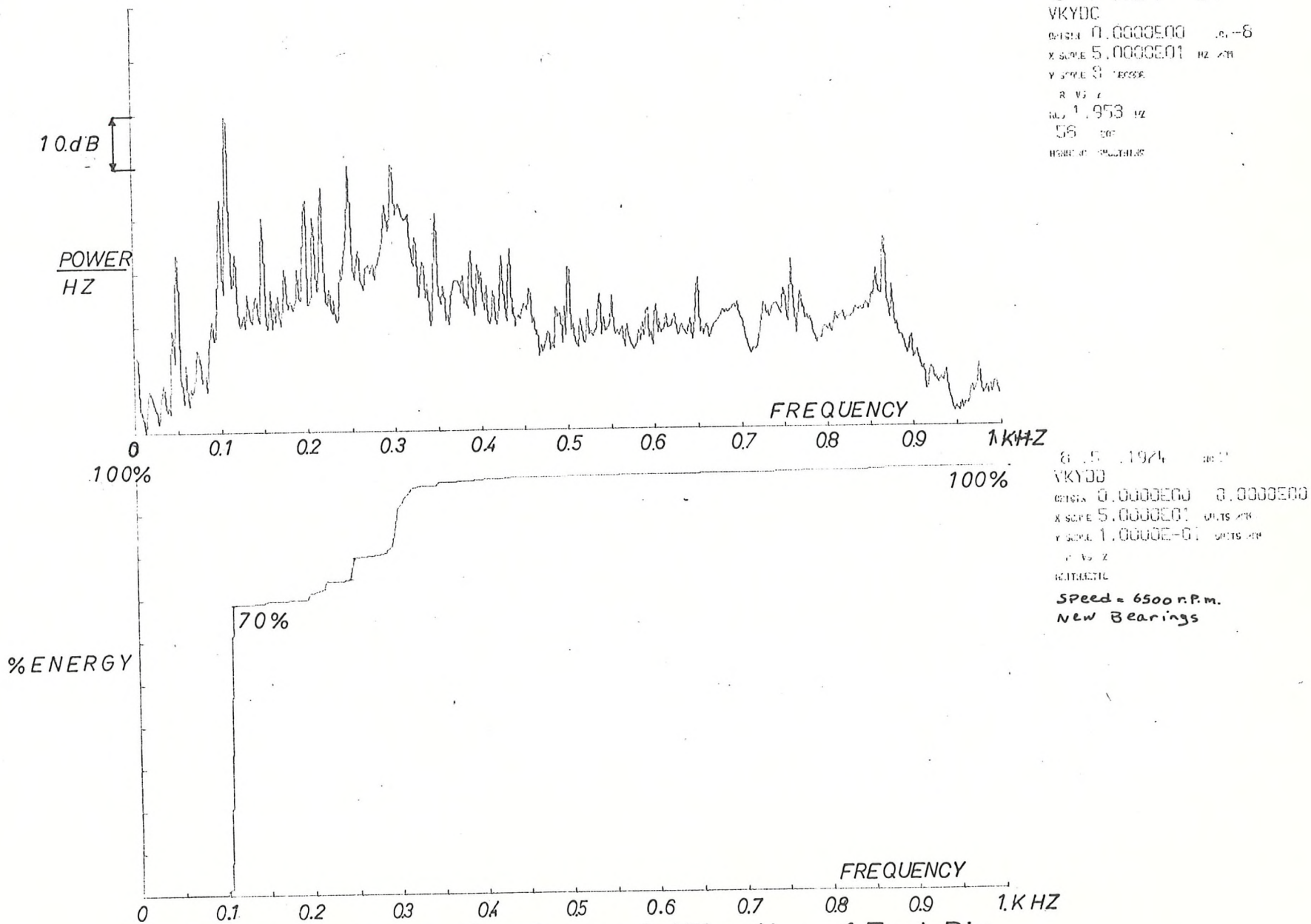

Fig 47 Frequency Spectrum of Vibration of Test Rig

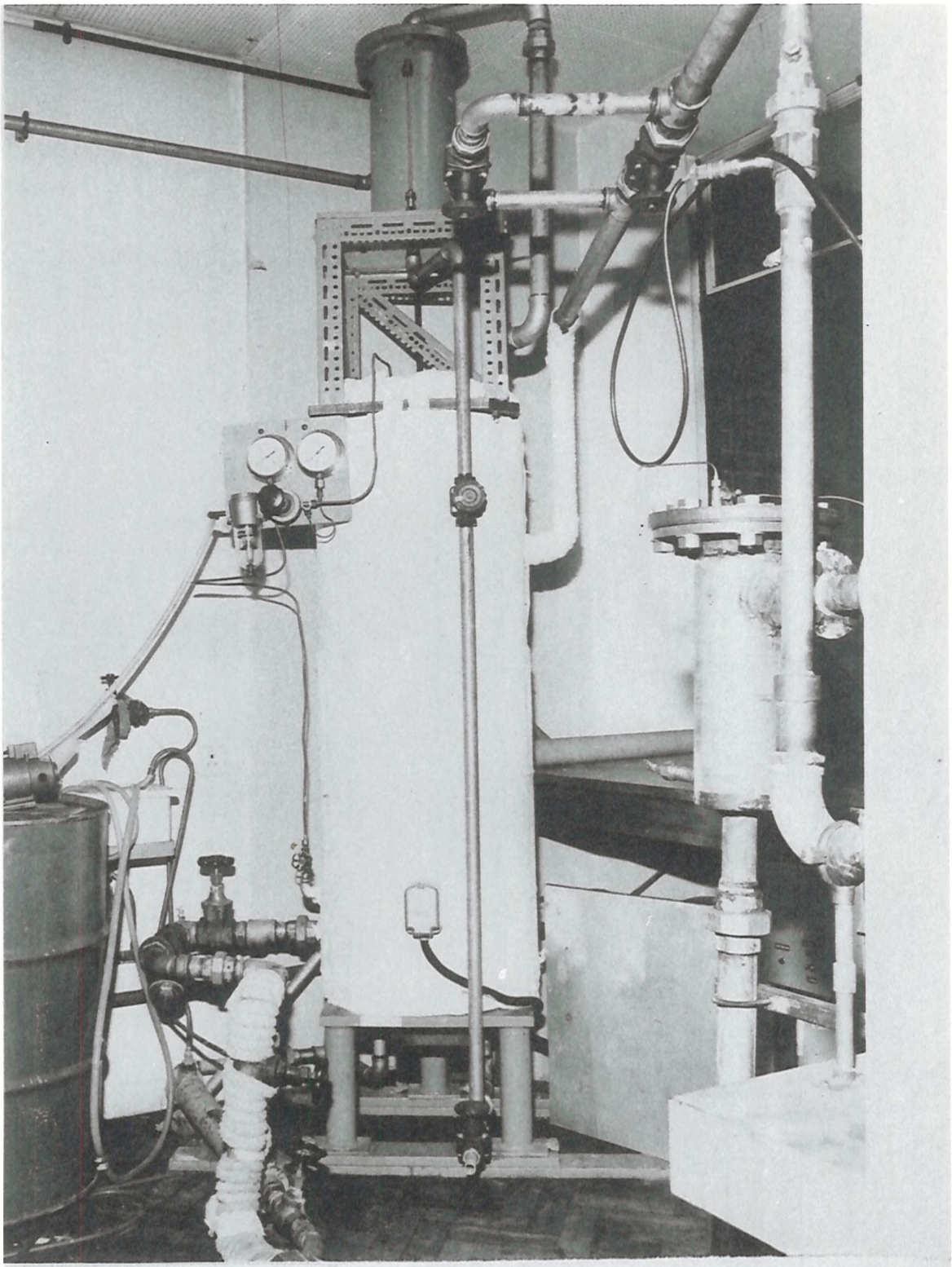

Fig 48 .Combination of Pressure & Expansion Tanks

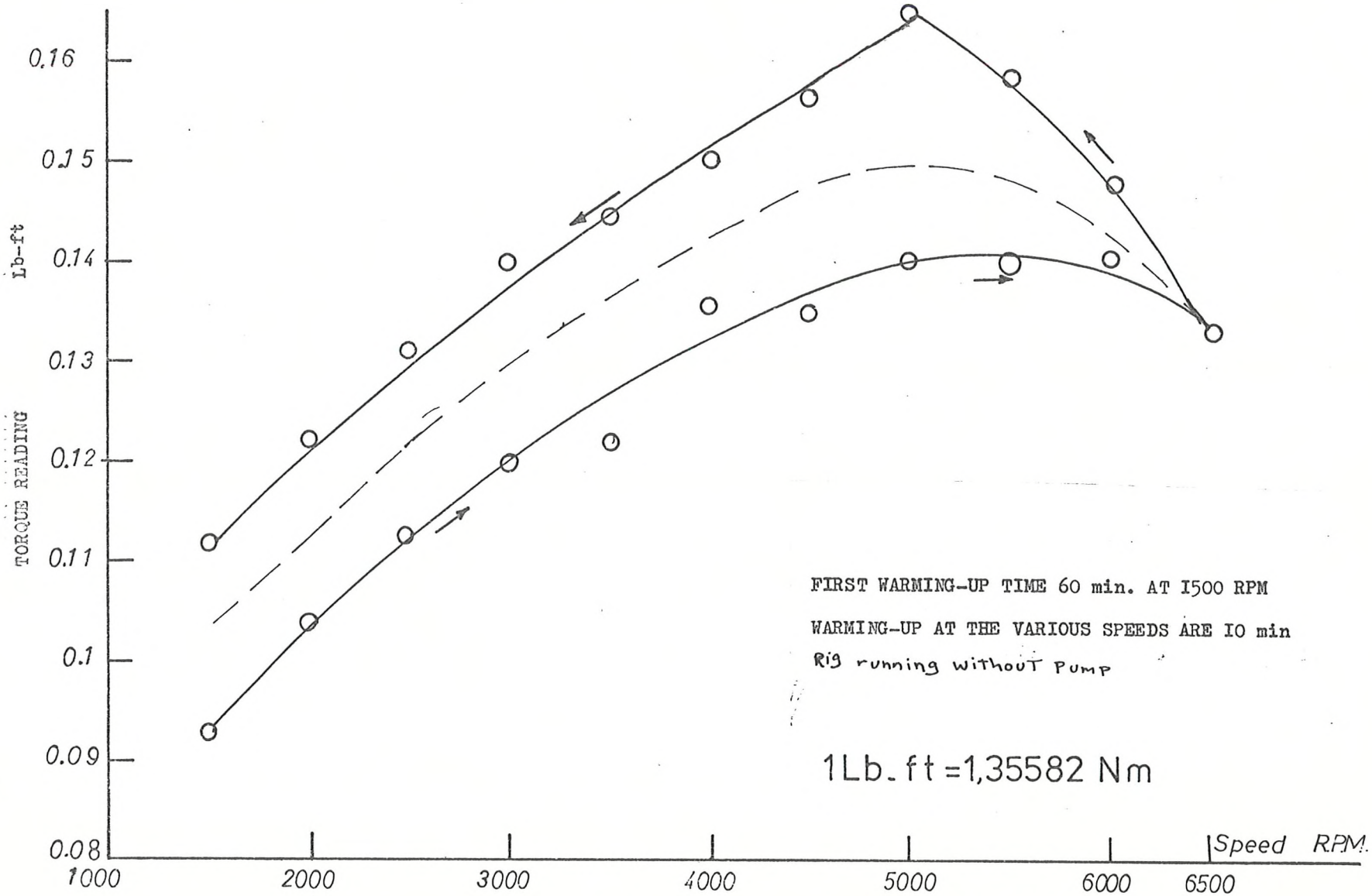

FIG 49: HISTERESIS IN TORQUE METER AFTER FINAL ATTENTION TO SYSTEM

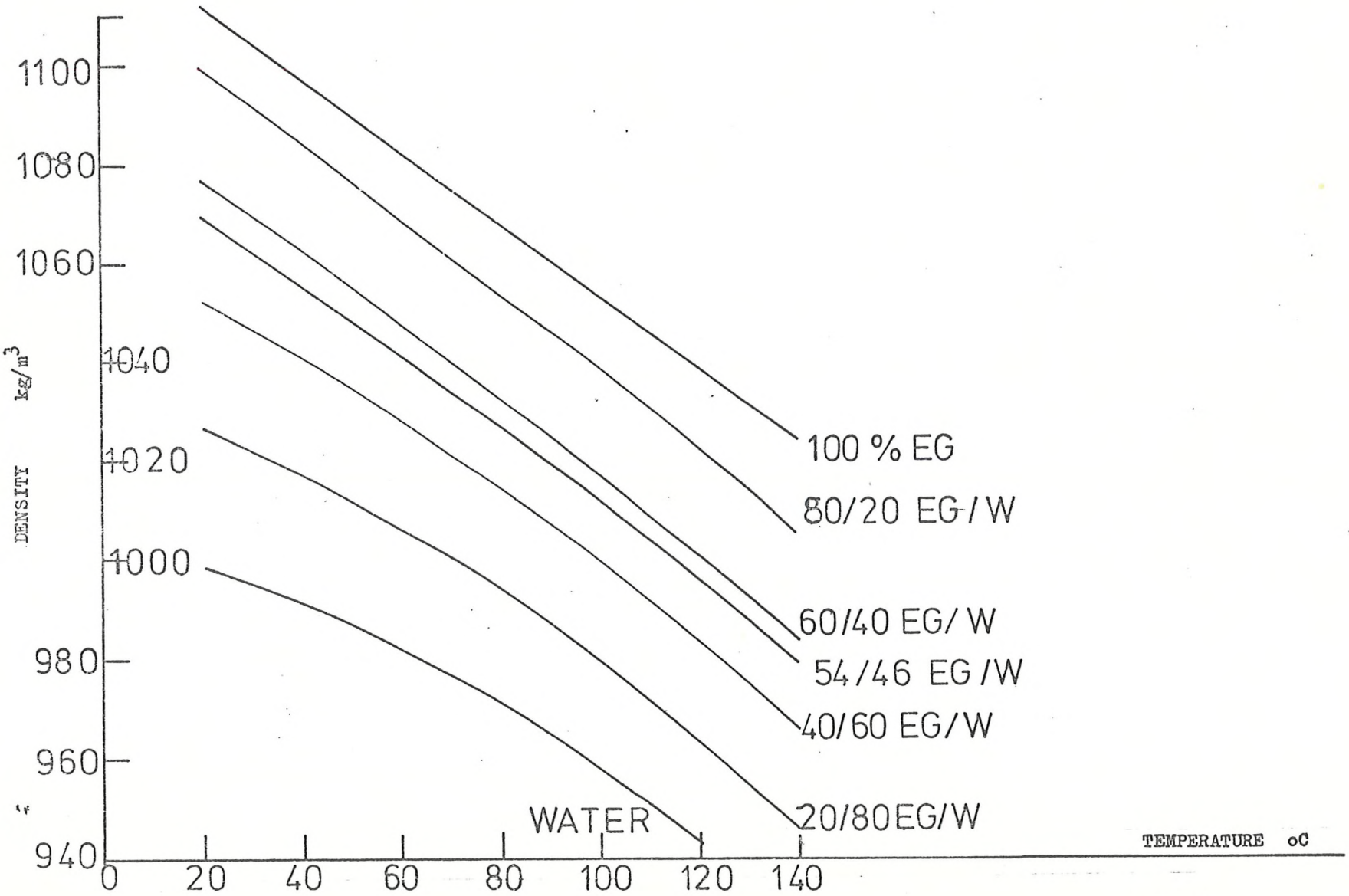

FIG 50: DENSITY OF ETHYLENE GLYCOL WATER MIXTURE AS A FUNCTION OF TEMPERATURE

Ref (78)

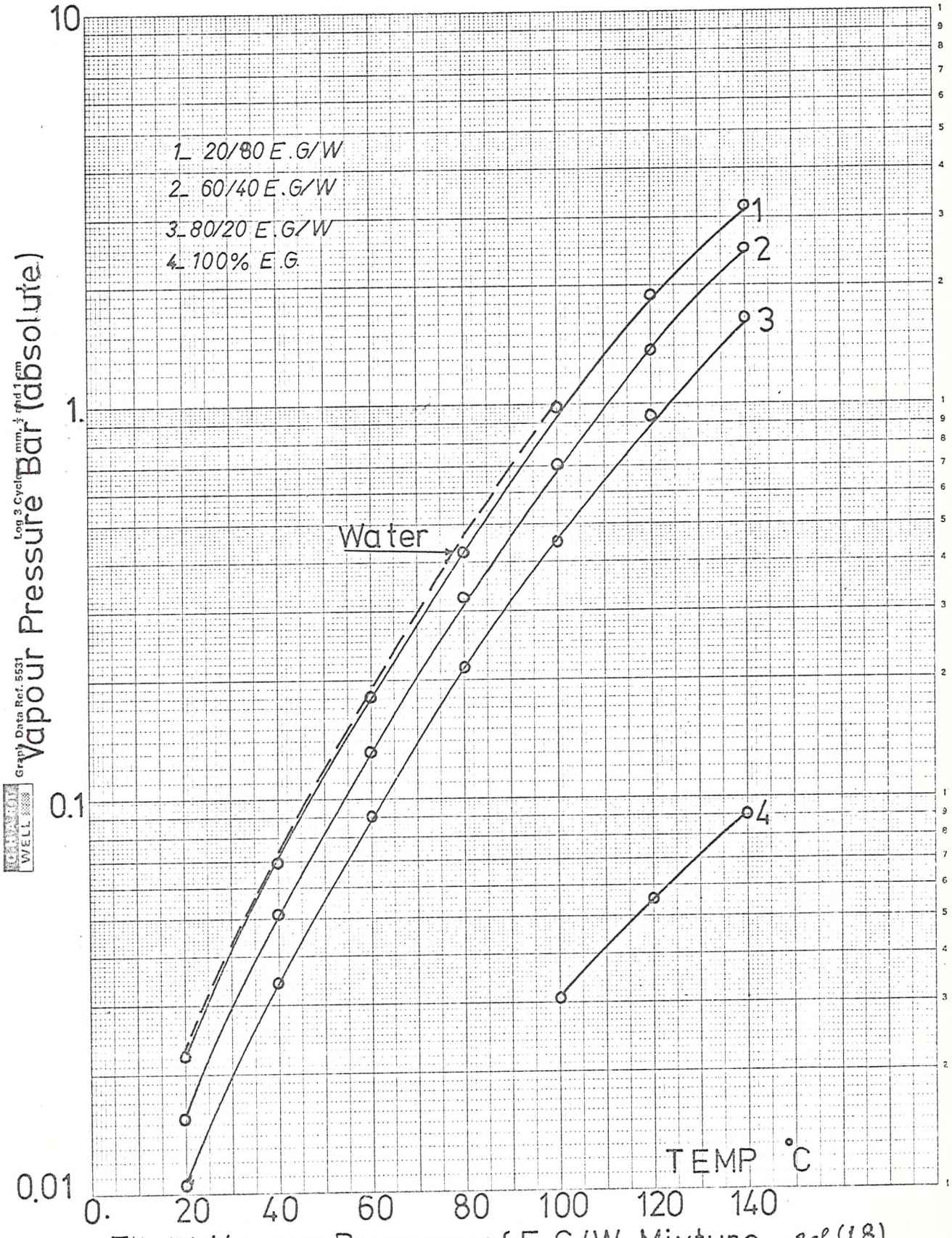

Fig 51 Vapour Pressure of E.G/W Mixture Ref (18)

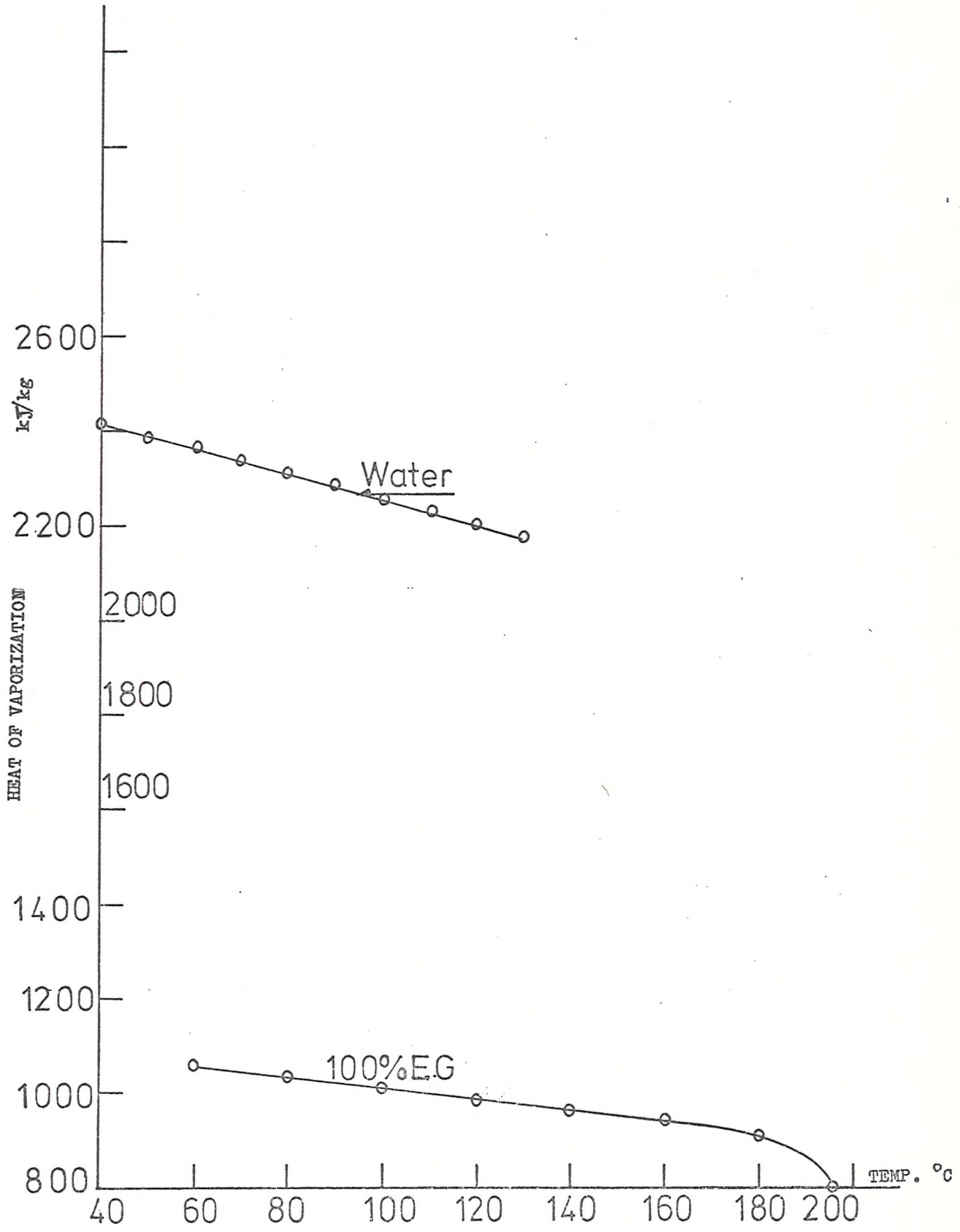

FIG 52: HEAT OF VAPORIZATION OF 100% ETHYLENE GLYCOL AND WATER Ref (18)

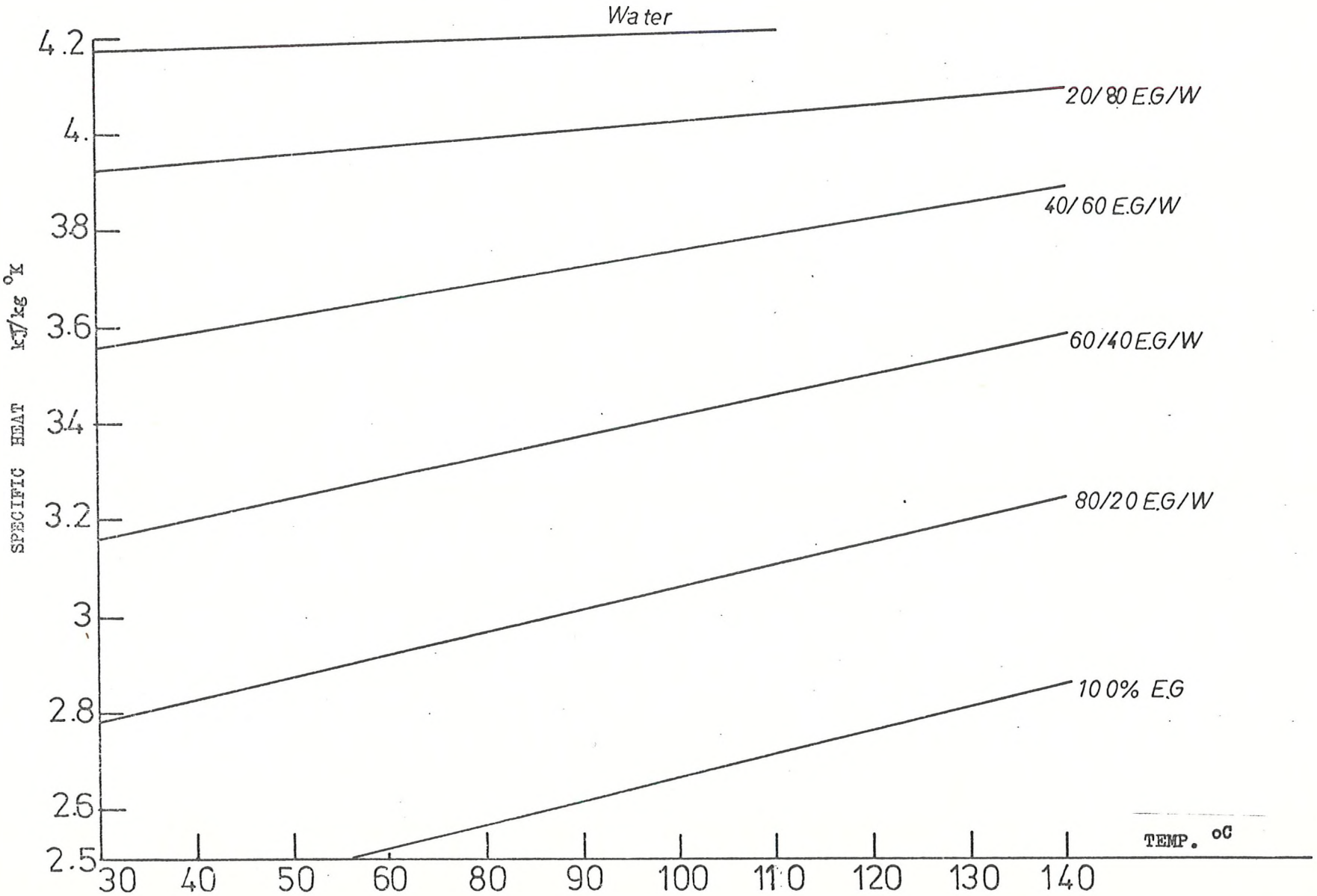

FIG 53: SPECIFIC HEAT OF ETHYLENE GLYCOL WATER MIXTURE Ref.(37) Ref (18)

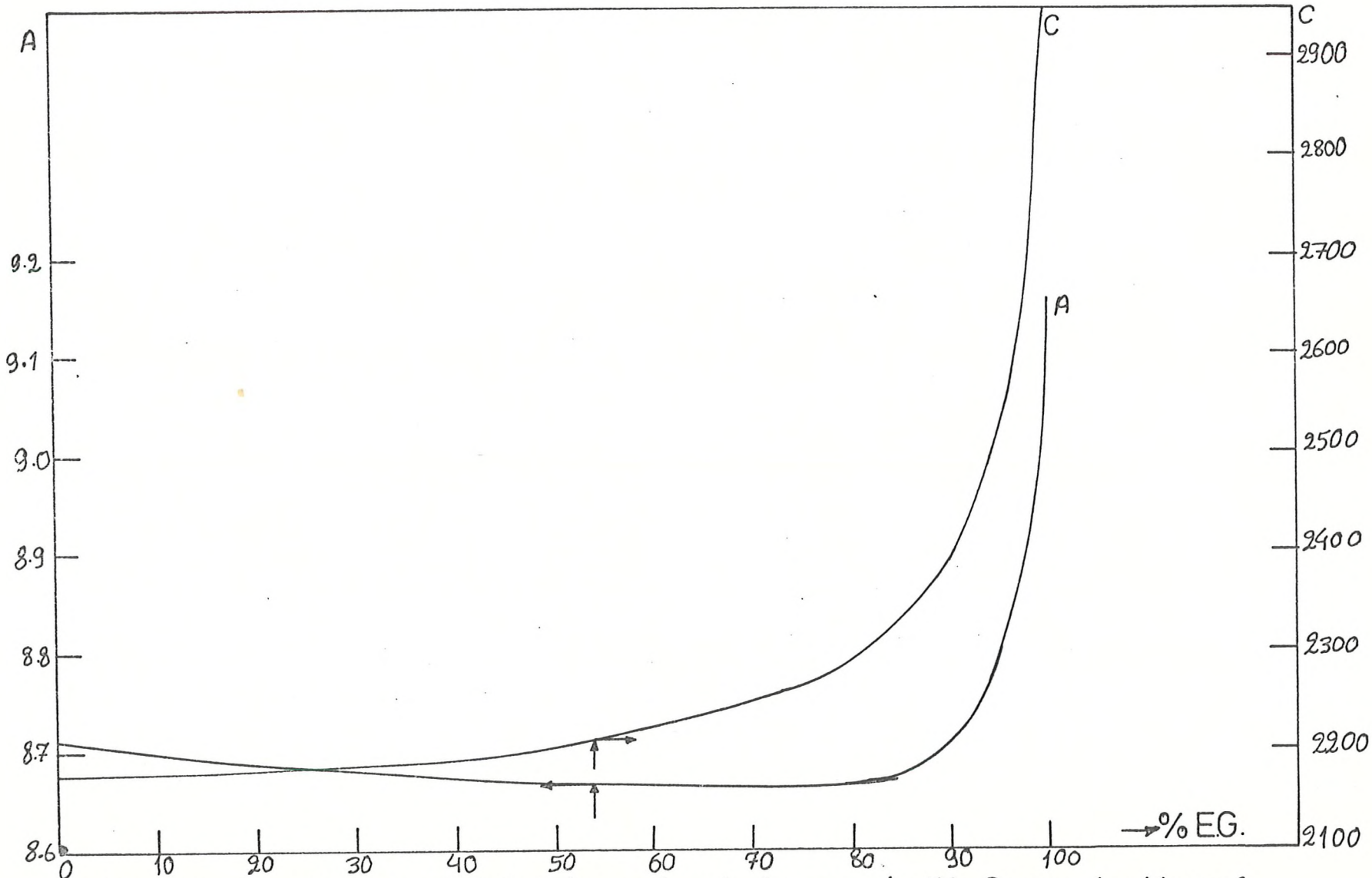

Fig 54 : Variation of A & C (constants in Eq. A6-13) with Concentration of EG/W Ref(21)

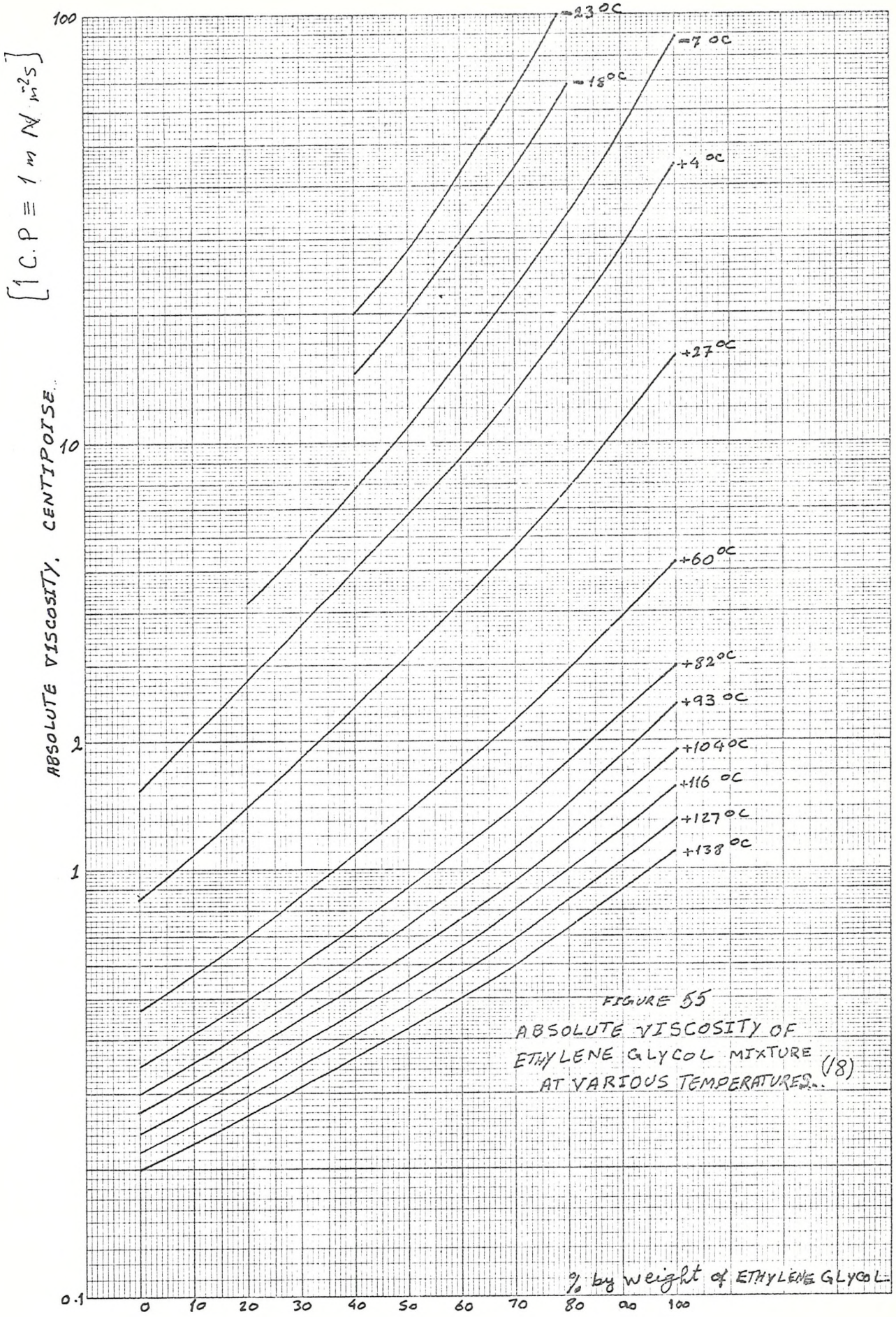

FIGURE 55
ABSOLUTE VISCOSITY OF ETHYLENE GLYCOL MIXTURE AT VARIOUS TEMPERATURES. (18)

FIG 55-

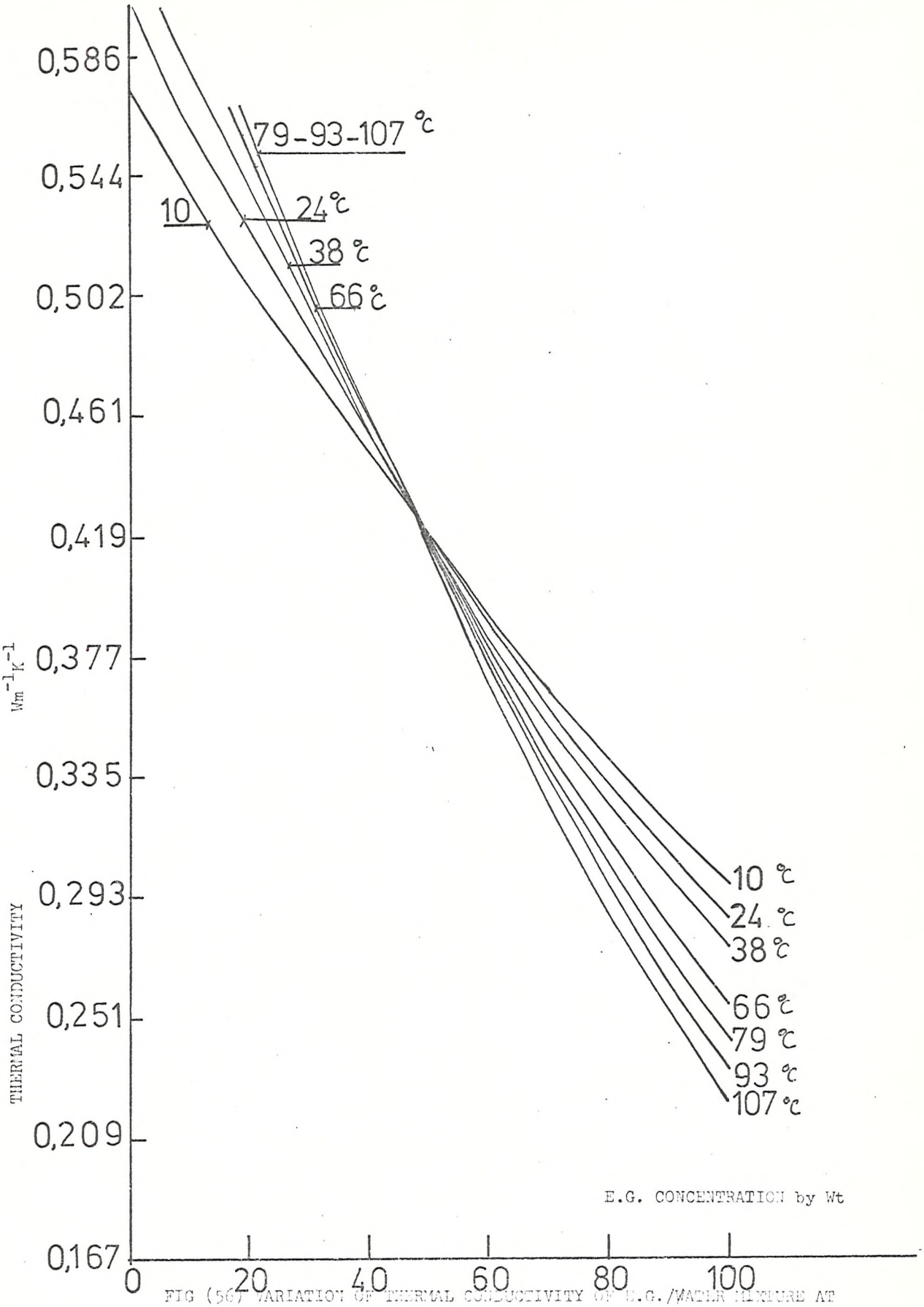

FIG (56) VARIATION OF THERMAL CONDUCTIVITY OF E.G./WATER MIXTURE AT VARIOUS TEMPERATURES Ref (18)

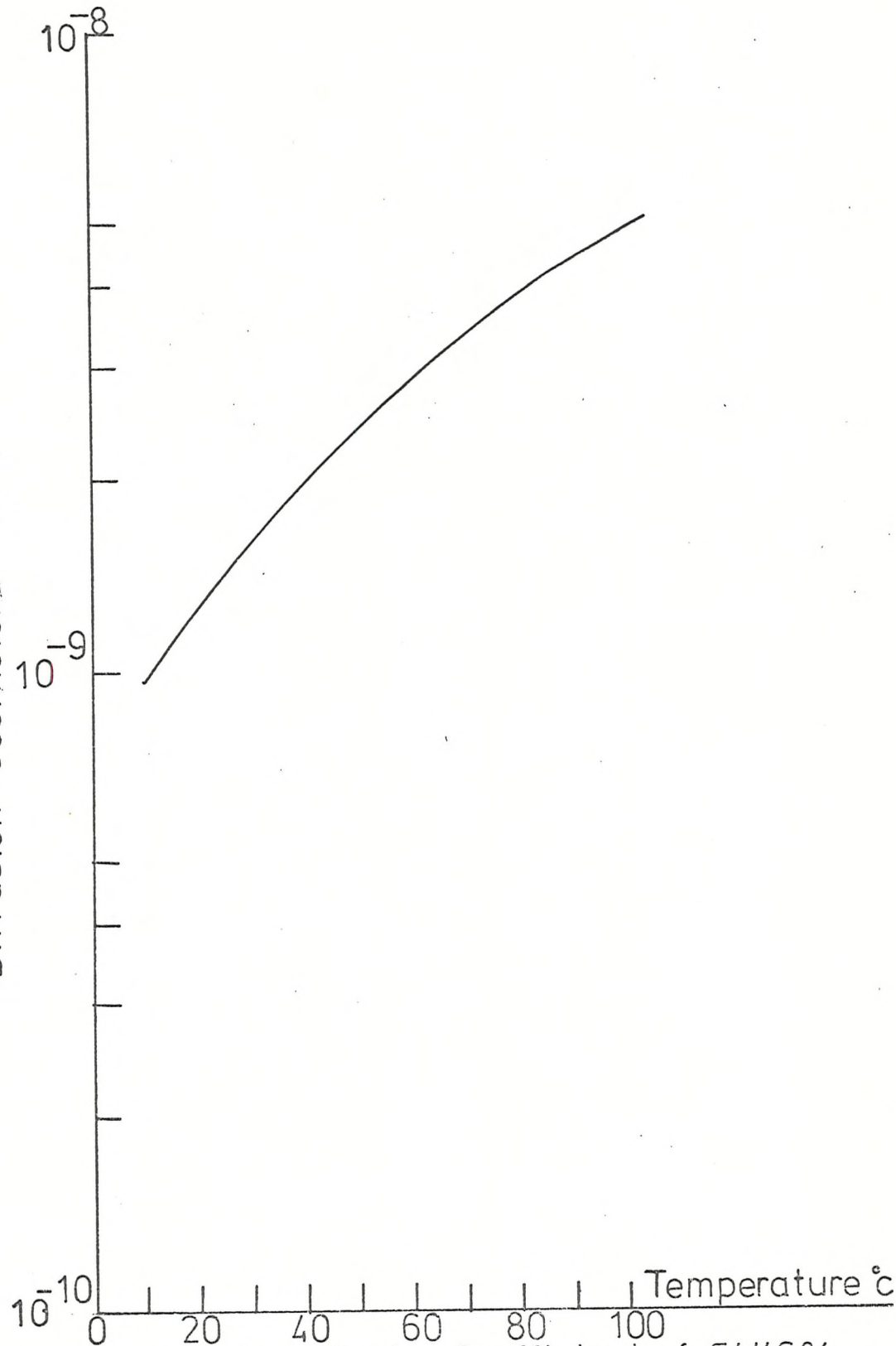

Fig 57- Diffusion Coefficient of 54/46% of E.G./W. at Various Temperatures (68)

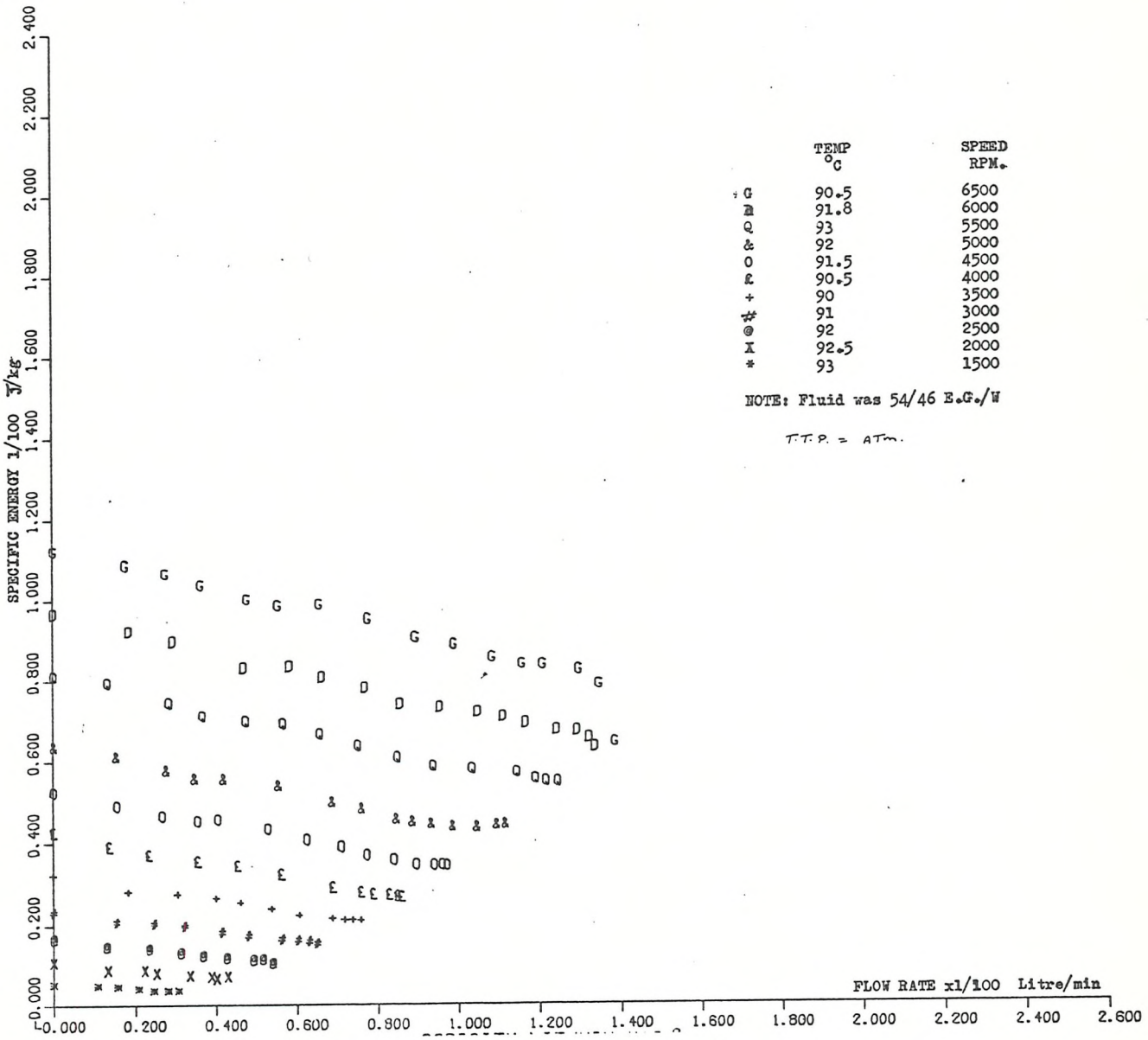

	TEMP °C	SPEED RPM.
G	90.5	6500
D	91.8	6000
Q	93	5500
&	92	5000
0	91.5	4500
£	90.5	4000
+	90	3500
#	91	3000
@	92	2500
X	92.5	2000
*	93	1500

NOTE: Fluid was 54/46 E.G./W

T.T.P. = ATm.

FIG 58: HEAD/FLOW CURVE FOR PUMP (B) AT 90 °C

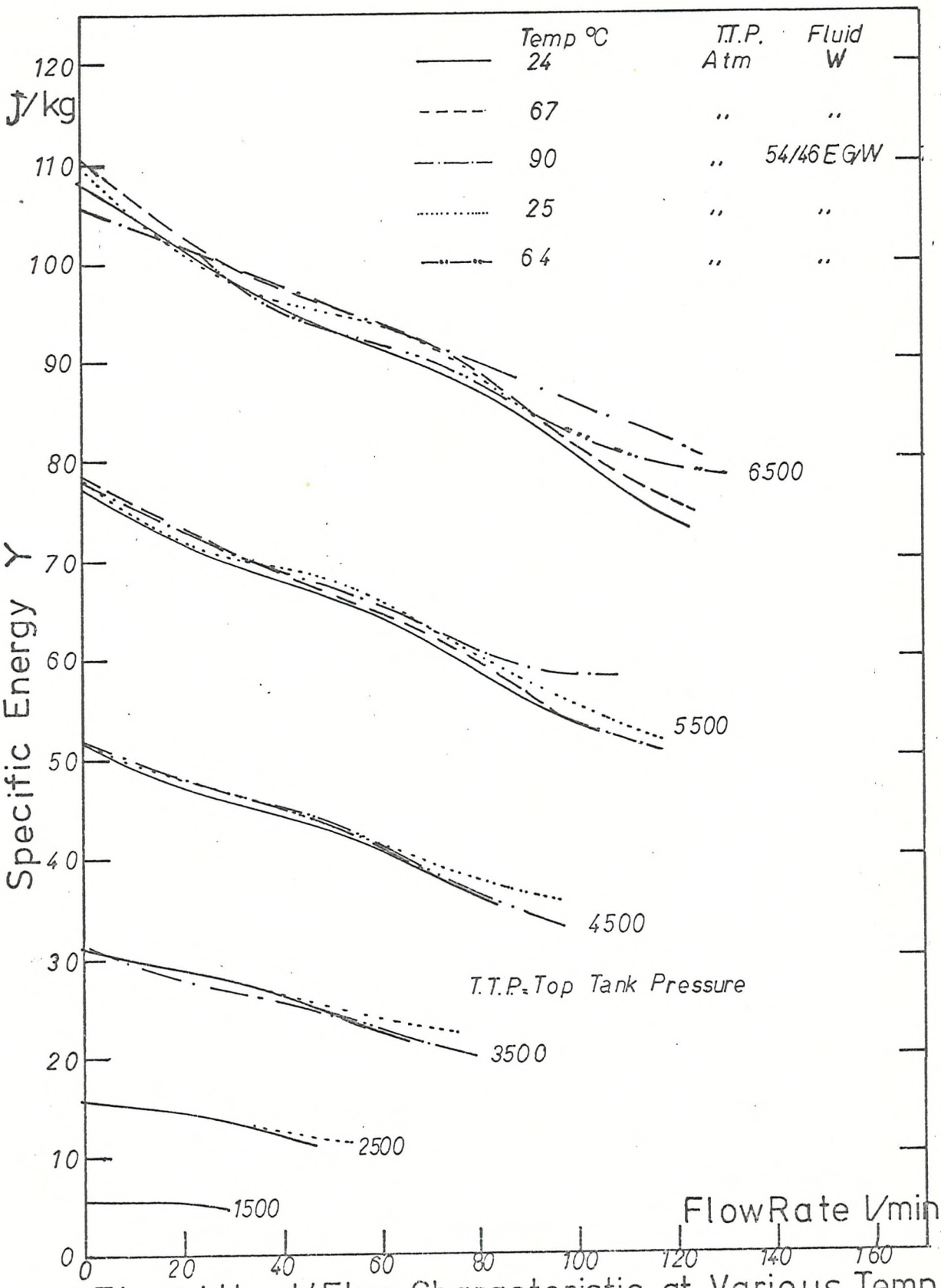

Fig 59 : Head/Flow Characteristic at Various Temp. in Pump B

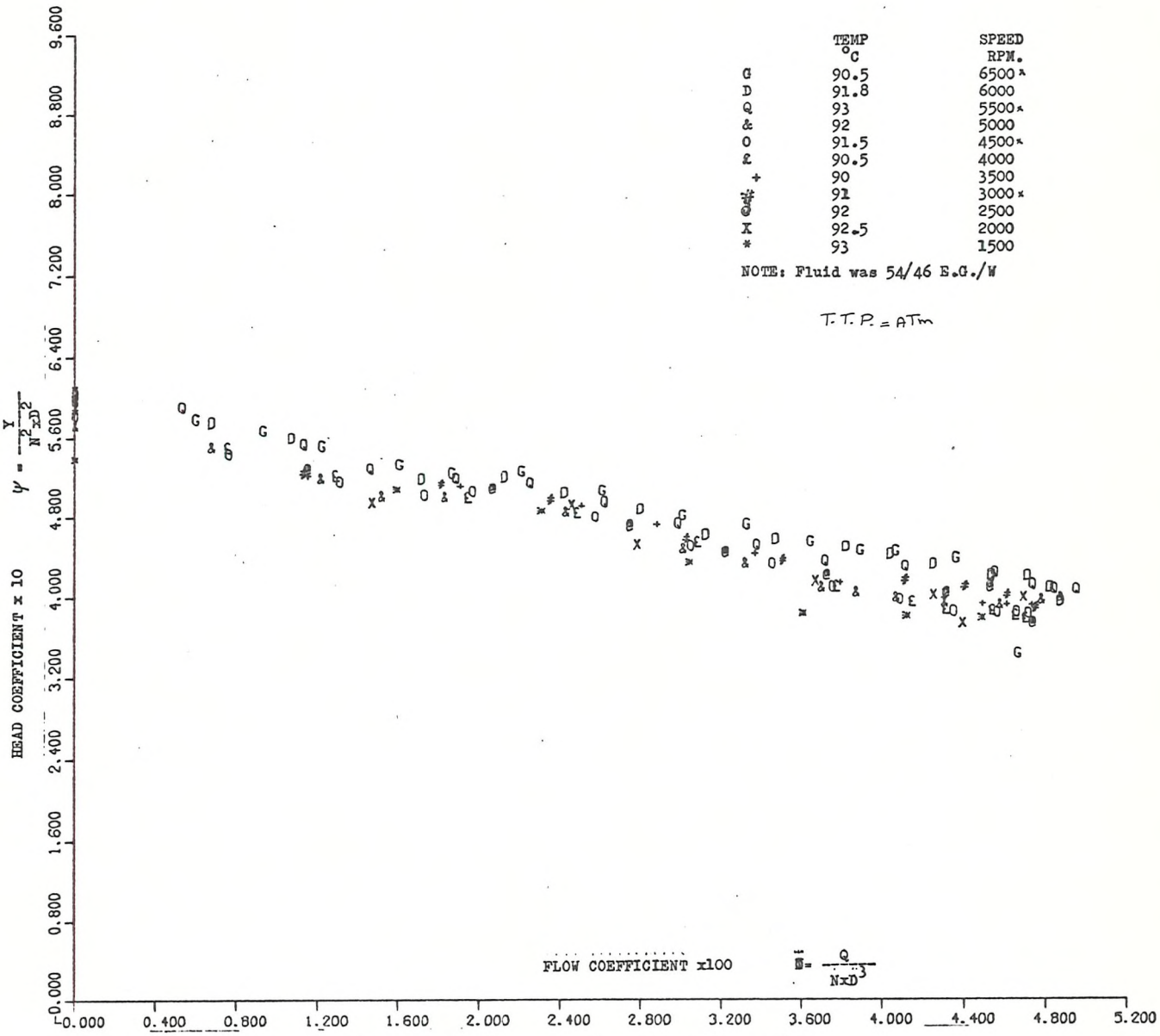

FIG 60: NON DIMENSIONAL FORM OF HEAD/FLOW CHARACTERISTIC AT 90°C AND VARIOUS SPEED ON PUMP (B).

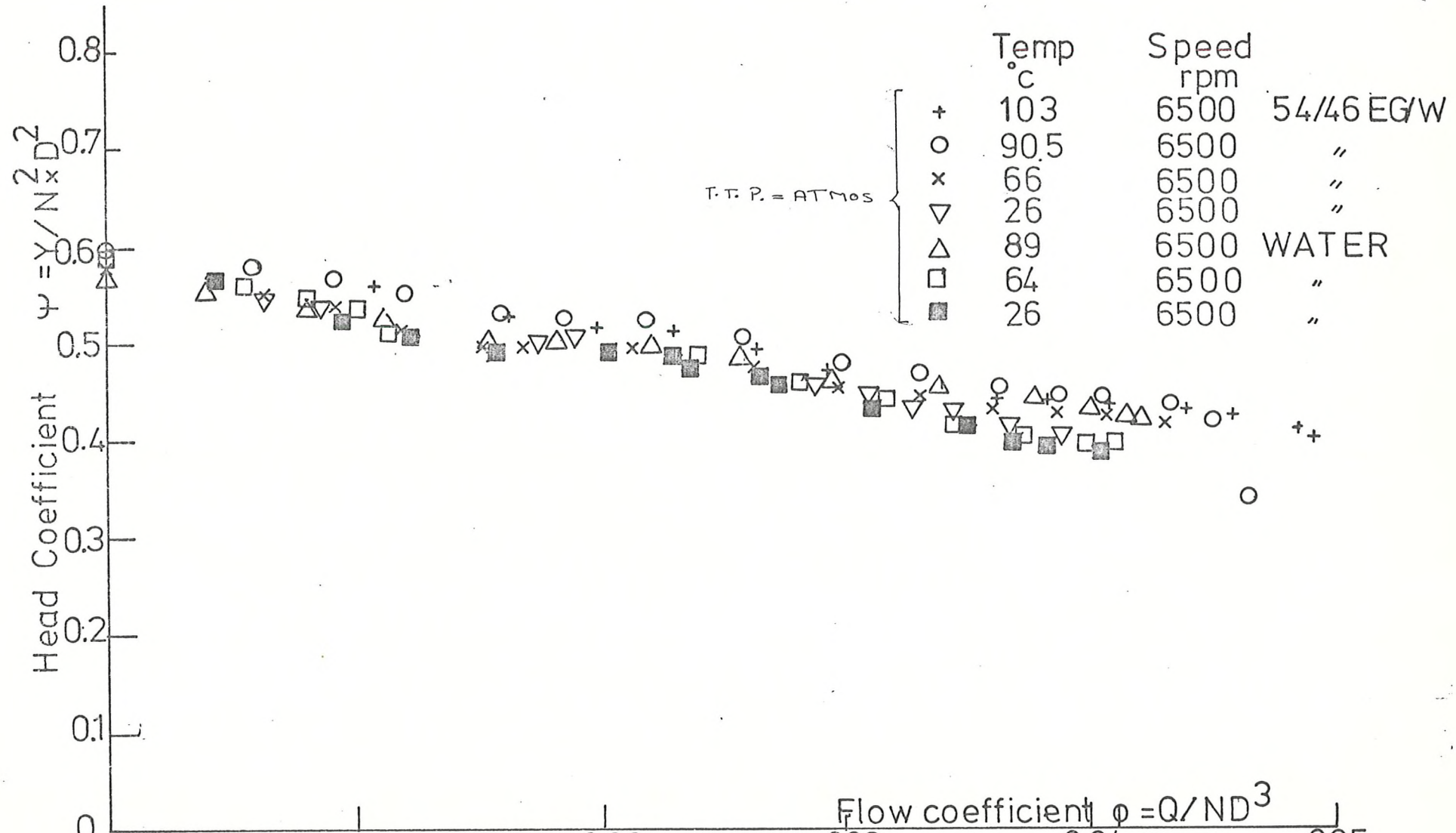

Fig 61: Nondimensional Head/Flow Characteristic at Various Temp. (pump B)

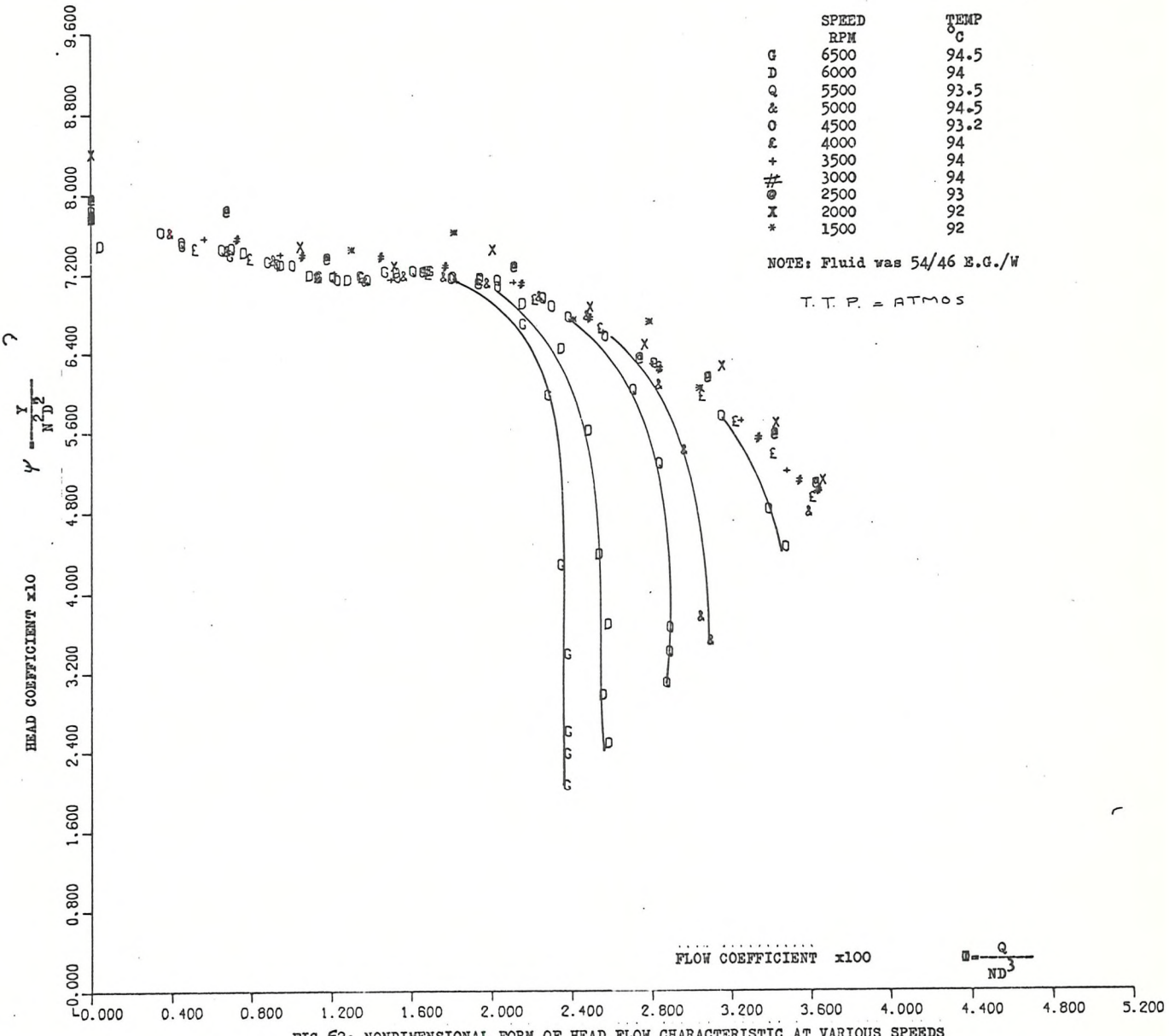

FIG 62: NONDIMENSIONAL FORM OF HEAD FLOW CHARACTERISTIC AT VARIOUS SPEEDS FOR PUMP (A)

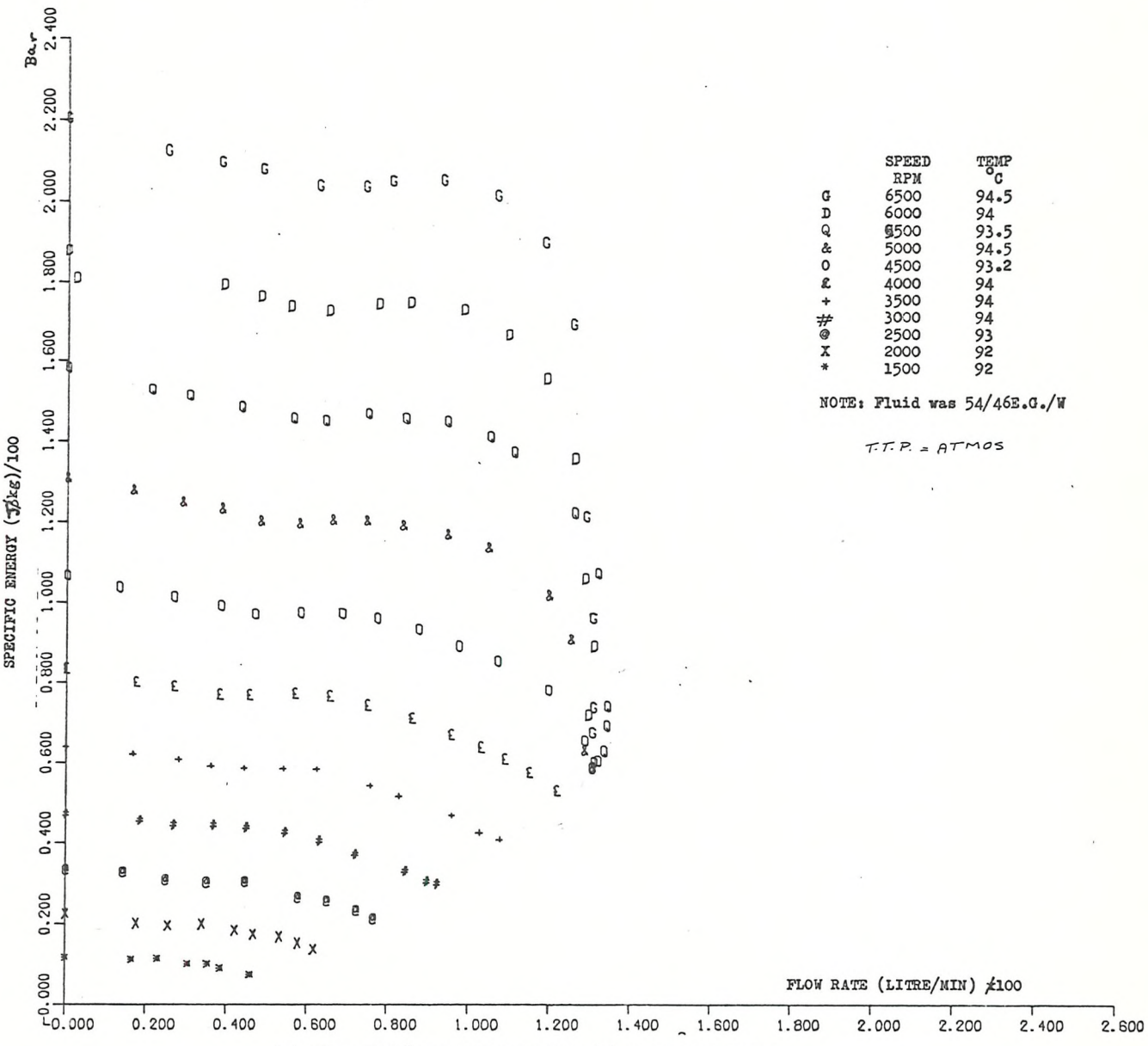

FIG 52-A: HEAD/FLOW CURVE FOR PUMP (A) AT VARIOUS SPEEDS

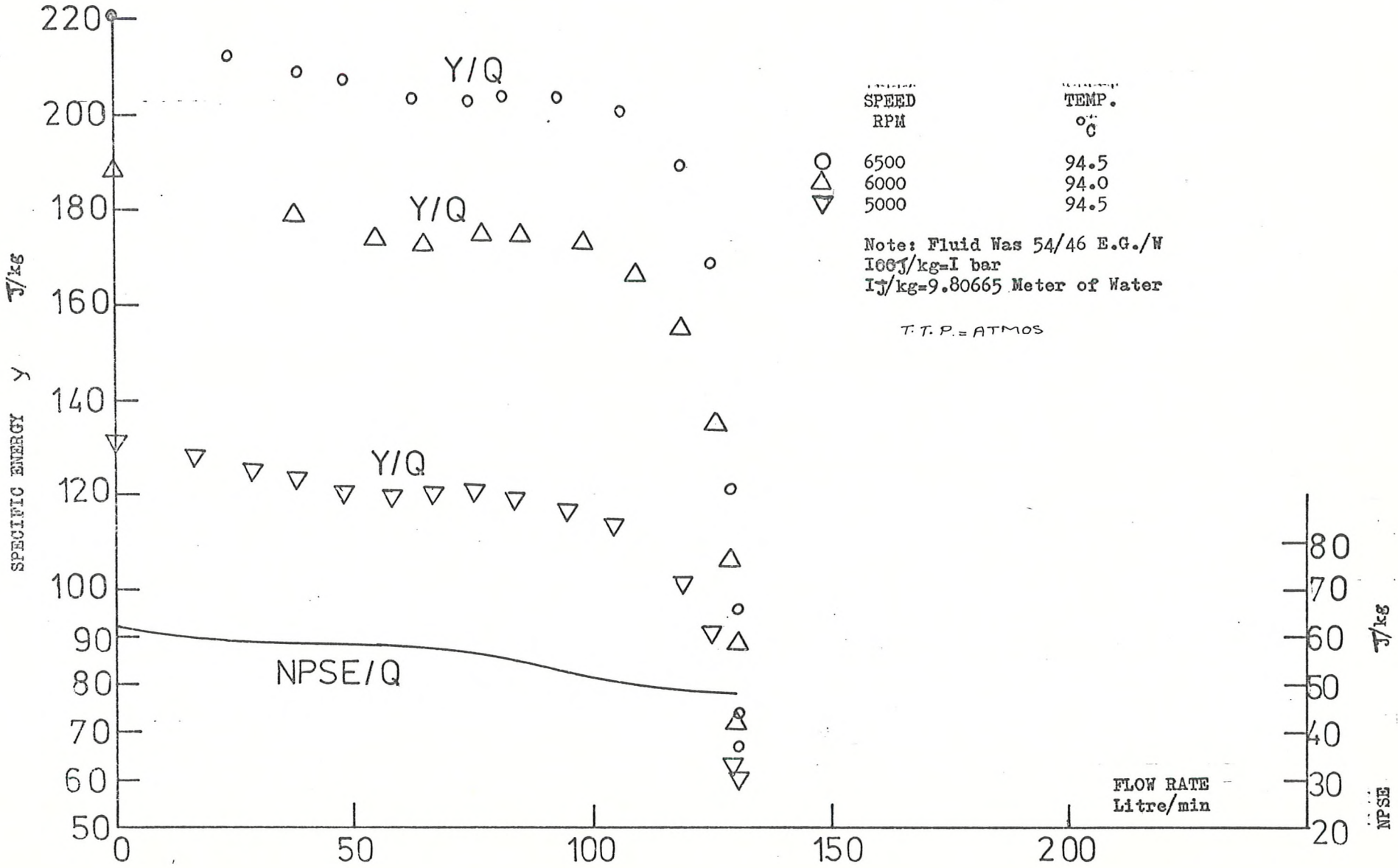

FIG.63: EFFECT OF SPEED ON FLOW RATE AT BREACKDOWN FOR PUMP (A)

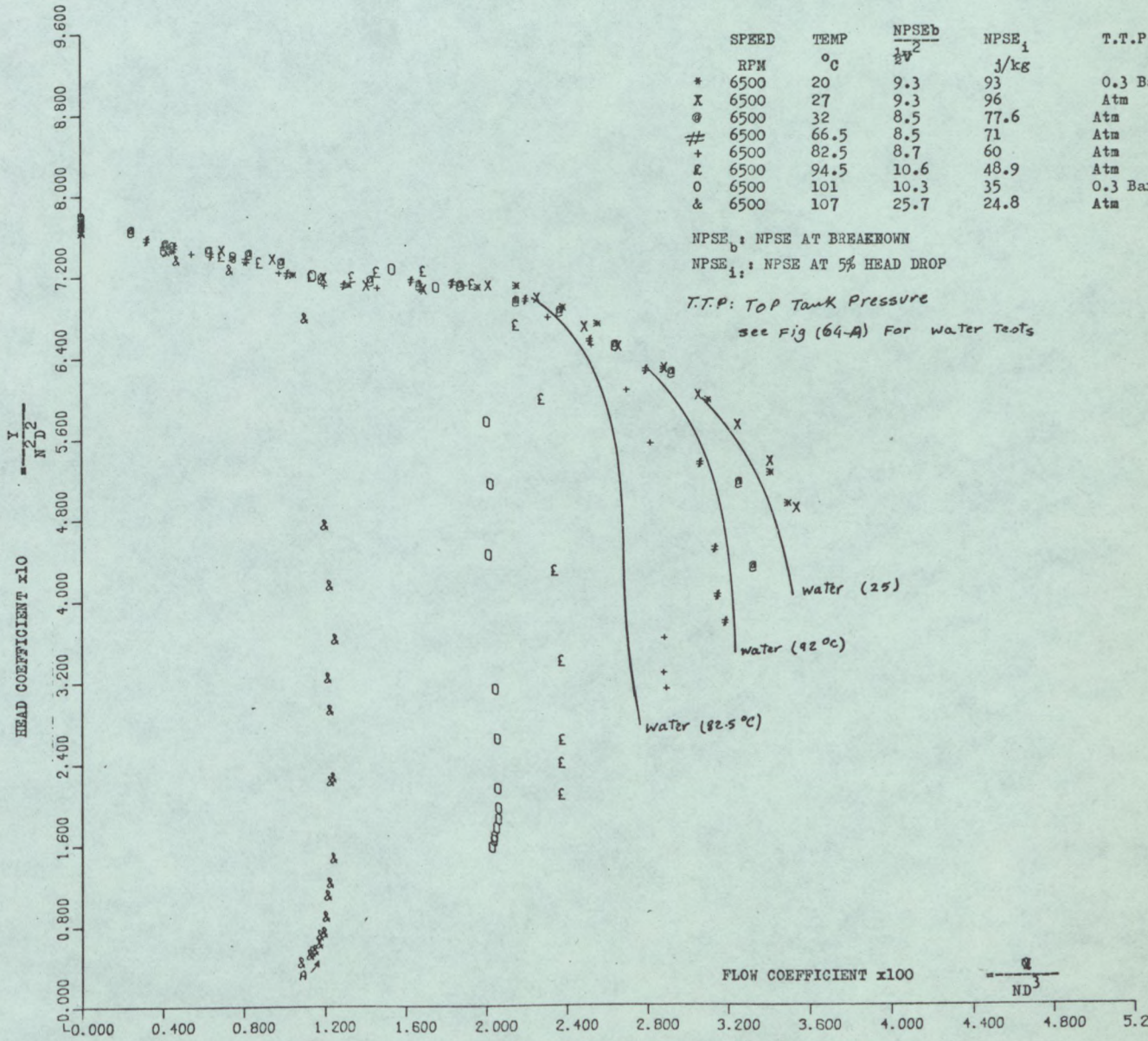

	SPEED RPM	TEMP °C	$\frac{NPSE_b}{\frac{1}{2}V^2}$	$NPSE_i$ J/kg	T.T.P
*	6500	20	9.3	93	0.3 Bar
X	6500	27	9.3	96	Atm
@	6500	32	8.5	77.6	Atm
#	6500	66.5	8.5	71	Atm
+	6500	82.5	8.7	60	Atm
£	6500	94.5	10.6	48.9	Atm
0	6500	101	10.3	35	0.3 Bar
&	6500	107	25.7	24.8	Atm

$NPSE_b$: NPSE AT BREAKDOWN

$NPSE_i$: NPSE AT 5% HEAD DROP

T.T.P: Top Tank Pressure

see Fig (64-A) For water Tests

FIG 64: NONDIMENSIONAL HEAD/FLOW CHARACTERISTIC AT VARIOUS TEMPERATURES IN PUMP (A) FOR 54/46 E.G./W &*WATER*

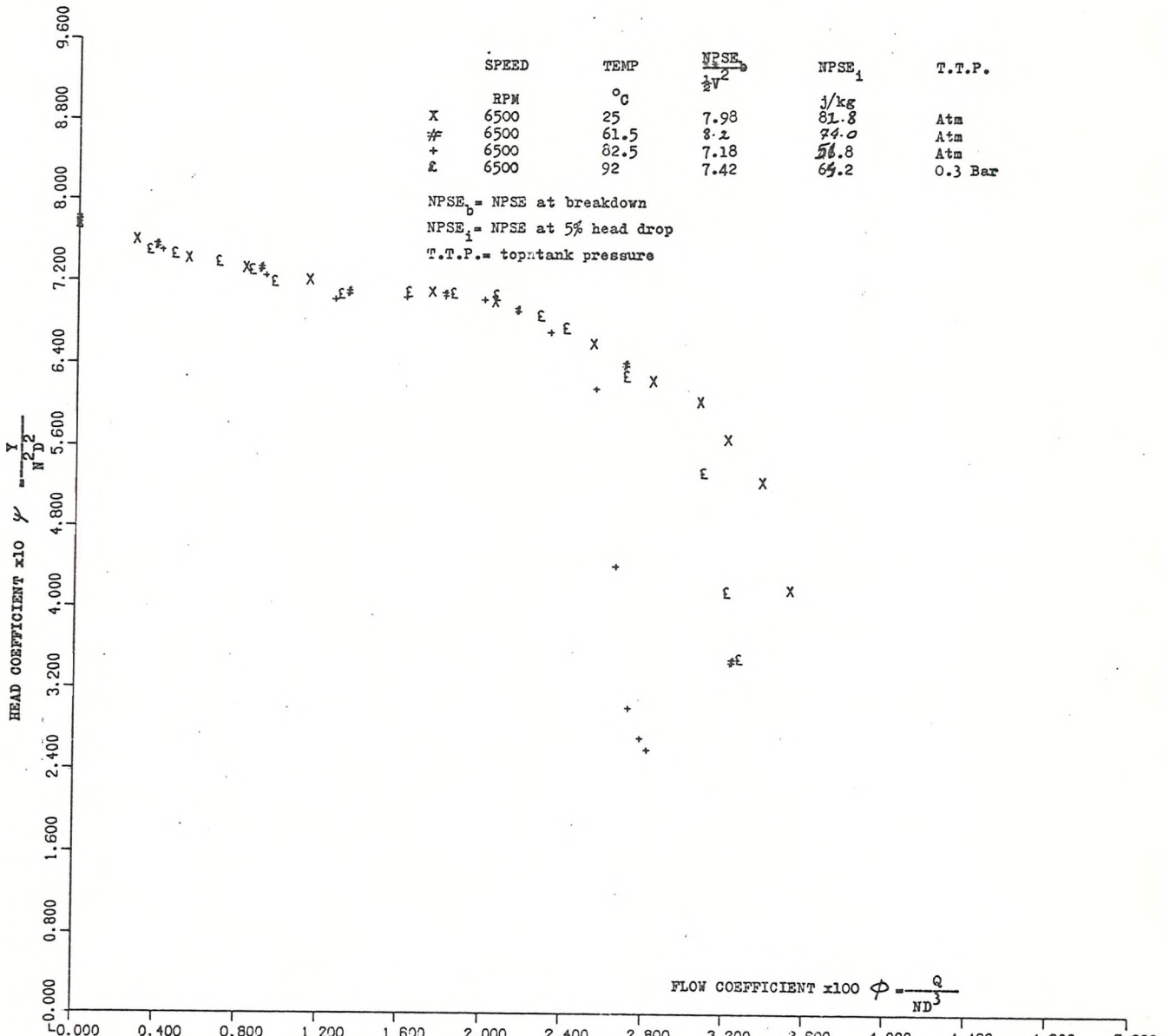

	SPEED	TEMP	$\frac{NPSE_b}{\frac{1}{2}V^2}$	$NPSE_i$	T.T.P.
	RPM	°C		j/kg	
X	6500	25	7.98	81.8	Atm
#	6500	61.5	8.2	74.0	Atm
+	6500	82.5	7.18	56.8	Atm
£	6500	92	7.42	65.2	0.3 Bar

$NPSE_b$ = NPSE at breakdown

$NPSE_i$ = NPSE at 5% head drop

T.T.P.= toptank pressure

FIG 4-A: NONDIMENSIONAL HEAD/FLOW CHARACTERISTIC AT VARIOUS TEMPERATURES IN PUMP (A) FOR WATER

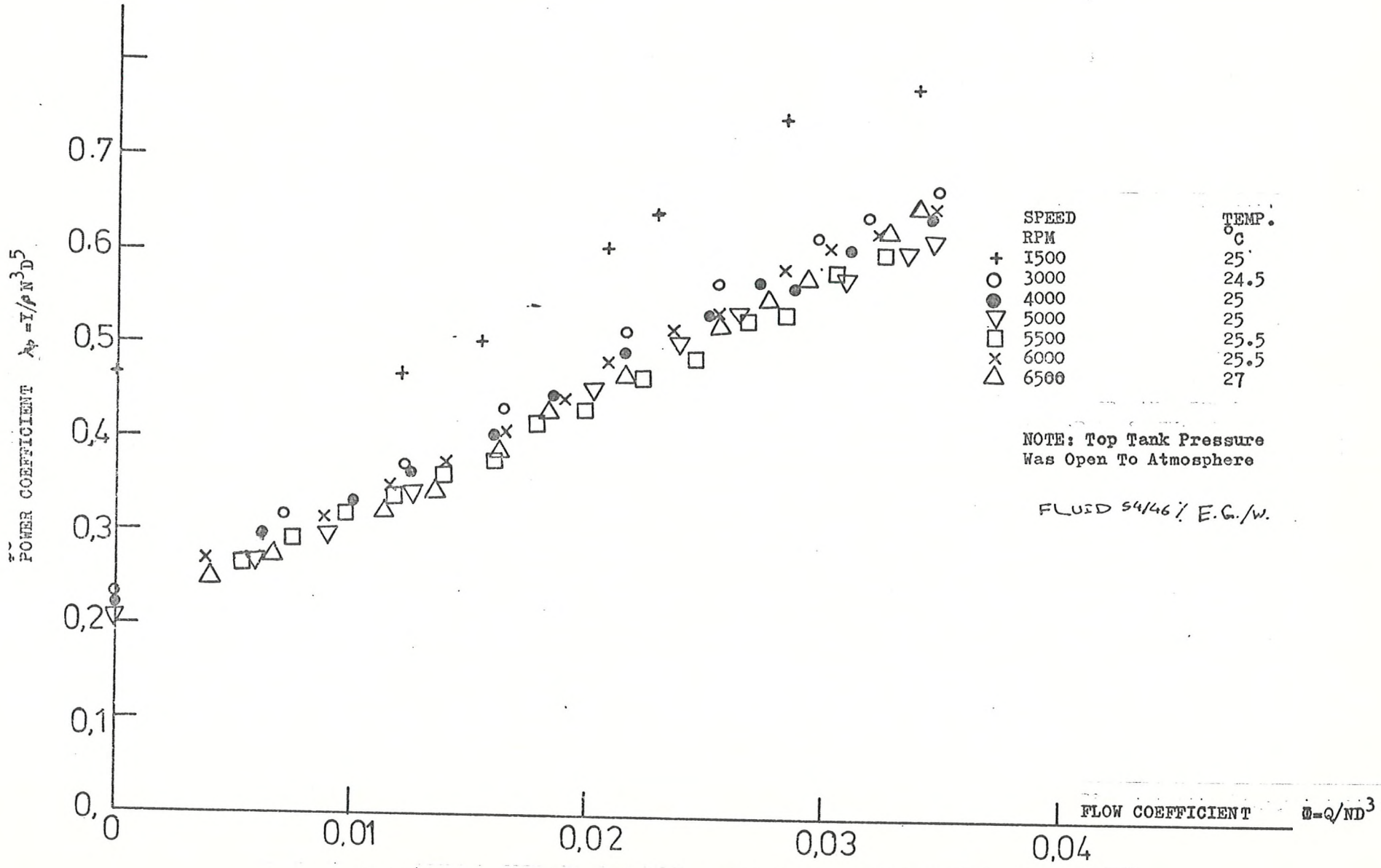

FIG 65: NONDIMENSIONAL FORM OF POWER/FLOW CHARACTERISTIC AT VARIOUS SPEEDS ON PUMP (A)

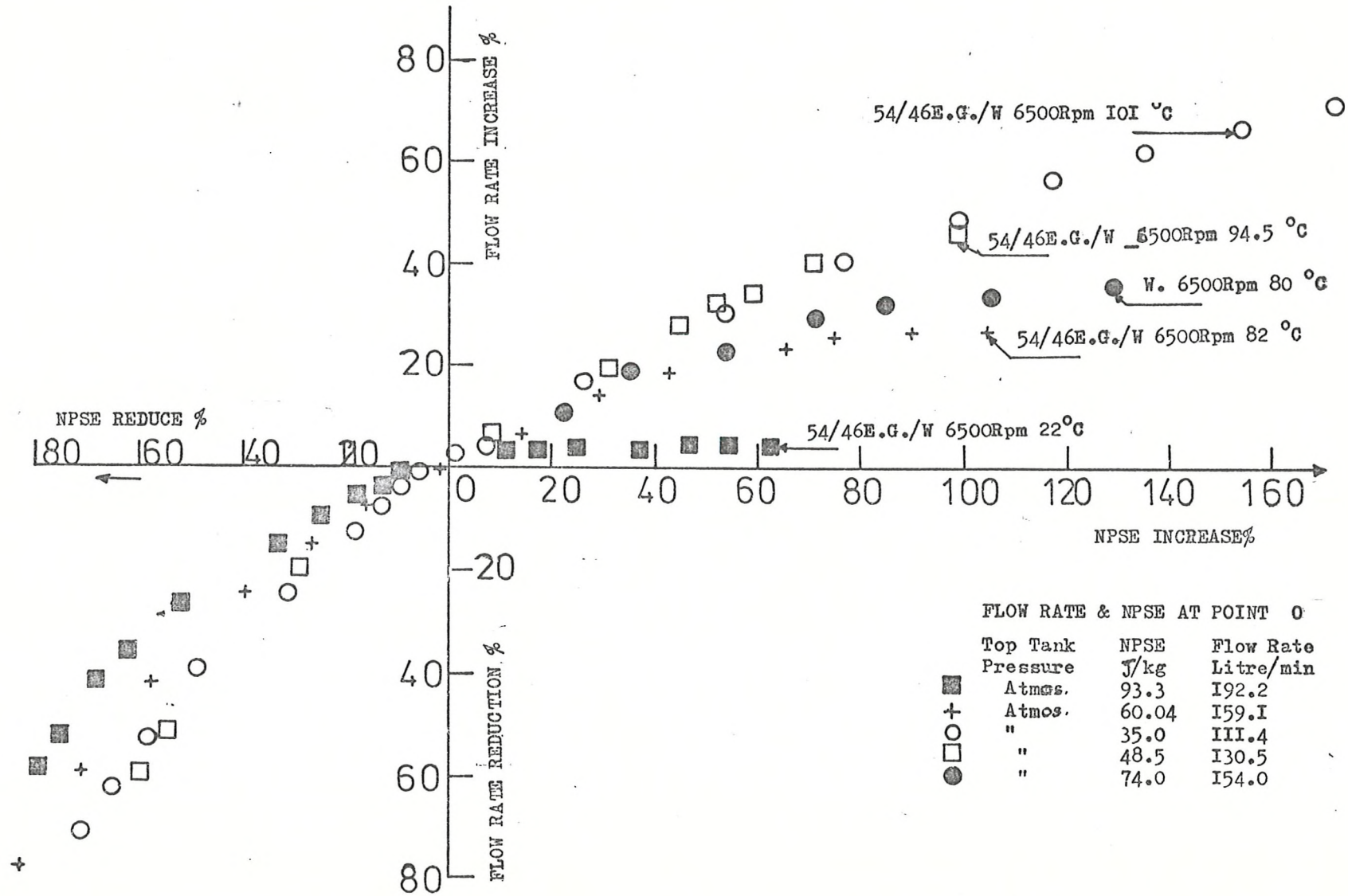

FIG 66: EFFECT OF EXTERNAL PRESSURE ON TOP TANK ON FLOW RATE ON PUMP A

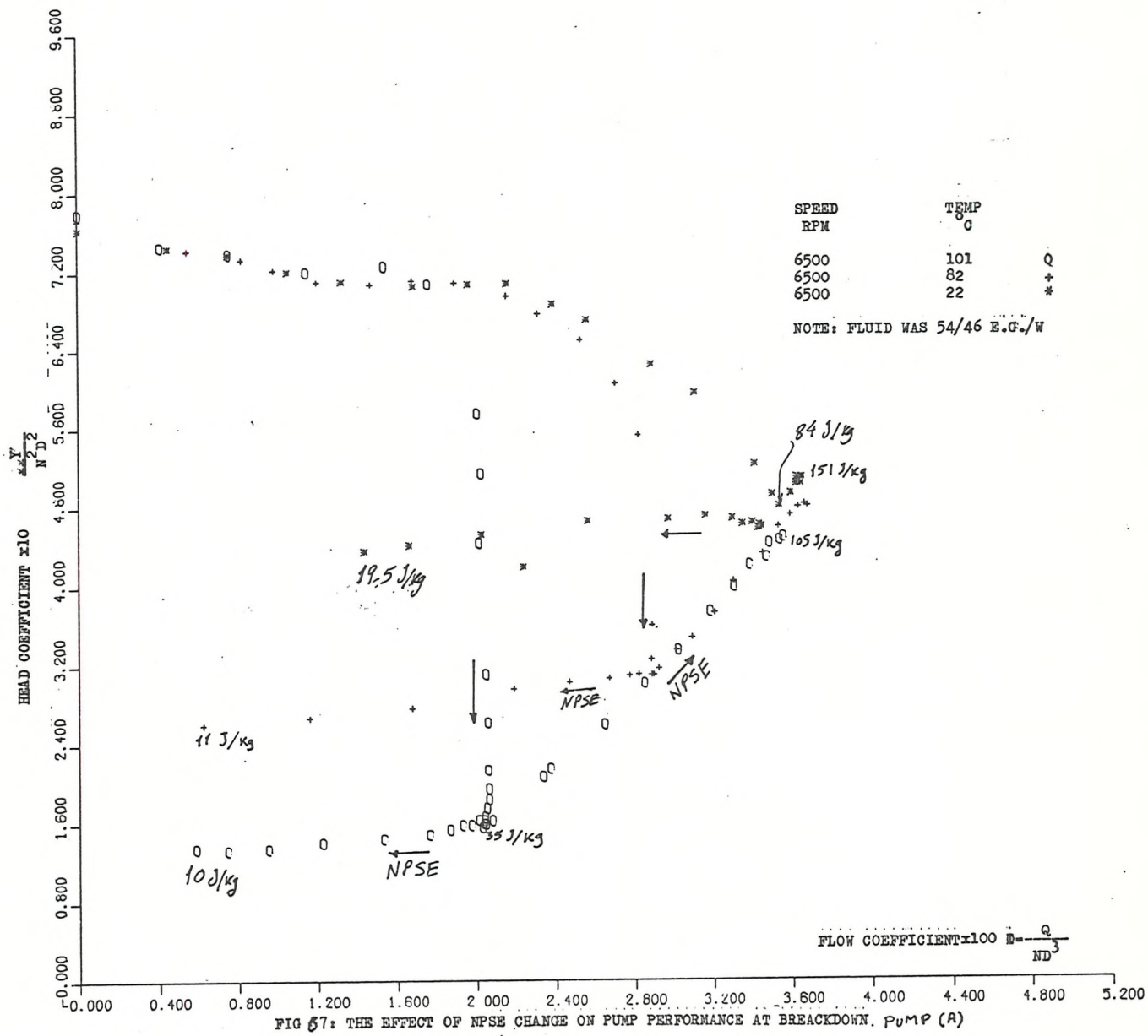

FIG 57: THE EFFECT OF NPSE CHANGE ON PUMP PERFORMANCE AT BREAKDOWN. PUMP (A)

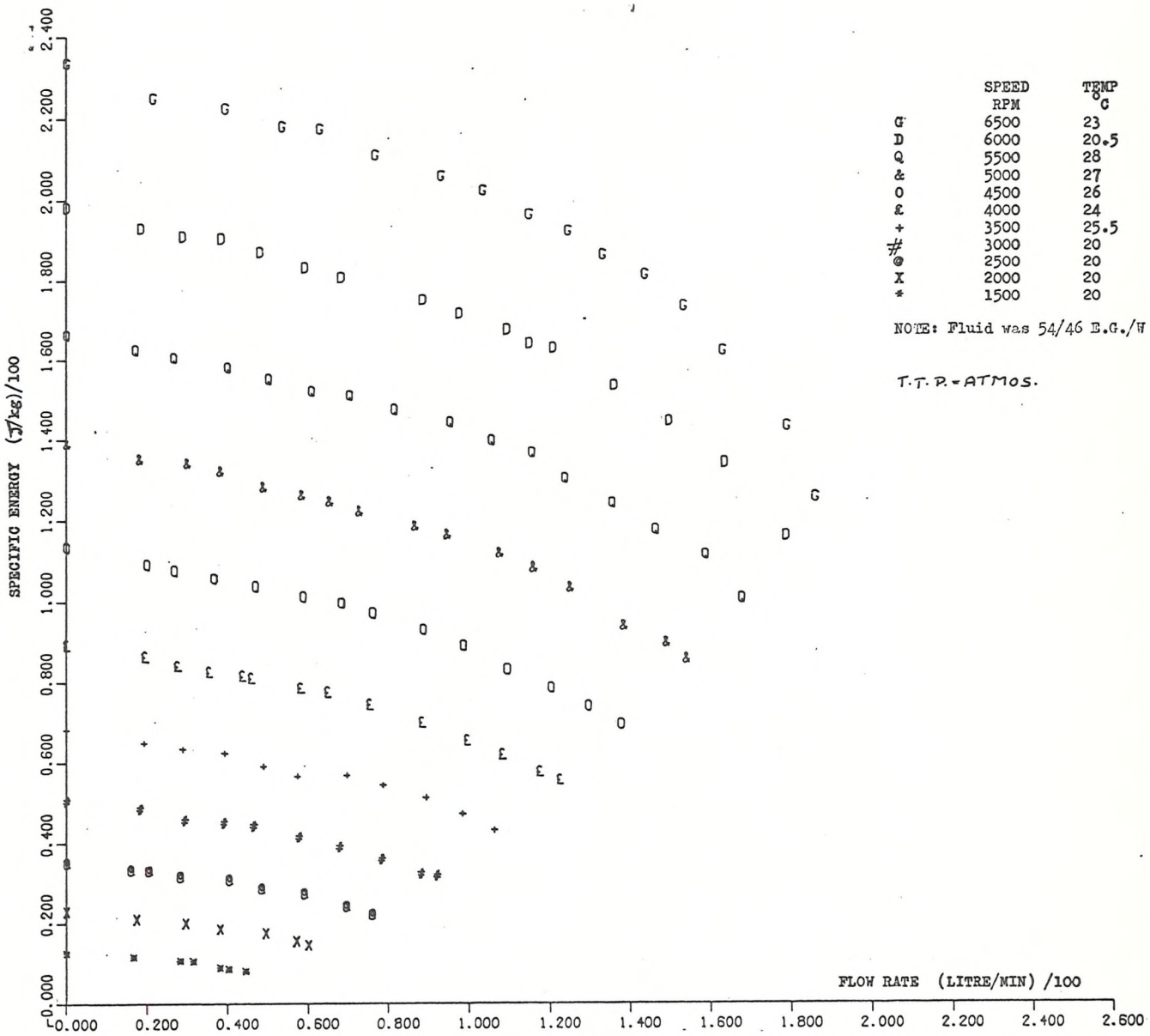

FIG 68: DIMENSIONAL HEAD/FLOW CHARACTERISTIC FOR PUMP (A_1^1) AT VARIOUS SPEEDS

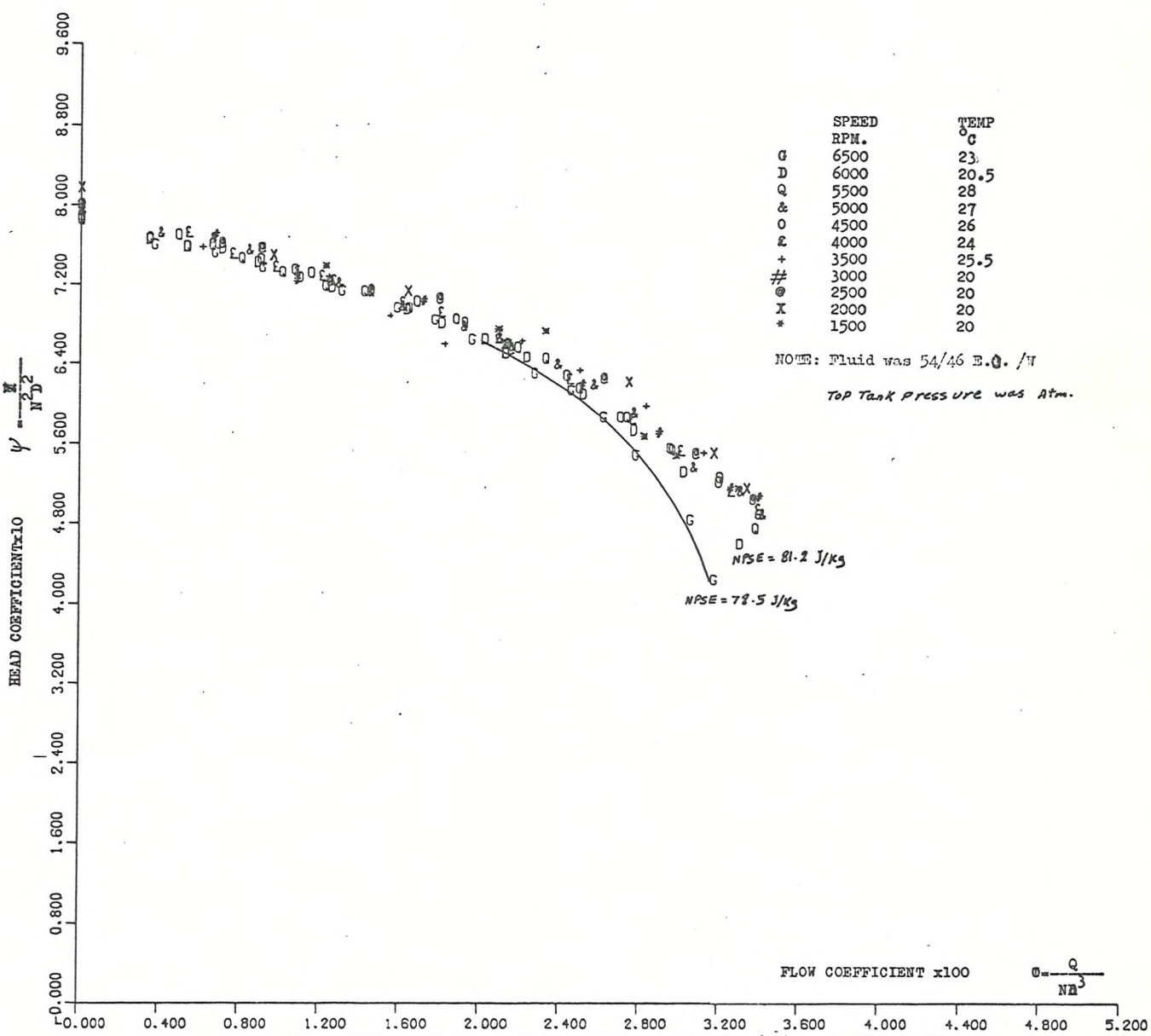

FIG 69: NONDIMENSIONAL HEAD FLOW CHARACTERISTIC FOR PUMP (A_1) AT VARIOUS SPEEDS

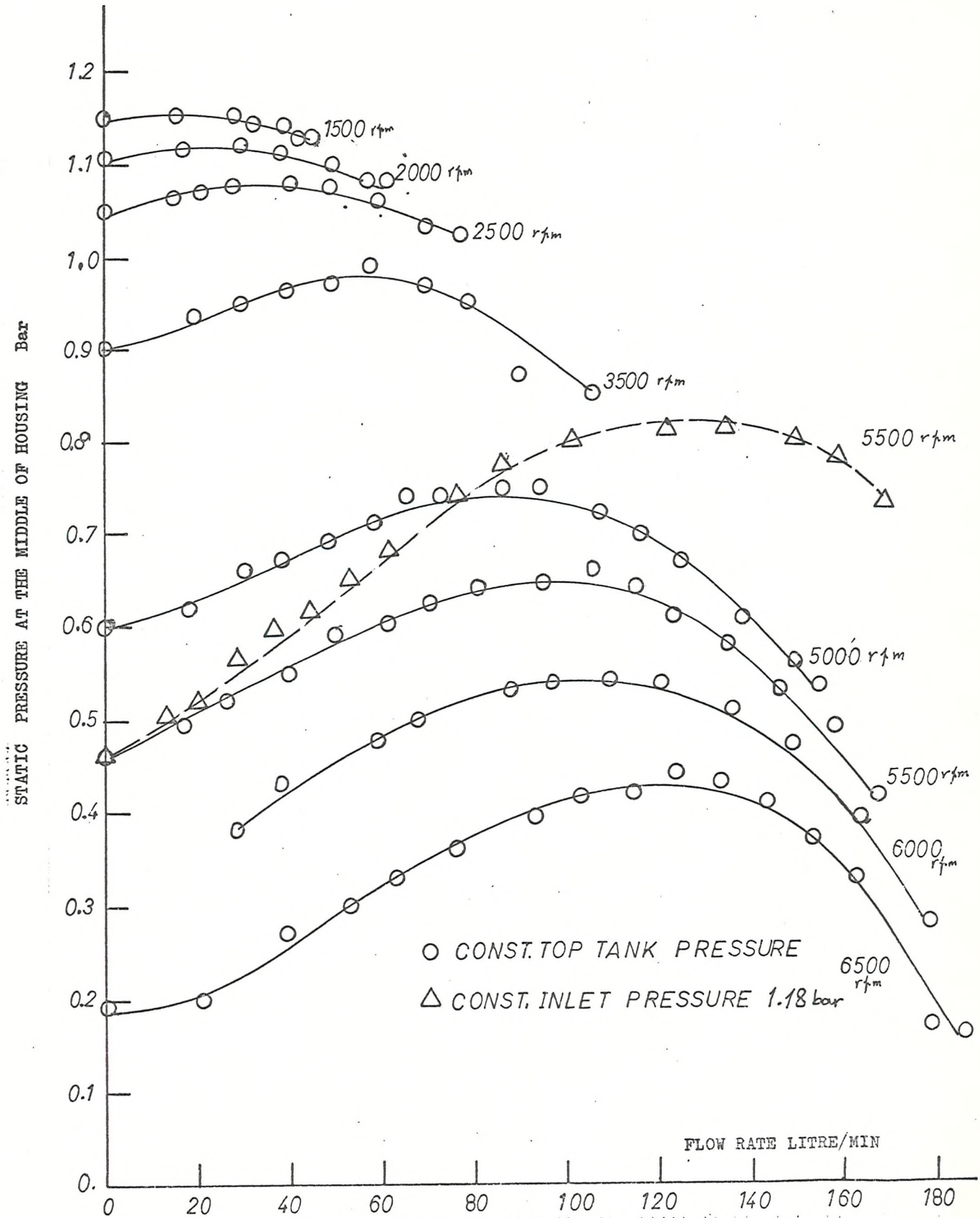

FIG 70: VARIATION OF STATIC PRESSURE IN THE MIDDLE OF THE HOUSING Vs FLOW RATE FOR VARIOUS SPEED AT 20°C IN PUMP A1

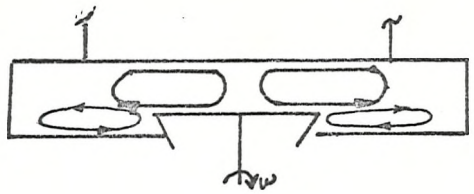

a - NO THROUGHFLOW

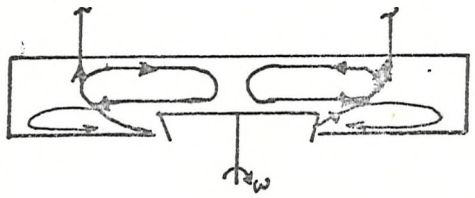

b- MEDIUM THROUGHFLOW

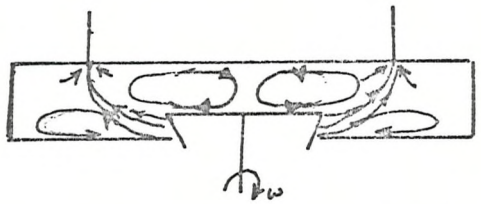

c - HIGH THROUGHFLOW

Fig 71: Velocity Distribution in the Square Housing.

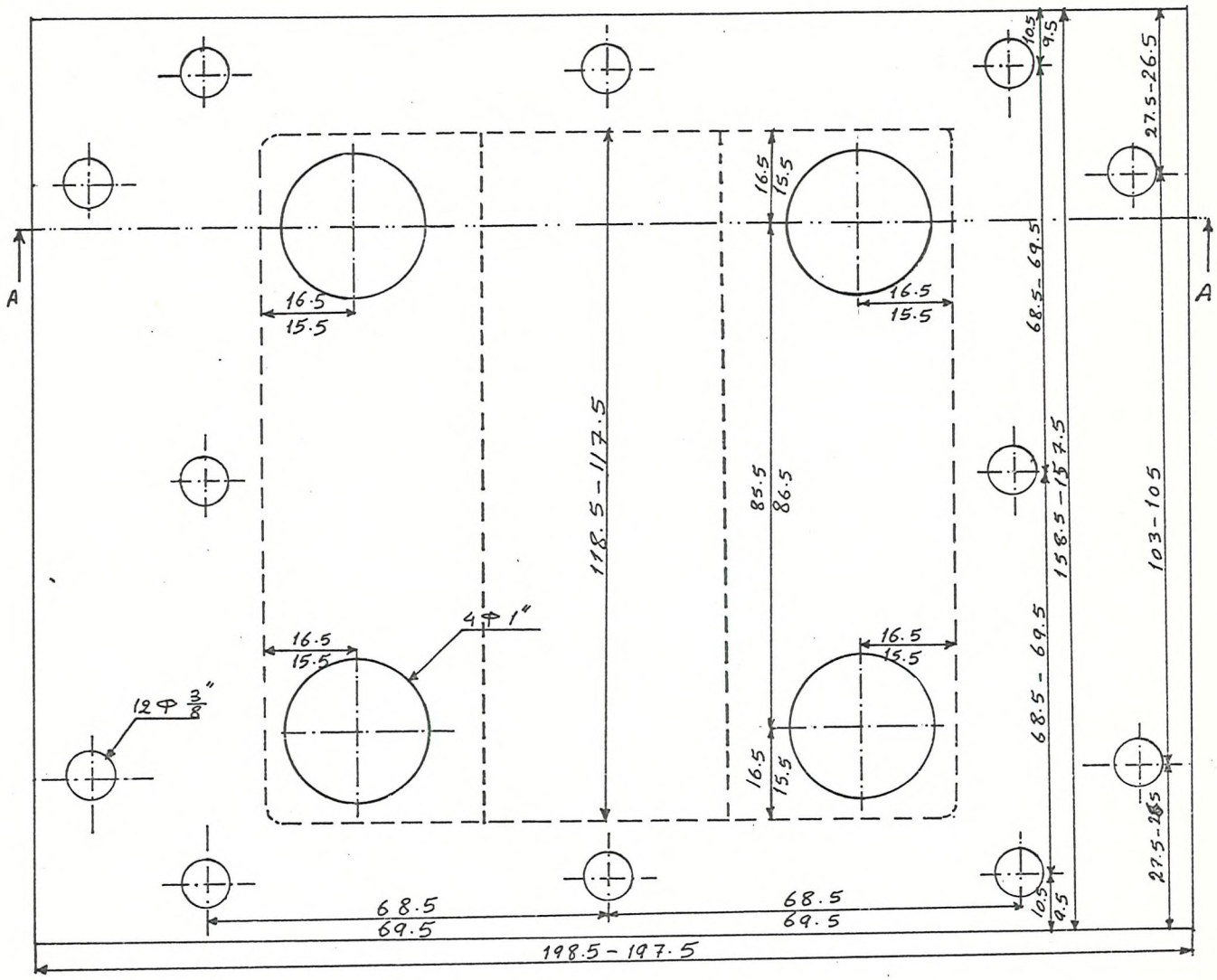

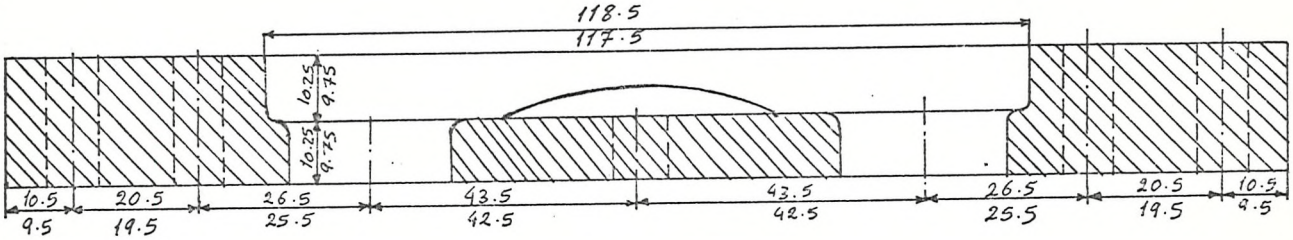

SECTION A-A

Fig. 72: Suggested Housing for Future Improvement

Good surface Machina

scale 1:1"

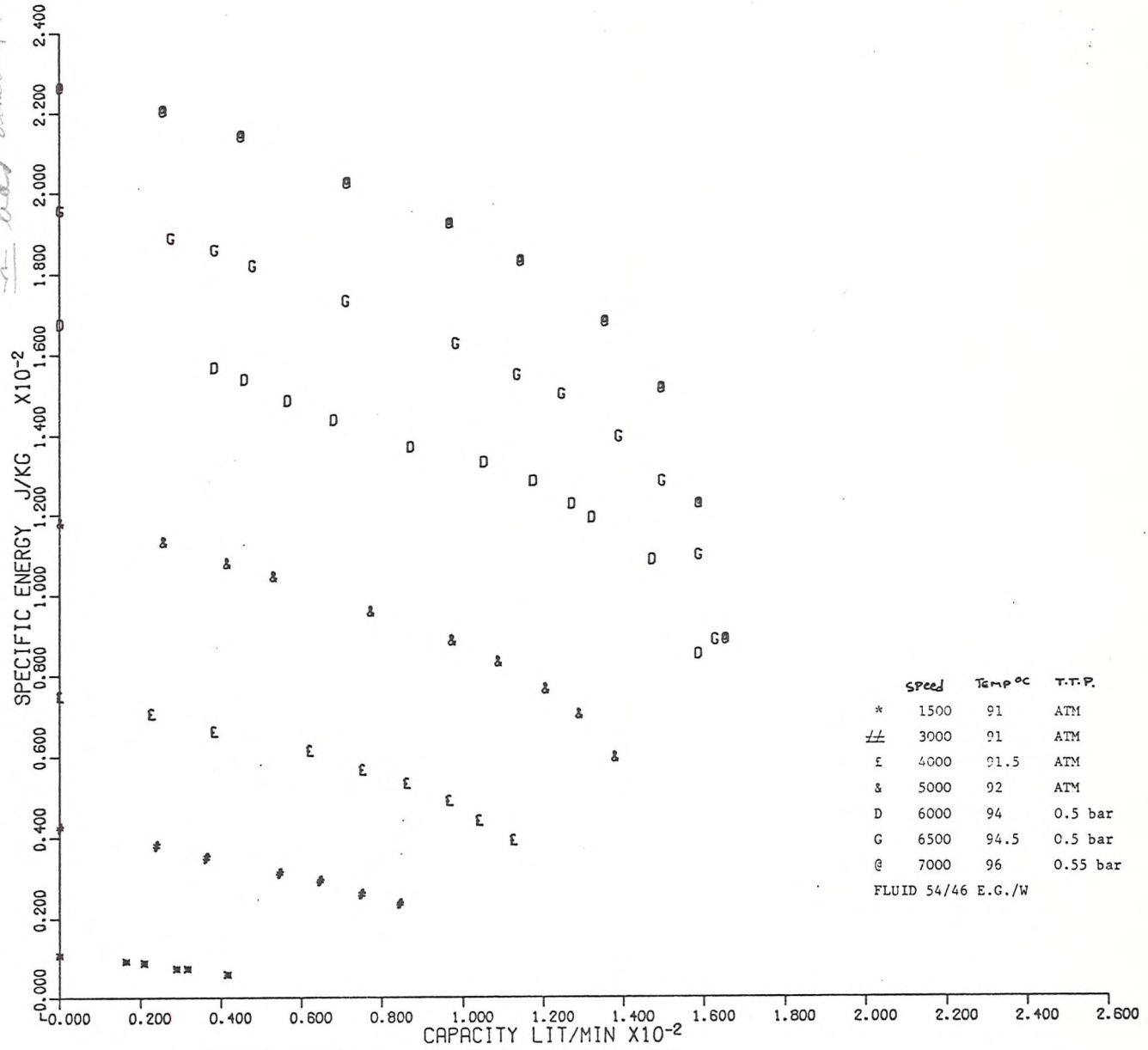

Fig (73). HEAD/Flow Curve FOR PUMP (C) AT VARIOUS SPEEDS.

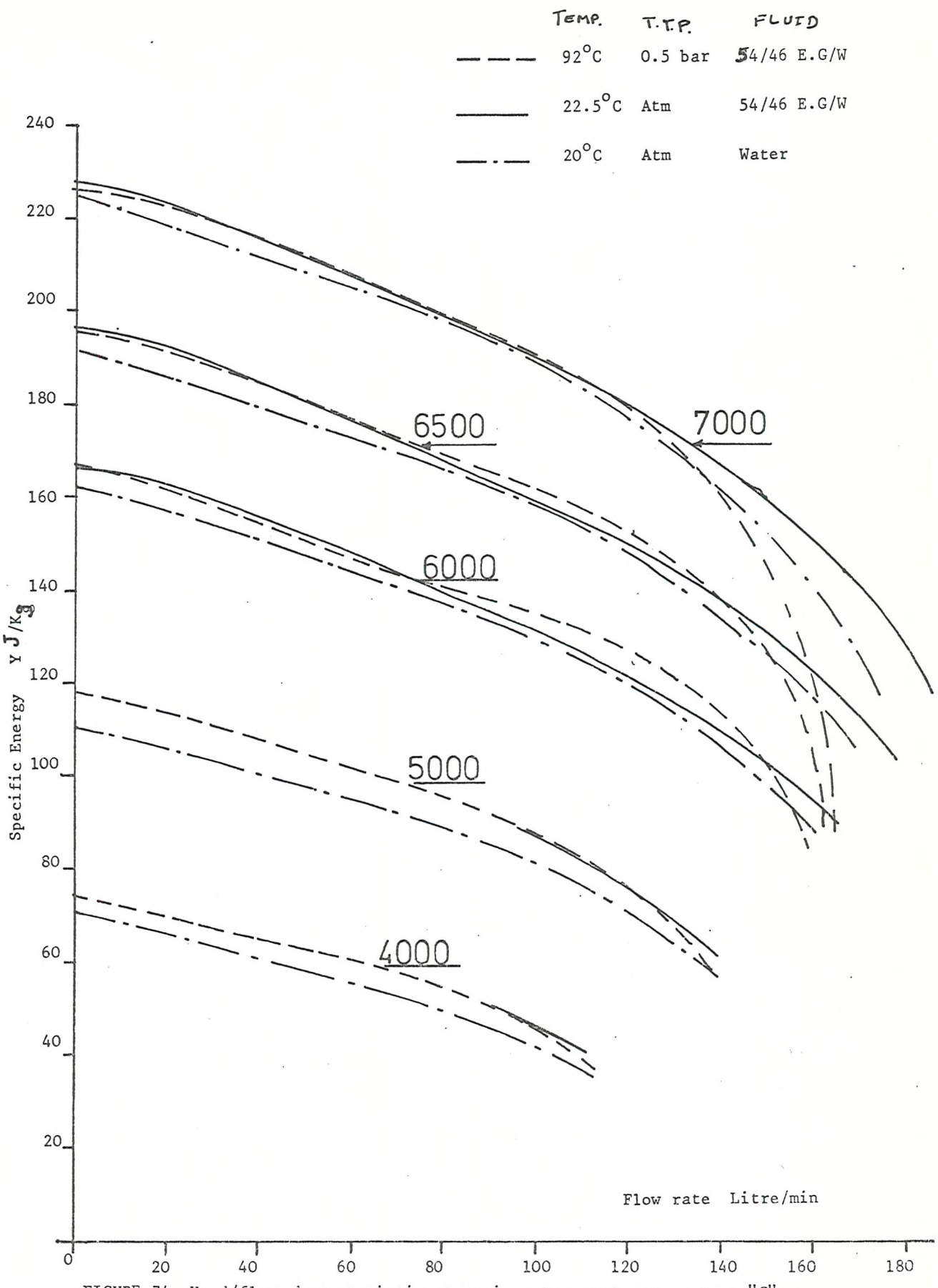

FIGURE 74 Head/flow characteristic at various temperatures on pump "C"

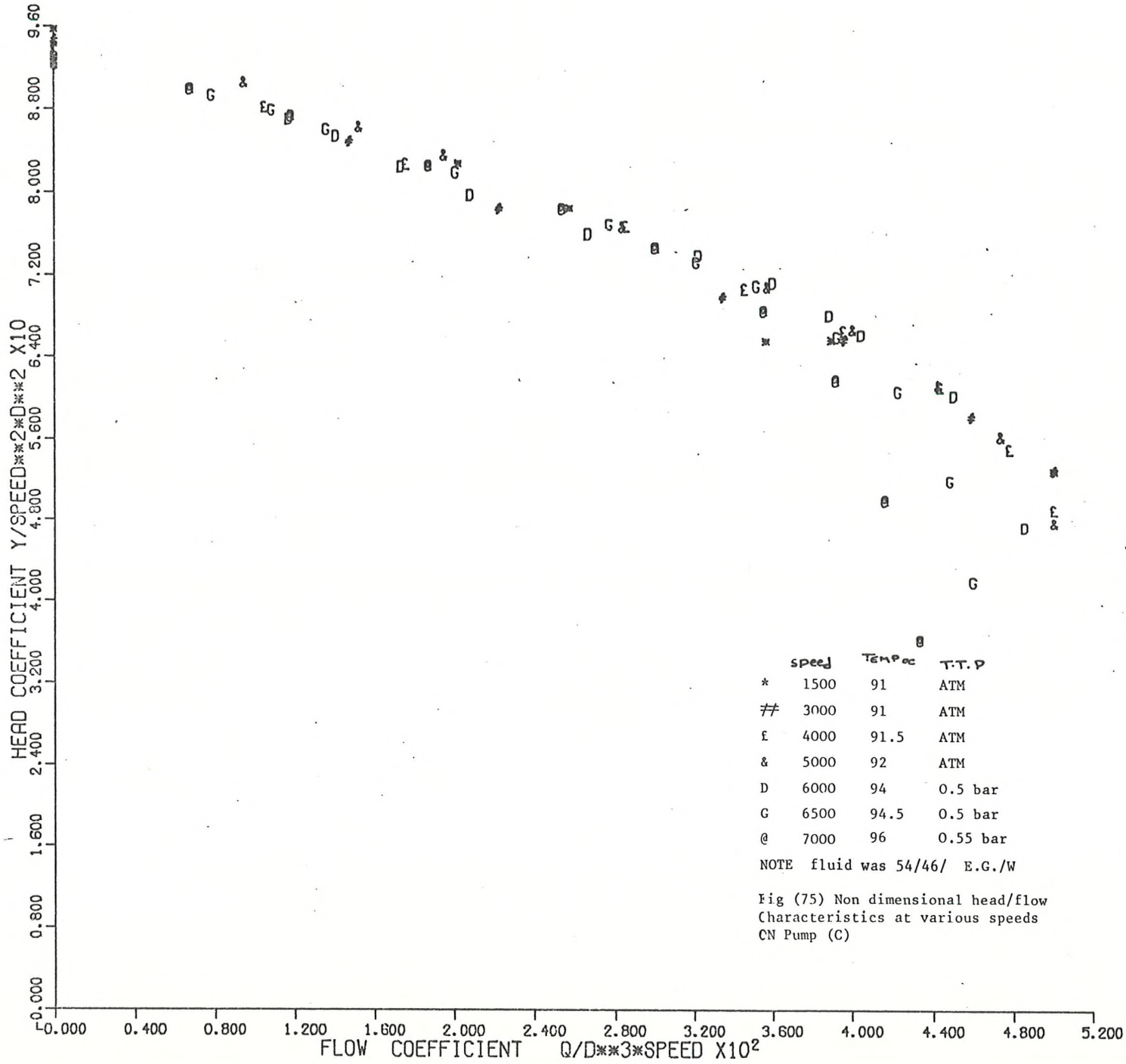

	speed	Temp oc	T.T.P
*	1500	91	ATM
##	3000	91	ATM
£	4000	91.5	ATM
&	5000	92	ATM
D	6000	94	0.5 bar
G	6500	94.5	0.5 bar
@	7000	96	0.55 bar

NOTE fluid was 54/46/ E.G./W

Fig (75) Non dimensional head/flow Characteristics at various speeds CN Pump (C)

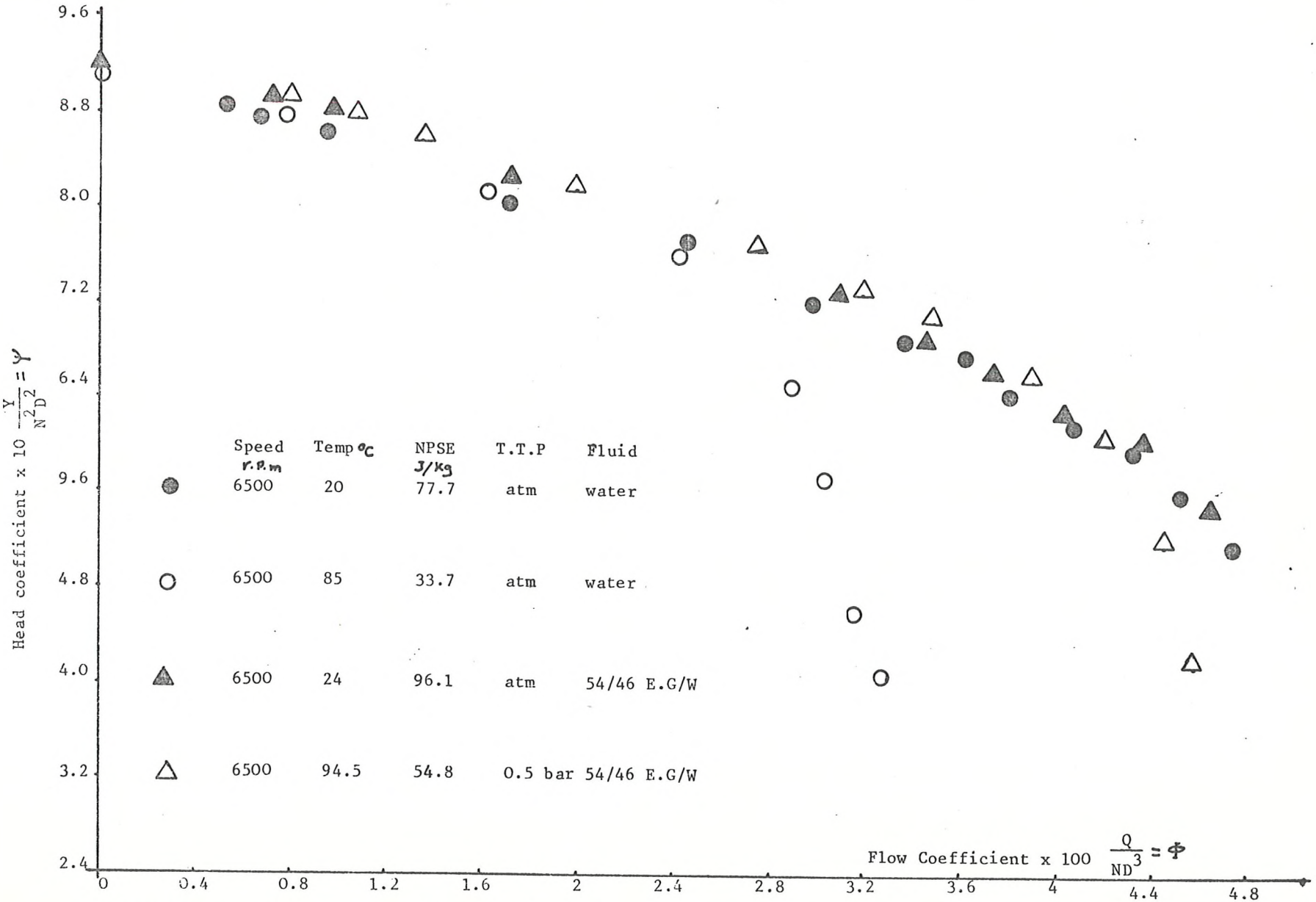

FIGURE 76 Non-dimensional head/flow characteristic at various temperatures on pump "C" for water & 54/46% E.G/W

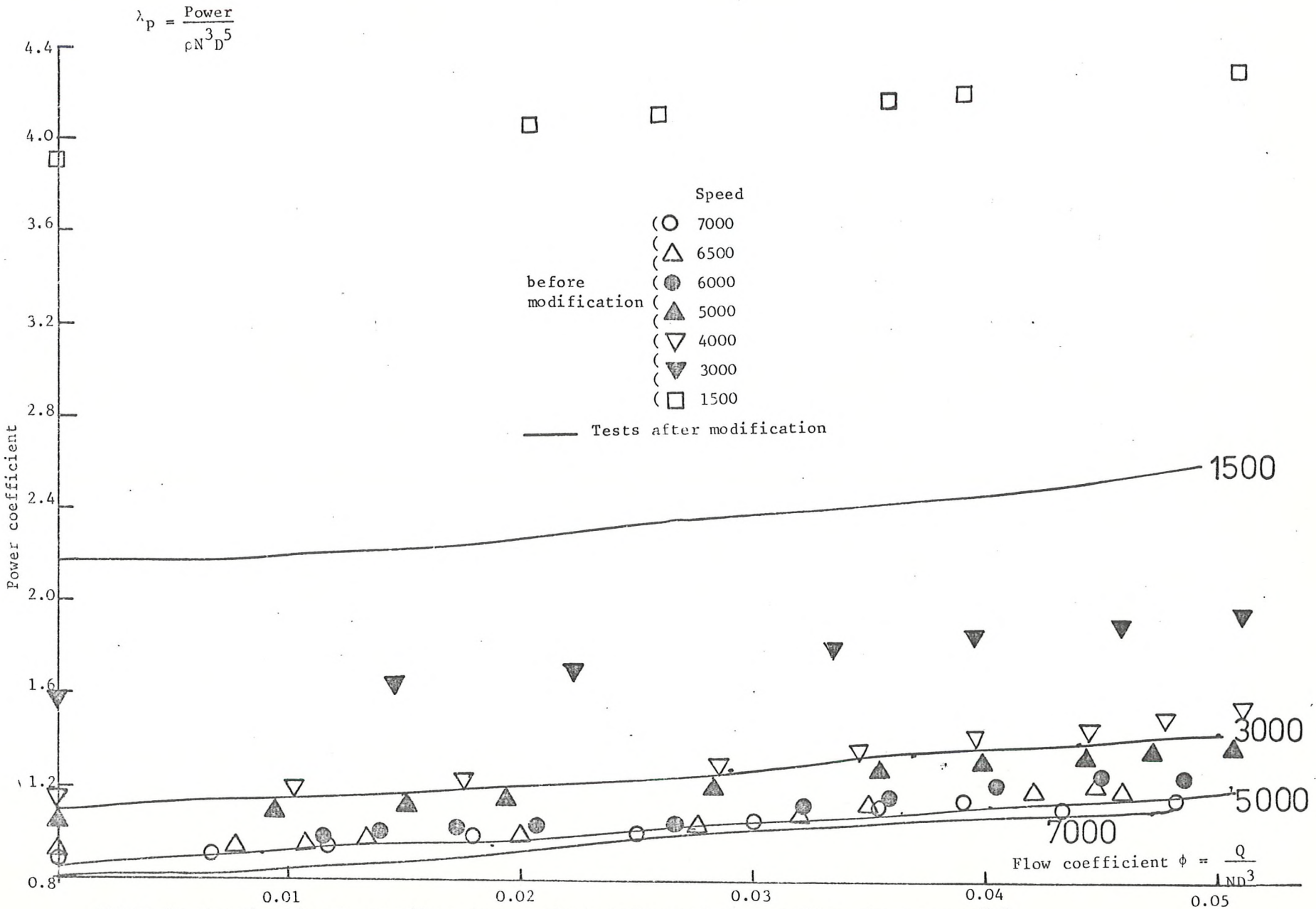

FIGURE 77 Non-dimensional power/flow characteristic before and after modification on pump "C"

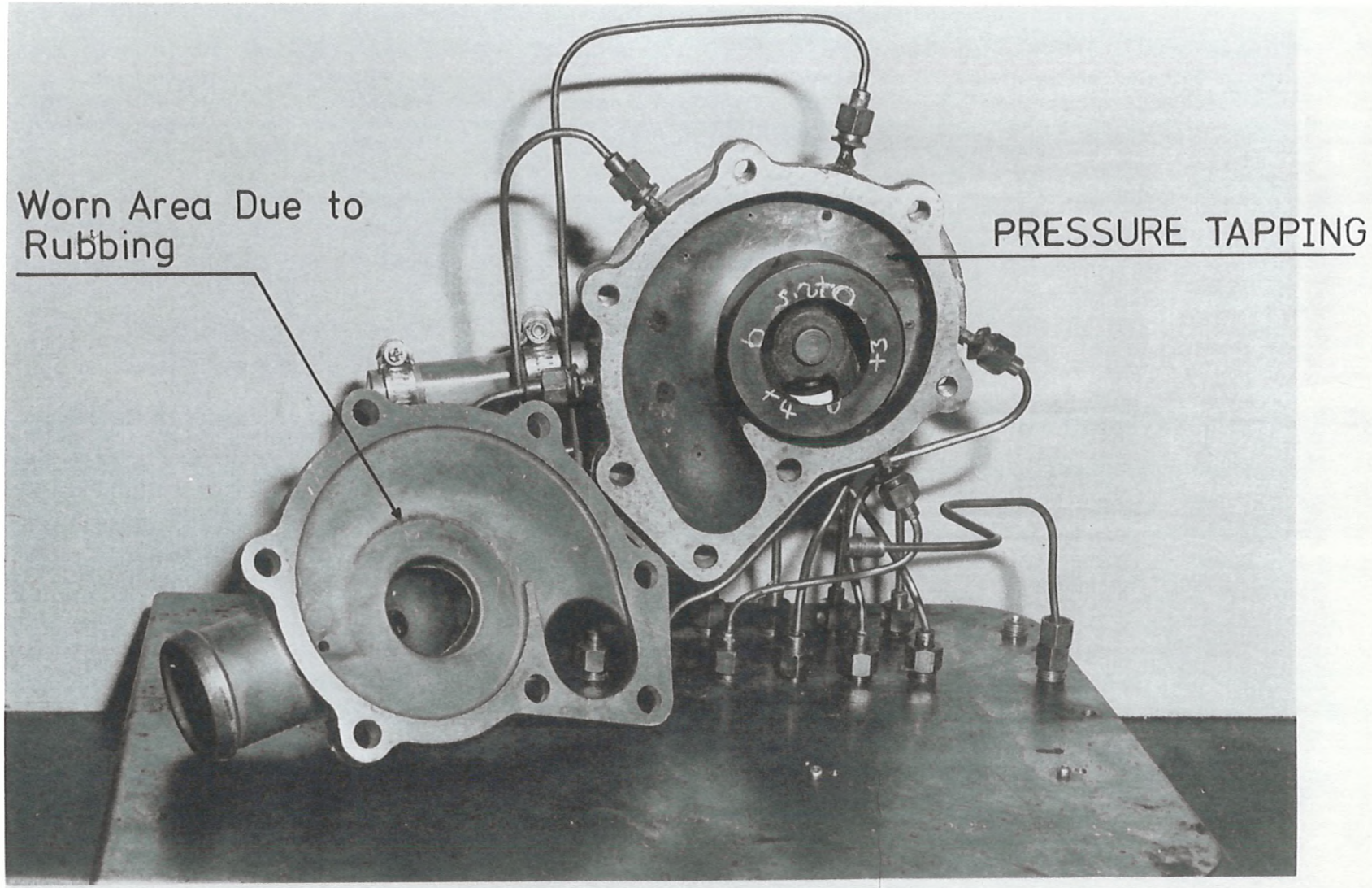

Fig 78 PUMP "C" BEFORE MODIFICATION

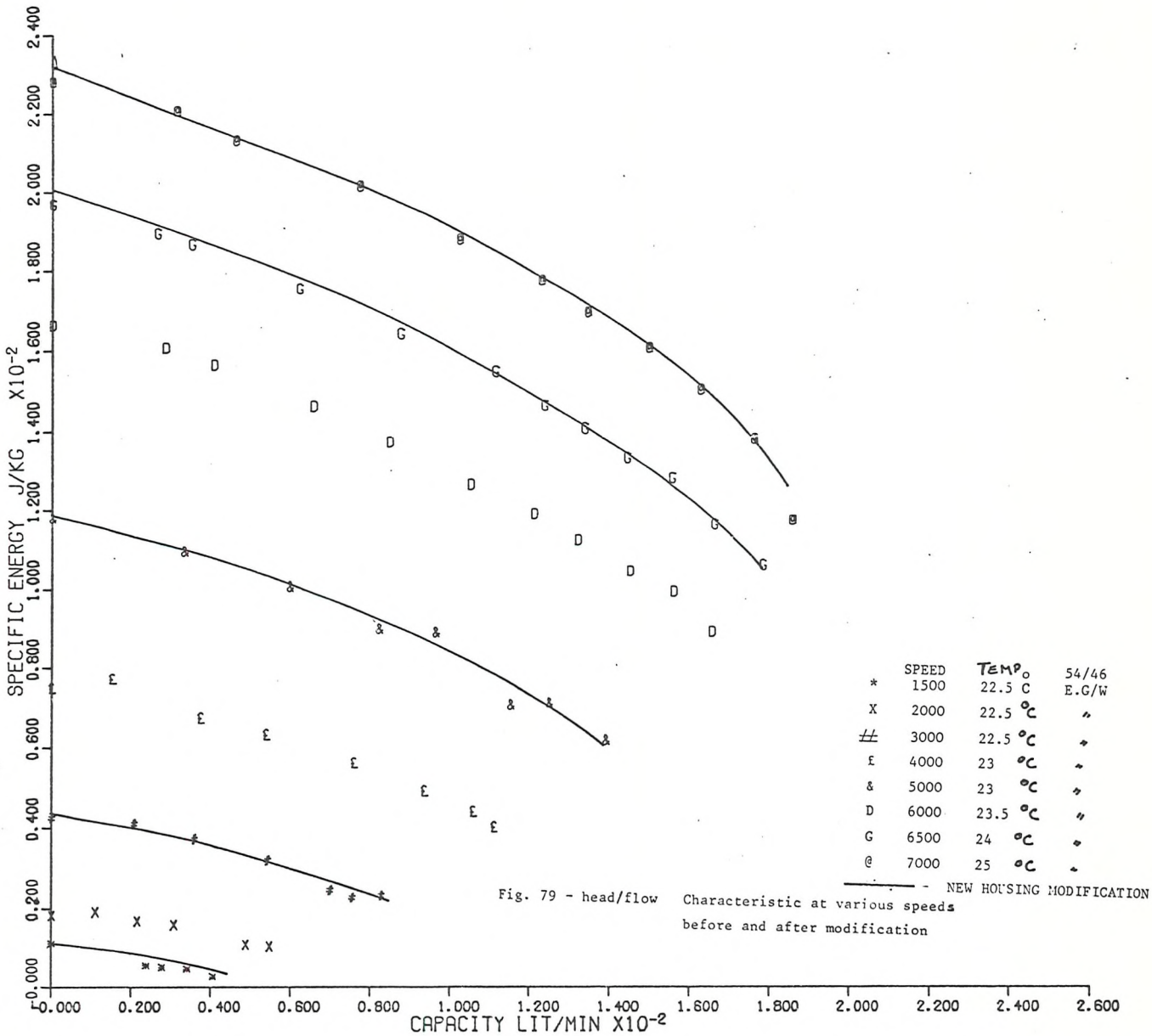

Fig. 79 - head/flow Characteristic at various speeds before and after modification

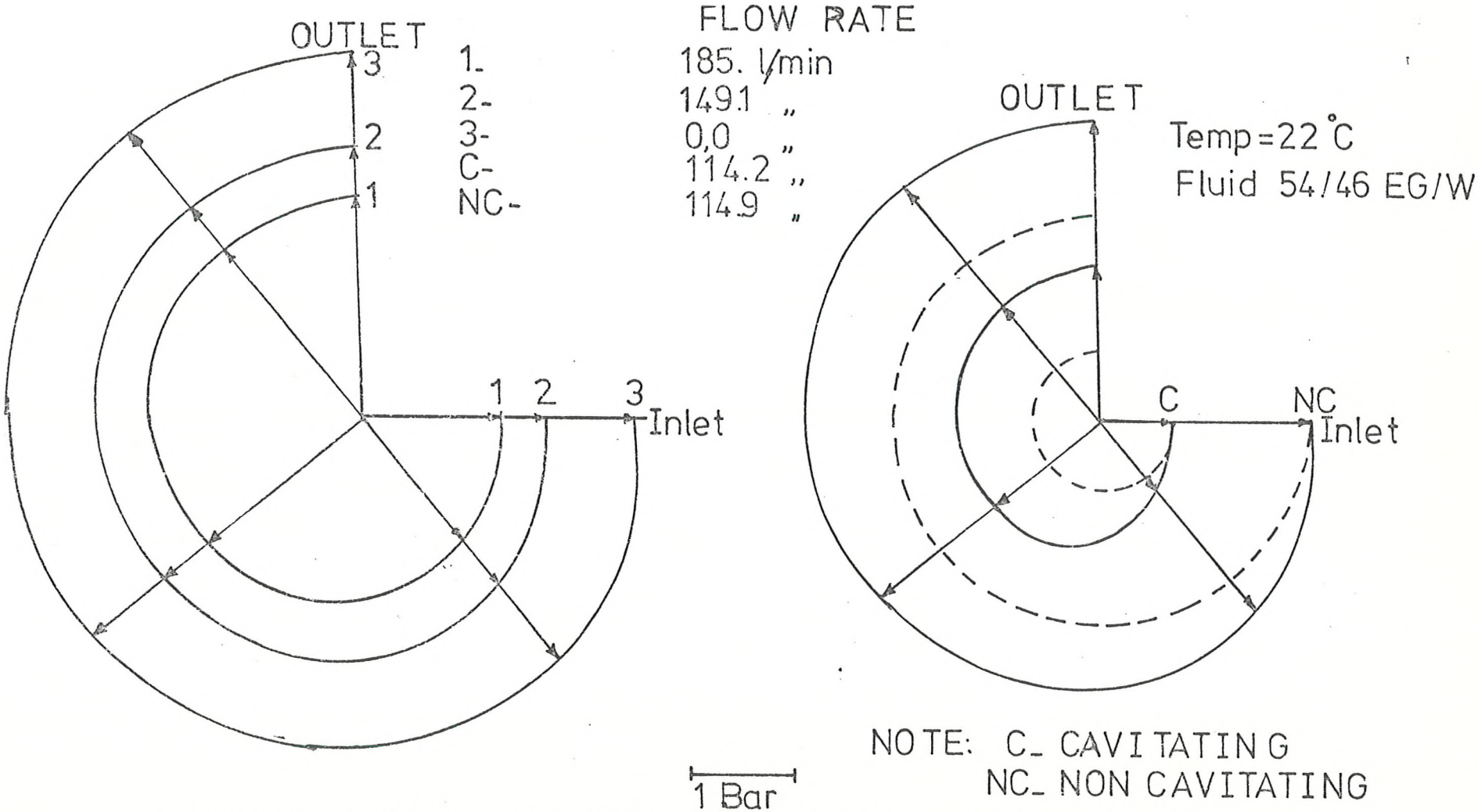

Fig 80 PRESSURE DISTRIBUTION IN THE VOLUTE OF PUMP "C" AT DIFFERENT FLOW RATE & 7000 RPM.

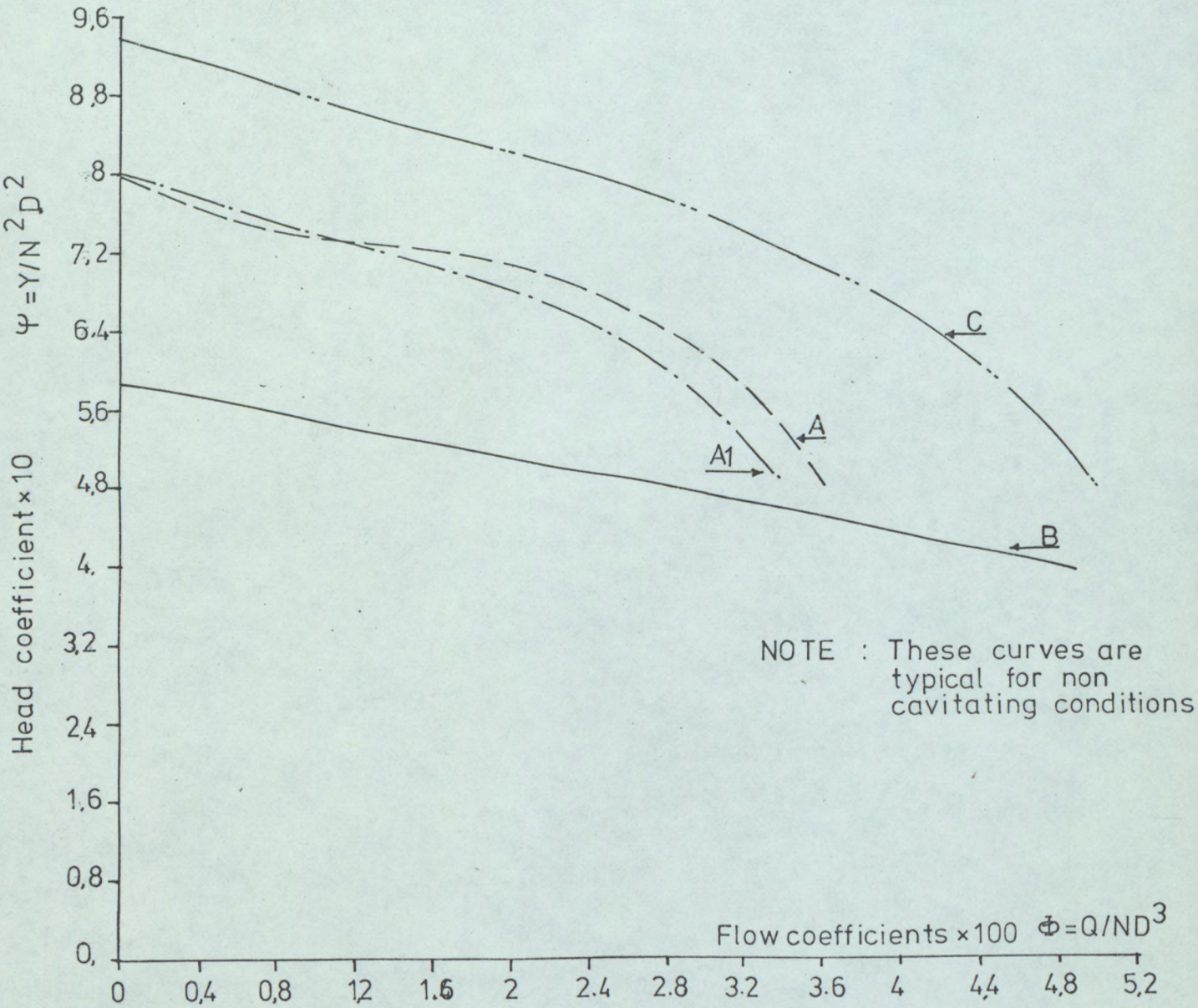

Fig 80-A Non dimensional head/flow characteristics for different geometry of tested pumps

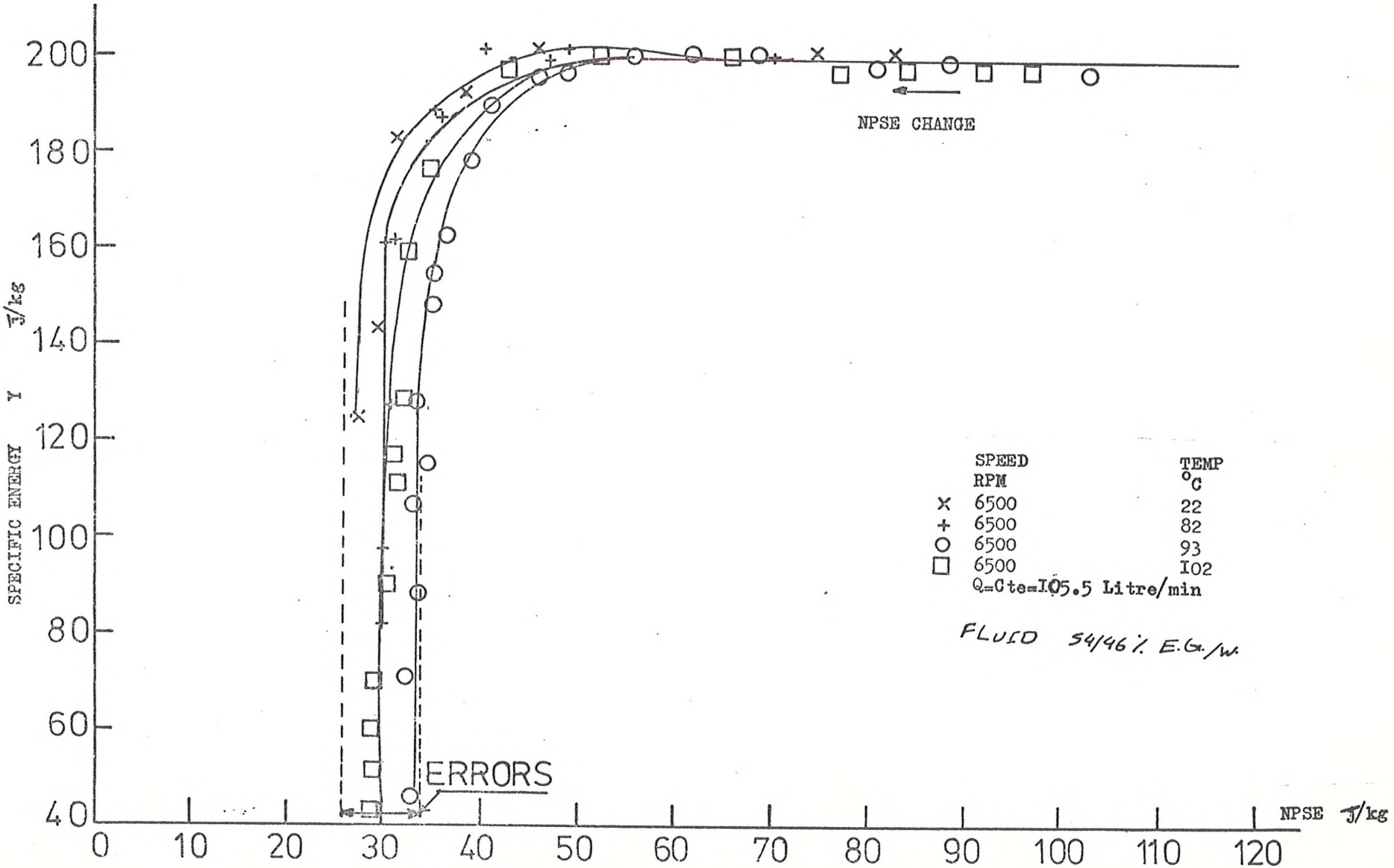

FIG 81 : SPECIFIC ENERGY CHANGE DUE TO NPSE CHANGE AT CONSTANT FLOW RATE AT VARIOUS TEMPERATURE ON PUMP (A)

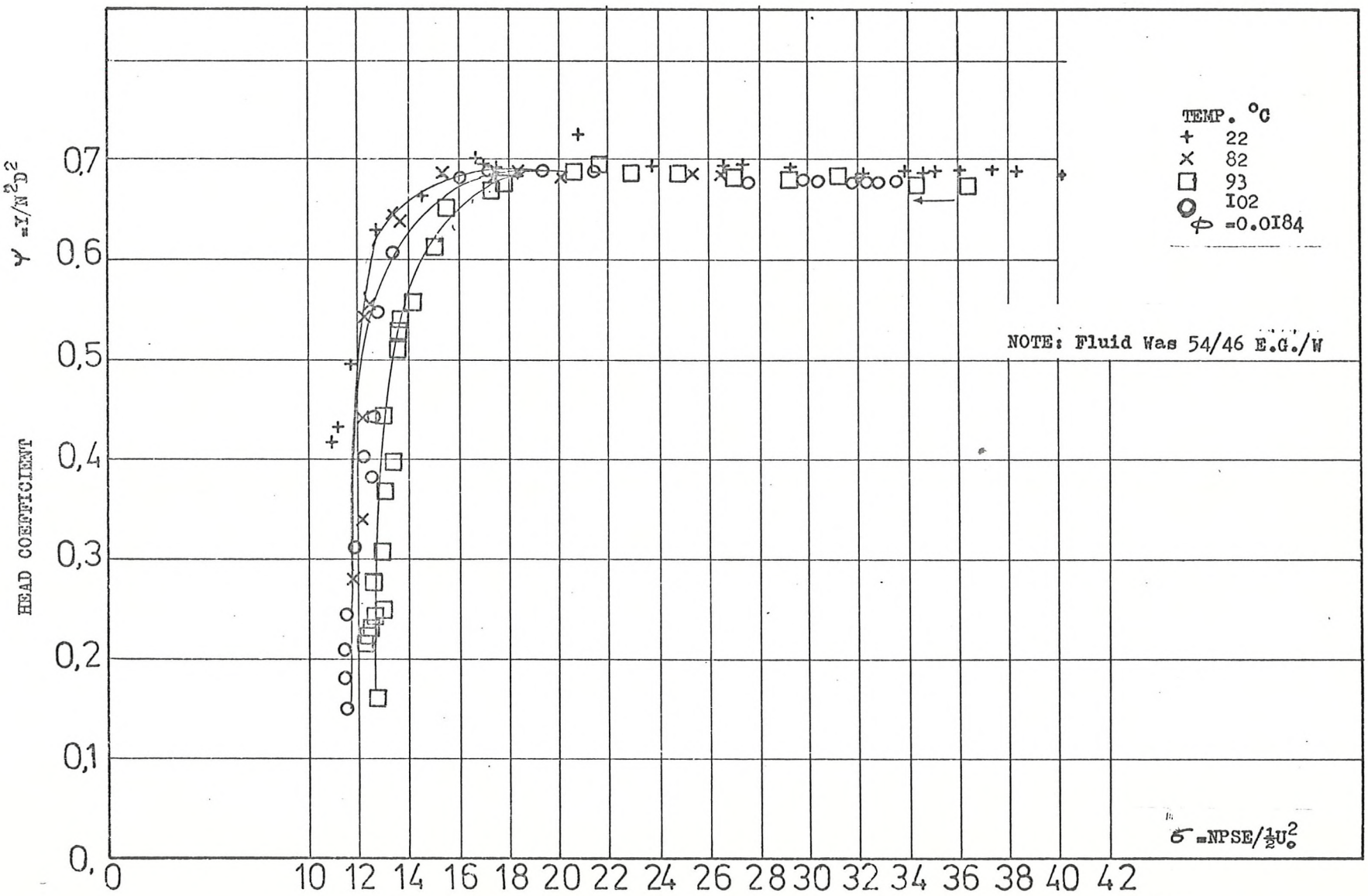

FIG 22: CAVITATION CHARACTERISTIC AT CONSTANT FLOW COEFFICIENT &6500 R.P.M IN PUMP (A)

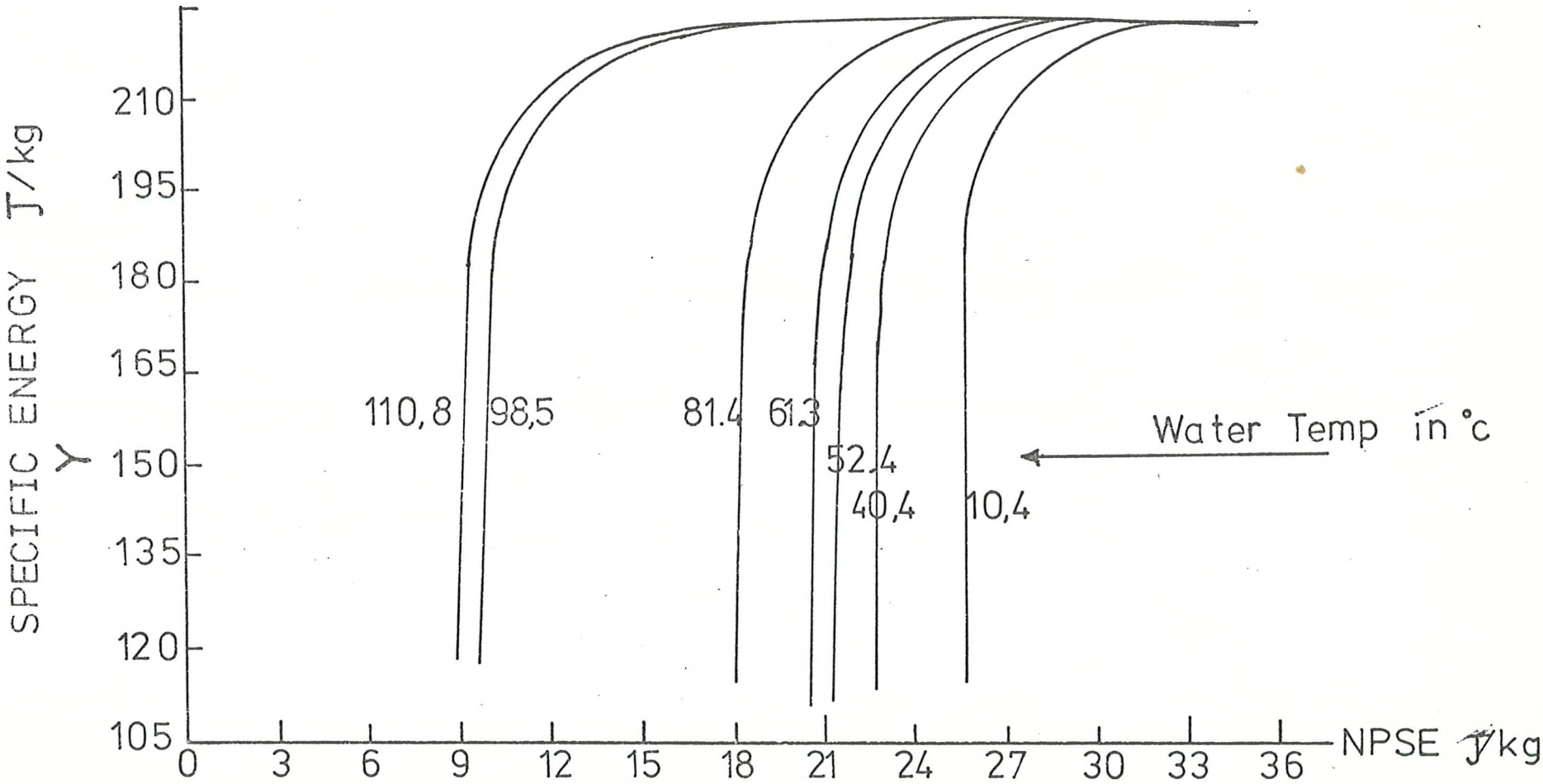

Fig 83 : EFFECT OF NPSE ON SPECIFIC ENERGY Ref (102)

FIG 84: |ΔNPSE| AS A FUNCTION OF THERMAL CAVITATION PARAMETER FOR E.G./W

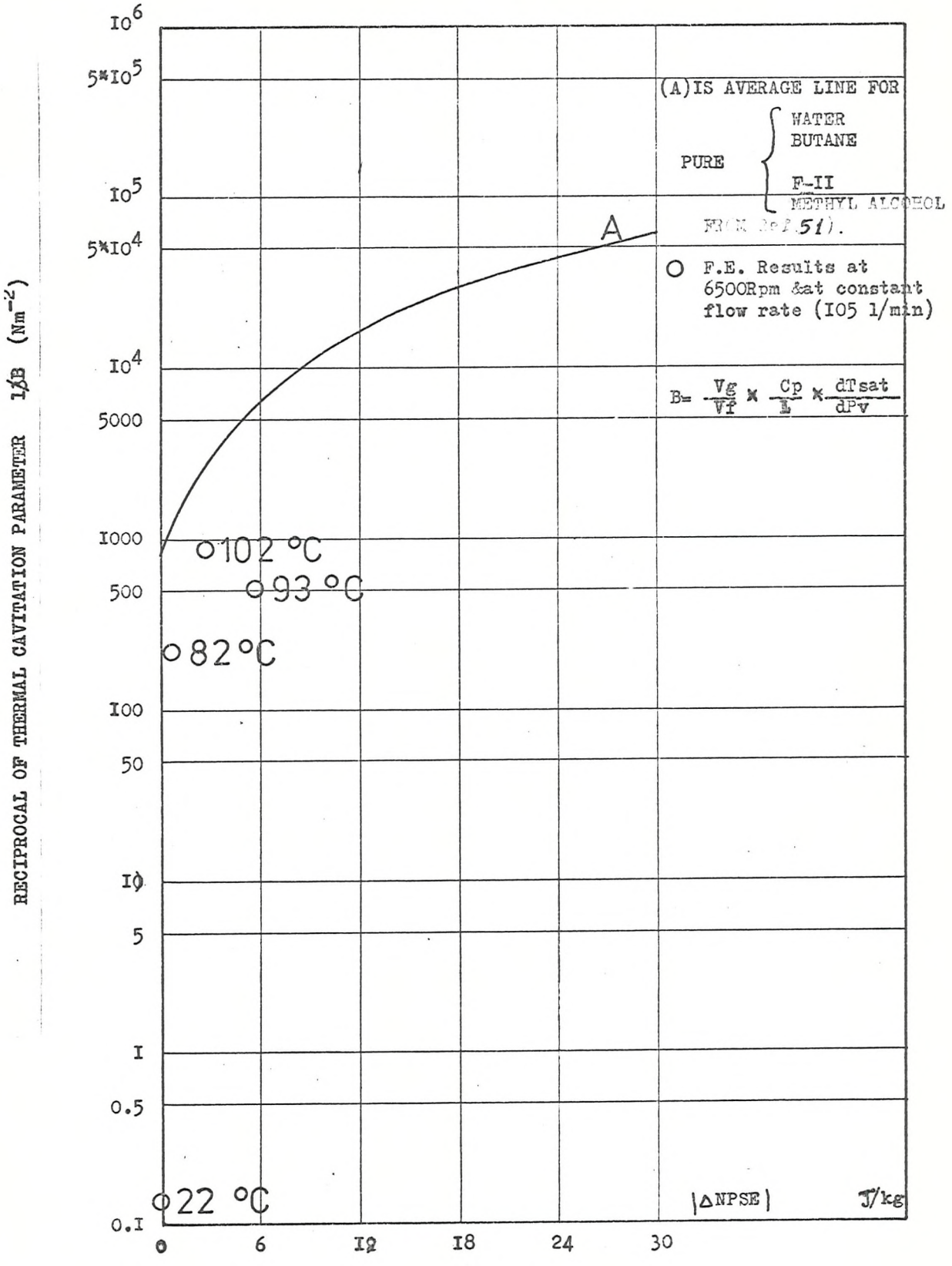

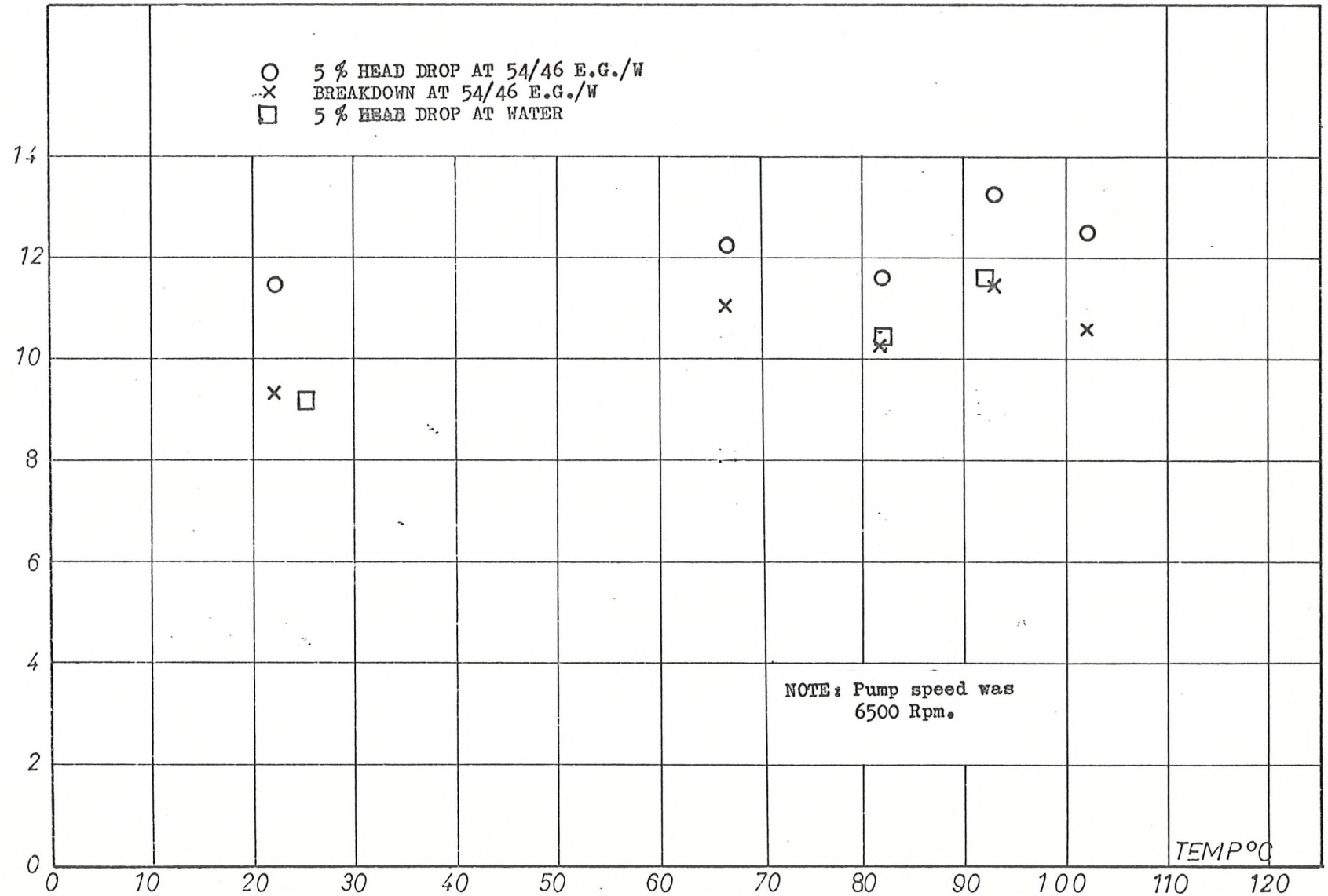

FIG 85: EFFECT OF TEMPERATURE ON CAVITATION PARAMETER WHEN FLUIDS WERE WATER & 54/46 E.G./W IN PUMP (A)

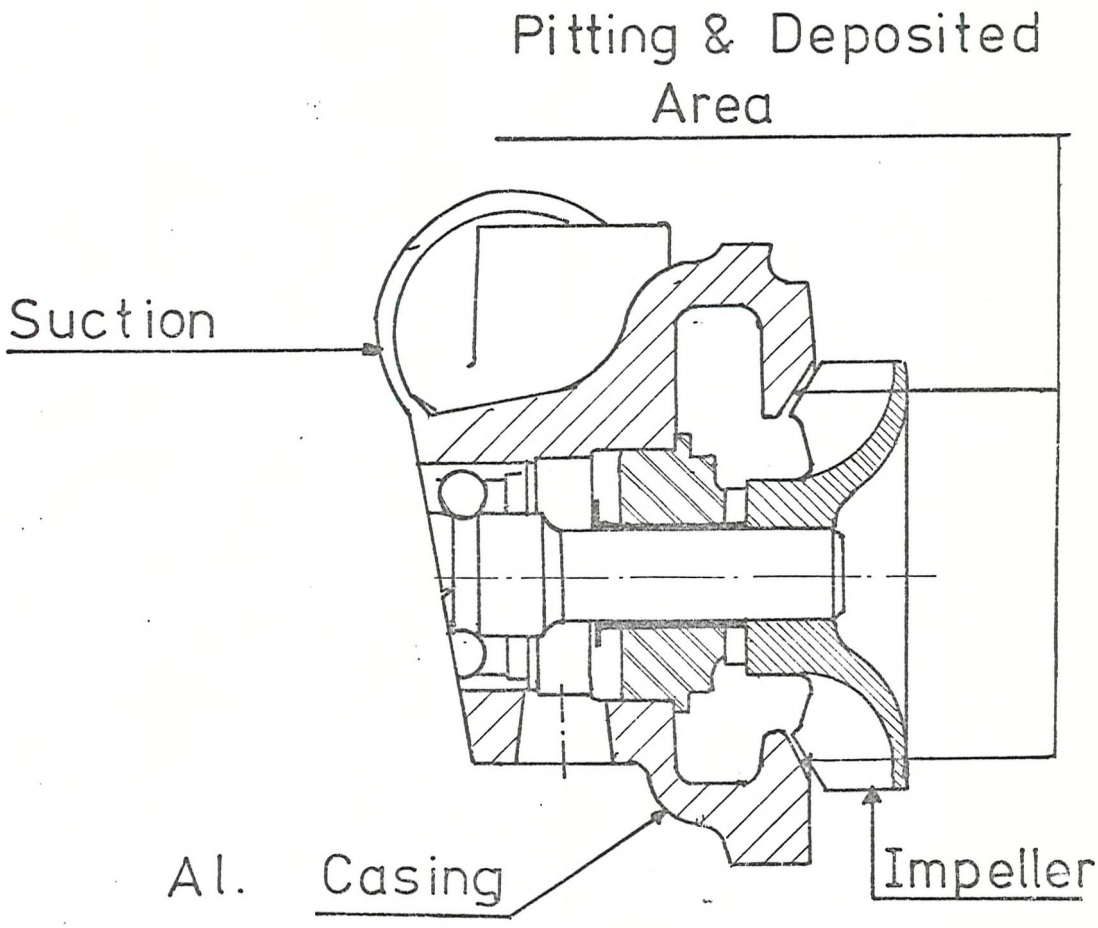

Fig86: Pitting in Pump (B)

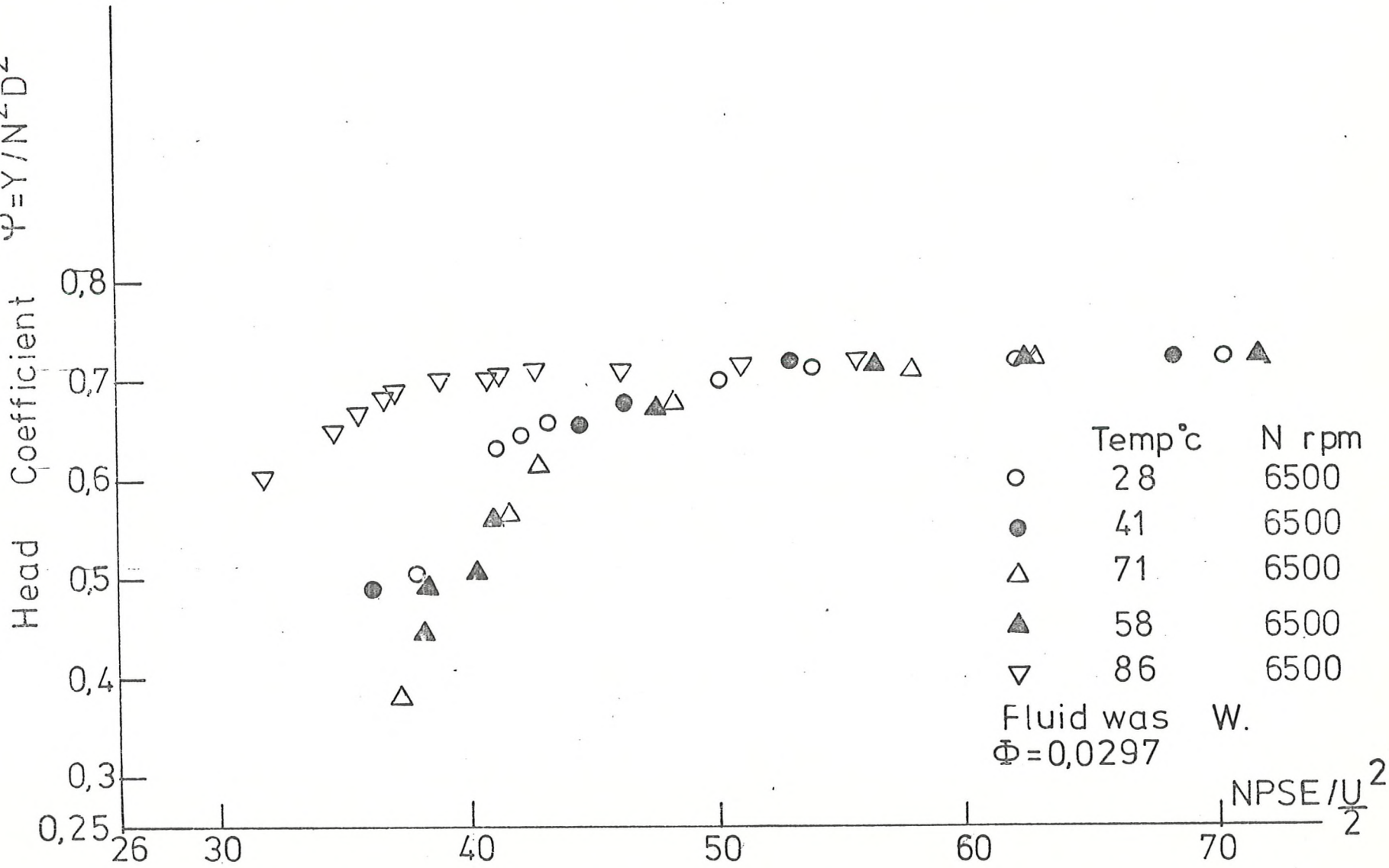

Fig 87 Dimensionless Cavitation Characteristic of Pump "C" at Various Temperatures.

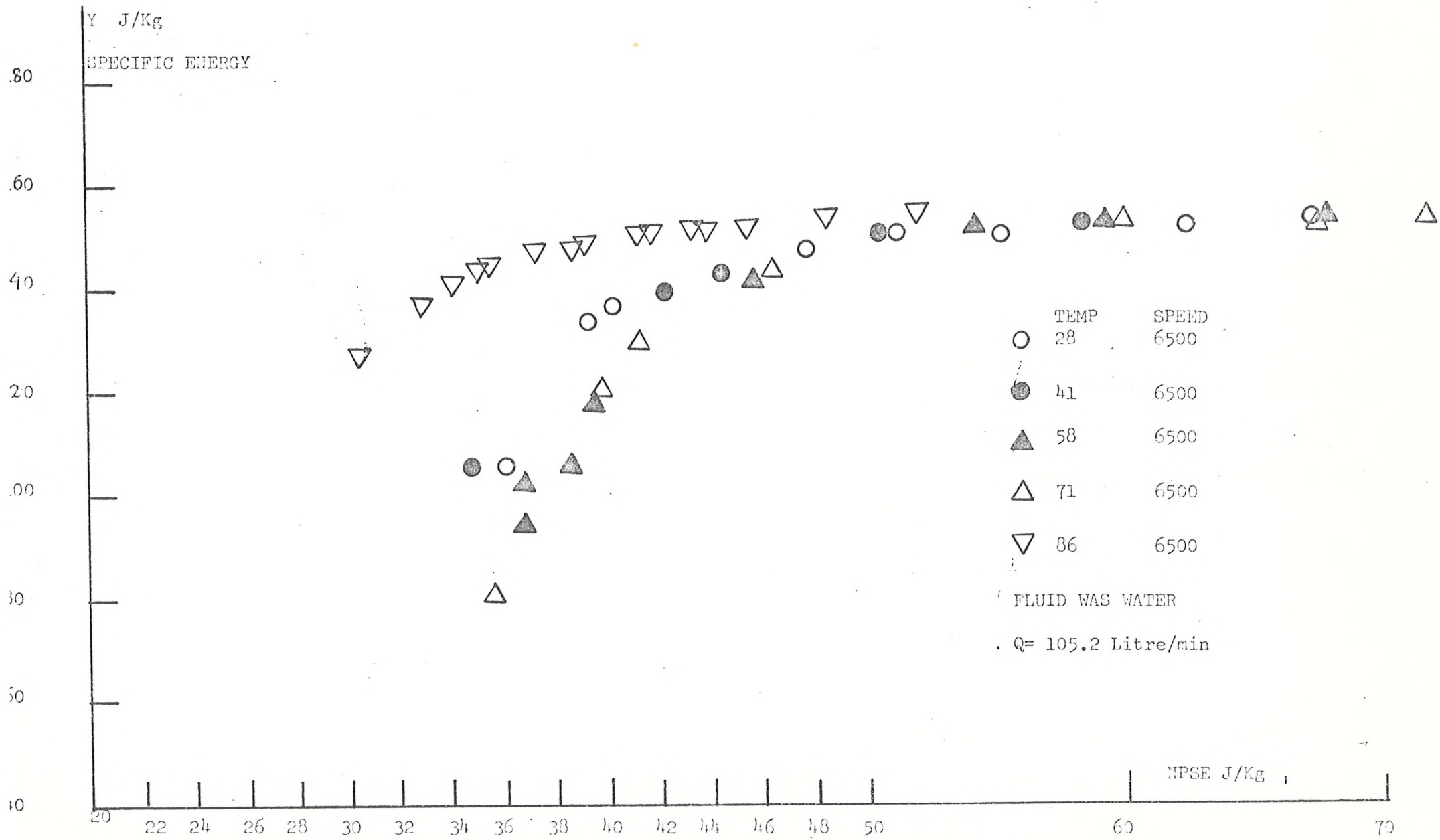

FIG 88 DIMENSIONAL CAVITATION CHARACTERISTIC OF PUMP "C" AT VARIOUS TEMPERATURES

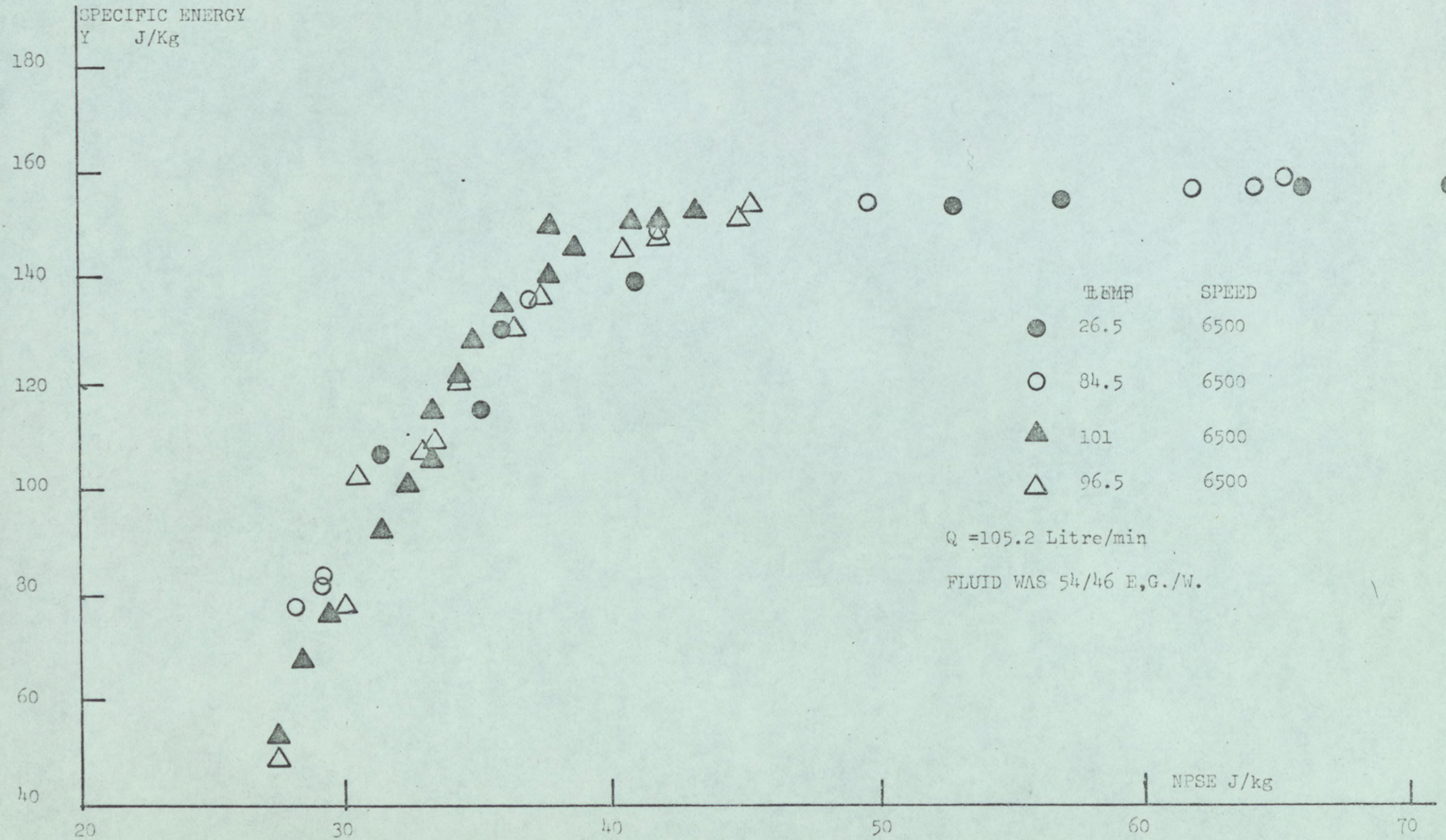

FIG 89 DIMENSIONAL CAVITATION CHARACTERISTIC OF PUMP "C" AT VARIOUS TEMPERATURES.

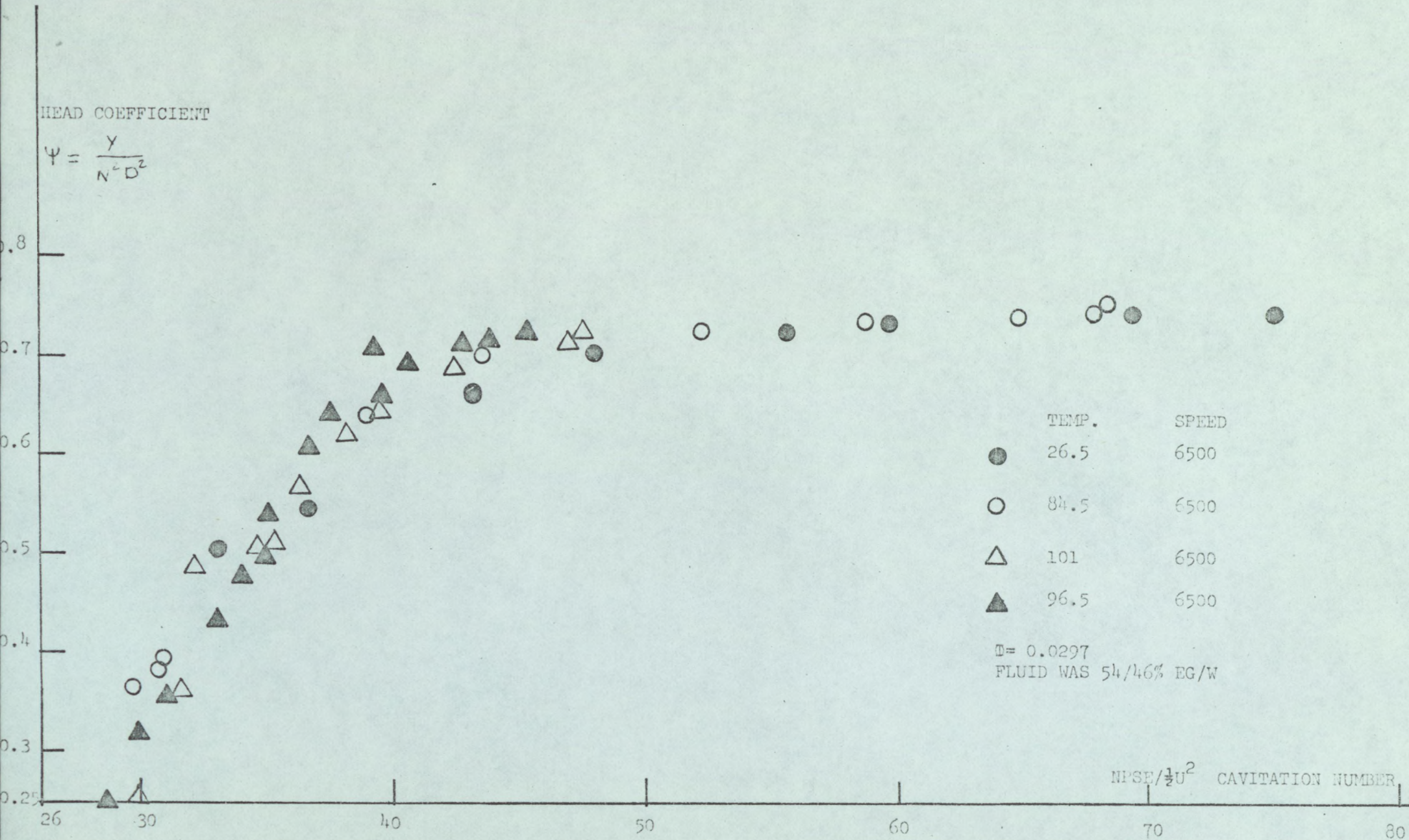

FIG 90 DIMENSIONLESS CAVITATION ######CHARACTERISTIC OF PUMP "C" AT VARIOUS TEMPERATURES.

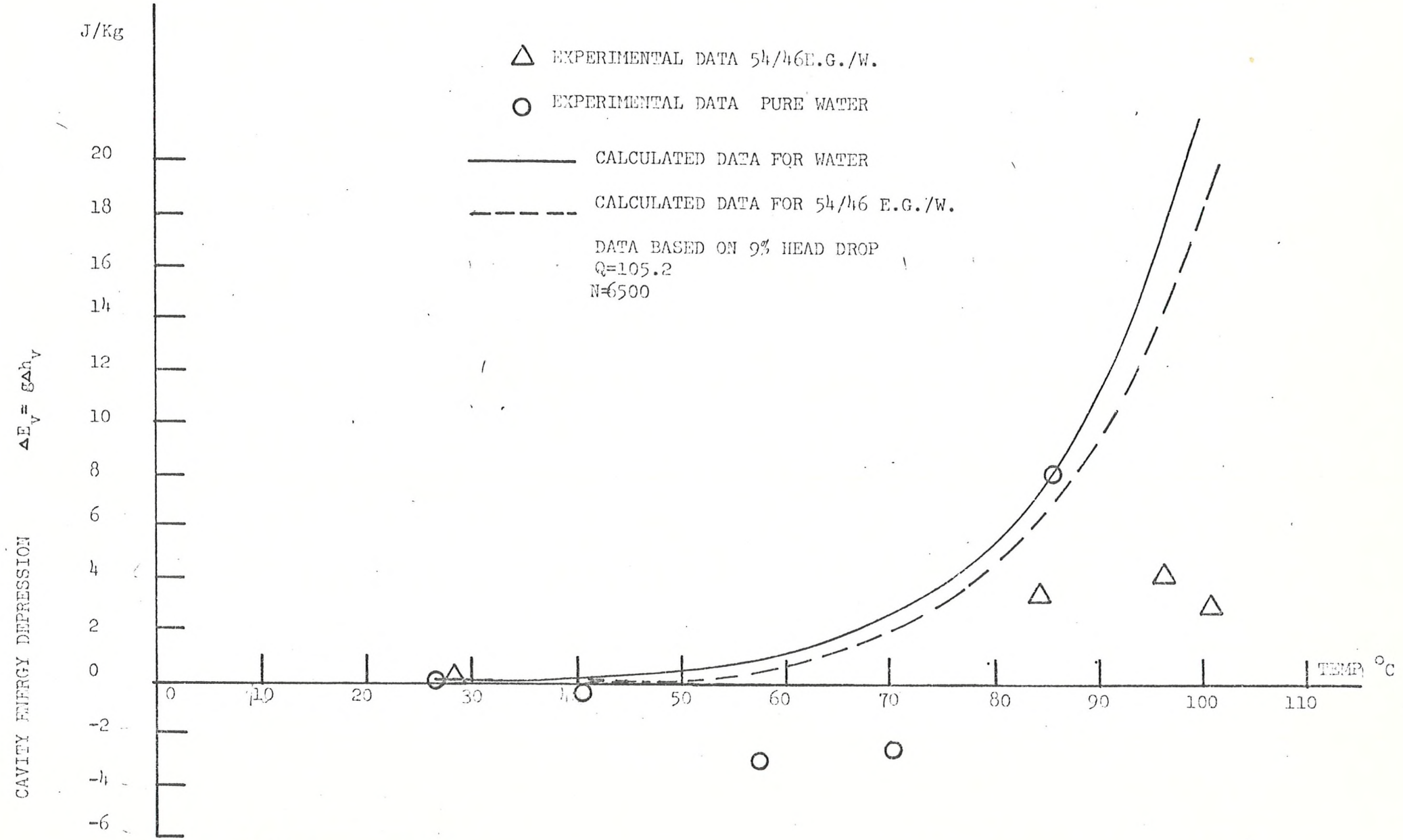

FIG 91 CALCULATED & EXPERIMENTAL CAVITY ENERGY DEPRESSION AT VARIOUS TEMPERATURES FOR PUMP "C"

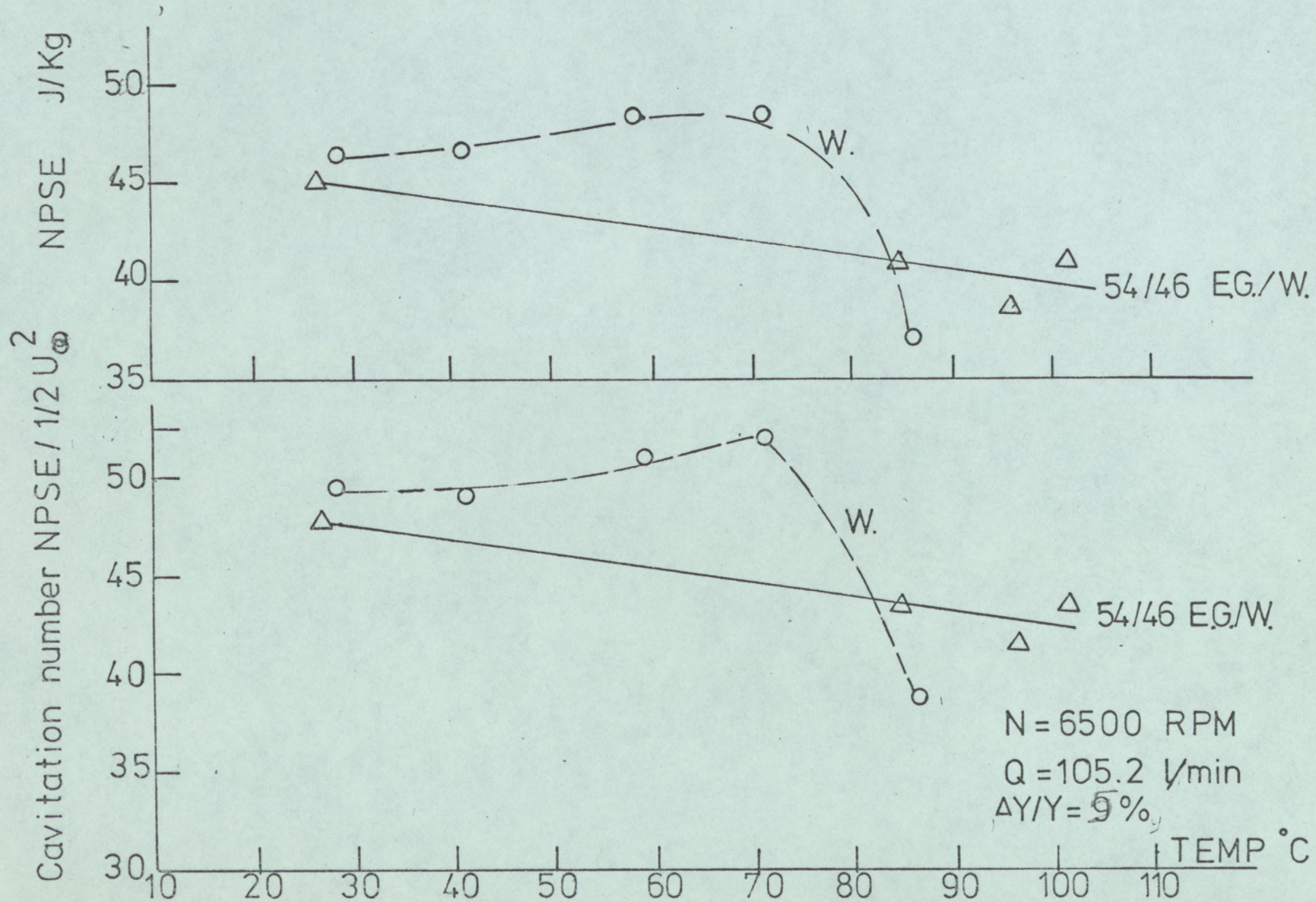

Fig 92 Effect of temp. on cavitation number & NPSE when fluids were water & 54/46EG/W on pump C

FIG. (93). $|\Delta N^{TP}|$ AS A FUNCTION OF THERMAL CAVITATION PARAMETER FOR WATER & E.G./W

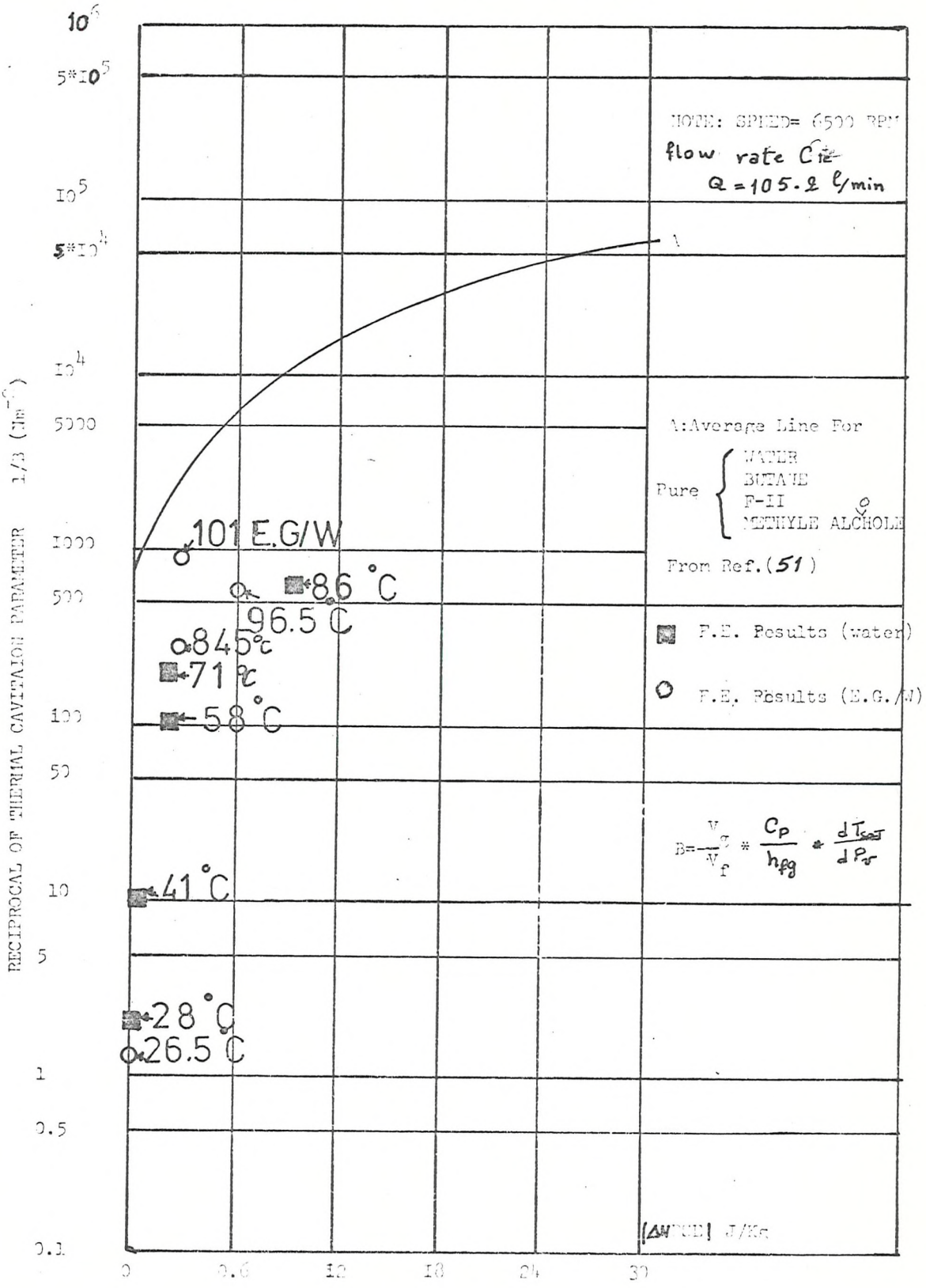

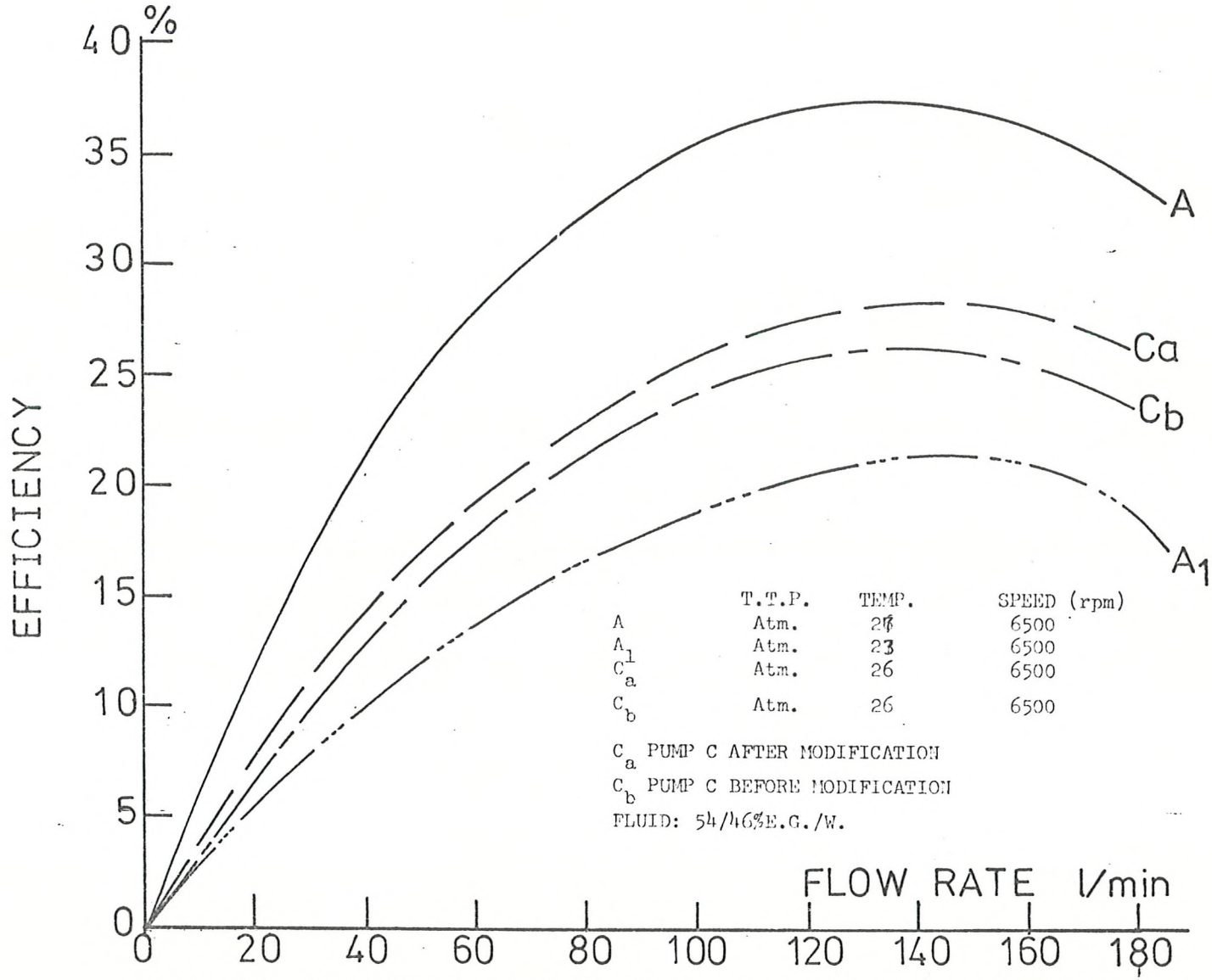

Fig 94 EFFICIENCY/FLOW CURVES AT VARIOUS PUMPS

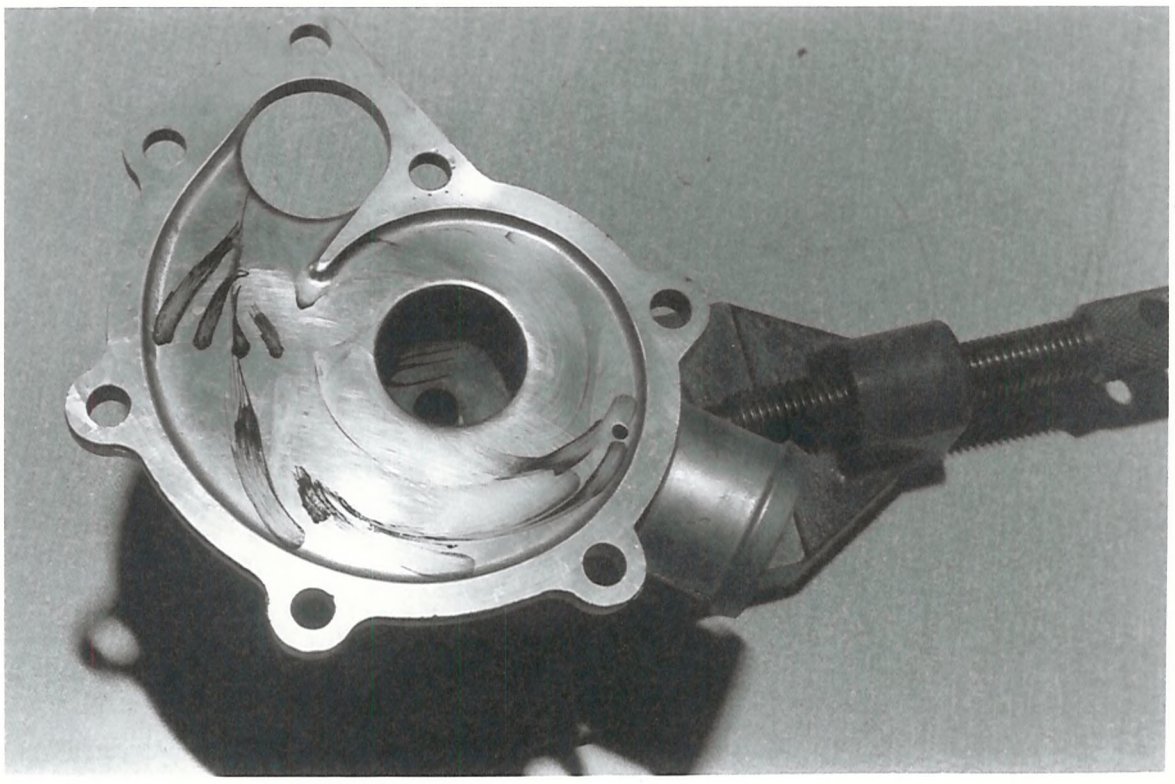

A- CAVITATING CONDITION Q=119.3 Litre/min N=7000 R.P.M.

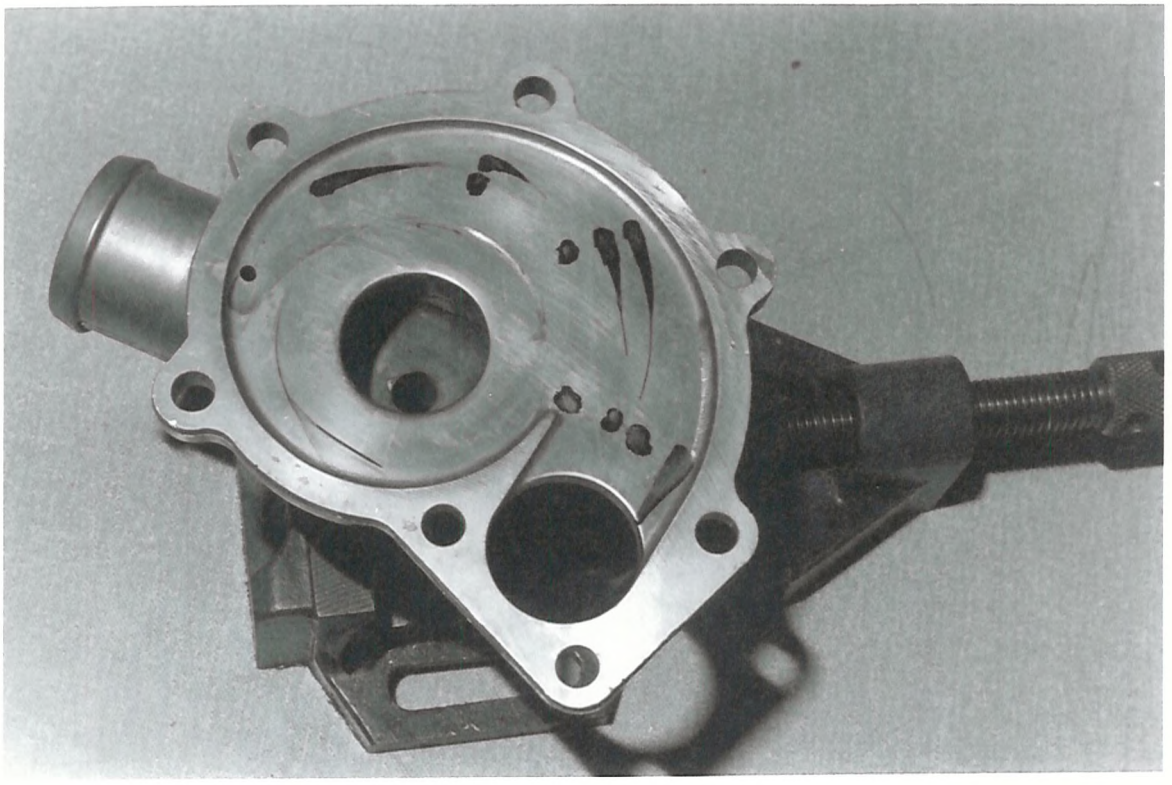

B- cavitating condition Q=118.4 Litre/min N=7000 R.P.M.

FIG 95- PAINT SPOT TESTS ON PUMP "C"

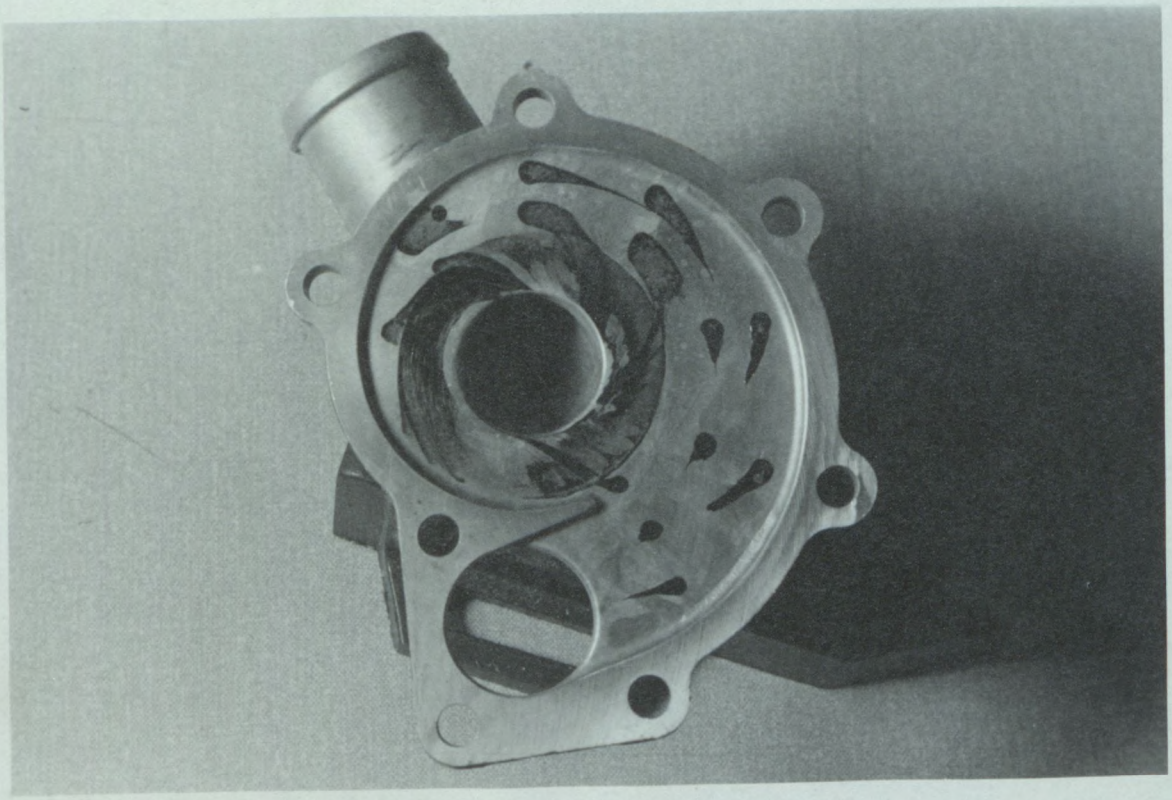

C- NON CAVITATING Q=82.1 Litre/min N=3200 R.P.M.

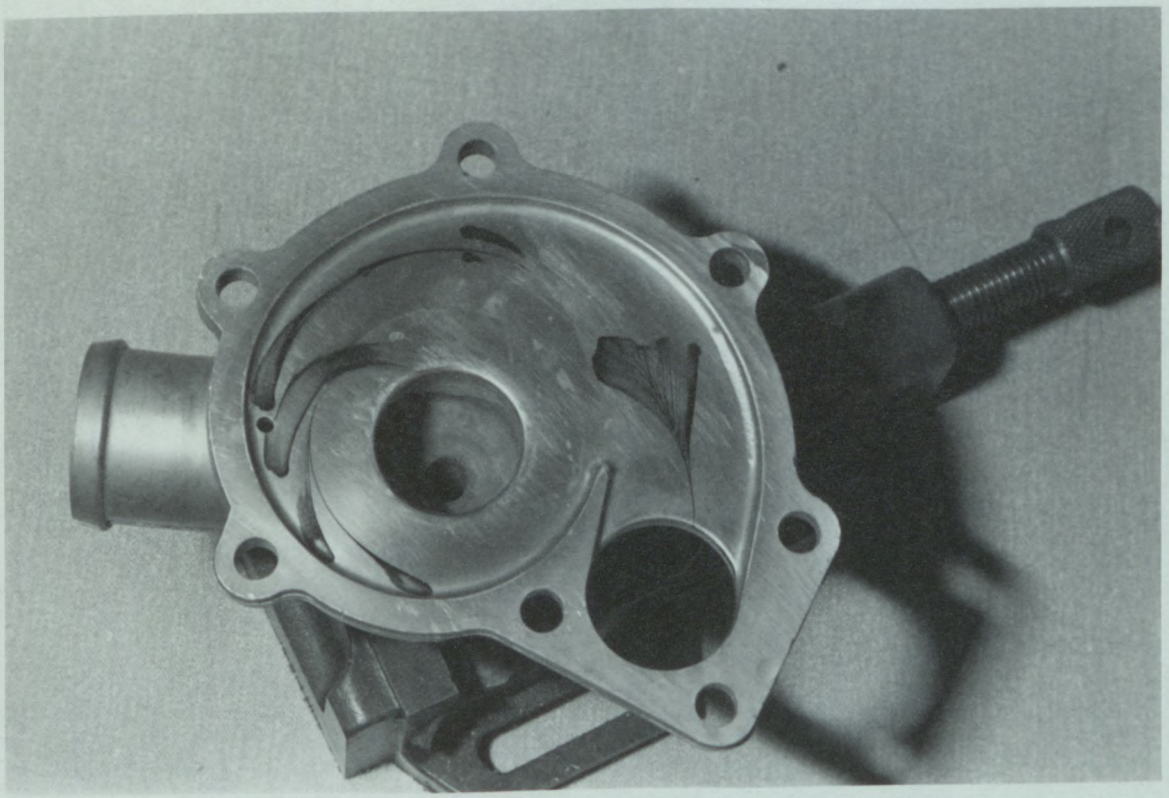

D- NON CAVITATING Q=177.8 Litre/min N=7000 R.P.M.

FIG 95- PAINT SPOT TESTS ON PUMP "C"

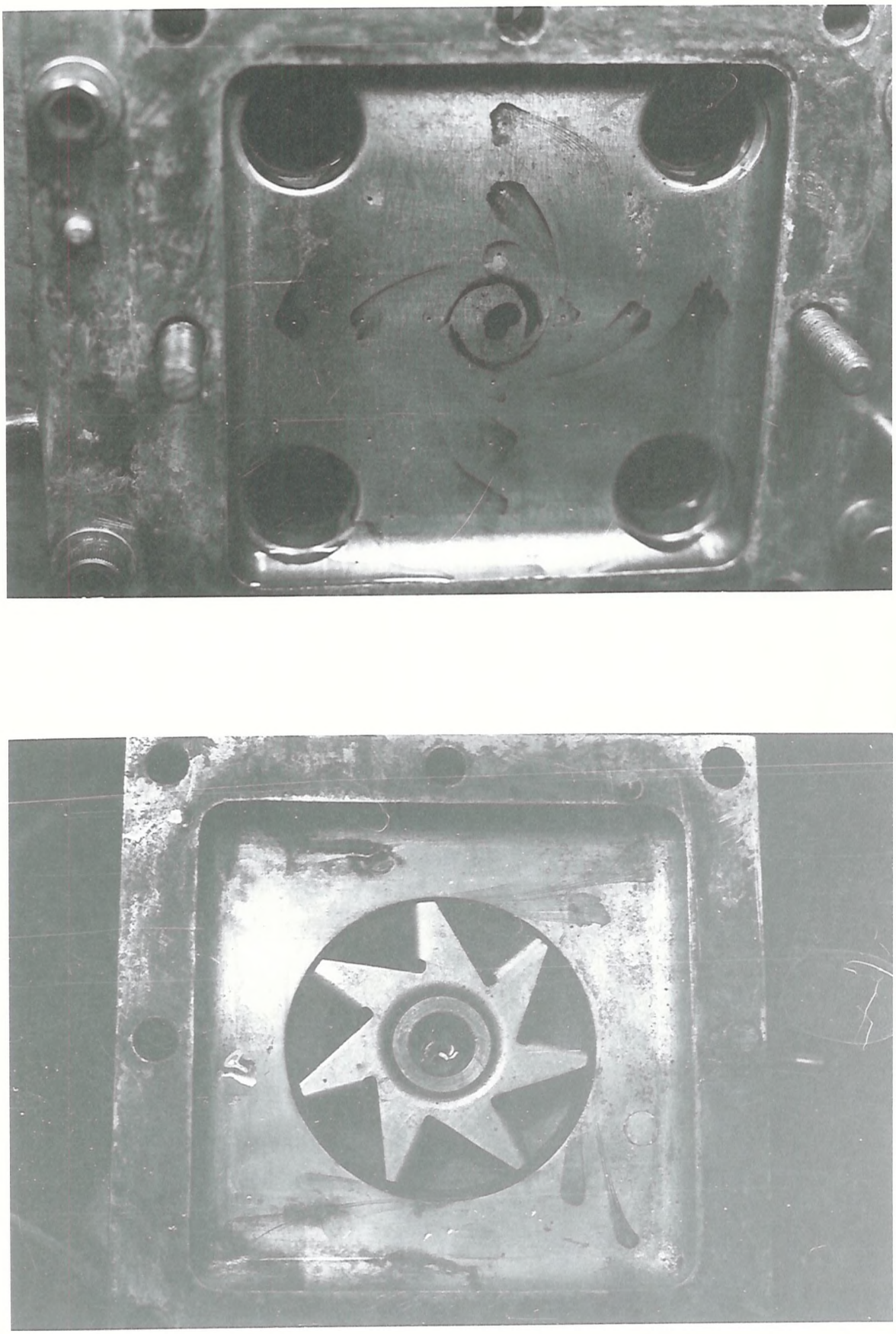

FIG 96-PAINT SPOT TESTS ON THE HOUSING OF PUMP A_1 (NO THROUGH-FLOW)

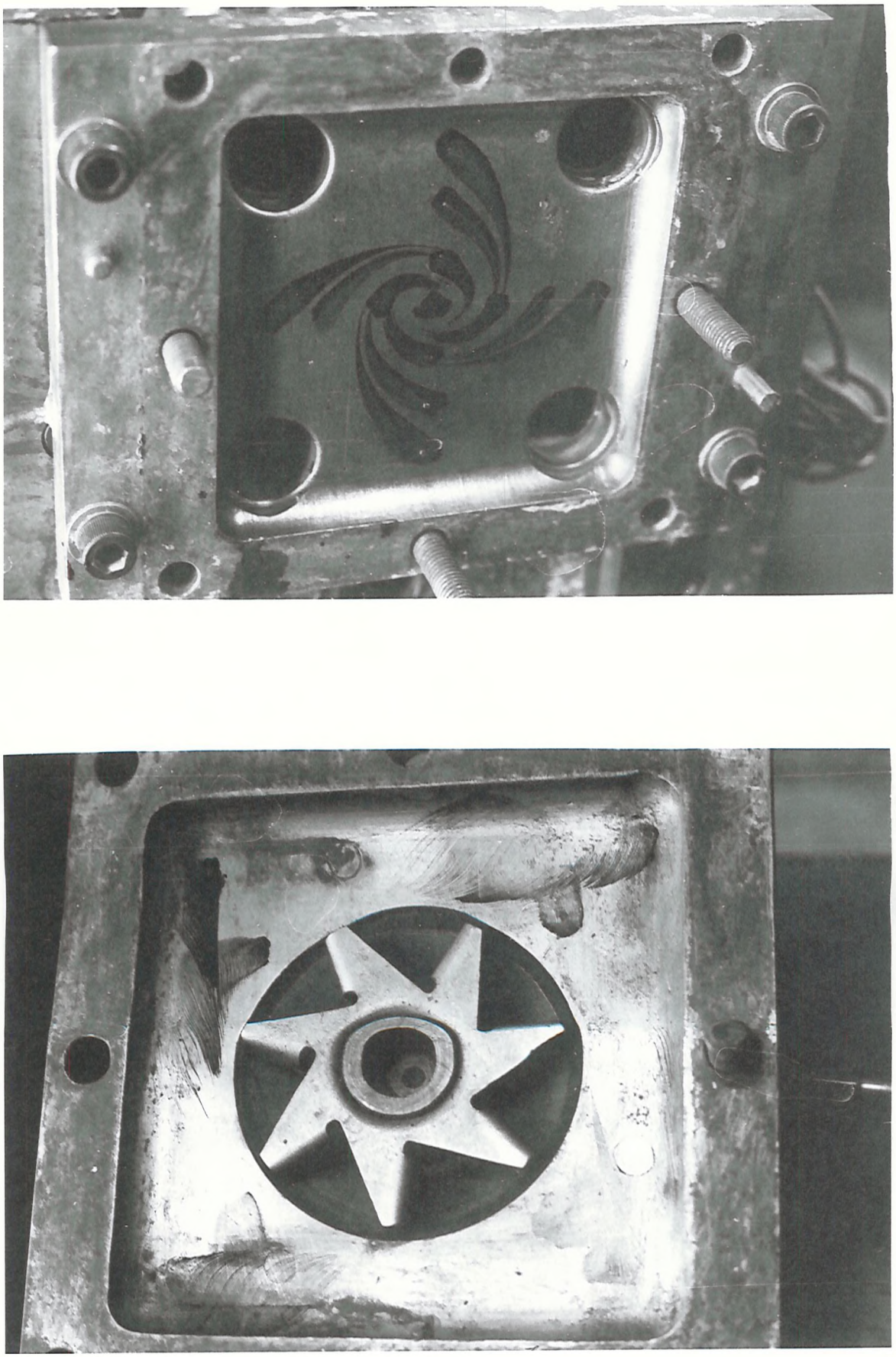

FIG 97 PAINT SPOT TESTS ON THE HOUSING OF PUMP A_1 (HIGH THROUGH_FLOW)

PUMP B_1 has less clearance between Impeller Vanes & Housing & modified Suction

PUMP B_2 Same as Pump B_1 BUT with Curved Vanes

PUMP B_1 has the flattest head flow characteristic of the pumps tested

T.T.P. = Atmos.

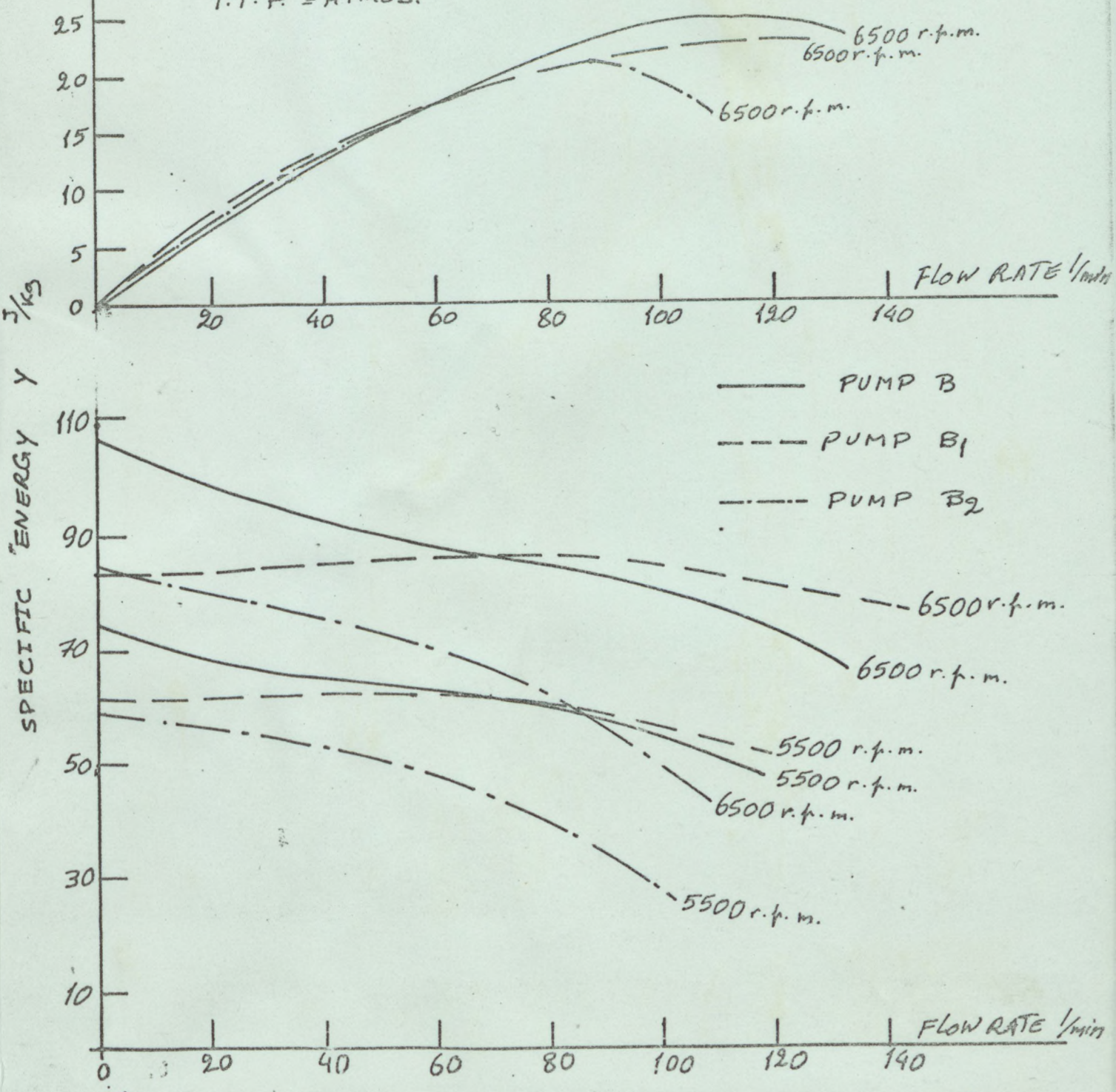

Fig 98 - Head/Flow Characteristics & Efficiency/Flow Curves for Pump B, B_1, B_2 at 20°C